AN ABSTRACT OF THE THESIS OF

Scott I. Goodall for the degree of Master of Science in Civil Engineering and Wood Science presented on March 8, 2010.
Title: Optimizing the Performance of Gypsum Wall Board in Wood Frame Shear Walls

Abstract approved:

_____

Rakesh Gupta

The overall goal of this project was to design a wood frame shear wall that could withstand greater displacement before damage occurred to the Gypsum Wall Board (GWB). More specifically, the objectives of the study were: (1) to evaluate damage to the GWB in alternative shear wall designs at 1%, 2% and 3% drift levels and compare these results to current performance-based design standards, (2) to evaluate quantitatively the relative displacement between the GWB and the wood frame under monotonic loading and (3) to evaluate the value of alternative shear wall designs considering damage sustained from design drift levels.

A total of 14 shear walls consisting of seven different designs with two walls built per design were tested to failure. Six of these walls had 1105 mm x 610 mm window openings and eight did not. All shear walls were 2440 mm x 2440 mm in size and built from 38 mm x 89 mm Douglas-fir (*Pseudotsuga menziesii*) studs at 610 mm on center (o. c.).

The seven shear wall designs tested included two control designs based on the minimum 2009 International Residential Code requirements. One control design

included a window opening and another did not. The SEPSTUD wall design included a larger screw to GWB edge distance, while the 3INNAIL design included a closer OSB nail spacing. The 2OSBWIN and 2OSB wall designs, respectively, with and without a window opening, included Oriented Strand Board (OSB) panels attached to both sides of the wood frame and the GWB attached on top of the OSB. The 4PNLWIN design attached the GWB as four different panels around the window opening, instead of two panels.

Shear wall test behavior generally agreed with the ASCE/SEI 41-06 performance-based drift criteria. 1% drift occurred between 57-80% of total wall capacity, 2% drift occurred between 84-97% of wall capacity and 3% drift occurred between 97-100% of wall capacity. The results of the visual failure comparison indicated that little damage was observed in the GWB for walls loaded to the NDS allowable strength.

The results of the shear wall visual failure comparison indicated that all innovative shear wall designs outperformed the control designs at 1% drift. This was because less GWB damage was observed in the innovative shear wall designs. At 2% and 3% drift, the 4PNLWIN and SEPSTUD designs performed worse than the control. The 3INNAIL design performed slightly better, and the 2OSB and 2OSBWIN designs performed superior to the control designs at 2% and 3% drift. The greater performance of all these designs can be attributed to the increase in strength and stiffness of these shear walls. However, superior performance of the 2OSB and 2OSBWIN designs was

due to the similar stiffness of both sides of the shear wall, resulting in equal load sharing and less damage to the GWB.

Shear walls with magnitudes of the relative displacement vectors above the visual failure limit of 3 mm exhibited inferior GWB performance, which is consistent with the visual failure results.

A shear wall value comparison indicated that the 3INNAIL, 2OSB and 2OSBWIN designs all exhibited a more efficient use of shear wall materials at 1% and 2% drift than the control designs. However, when considering a design earthquake drift level, 2OSB and 2OSBWIN designs demonstrate the most efficient use of shear wall materials.

OPTIMIZING THE PERFORMANCE OF GYPSUM WALL BOARD IN WOOD FRAME SHEAR WALLS

by
Scott I. Goodall

A THESIS

submitted to

Oregon State University

in partial fulfillment of
the requirements for the
degree of

Master of Science

Presented March 8, 2010
Commencement June 2010

Master of Science thesis of Scott I. Goodall presented on March 8, 2010

APPROVED:

_____

Major Professor, representing Wood Science and Civil Engineering

_____

Head of the School of Civil and Construction Engineering

_____

Head of the Department of Wood Science and Engineering

_____

Dean of the Graduate School

I understand that my thesis will become part of the permanent collection of Oregon State University libraries. My signature below authorizes release of my thesis to any reader upon request.

_____

Scott I. Goodall, Author

ACKNOWLEDGMENTS

I would like to thank the following people for their support in helping me complete this project:

- Dr. Rakesh Gupta for his guidance, support and leadership in this project.
- Milo Clauson for his problem solving ability in and out of the lab, help with instrumentation, test setup and implementation, and general guidance and support.
- Dr. Thomas Miller for his guidance, support and assistance.
- Stephanie Sireix, David Linton, Jeff Vaughn, Denis Hilbert and Mike Karas for help in the lab.
- All my friends and family for their unending support and encouragement.

TABLE OF CONTENTS

Page

Introduction 1

Methods and Materials 8

Preliminary Testing 9

GWB Connection Testing 9

GWB Flexural Strength Testing 9

Shear Wall Specimens 10

Shear Wall Designs without Openings 11

Shear Wall Designs with Openings 13

Test Setup 15

Monotonic Testing 15

Visual Failure Comparison 16

Instrumentation 16

Test Matrix 18

Results and Discussion 26

Preliminary Testing 26

Shear Wall Behavior 27

Shear Wall Drift Levels and Performance 29

Shear Wall Visual Failure Comparison 31

Shear Wall Comparison at Drift Criteria 32

Shear Wall Comparison at Allowable Strength 36

Shear Wall Relative Displacement Comparison 37

TABLE OF CONTENTS

Page

Qualitative Relative Displacement Comparison 37

Displacement Vector Magnitude Comparison 40

Shear Wall Value Comparison 43

Conclusions 54

References 58

LIST OF FIGURES

Figure Page

Figure 1. IRC Shear Wall Design 20

Figure 2. SEPSTUD Shear Wall Design 20

Figure 3. 3INNAIL Shear Wall Design 21

Figure 4. 2OSB Shear Wall Design 21

Figure 5. IRCWIN Shear Wall Design 22

Figure 6. 2OSBWIN Shear Wall Design 22

Figure 7. 4PNLWIN Shear Wall Design 23

Figure 8. Shear Wall Test Setup 23

Figure 9. Schematic of Displacement Sensor Locations 24

Figure 10. GWB Failure Modes 46

Figure 11. IRC Shear Wall Design Load Displacement Curve 46

Figure 12. Shear Wall Damage Observations 47

Figure 13. Shear Wall Global Connection Failure Comparison 48

Figure 14. Classical Wood Frame Deformation and GWB Rotation Model 48

Figure 15. Relative Displacement Photos of Shear Walls at Failure 49

Figure 16. GWB Relative Displacement Vectors at 1% Drift for IRC Design 49

Figure 17. Relative Displacement Comparison for Shear Walls without Openings 50

Figure 18. Relative Displacement Comparison for Shear Walls with Openings 50

Figure 19. Shear Wall Value Comparison 51

LIST OF TABLES

Table Page

Table 1. Modulus of Elasticity for Various Sheathing Materials 7

Table 2. Test Matrix 25

Table 3. Shear Wall Mechanical Properties 52

Table 4. Percentage of Maximum Load at Drift Criteria 52

Table 5. Global Connection Failure Observed at Allowable Strength 53

LIST OF APPENDICES

Appendix Page

Appendix A: Wood Frame Materials 61

Appendix B: GWB Materials 70

Moisture Content of GWB Panels Applied to Shear Walls 70

ASTM C473 GWB Flexural Strength Test 70

GWB Connection Tests 71

Appendix C: Visual Comparison Analysis 86

Appendix D: Displacement Sensor Configuration and Calibration 103

Appendix E: Shear Wall Test Raw Data 107

Appendix F: Shear Wall Backbone Curves 123

Appendix G: Sensor Vectors and Angles 128

Appendix H: Further Discussion of Relative Displacement Vectors 158

Shear Walls without Openings 158

Shear Walls with Openings 160

Appendix I: Discussion of Shear Wall Performance at Low Displacements 166

Appendix J: Shear Wall Value Comparison Figures 168

Appendix K: Discussion of Variability in Results 171

Variation in Mechanical Property Results 171

Variation in Visual Failure Comparison Method 171

Appendix L: Shear Wall Allowable Strengths 173

LIST OF APPENDIX FIGURES

Figure Page

Figure A1. IRC and 2OSB Designs Wood Frame Systems 62

Figure A2. SEPSTUD and 3INNAIL Designs Wood Frame Systems 62

Figure A3. IRCWIN and 2OSBWIN Designs Wood Frame Systems 63

Figure A4. 4PNLWIN Design Wood Frame System 63

Figure B1. GWB Panel Locations 74

Figure B2. GWB Flexural Test Setup 74

Figure B3. GWB Flexural Sample Locations 75

Figure B4. GWB Flexural Tests Load Displacement Curves 76

Figure B5. GWB Connection Test Setup 77

Figure B6. Load Displacement Curve for 9.5 mm Edge Distance GWB Tests 77

Figure B7. Load Displacement Curve for 19.1 mm Edge Distance GWB Tests 78

Figure B8. Load Displacement Curve for 57.2 mm Edge Distance GWB Tests 79

Figure B9. Average GWB Sample Maximum Load 79

Figure B10. Average GWB Sample Displacement at Maximum Load 80

Figure B11. GWB Sample Displacement at Visual Failure 80

Figure B12. GWB Connection Test Photographs 81

Figure C1. Visual Failure Comparison Locations 88

Figure D1. Instrumentation Panel 104

Figure D2. Displacement Sensor Schematic 104

Figure D3. Instrumentation Setups 105

Figure D4. Displacement Sensor 1 Calibration Summary 105

LIST OF APPENDIX FIGURES

Figure Page

Figure E1. Displacement Sensor Locations 108

Figure E2. IRC-E Raw Data 109

Figure E3. IRC-M Raw Data 110

Figure E4. SEPSTUD-E Raw Data 111

Figure E5. SEPSTUD-M Raw Data 112

Figure E6. 3INNAIL-E Raw Data 113

Figure E7. 3INNAIL-M Raw Data 114

Figure E8. 2OSB-E Raw Data 115

Figure E9. 2OSB-M Raw Data 116

Figure E10. IRCWIN-E Raw Data 117

Figure E11. IRCWIN-M Raw Data 118

Figure E12. 2OSBWIN-E Raw Data 119

Figure E13. 2OSBWIN-M Raw Data 120

Figure E14. 4PNLWIN-E Raw Data 121

Figure E15. 4PNLWIN-M Raw Data 122

Figure F1. IRC Design Backbone Curves 124

Figure F2. SEPSTUD Design Backbone Curves 124

Figure F3. 3INNAIL Design Backbone Curves 125

Figure F4: 2OSB Design Backbone Curves 125

Figure F5. IRCWIN Design Backbone Curves 126

Figure F6: 2OSBWIN Design Backbone Curves 126

LIST OF APPENDIX FIGURES

Figure Page

Figure F7. 4PNLWIN Design Backbone Curves 127

Figure G1. Sensor and Vector Directions for Shear Walls besides 4PNLWIN 129

Figure G2. Sensor and Vector Directions for 4PNLWIN 129

Figure G3. IRC Top End Sensor Displacements and Vector Angles 130

Figure G4. IRC Bottom End Sensor Displacements and Vector Angles 131

Figure G5. IRC Top Middle Sensor Displacements and Vector Angles 132

Figure G6. IRC Bottom Middle Sensor Displacements and Vector Angles 133

Figure G7. SEPSTUD Top End Sensor Displacements and Vector Angles 134

Figure G8. SEPSTUD Bottom End Sensor Displacements and Vector Angles 135

Figure G9. SEPSTUD Top Middle Sensor Displacements and Vector Angles 136

Figure G10. SEPSTUD Bottom Middle Sensor Displacements and Vector Angles . 137

Figure G11. 3INNAIL Top End Sensor Displacements and Vector Angles 138

Figure G12. 3INNAIL Bottom End Sensor Displacements and Vector Angles 139

Figure G13. 3INNAIL Top Middle Sensor Displacements and Vector Angles 140

Figure G14. 3INNAIL Bottom Middle Sensor Displacements and Vector Angles... 141

Figure G15. 2OSB Top End Sensor Displacements and Vector Angles 142

Figure G16. 2OSB Bottom End Sensor Displacements and Vector Angles 143

Figure G17. 2OSB Top Middle Sensor Displacements and Vector Angles 144

Figure G18. 2OSB Bottom Middle Sensor Displacements and Vector Angles 145

Figure G19. IRCWIN Top End Sensor Displacements and Vector Angles 146

Figure G20. IRCWIN Bottom End Sensor Displacements and Vector Angles 147

LIST OF APPENDIX FIGURES

Figure Page

Figure G21. IRCWIN Top Middle Sensor Displacements and Vector Angles 148

Figure G22. IRCWIN Bottom Middle Sensor Displacements and Vector Angles.... 149

Figure G23. 2OSBWIN Top End Sensor Displacements and Vector Angles 150

Figure G24. 2OSBWIN Bottom End Sensor Displacements and Vector Angles..... 151

Figure G25. 2OSBWIN Top Middle Sensor Displacements and Vector Angles 152

Figure G26. 2OSBWIN Bottom Middle Sensor Displacements and Vector Angles. 153

Figure G27. 4PNLWIN Top End Sensor Displacements and Vector Angles..... 154

Figure G28. 4PNLWIN Bottom End Sensor Displacements and Vector Angles..... 155

Figure G29. 4PNLWIN Top Middle Sensor Displacements and Vector Angles 156

Figure G30. 4PNLWIN Bottom Middle Sensor Displacements and Vector Angles. 157

Figure H1. Classical Wood Frame Deformation and GWB Rotation Model 162

Figure H2. Relative Displacement Photos of Shear Walls at Failure 162

Figure H3. Relative Displacement Vectors for Shear Walls without Openings..... 163

Figure H4. Relative Displacement Vectors for Shear Walls with Openings 164

Figure H5. Uplift of the Middle Stud at Failure in Double Middle Stud Designs..... 165

Figure H6. Load Path Schematic of Double Middle Stud Shear Walls..... 165

Figure I1: Connection Failure of Walls without Openings at Low Displacements ... 167

Figure I2: Failure Comparison of Walls with Openings at Low Displacements..... 167

Figure J1. Value Comparison at 1% Drift for Shear Walls without Openings..... 169

Figure J2. Value Comparison at 2% Drift for Shear Walls without Openings..... 169

Figure J3. Value Comparison at 1% Drift for Shear Walls with Openings..... 170

LIST OF APPENDIX FIGURES

Figure Page

Figure J4. Value Comparison at 2% Drift for Shear Walls with Openings 170

LIST OF APPENDIX TABLES

Table Page

Table A1. IRC-E Wood Frame Properties 64
Table A2. IRC-M Wood Frame Properties 64
Table A3. 2OSB-E Wood Frame Properties 64
Table A4. 2OSB-M Wood Frame Properties 65
Table A5. SEPSTUD-E Wood Frame Properties 65
Table A6. SEPSTUD-M Wood Frame Properties 65
Table A7. 3INNAIL-E Wood Frame Properties 66
Table A8. 3INNAIL-M Wood Frame Properties 66
Table A9. IRCWIN-E Wood Frame Properties 66
Table A10. IRCWIN-M Wood Frame Properties 67
Table A11. 2OSBWIN-E Wood Frame Properties 67
Table A12. 2OSBWIN-M Wood Frame Properties 68
Table A13. 4PNLWIN-E Wood Frame Properties 68
Table A14. 4PNLWIN-M Wood Frame Properties 69
Table B1. Moisture Contents of GWB Panels Applied to Shear Walls 83
Table B2. Flexural Strength of Perpendicular GWB Samples 84
Table B3. Flexural Strength of Parallel GWB Samples 84
Table B4. Moisture Contents of GWB Samples 84
Table B5. Test Results from Connection Tests 85
Table C1. Visual Failure Comparison Results from IRC-E 89
Table C2. Visual Failure Comparison Results from IRC-M 90

LIST OF APPENDIX TABLES

Table Page

Table C3. Visual Failure Comparison Results from SEPSTUD-E 91

Table C4. Visual Failure Comparison Results from SEPSTUD-M 92

Table C5. Visual Failure Comparison Results from 3INNAIL-E 93

Table C6. Visual Failure Comparison Results from 3INNAIL-M 94

Table C7. Visual Failure Comparison Results from 2OSB-E 95

Table C8. Visual Failure Comparison Results from 2OSB-M 96

Table C9. Visual Failure Comparison Results from IRCWIN-E 97

Table C10. Visual Failure Comparison Results from IRCWIN-M 98

Table C11. Visual Failure Comparison Results from 2OSBWIN-M 99

Table C12. Visual Failure Comparison Results from 2OSBWIN-E 100

Table C13. Visual Failure Comparison Results from 4PNLWIN-E 101

Table C14. Visual Failure Comparison Results from 4PNLWIN-M 102

Table D1. Maximum Displacement Sensor Error Summary 106

Table K1: Difference in Percent Global Connection Failure 172

OPTIMIZING THE PERFORMANCE OF GYPSUM WALL BOARD IN WOOD FRAME SHEAR WALLS

INTRODUCTION

Eighty to ninety percent of all structures in the United States are wood frame. An even higher percentage of residential structures use wood as the main structural material. A residential structure is generally the greatest personal investment of anyone in the US and represents a great value to society (McMullin and Merrick, 2002). Protecting this investment from natural disasters such as earthquakes is an important task for engineers. Fortunately, wood generally performs very well during seismic events. The two reasons for this are: (1) wood's high strength to weight ratio and (2) its load duration properties i.e. wood can withstand a large load for a short period of time, such as an earthquake. However, the Northridge Earthquake of 1994 changed the way engineers viewed the resilience of wood structures in earthquakes. An estimated 20 billion dollars in damage occurred to wood structures in the Northridge Earthquake (Seible et al., 1999). However, much of these failures were concentrated in nonstructural components such as Gypsum Wall Board (GWB) (Schierle, 2003).

Shear walls are the main component in a wood frame structure that resists seismic loads and consist of a wood frame, anchorage, fasteners, structural sheathing and nonstructural sheathing. The wood frame is generally made from dimensional lumber. Shear wall anchorage consists of mechanical devices called hold downs and anchor bolts that connect the wood frame to the foundation of a wood frame structure. Fasteners are generally nails or screws that attach the sheathing to the wood frame.

Structural sheathing is often Oriented Strand Board (OSB) or plywood, while nonstructural sheathing is usually GWB. OSB is a wood composite panel used for its shear strength and stiffness. It is usually installed on the outside of a structure, but covered by some sort of building envelope, for example siding. GWB is a panel installed on the inside of a building as an architectural finish and is also used as fire protection.

Shear walls resist seismic loads in two different ways: load transfer and energy dissipation. The horizontal seismic loads are transferred vertically by the frame interacting with the sheathing. Fastener yielding and inelastic behavior dissipates energy to resist seismic loads as well. Current building design codes do not include the addition of the nonstructural GWB into shear wall mechanical behavior. This was believed to be a conservative assumption until the wood frame shear walls in the Northridge Earthquake experienced severe damage. Table 1 identifies GWB as a stiffer material than OSB. The greater stiffness of the GWB compared to the OSB results in uneven load sharing between the two materials and extreme damage in the GWB (Sinha, 2007). The stiffer GWB attracts the seismic load at low deflections until a brittle failure of the GWB results, and then the load is transferred to the OSB.

McMullin and Merrick (2002) performed testing of 2440 x 4877 mm partition walls with openings for windows and doors sheathed with GWB on one side. This study concluded that cosmetic damage to the GWB begins at 0.25% drift and total economic loss of the wall occurs at 2% drift. Damage thresholds were identified as

cracking of the GWB at the door openings near 0.25-0.75% drift and cracking of the paint over the fastener head occurring at 0.25-0.75% drift. The maximum load occurred around 1.0-1.5% drift. Different GWB connection systems were tested including the use of innovative fasteners, fiber reinforced wallboard and floating edge construction. The two types of innovative fasteners used, screws with larger heads and countersunk washers, both retarded the propagation of cracks around window openings during testing. Innovative fasteners and fiber reinforced wallboard both increased the ultimate strength of the walls. However, using fiber reinforced wallboard did not affect the damage observed in the GWB. Floating edge construction decreased the damage from cracking of the paint over the fastener head. Beyond this, it did not affect the stiffness or strength of the wall. Additionally, outcomes of monotonic tests predicted those of cyclic tests with the backbone curve of the cyclic tests lying within the monotonic curve. However, strength and stiffness degradation were seen after 1% drift in the cyclic tests compared to the monotonic tests. Cracking of the GWB panels around the corners of door and window openings was a common failure progression for all the walls.

Sinha (2007) tested sixteen 2440 x 2440 mm shear walls, some sheathed with OSB and GWB, others with only OSB, to determine load sharing between the GWB and the OSB. Sinha concluded that GWB does transfer load, but only at low forces and deflections. Beyond 60% of the wall capacity, the OSB begins to transfer most of the load. The addition of GWB was found to only contribute 0.8% to the overall

strength of the wall, while it contributed 50% to the elastic shear stiffness. The strength and stiffness contributions from GWB were also recorded by Uang and Gatto (2003) with similar results. An increase in average strength by 12% and an increase in initial stiffness by 48% were recorded by Uang and Gatto (2003). Other studies (Karacabeyli and Ceccotti [1996], Wolfe [1983], and Toothman [2003]) have concluded that GWB increases stiffness and strength but lowers ductility. The theory that the superposition of all shear wall elements can be assumed has been disputed. Some research has concluded it is always true (Wolfe, 1983). Others have concluded it is not true (Toothman, 2003) and still others have concluded it is only true to 1.3% drift (Karacabeyli and Ceccotti, 1996).

Sinha's conclusion that the failure of the GWB occurs before the OSB was witnessed in the aftermath of the 1994 Northridge Earthquake (Schierle, 2003) and the 1971 San Fernando Earthquake (Lagorio, 1990). Following the Northridge Earthquake, field investigations were carried out by the Consortium of Universities for Research in Earthquake Engineering (CUREE) task force in the City of Los Angeles (Schierle, 2003). According to on-site investigations of 1230 randomly selected buildings, nonstructural damage was the most frequent and expensive repair for single family dwellings, costing an average of $7,989 (Schierle, 2003). Another study on other historic earthquakes found that nonstructural damage can account for a maximum of 70% of future repair costs (Lagorio, 1990). For multifamily dwellings, shear walls were the most frequently damaged and expensive repair, costing an

average of $215,765 (Schierle, 2003). Failures in nonstructural components and shear walls compromised the majority of the damage done to wood frame structures in the Northridge Earthquake (Seible et al., 1999). A similar study was done on the San Fernando Earthquake by Oakeshott (1975). Of the 12,000 buildings surveyed, 89% had some sort of damage to the GWB. While the majority of this damage could be repaired by simple spackling, the overall cost was still great due to the high frequency of this problem.

Due to the property loss from the Northridge Earthquake related to GWB and shear walls (Schierle, 2003), currently implemented shear wall designs must be updated. A major cause of this past damage is from the different stiffnesses of the GWB and OSB (Sinha, 2007). The stiffer GWB will cause an increased strength and stiffness, but reduced ductility of the wall (Uang and Gatto, 2003). The recommendations of CUREE are to consider this change in shear wall behavior in design (Cobeen et al., 2004). Specifically, CUREE recommends future studies to understand how these shear wall components interact with each other. Additional recommendations include that design should codes account for the increased strength from finish materials such as GWB, their decreased ductility by reducing the R-factor, and their increased initial stiffness at low drifts.

The overall goal of this project was to design a shear wall that can withstand greater displacement before damage occurs to the GWB. Using the previous research

and CUREE recommendations, seven new shear walls designs were fabricated, tested and compared.

This project capitalized on using common materials and practices. Using common practices, the alternative designs could be employed by "do it yourselfers" and contractors. With common materials, the upfront cost of buildings remains similar. Both of these factors allow for an improved design to be incorporated into standard practices quickly and efficiently.

By comparing the performance of different wood frame designs with and without window openings, the value of these designs could be applied to residential housing. Comparing the behavior of these shear walls required additional knowledge of shear wall behavior than was available in the literature. Information regarding a visual failure criteria as well as movement of individual elements of the shear walls was required. The specific objectives of the project were:

1) To evaluate damage to the GWB in alternative shear wall designs at 1%, 2% and 3% drift levels and compare these results to current performance-based design standards.
2) To evaluate quantitatively the relative displacement between the GWB and the wood frame under monotonic loading.
3) To evaluate the value of alternative shear wall designs considering damage sustained from design drift levels.

Table 1. Modulus of Elasticity for Various Sheathing Materials (Sinha, 2007)

Material	Modulus of Elasticity	Source
OSB	4.8 to 8.3 GPa	USDA Forest Service (2004)
GWB	5.0 to 12.0 GPa	Deng and Furono (2001)

METHODS AND MATERIALS

Because only common materials and practices were used, the primary means of damage prevention to the GWB was through changes in shear wall construction. The construction was altered to obtain the following changes in shear wall behavior:

1) Increased strength
2) Increased stiffness
3) Stronger connection between the GWB and the wood frame
4) Stronger connection between the OSB and the wood frame

A timeline of this project was as follows:

1) Perform preliminary testing of GWB and wood frame connections to determine the effects of screw edge distance on connection strength and displacement at maximum load. Also, identify GWB screw connection failure modes and displacements at which those failure modes occurred.
2) Design three innovative shear wall systems without openings which prevent damage to the GWB.
3) Test the innovative shear walls without openings to failure under monotonic loading.
4) Compare performance of innovative shear walls against a control design based on the minimum 2009 International Residential Code (IRC) requirements.

5) Using knowledge gained; design two additional shear walls systems with window openings.
6) Test the innovative shear walls with window openings to failure under monotonic loading.
7) Compare performance of innovative shear walls with openings against the control design with a window opening.

Preliminary Testing

GWB Connection Testing

GWB connections were tested to achieve the following goals:

1) Identify how GWB screw edge distance affects connection strength and displacement at maximum load.
2) Identify visual failure modes of GWB and displacements at which those failures occurred.

Fifteen GWB connections were tested in tension at one of three edge distances. These edge distances were the distance between the screw and the edge of the GWB panel. The three edge distances considered were 9.5, 19.1 and 57.2 mm which correspond to the edge distances found in all shear wall specimen designs considered in this study. Appendix B describes sample properties and test procedure.

GWB Flexural Strength Testing

The flexural strength of GWB shipment used in this study was determined in accordance with Method B of the ASTM C473 test (ASTM 2007). The primary goal

of this test was to determine the variability in the GWB shipment received and to validate that the flexural strength was above ASTM C1396 requirements (ASTM 2006). The ASTM C1396 test requires that the flexural strength of four 305 x 406 x 12.7 mm samples of GWB, two tested parallel and two tested perpendicular to the 2400 mm panel edge, be tested from three GWB panels in the shipment. Appendix B outlines additional details of this procedure.

Shear Wall Specimens

All shear walls were 2440 mm x 2440 mm in size and contained double top plates and double end studs. Aside from the headers used in window openings, all framing was 38 mm x 89 mm (51 mm x 102 mm or 2 x 4 nominal size) No. 1 and Better grade kiln dried Douglas-fir (*Pseudotsuga menziesii*) dimension lumber. The specific gravity and modulus of elasticity of all lumber, excluding headers, is included in Appendix A. Vertical studs for walls were spaced at 610 mm on center (o. c.). Double top and bottom plates, end studs and all vertical studs in which two stud faces contacted were face nailed together at 610 mm o. c. using two 10d (3.3 x 75 mm) SENCO® framing nails. All connections of the top and bottom plates to vertical studs were end nailed with two 16d (3.4 x 88 mm) Bostitch® framing nails for each stud connection. Framing nails were all full round head, strip cartridge, smooth shank nails driven using a SENCO® SN 65 or Bostitch® N90RHN framing nailer.

Walls were vertically sheathed with two 1220 mm x 2440 mm x 11.1 mm 24/16 APA rated OSB panels. On the opposite side, walls were vertically sheathed

with two 1220 mm x 2440 mm x 12.7 mm GWB panels. OSB panels were connected to the wood frame using 8d (2.9 mm x 60 mm) SENCO® framing nails with two different nail spacings outlined in the individual wall specimen designs. GWB panels were attached vertically to the wood frame using 41.3 mm long Bugle Coarse Grade 25 drywall screws 305 mm o. c. The edge distance (ED) of all shear wall designs is indicated in their respective figures.

All walls were anchored to a fabricated steel beam that was welded to the strong floor to simulate a rigid foundation. The double end studs were anchored to this fabricated steel beam using two SIMPSON Strong-Tie PHD5-SDS3 and 15.9 mm diameter bolts. Additionally, two 63.5 mm x 63.5 mm x 12.7 mm base plates with 15.9 mm diameter anchor bolts were placed 305 mm from the end studs to anchor the bottom plate.

Seven wall specimen designs were used in this project. Of these seven, three had window openings and four did not.

Shear Wall Designs without Openings

IRC Shear Wall Design

The IRC design, shown in Figure 1, was the control design for shear walls without openings. The IRC design represented the minimum requirements for a shear wall in the 2009 IRC (International Code Council, 2009), and so is called the IRC design.

SEPSTUD Shear Wall Design

Preliminary testing of the GWB indicated that the distance between where a screw was placed to the edge of a GWB panel affects the strength of the GWB wood frame connection. A larger edge distance was found to result in a stronger connection. The SEPSTUD design, shown in Figure 2, was built to increase this edge distance and as a result increase the strength of the GWB connection. To accomplish this, a double bottom plate was installed as well as a double middle stud. The two middle studs were separated by 114 mm to allow for a 57.2 mm edge distance around the entire GWB panel. This separated stud design was abbreviated SEPSTUD design.

3INNAIL Shear Wall Design

The 3INNAIL design, shown in Figure 3, was built to see how an increase in the strength of the shear wall and stiffness of the OSB side of the wall affects the performance of the GWB. As concluded by Sinha (2007) unequal load sharing of the GWB and OSB lead to greater initial damage to the GWB. This unequal load sharing was due to the greater stiffness of the GWB compared to the OSB. Stiffening the OSB side of the wall was thought to cause more equal load sharing between the GWB and the OSB. To accomplish this, the OSB to wood frame connection was altered by decreasing the nail spacing by a factor of two. This resulted in an edge nailing of 76.2 mm o. c, or three inches and indicated by the name 3INNAIL, and a field nailing of 152 mm o. c. A double bottom plate and double middle studs were also added to the wood frame. This was to insure that the heavy nailing pattern would not split the kiln

dried wood studs. The double bottom plate and middle studs also allowed for a larger edge distance for the GWB.

2OSB Shear Wall Design

Like the 3INNAIL design, the 2OSB wall design was built to more evenly distribute the load between the GWB and OSB. This design, shown in Figure 4, was exactly like the IRC design except that OSB panels were applied to both sides of the wood frame as indicated by the name 2OSB. The GWB panels were then applied on top of the additional OSB panels. Applying materials with equal stiffness to each side of the wood frame was thought to share load more evenly and put less strain on the GWB. The nailing pattern for the OSB to wood frame connection was the same on both sides of the wood frame as the IRC wall design.

Shear Wall Designs with Openings

IRCWIN Shear Wall Design

The IRCWIN design, shown in Figure 5, was the control design for shear walls with openings and the adaptation of the IRC design to have window openings. Each shear wall with a window opening had a header and opening sill to frame the opening. The openings were 1105 mm x 610 mm located in the very center of the wall. The header consisted of two 38 mm x 140 mm (51 x 152 mm or 2 x 6 nominal size) No. 2 and Better grade kiln dried Douglas-fir (*Pseudotsuga menziesii*) lumber lengths with an 11.1 mm OSB spacer in between. Jack studs and a cripple stud were placed above the header and beneath the opening sill, respectively. Two 16d nails were used to end

nail horizontal members to vertical members such as the header to the vertical studs. The nailing pattern for the OSB to wood frame connection was the same as the IRC design.

2OSBWIN Shear Wall Design

The 2OSBWIN design, as shown in Figure 6, was the adaptation of the 2OSB design to have window openings. This design was exactly like the IRCWIN design except that OSB panels were applied to both sides of the wood frame. The GWB was then attached to the top of the additional OSB panels. The nailing pattern for the OSB to wood frame connection was the same on both sides of the wood frame as the IRCWIN design.

4PNLWIN Shear Wall Design

McMullin and Merrick (2002) noted that one method of failure for partition walls with openings was cracking of the GWB near the corners of the openings. The 4PNLWIN design, as shown in Figure 7, was built to prevent this sort of failure mode. GWB panels were cut and applied such that they connected at the window opening corners. This allowed for a gap between panels near the corners which could allow panel rotation before cracking occurred. Additional jack studs above the windows were required so that the panels could be applied in this way. The nailing pattern for the OSB to wood frame connection was the same as the IRCWIN design.

Test Setup

Testing was conducted in the Gene D. Knudson Wood Engineering Laboratory in Richardson Hall at Oregon State University. A typical wall setup is shown in Figure 8. All walls were anchored to a fabricated steel beam which was welded to the strong floor to simulate a rigid foundation. The double top plate was bolted to a 2700 mm long load head with two 22.2 mm diameter bolts and two 12.7 mm diameter bolts spaced from each end at 127 mm and 330 mm, respectively. The load head was attached to a 49 kN capacity, 254 mm stroke, hydraulic actuator. The hydraulic actuator was attached to the reaction wall. This actuator was controlled by a MTS 406 servo controller. A 111 kN load cell was attached to the actuator to provide force measurements, while the actuator provided global displacement data. Additionally, this actuator was supported by a 102 mm hydraulic cylinder such that the weight of the hydraulic actuator was not applied to the wall. Force and displacement data were recorded on a computer using the LabView 8.6i program.

Monotonic Testing

Testing was based on the ASTM E 564-06 (ASCE, 2006) standard shear wall static load test. All monotonic tests were stopped at 4.0, 8.0, 12.0, 16.0, 20.0, 24.4, 48.8 and 73.2 mm for failure maps of the walls to be created. The 24.4, 48.8 and 73.2 mm stops were consistent with 1%, 2% and 3% drift of the wall height. These tests were performed at two different loading rates. For all loading between 0 and 24.4 mm, the loading rate was 4.0 mm/min. For all loading between 24.4 mm to failure, a

loading rate of 10.0 mm/min was used. This resulted in wall testing taking about two hours per wall test.

Visual Failure Comparison

At each stop in the monotonic test, a visual failure map of the wall was constructed. A detailed screw pattern was drawn and numbered on each GWB panel so that all walls with the same design had the same screw attachment and the exact location of each connection failure could be recorded. While visually based, these criteria allowed for an objective analysis of screw connection failure. For each failure map, the number of screw connections failed, the failure mode of each connection, and the locations of the failed connections were recorded.

Instrumentation

Preliminary testing indicated that increased relative displacement between GWB and the wood studs increased damage to the GWB. As a result, an instrumentation setup was devised to measure the relative displacement between the wood studs and the GWB panels in the shear walls. When the shear walls were loaded, the wood frame deformed differently than the GWB. This resulted in a relative displacement between the GWB and the wood frame. This relative displacement increased as displacement was applied along with the damage to the GWB. This method was used to compare wall performance and support the results of the visual failure comparison. It was believed that fewer screw connection failures at certain

global displacements would have lower relative displacements at those global displacements.

To determine the relative movement of the GWB panels, spring return linear position (displacement) sensors were used. These displacement sensors were manufactured by BEI Duncan Electronics ®. The displacement sensors were super glued to 69.0 x 12.7 x 1.59 mm aluminum sensor arms. These arms were loosely attached to the aluminum panel using 440 thread countersunk nuts and bolts which were free to rotate about the pivot bolt. This panel was rigidly attached to the surface of the GWB using a Devcon ® High Strength Five Minute Epoxy. Sensors were attached in sets of two perpendicular to each other and contained a loop attachment at one end of each sensor. Each loop attachment was a 19 mm long piece of 1.59 mm diameter welding rod. One end was bent into a loop such that an 8d nail could be placed through it, and the other end was rigidly attached to the displacement sensor plastic slug using the five minute epoxy.

A hole was drilled through the GWB, and also the OSB for 2OSB and 2OSBWIN designs, and a nail placed through both loop attachments for each set of sensors and into the wood frame. This allowed the displacement sensors to extend or contract when the GWB panel moved relative to the wood frame. Because these sensors were setup perpendicular to each other, they could measure vertical and horizontal motions.

Due to laboratory constraints, only two such panels could be developed and instrumented. These panels were attached in four locations as in Figure 9. These four locations were the lower end stud, upper end stud, lower middle stud and upper middle stud. The data from panel attachments at all four locations were acquired by having the panels attached at two of the locations in one test, and the other two in another test of an identical wall design. Tests in which the panels were attached to the end (uplift) stud were indicated by a '-E' at the end of the test name. Tests in which the panels were attached to the middle stud were indicated by a '-M' at the end of the test name.

Each panel contained two sets of two sensors as shown in Figure 9. These sensors were named by number and in which setup each sensor was used. Sensors labeled 'E' were used in the end setup and represent motion near the end stud. Sensors labeled 'M' were used in the middle stud and represent motion near the middle stud. Each set of two sensors was also named by the location at which they are attached to on the wood frame. Sets of sensors attached to the horizontal top or bottom plate were labeled as such as well as those attached to the middle or end vertical studs. These sets of sensors represent the horizontal and vertical relative displacement between the wood frame and the GWB at the locations indicated in Figure 9.

Test Matrix

A total of 14 walls were tested to failure in this study as shown in Table 2. Seven shear wall designs were implemented with two walls built per wall design. Each wall design had one wall where the instrumentation panels were attached to the GWB

near the end stud, and one wall where the instrumentation panel was attached to the GWB near the middle stud. Six of these walls had window openings, and eight did not. Two additional preliminary wall tests were performed on IRC design walls. The results from these walls were not included in this study as they were tested to verify the test system, instrumentation and visual failure modes.

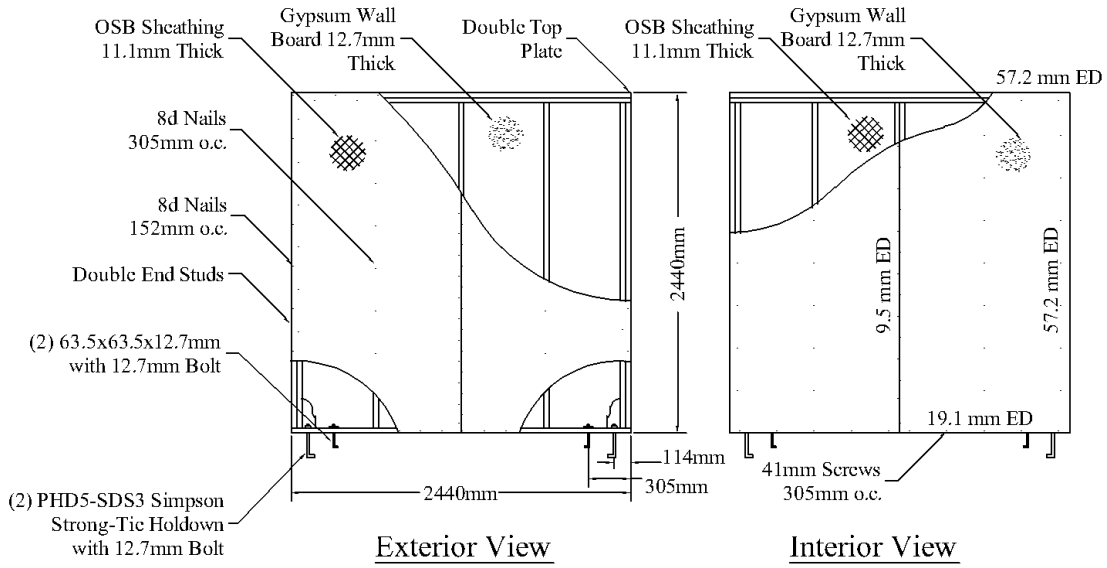

Figure 1. IRC Shear Wall Design

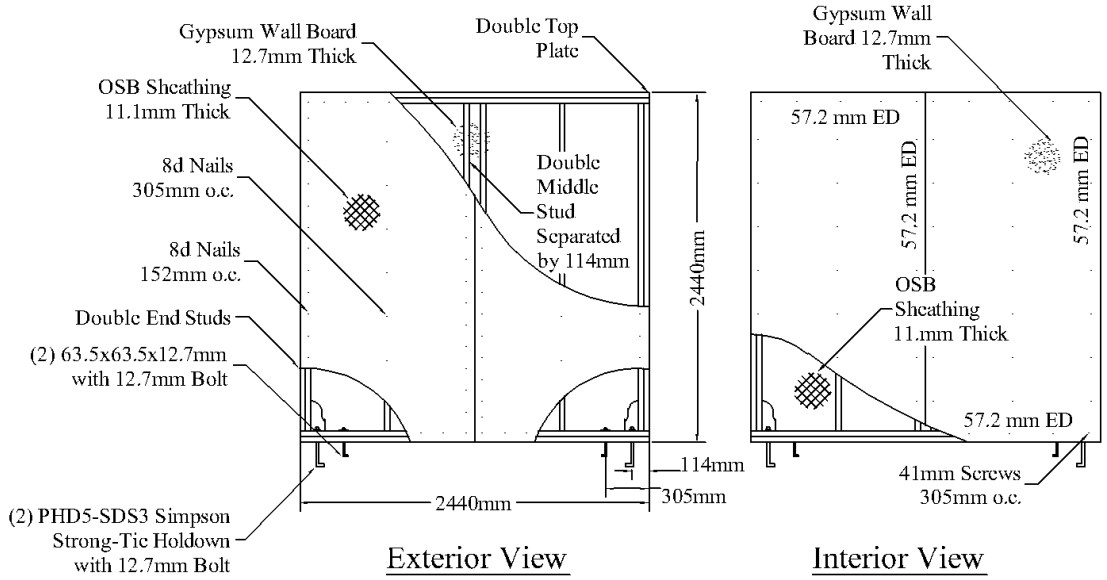

Figure 2. SEPSTUD Shear Wall Design

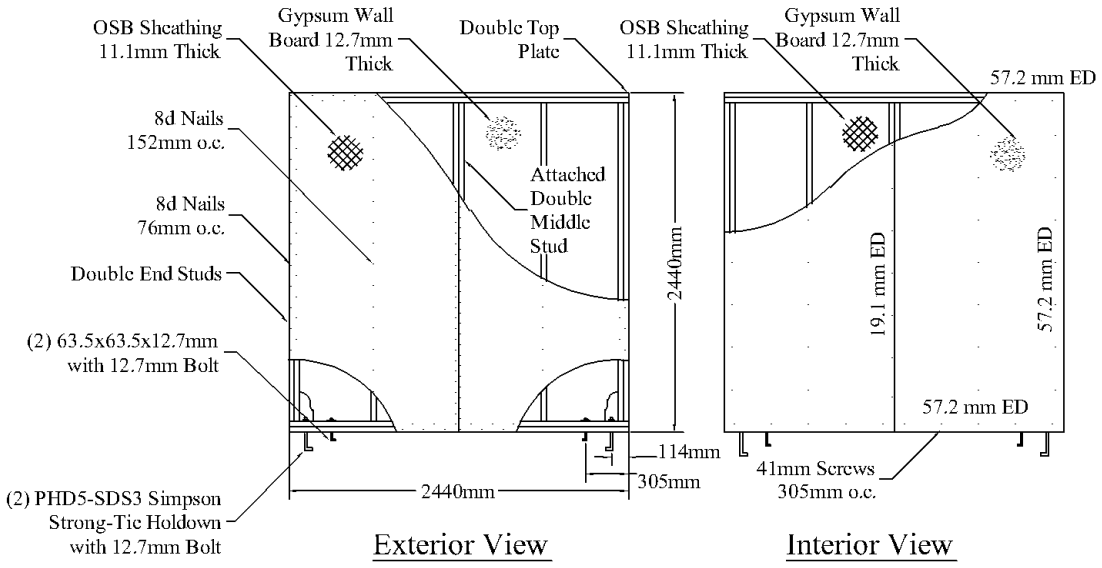

Figure 3. 3INNAIL Shear Wall Design

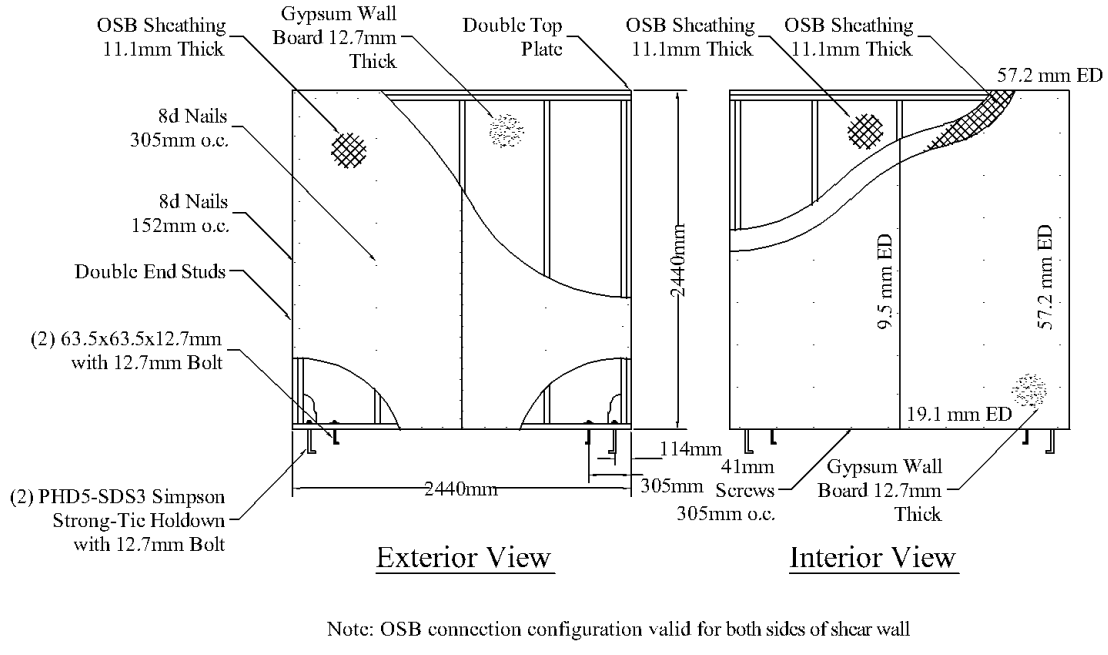

Note: OSB connection configuration valid for both sides of shear wall

Figure 4. 2OSB Shear Wall Design

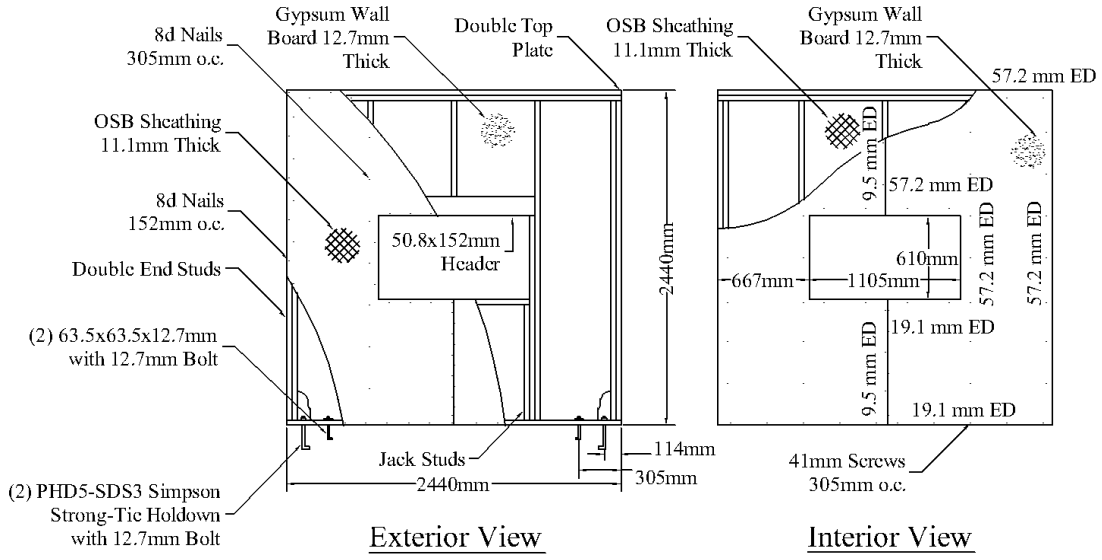

Figure 5. IRCWIN Shear Wall Design

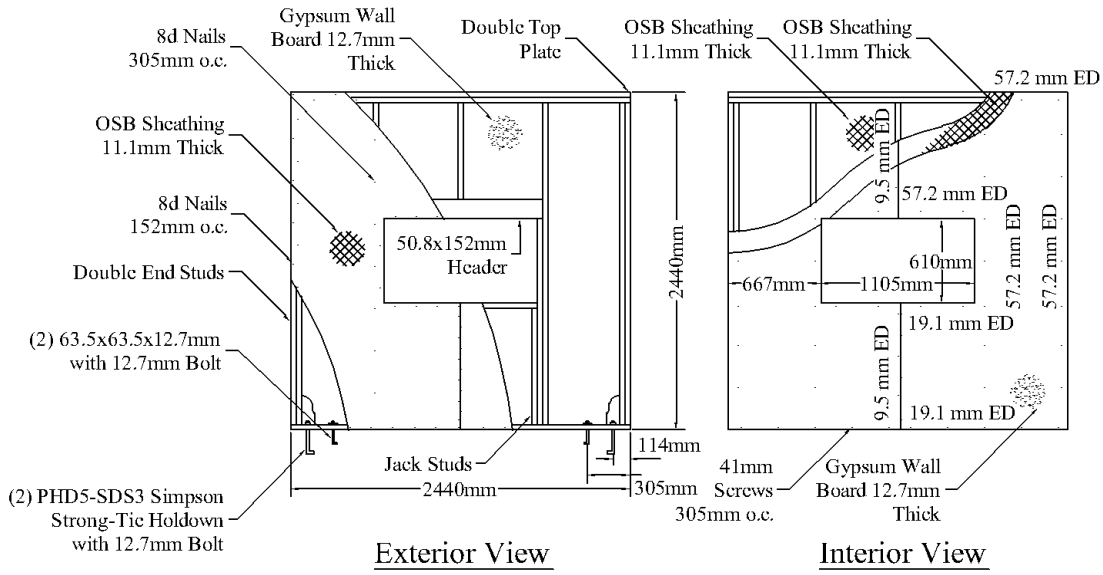

Note: OSB connection configuration valid for both sides of shear wall

Figure 6. 2OSBWIN Shear Wall Design

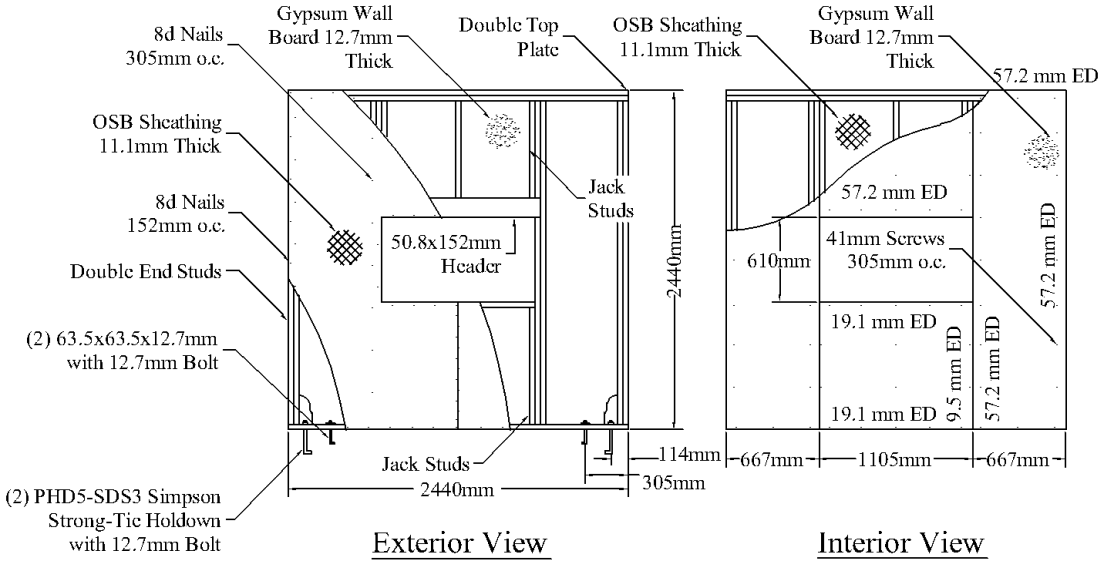

Figure 7. 4PNLWIN Shear Wall Design

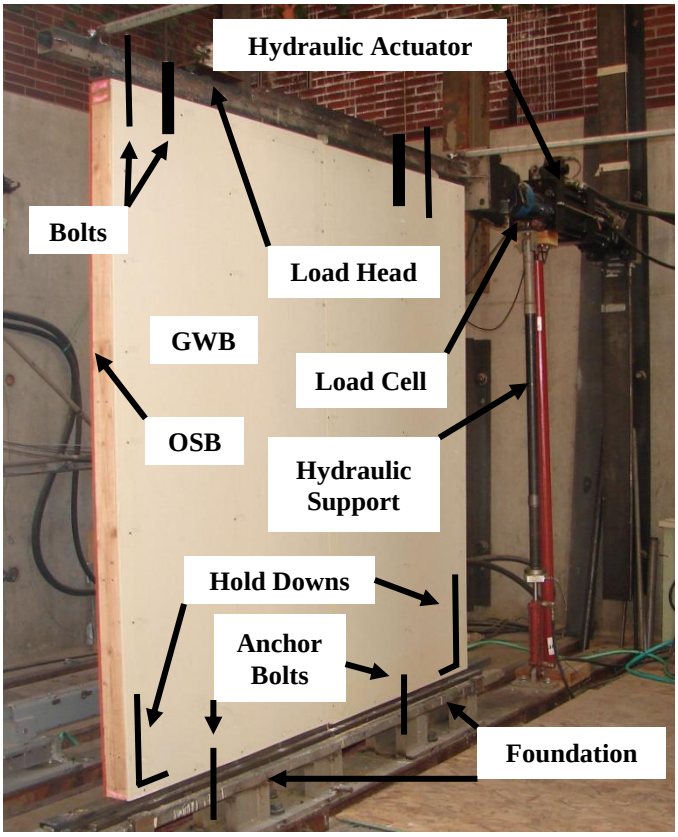

Figure 8. Shear Wall Test Setup

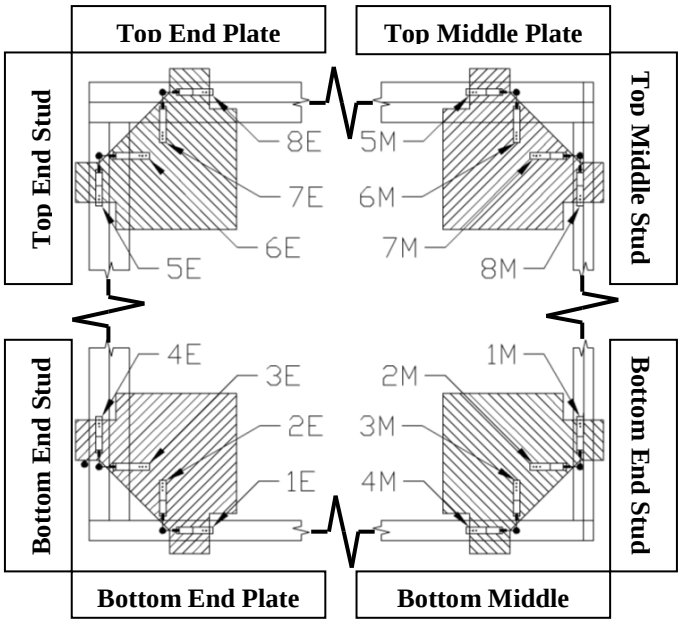

Figure 9. Schematic of Displacement Sensor Locations

Table 2. Test Matrix

Test Name	Shear Wall Design	Instrumentation Setup	Window Opening	Wall Design Description
IRC-E	IRC	End Stud	No	152 mm edge and 305 mm field nailing. IRC minimum requirements.
IRC-M		Middle Stud	No	
SEPSTUD-E	SEPSTUD	End Stud	No	152 mm edge and 305 mm field nailing. Additional separated middle stud and bottom plate.
SEPSTUD-M		Middle Stud	No	
3INNAIL-E	3INNAIL	End Stud	No	76.2 mm edge and 152 mm field nailing. Additional attached middle stud and bottom plate.
3INNAIL-M		Middle Stud	No	
2OSB-E	2OSB	End Stud	No	152 mm edge and 305 mm field nailing. OSB applied to both sides of wood frame.
2OSB-M		Middle Stud	No	
IRCWIN-E	IRCWIN	End Stud	Yes	152 mm edge and 305 mm field nailing. IRC minimum requirements.
IRCWIN-M		Middle Stud	Yes	
2OSBWIN-E	2OSBWIN	End Stud	Yes	152 mm edge and 305 mm field nailing. OSB applied to both sides of wood frame.
2OSBWIN-M		Middle Stud	Yes	
4PNLWIN-E	4PNLWIN	End Stud	Yes	152 mm edge and 305 mm field nailing. GWB panel seams are at window opening corners.
4PNLWIN-M		Middle Stud	Yes	

RESULTS AND DISCUSSION

Preliminary Testing

The following failure modes of the GWB were observed through preliminary connection testing:

1) Tearing or cracking of the GWB near or around a screw connection (Figure 10a).
2) Pull-through of the screw into the back of the GWB by at least 2 mm (Figure 10b).
3) Local crushing of the GWB indicated by a visible bubble around the screw connection (Figure 10c).

The strength and displacement at maximum load of the GWB screw connections depended on edge distance. The average connection strength was similar for 19.1 and 57.2 mm edge distances, but about 29% lower for the 9.5 mm edge distance compared to the other edge distances. The displacement at maximum load for the 57.2 mm edge distance was 24% and 192% greater than those observed in the 19.1 and 57.2 mm edge distances, respectively. The 57.2 mm edge distance was utilized in the SEPSTUD design because of this increased strength and displacement at maximum load. Noticeable visual failures were observed to occur abruptly, not gradually as relative displacement increased. This occurred at about 3 mm of displacement which was taken as the visual failure limit.

The flexural strengths of all GWB panels were found to be 23% and 71% higher than the ASTM C1396 required flexural strength in the perpendicular and parallel directions, respectively (ASTM, 2006). If the flexural strength of other GWB panels is much different than what was found in this study, the results of this study may not apply to those GWB panels. The resultant Coefficient of Variation (COV) found for the perpendicular and parallel directions were 4% and 15%. This variation was determined acceptable for this study such that the results determined from the connection tests performed on one GWB panel could be applied to the entire GWB shipment used in the shear wall tests. Details and additional discussion of preliminary testing and results are shown in Appendix B.

Shear Wall Behavior

Table 3 describes the maximum load and stiffness of the shear walls tested. The stiffness of all shear walls was calculated by dividing 80% of maximum load by the global displacement observed at that load. This method was used in CUREE W13 (Uang and Gatto, 2003). ASTM E564 (ASTM, 2006) mentions using 33% of maximum load, which results in a much higher stiffness (by a factor of two), but allows the researcher to use other reference load levels to determine the stiffness. Using a lower load level, such as 33% of maximum load, results in an initial stiffness which is more representative of the testing procedure and setup than actual wall behavior. Additionally, using 80% maximum load method was shown to predict cyclic

performance from monotonic tests (Uang and Gatto, 2003), which is of interest in the application of the results of this study to dynamic earthquake loading.

Shear wall designs 2OSB, 3INNAIL and 2OSBWIN all exhibited the greatest strengths with similar maximum loads. This similarity can be attributed to the same number of fasteners used to connect the OSB to the wood frame in all of these designs, which resulted in a stronger connection. Much lower average maximum loads were observed in the IRC, SEPSTUD, IRCWIN and 4PNLWIN designs due to fewer fasteners used to connect the OSB to the wood frame resulting in a weaker OSB connection. Little change in strength was observed between the IRC to IRCWIN design and the 2OSB to 2OSBWIN design, contrary to what was predicted by current design codes. The National Design Specification (NDS) predicted a 55% reduction in strength (AFPA, 2005), but almost no change was observed. The calculation of the allowable strength of these walls is shown in Appendix L.

Much like maximum load performance, shear wall designs 2OSB, 3INNAIL and 2OSBWIN exhibited the greatest stiffnesses, while the IRC, SEPSTUD, IRCWIN and 4PNLWIN designs exhibited lower stiffnesses. The 2OSB, 3INNAIL and 2OSBWIN designs all had greater stiffnesses than other designs due to the greater number of fasteners used to connect the OSB to the wood frame. Because the 4PNLWIN design had four GWB panels attached instead of two, the GWB panels were free to rotate resulting in the lowest stiffness of all designs.

Variation in mechanical properties was high in this study for the more unconventional SEPSTUD and 4PNLWIN designs due to their sensitivity to construction changes. For the other wall designs, the variation in mechanical properties was within acceptable values for ASTM E564 (ASTM 2006). A further discussion of this variation is included in Appendix K.

Shear Wall Drift Levels and Performance

Figure 11 shows the 1%, 2% and 3% drift criteria using ASCE/SEI 41-06 (ASCE, 2006), the allowable strength using the NDS (AFPA, 2005) and the 2% drift limit using ASCE 7-05 (ASCE, 2005) for the IRC-E shear wall specimen. As can be seen, the displacement observed at the allowable strength as determined by the NDS falls well below any of the drift criteria.

Most buildings in the United States are built to a life safety design level using ASCE 7-05 (ASCE, 2005) which sets a 2% drift limit on most wood frame structures. This is consistent with the ASCE/SEI 41-06 (ASCE, 2006) life safety structural performance level. According to the ASCE/SEI 41-06 life safety structural performance level, "…a structure has damaged components but retains a margin against onset of partial or total collapse…" In wood stud walls this occurs at 2% transient drift and relates to "moderate loosening of connections and minor splitting of members". Figure 12a shows the observed shear wall minor member splitting and connection loosening at 2% drift which is consistent with the ASCE 41-06 life safety performance level description.

Table 4 indicates the average percentage of maximum load observed in all shear wall designs at 1%, 2% and 3% drift. The ASCE 41-06 required margin against collapse at 2% drift for the IRC, SEPSTUD and IRCWIN was very small. This small margin against collapse was indicated by the walls being loaded to 94% - 97% of their full capacity and calls into question whether these walls meet life safety performance levels. Other wall designs were loaded below 88% of their full capacity, which represented a slightly larger margin against collapse.

Besides life safety, the other performance levels defined in ASCE/SEI 41-06 are immediate occupancy and collapse prevention. Immediate occupancy occurs at 1% transient drift in wood frame buildings and is defined as "…the postearthquake damage state in which a structure remains safe to occupy, essentially retains its pre-earthquake design strength and stiffness…" (ASCE, 2006). In wood frame structures this level is associated with "…minor hairline cracking of the gypsum…" (ASCE, 2006). The hairline GWB cracking observed in shear wall tests is shown in Figure 12b and is consistent with the ASCE 41-06 immediate occupancy performance level description. Additional observations at 1% drift include walls being loaded from 57% to 80% of their total capacity.

The collapse prevention performance level is associated with 3% transient drift in wood frame buildings and is defined as "…the postearthquake damage state in which a structure has damaged components and continues to support gravity loads, but retains no margin against collapse…" (ASCE, 2006). This is characterized by

"…Connections loose. Nails partially withdrawn. Some splitting of members…" (ASCE, 2006). Instead of the withdrawal of nails described in ASCE 41-06, nail pull through was a much more common failure in OSB sheathing. The observed nail pull through and the loose connections of shear walls at 3% drift are shown in Figure 12c, the loose connections are consistent with the ASCE 41-06 collapse prevention performance level. The lack of a margin against collapse at this drift level is evident in Table 4 as all walls were loaded from 97% to 100% of their full capacity.

ASCE/SEI 41-06 drift criteria generally agreed with observed behavior. The possible exceptions to this were the small margins against collapse observed in the IRC, SEPSTUD and IRCWIN designs.

Shear Wall Visual Failure Comparison

Shear wall loading was stopped at ten different displacements, including 1%, 2% and 3% drifts, where visual failure maps were created. A percentage of the global connection failures were computed at each displacement stop for each wall. This percent global connection failure was the number of failed fastener connections divided by the total number of fasteners used to connect the GWB panels to the wood frame for a particular wall design.

This percentage was used instead of the number of connections failed because not all shear wall designs had the same number of fasteners used to connect the GWB to the wood frame. The few initial connection failures caused by overdriving the fasteners or placing fasteners too close to the edge of the GWB were removed from

this analysis by subtracting them from subsequent failures at greater displacements. Because two identical specimens were tested from every wall design, the average global connection failure percentage of the two is presented in the following sections. A discussion on the variation between identical wall specimens is included in Appendix K.

Shear Wall Comparison at Drift Criteria

A visual connection failure comparison between shear walls is shown in Figure 13. At 1% drift, all innovative shear wall designs outperformed the control designs. The SEPSTUD and 4PNLWIN designs performed moderately better than the IRC and IRCWIN designs, but the 3INNAIL, 2OSB and 2OSBWIN designs exhibited the best GWB performance.

At 2% drift the SEPSTUD and 4PNLWIN design performed worse than the IRC and IRCWIN designs, while the 3INNAIL design performed only slightly better. The 2OSB and 2OSBWIN designs exhibited superior GWB performance with only an 11% and 7% global connection failure, respectively. The IRC and IRCWIN designs exhibited a 62% and 65% global connection failure, respectively. These large global connection failures in the IRC and IRCWIN designs are consistent with the large economic loss observed in previous test results of GWB partition walls (McMullin and Merrick, 2002) which identified a total economic loss of the GWB at 2% drift.

Similar trends were shown at 3% drift with the 4PNLWIN and SEPSTUD designs exhibiting similar performance to the IRC and IRCWIN designs. The

3INNAIL design performed only slightly better than the IRC design at 3% drift. However, the 2OSB and 2OSBWIN designs exhibited superior GWB performance even at 3% drift. While all innovative designs performed better at 1% drift, the 3INNAIL, 2OSB and 2OSBWIN designs performed better at all drifts, with the 2OSB and 2OSBWIN designs exhibiting superior overall performance.

In all wall designs besides the 2OSB and 2OSBWIN designs, a minimum of 51% global connection failure was observed at 2% drift. This implies that walls loaded to 2% drift, or the maximum ASCE 7-05 allowable displacement (ASCE, 2005), in a seismic event will sustain substantial damage to the GWB. This amount of damage is consistent with what was observed in the aftermath of the Northridge Earthquake (Seible et al., 1999).

The 3INNAIL, 2OSB and 2OSBWIN designs all had the highest strengths and exhibited the best GWB performance. As expected, increasing the strength and stiffness of a shear wall made it more resistant to damage in the GWB. Increasing the stiffness of a wood frame structure will either reduce or not affect the seismic load applied to it from a design response spectrum. This is because an increase in stiffness would lead to a decrease in natural period, which would either reduce or not affect the spectral response acceleration applied to it from a design response spectrum. The less spectral response acceleration applied to a structure, the less seismic load would be applied to the structure and the less it would be damaged. This higher stiffness of the

3INNAIL, 2OSB and 2OSBWIN designs could lead to even less damage in the GWB caused by seismic loading from a design response spectrum than shown in this study.

The 3INNAIL, 2OSB and 2OSBWIN designs exhibited good GWB performance, but the 2OSB and 2OSBWIN designs exhibited the best GWB performance. This better performance was observed at 2% and 3% drifts, and occurred even with comparable strength and stiffness values between all three wall designs. This implied that an additional factor caused the superior performance of the 2OSB and 2OSBWIN designs.

The 2OSB and 2OSBWIN designs performed so well due to similar stiffness of both sides of the shear wall. In all other walls, the stiffer GWB on one side of the wall attracted more load until the GWB began to transfer load to the OSB (Sinha, 2007). If OSB was applied to both sides of the frame, and GWB attached to the OSB, both sides of the frame would have similar stiffness. This similar stiffness allowed the OSB on both sides of the frame to share load equally and apply less load to the GWB. With less load applied to the GWB, less damage would occur to the GWB.

The 3INNAIL wall was designed to employ this same strategy to increase GWB performance. The stiffness of the OSB side of the wall was increased by decreasing the nail spacing, theoretically making both sides of the wall closer in stiffness. However, load was still transferred to the GWB resulting in the damage evident in the 3INNAIL design. It may be possible to design an OSB connection with

the same stiffness as the GWB connection, but this would require further testing of the stiffness of these types of connections.

Strengthening the GWB and wood frame connection by increasing the GWB edge distance in the SEPSTUD design only improved GWB performance up to 1% drift. This altered GWB connection behaved like the IRC wall at 2% and 3% drift. This behavior implies that this stronger 57.2 mm edge distance connection failed somewhere between 1% and 2% drift, or failure began in another element of the shear wall. In the case of the SEPSTUD wall design, this failure was observed in the uplift of the top plate due to the lack of attachment between the middle studs as described in Appendix H.

The 4PNLWIN design was built to withstand the expected cracking around the corners of the window openings as seen in previous studies (McMullin and Merrick, 2002). However, cracking around the window openings only occurred in a few walls and only at displacements beyond 3% drift. Regardless, the 4PNLWIN design exhibited better GWB performance compared to the IRCWIN design at displacements up to 1% drift as shown in Figure 13.

The decrease in stiffness on the GWB side of the wall was the reason for the improved performance of the 4PNLWIN design. This is evident from the 28% decrease in stiffness between the 4PNLWIN design and the IRCWIN design as shown in Table 3. The 4PNLWIN design exhibited decreased stiffness because the GWB was applied as four smaller panels that rotated independently, instead of two larger panels.

This decrease in stiffness of the GWB side allowed for a similar stiffness on both sides of the wall, and more equal load sharing between the GWB and the OSB, resulting in less load and damage applied to the GWB. However, this behavior was only true to 1% drift. Observations at 2% and 3% drift indicated the GWB panels began to rack, increasing the stiffness of the GWB side of the wall. This increase in stiffness caused unequal load sharing between the GWB and the OSB and increased the damage to the GWB resulting in poor performance of 4PNLWIN after 1% drift.

Shear Wall Comparison at Allowable Strength

The GWB damage observed at the allowable strength of shear walls was much less than the damage observed in shear walls at 1% and 2% drift. As shown in Figure 11, the displacement at which the allowable strength was reached falls well below the ASCE 7-05 (ASCE, 2005) drift limits or ASCE/SEI 41-06 (ASCE, 2006) drift criteria. Table 5 shows the NDS allowable strength (AFPA, 2005) of each shear wall, the average displacements at which each shear wall reached allowable strength and the percent global connection failure observed at allowable strength. Table 5 also shows the displacement stop at which the percent global connection failure was observed for each shear wall allowable strength, as tests were not stopped exactly at the displacement where allowable strength was reached.

All shear walls reached allowable strength between displacements of 1.4 and 9.7 mm. At these low displacements, very little damage to the GWB was observed. For the IRC and SEPSTUD designs, an average of 2% global connection failure was

observed at allowable strength while 1% was observed in 3INNAIL and 2OSB designs. No connection failure was observed in any design with window openings at allowable strength. This observation agrees with the result that all walls with window openings exhibited higher maximum loads than predicted by NDS allowable strengths. A lower NDS allowable strength would occur at a lower displacement, and result in lower GWB damage.

In the Northridge Earthquake, damage to the GWB was the most frequent and expensive repair for single family dwellings, costing an average of $7,989 in the 1230 households surveyed (Schierle, 2003). This level of GWB damage is much greater than the few failed fasteners observed at allowable strength in the shear wall tests of this study. This implies that shear walls in the Northridge Earthquake experienced much higher loads than shear wall allowable strengths. The amount of damage seen from the Northridge Earthquake (Schierle, 2003) was more consistent with damage observed in shear walls loaded beyond 1% drift in this study.

Shear Wall Relative Displacement Comparison

Qualitative Relative Displacement Comparison

Figure 14 shows a classical linear elastic model of structural sheathing rotation and wood frame deflection as described in CUREE W-30 (Cobeen et al., 2004) and by others (Foltz and Filiatrault, 2001). In this model, the wood frame deformed into a parallelogram and the panels rotate about the centroid of the fasteners. This centroid of the fasteners was equivalent to the centroid of the panel if fasteners are placed

symmetrically around the panel. This model of structural sheathing can be applied to the rotation of the GWB panels as well. The classical model implies a relative displacement between the GWB panels and the wood frame shown by the arrows in Figure 14. This relative displacement was observed at failure as shown by the test photos in Figure 15. A qualitative comparison of the directions of the relative displacements in these photos is consistent with those in the classical model.

Relative displacement occurred because the GWB panels displaced differently than the wood frame. The GWB panels would rotate more than the wood frame would deform in some locations, and less in others. In Figures 15a and 15b the top plate of the wood frame was pulled more than the GWB panels rotated, resulting in relative displacement in the direction opposite the imposed displacement. In Figures 15c and 15d, the GWB panels rotated more than fixed bottom plate, resulting relative displacement in the direction of the imposed displacement.

The relative displacement of the GWB to the wood frame was quantified by the measurements made by the displacement sensors. Each set of displacement sensors was set up perpendicular to each other and attached to a single nail driven into the wood frame. These sets of displacement sensors are labeled in Figure 9. The sensor outputs from these perpendicular displacement sensors could be resolved into a displacement vector by taking the sum of the squares to find the magnitude, and trigonometry to find the angle from the horizontal. This displacement combination method has been used in analytical models to determine the relative displacement of a

generic fastener (Folz and Filiatrault, 2001). The eight vectors that described displacement of the GWB relative to the wood frame were the top and bottom middle stud, top and bottom end stud, top and bottom middle plate and top and bottom end stud vectors.

The displacement vectors of the IRC design shear wall at 1% drift are shown in Figure 16. The displacement vectors for all walls and associated discussion are given in Appendix G. 1% drift was chosen because it was the highest level of displacement that the sensors could be displaced to where a visual failure map was recorded. The angle of these vectors did change much over the global displacement as is shown in Appendix G. The displacement vectors in Figure 16 are shown at their true angles and scaled 100 times their length. The directions of the relative displacement vectors are consistent with those predicted by the classical GWB rotation model in Figure 14 and with those observed qualitatively in Figure 15. This is especially true for the IRC, 2OSB, IRCWIN and 2OSBWIN designs. These designs had wood frames and sheathing attachments most like those used in the classical model.

For the SEPSTUD and 3INNAIL designs, the double middle stud created a different load path which resulted in different displacement vectors from all other wall designs. Due to sheathing shear transfer, the middle stud closest to the actuator would uplift causing the top plate to uplift, as observed in the SEPSTUD and 3INNAIL designs. This behavior was recorded by a larger top middle plate displacement vector in the SEPSTUD and 3INNAIL designs compared to other designs.

For the 4PNLWIN design, the GWB attachment around the window openings resulted in other differences in displacement vectors. Because the sensors on the middle stud were applied near the middle of the GWB panel, they were much lower in magnitude compared to other wall designs, and the direction was nearly horizontal. Additional information about how the measured relative displacement vectors related to changes in shear wall design is discussed in Appendix H.

Displacement Vector Magnitude Comparison

In the preliminary GWB connection testing, it was observed that visual failures occurred abruptly, not gradually, with relative displacement. The average displacement at which visual failures were observed in preliminary testing was 3 mm. This was taken as the average visual failure limit, or the relative displacement at which visual failure criteria was met. Preliminary GWB flexural testing indicated that the variation in flexural strength of all panels in the shipment was sufficient to apply this visual failure limit observed on one GWB panel to all GWB panels tested on walls. This deduction assumed that variation in flexural strength of the GWB panels would influence the visual failure limit of those panels.

Because this failure limit was discrete, it was expected that shear walls with the greatest amount of relative displacement above the visual failure limit should have the greatest amount of visual failure. The amount of relative displacement above the visual failure limit could be measured by the number of relative displacement vectors or the magnitude of certain vectors above the visual failure limit. The cause of visual

failure was determined by the number of and magnitudes of certain vectors, not the averages of all vectors.

The magnitudes of the displacement vectors for shear walls without openings at 1% drift are shown in Figure 17. The 40% global connection failure observed in the IRC wall at 1% drift, shown in Figure 13, is consistent with the six relative displacement vector magnitudes above the visual failure limit. This implies that much of the GWB panel was displaced above the 3 mm visual failure limit.

The 31% global connection failure observed in the SEPSTUD design at 1% drift, shown in Figure 13, is consistent with two relative displacement vector magnitudes above the visual failure limit. The SEPSTUD design had a 33% larger top middle plate displacement vector magnitude than the 3INNAIL design. This is because of the greater uplift of the top plate due to no connection between the two middle studs in the SEPSTUD design. This top plate vector was the largest recorded relative displacement magnitude and explains the large global connection failure in the SEPSTUD design at 1% drift. Like the 3INNAIL design, visual failures were recorded near the top middle plate and bottom end plate. Only two visual failures were recorded near the middle stud of all the 3INNAIL or SEPSTUD design walls. This is much less than for IRC design walls where nearly all fastener connections on the middle stud were determined to have failed at 1% drift. This implied that in the double middle stud walls the GWB panel stayed mostly attached to the middle stud, while not to the top plate.

The 3INNAIL design exhibited an 8% global connection failure at 1% drift which was concentrated near the top end plate and bottom end plate. This is consistent with vector magnitudes greater than the visual failure limit of the bottom end plate and top middle plate. These vectors are close in magnitude due to the heavy sheathing attachment and attachment of the middle studs which resulted in a greater force transfer.

At 1% drift, the 2OSB design exhibited a 3% global connection failure as shown in Figure 13. The resultant few fastener connection failures are consistent with relative displacement vector magnitudes below the visual failure limit. The bottom end stud vector is very close to this limit with a magnitude of 2.98 mm, but the 2OSB design still exhibited the least amount of relative displacement above the visual failure limit to all other designs.

The magnitudes of the displacement vectors for shear walls with openings at 1% drift are shown in Figure 18. Similar to the IRC design, the IRCWIN design exhibited a 38% average global connection failure at 1% drift as shown in Figure 13. This is consistent with the six displacement vector magnitudes above the visual failure limit. Four of these vectors are the same as for the IRC design.

Both 2OSBWIN and 4PNLWIN designs did not exhibit any relative displacement magnitudes above the visual failure limit. While this is consistent for the 2OSBWIN design in which only a 1% global connection failure was observed, it is not consistent for the 4PNLWIN design in which 17% global connection failure was

observed. Because of the very different GWB panel attachment in the 4PNLWIN design compared to other designs, the relative displacement vector magnitudes may not be comparable to other designs. Additionally, the relative displacement magnitudes observed at the middle stud in the 4PNLWIN design are less than those of other walls because they are measured near the middle of the GWB panel, not the edges. The GWB panel rotates about its center which causes more displacement near the edges of the panel than near the center.

Shear wall designs, except in the 4PNLWIN design, with more relative displacement measurements above the visual failure limit exhibited more visual GWB damage, which validates the visual failure results. However, this type of measurement may not be the optimum way to determine damage to GWB. For example, the SEPSTUD design exhibited much higher visual damage than 3INNAIL even though it exhibited the same number of relative displacement vector magnitudes above the visual failure limit. Perhaps more sensor measurements along the panel edge between studs or at intermediate studs would give a more complete picture of the relative displacements of the GWB panels in all instances, and give a better indication of visual failure behavior.

Shear Wall Value Comparison

Implementation of any type of new construction method is directly related to the cost and value of using that method. The material cost of all shear walls used in this study is shown in Appendix J. A 27% increase in material cost was observed for

the IRC to 2OSB and IRCWIN to 2OSBWIN designs. This increase in cost must be justified by an increase in performance for the 2OSB and 2OSBWIN designs to be implemented as a new construction method.

To investigate how each shear wall performed in relation to its material cost, a shear wall value comparison was performed. The goal of this value comparison was to rank the performance of each shear wall design while considering their material cost and to see which shear wall design demonstrated the most efficient use of materials. The shear wall value index was calculated by dividing the percent global remaining connections at 1% and 2% drift levels by the material cost of the shear wall. 3% drift level was not included because the cost of the GWB would not be an important factor in repairs for a building subjected to 3% drift. The percent global connection failure was calculated from the visual failure results and the percent global remaining fasteners was calculated by 100% - percent global connection failure. The shear wall value index was calculated by the formula:

$$Shear\ Wall\ Value\ Index = \frac{(100\% - \%\ Global\ Connection\ Failure)}{Material\ Cost\ (\$)}$$

This value comparison for all shear wall designs is shown in Figure 19. All innovative shear wall designs exhibited greater value than the control at 1% drift. The design with the greatest value was the 3INNAIL design with the largest shear wall value index compared to the IRC design. This shows that the 3INNAIL design demonstrates the most efficient use of materials at 1% drift. The 2OSB and 2OSBWIN

designs also displayed higher value compared to the IRC or IRCWIN designs at 1% drift.

At 2% drift, the range in shear wall value indexes was much higher. The 2OSB and 2OSBWIN designs exhibited the greatest value with the greatest increases in shear wall value index from the IRC or IRCWIN designs. These results showed that sheathing a shear wall with OSB on both sides resulted in the most efficient use of materials at 2% drift.

While the 3INNAIL design exhibited the greatest value at 1% drift, the 2OSB and 2OSBWIN designs demonstrated a greater value overall. This is because shear walls are generally built to be displaced to the life safety drift (ASCE [2005], ASCE [2006]) of 2%. At this 2% drift, the 2OSB and 2OSBWIN designs both showed superior value above all other shear walls.

This shear wall value index could only be used for comparison purposes. It is difficult to assign an economic value to each connection failure, and the economic losses to shear walls are more likely a step function than a continuous loss (McMullin and Merrick, 2002). Additionally, only the material cost of each shear wall was considered. In construction, the added labor cost for two additional OSB panels on the wood frame was much greater than adding additional nailing or a middle stud. By not including this labor cost, the value comparison favored the 2OSB and 2OSBWIN designs. To determine the additional labor costs, a professional framer would need to be hired to build the walls.

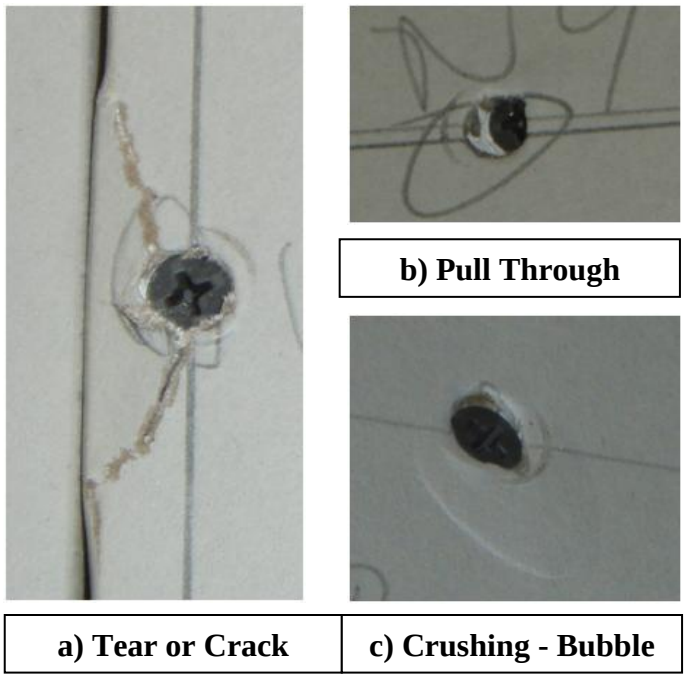

Figure 10. GWB Failure Modes

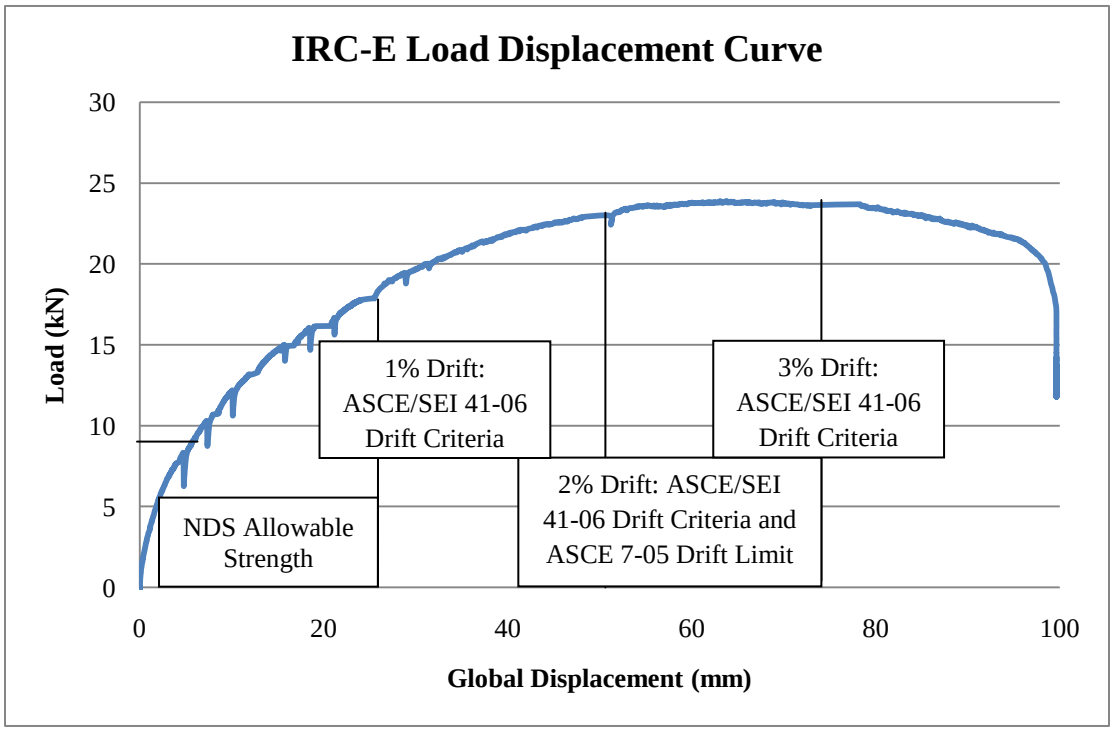

Figure 11. IRC Shear Wall Design Load Displacement Curve

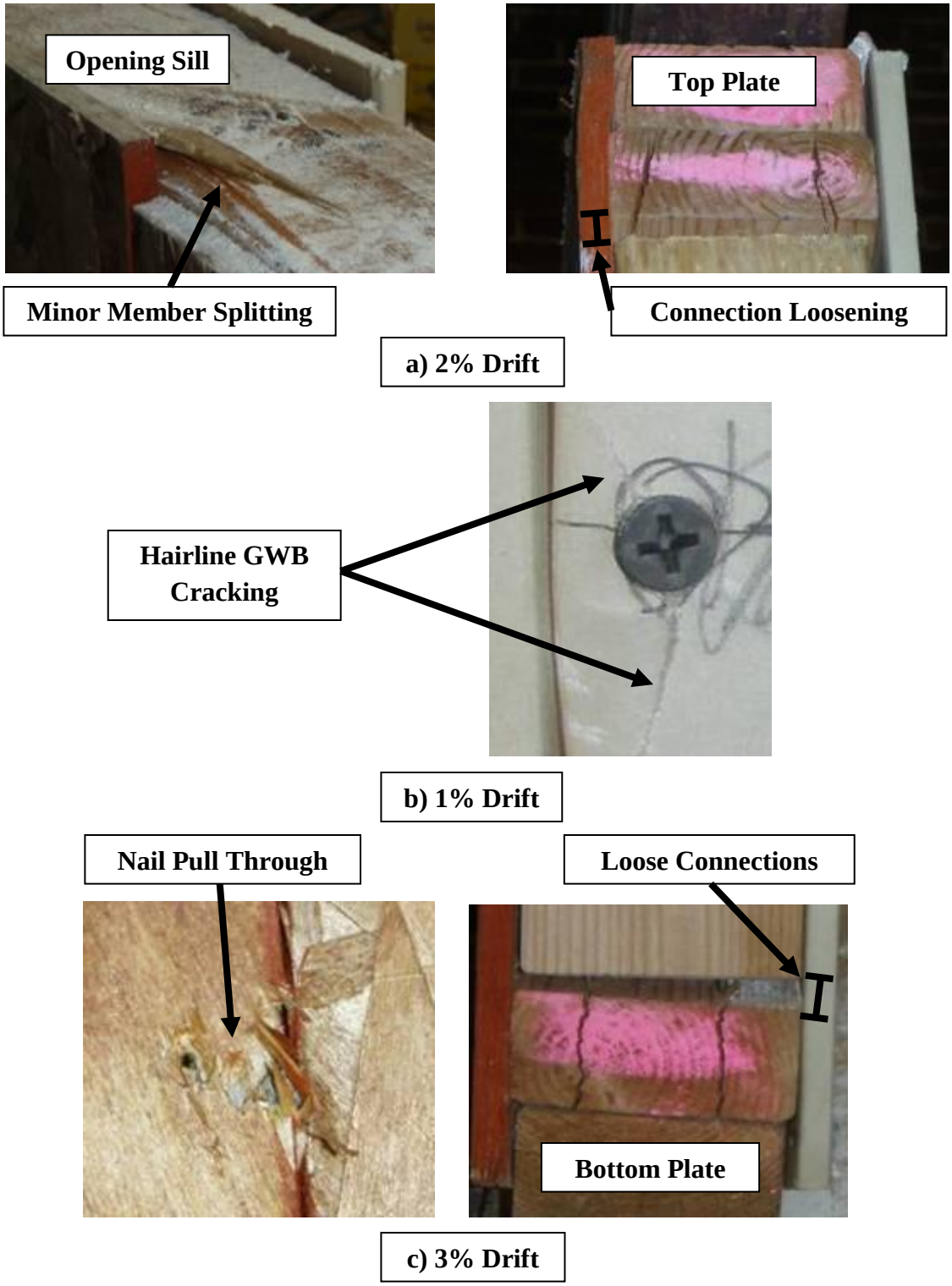

Figure 12. Shear Wall Damage Observations

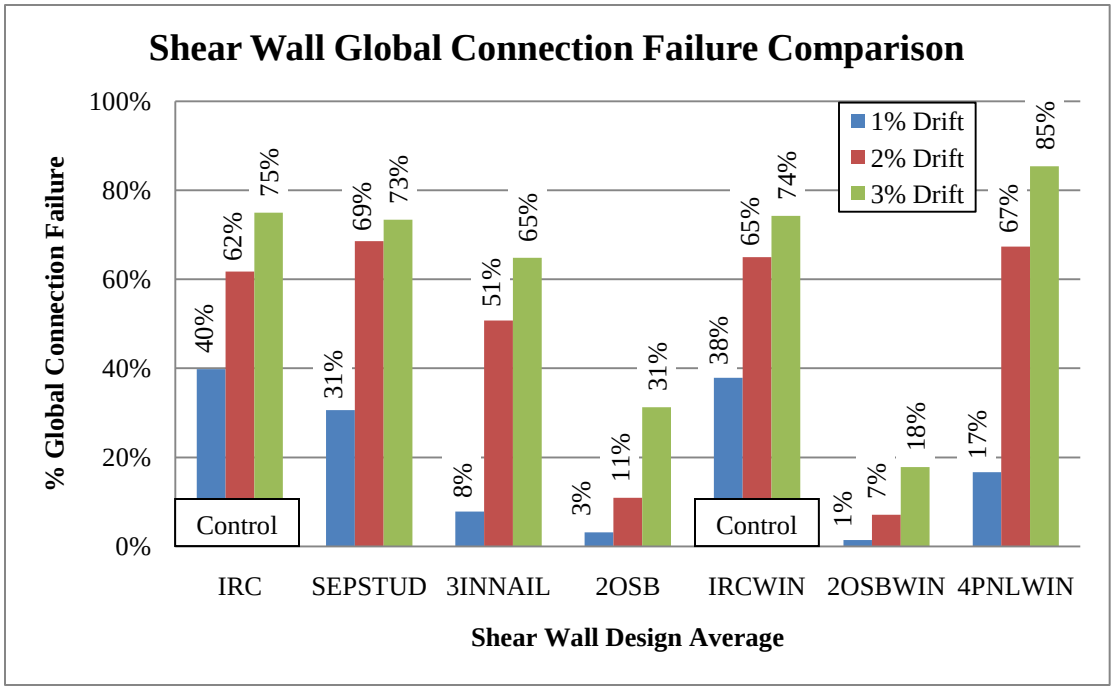

Figure 13. Shear Wall Global Connection Failure Comparison

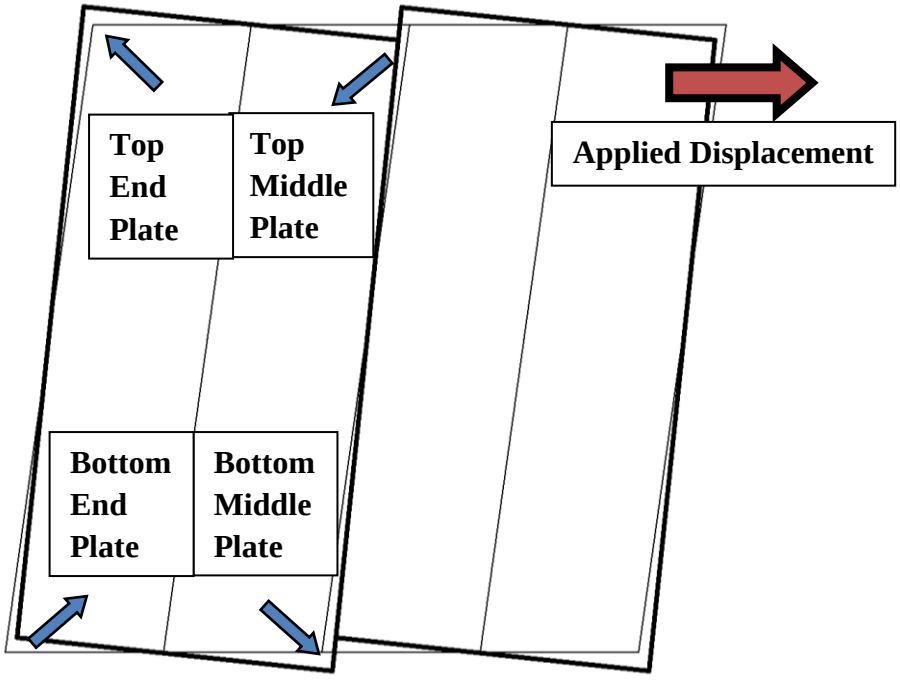

Figure 14. Classical Wood Frame Deformation and GWB Rotation Model

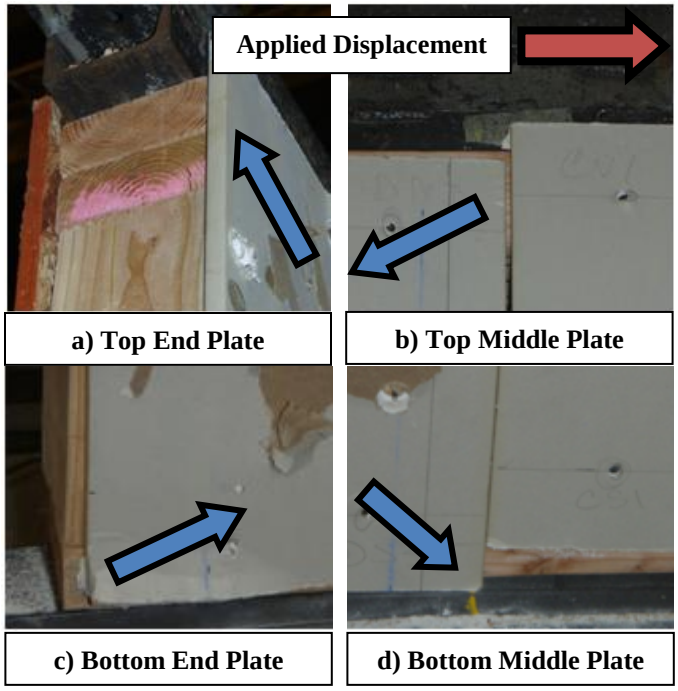

Figure 15. Relative Displacement Photos of Shear Walls at Failure

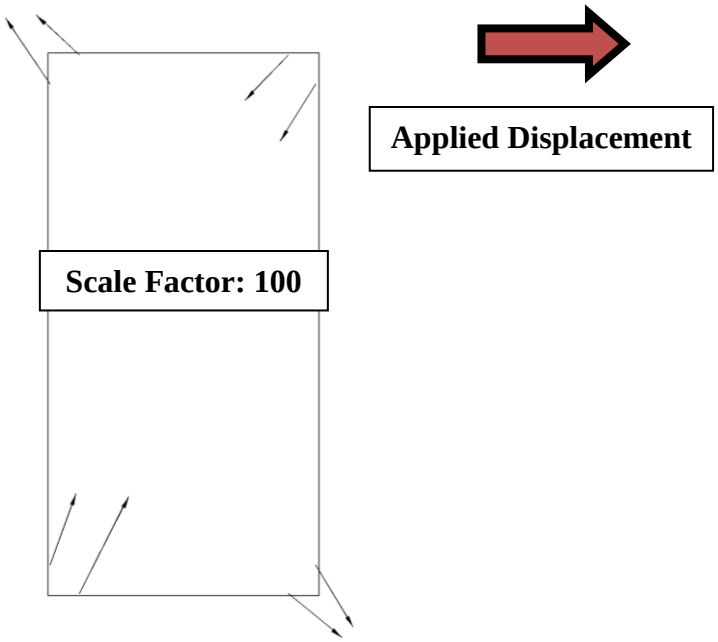

Figure 16. GWB Relative Displacement Vectors at 1% Drift for IRC Design

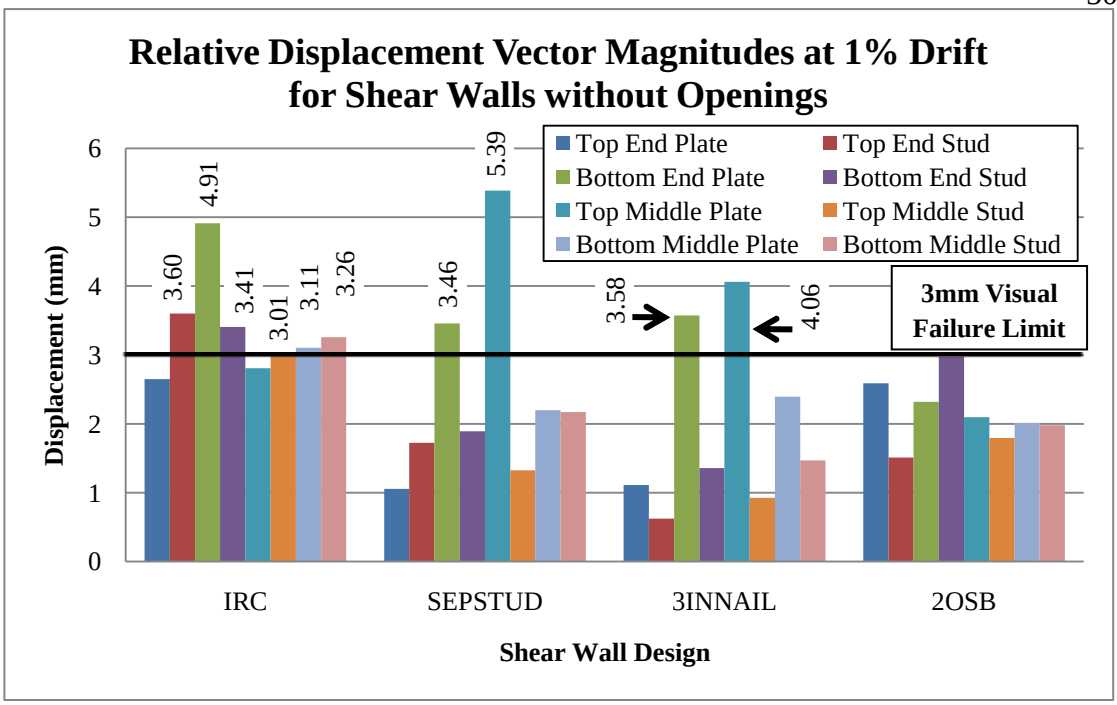

Figure 17. Relative Displacement Vector Comparison for Shear Walls without Openings

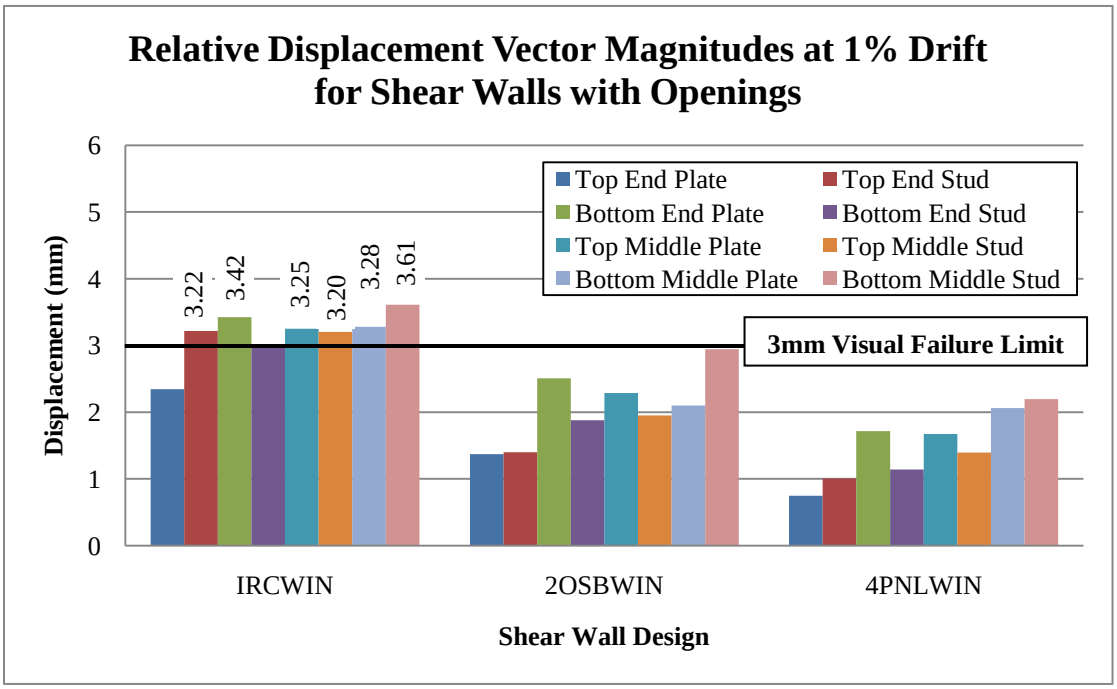

Figure 18. Relative Displacement Vector Comparison for Shear Walls with Openings

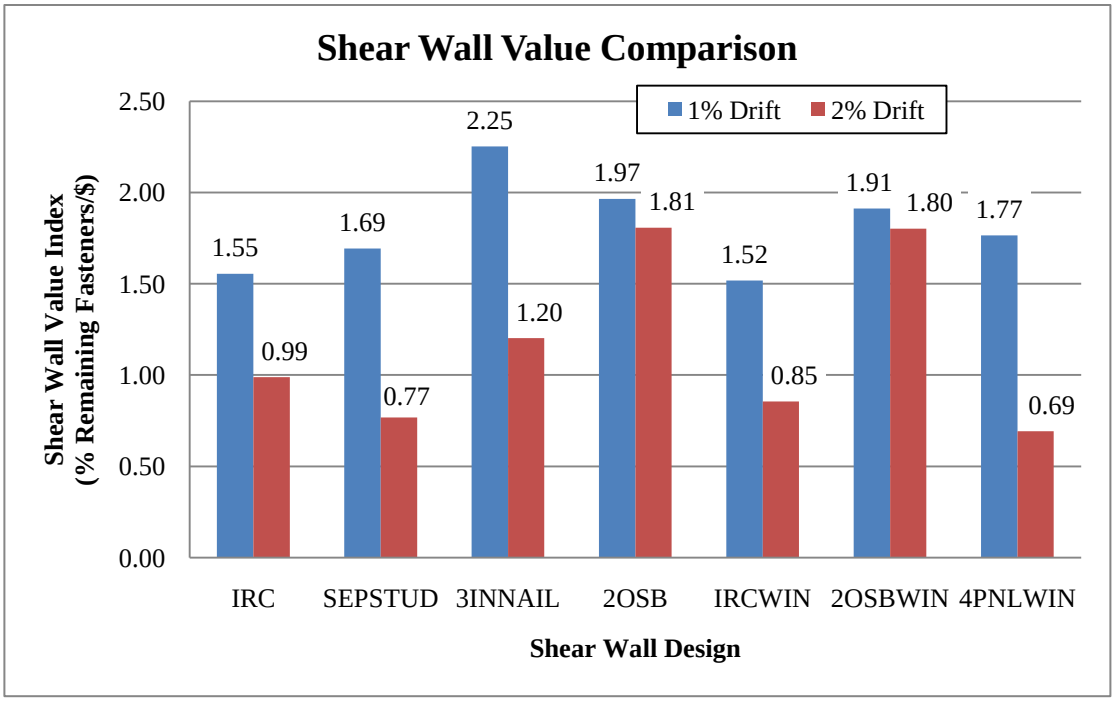

Figure 19. Shear Wall Value Comparison

Table 3. Shear Wall Mechanical Properties

Wall Test	Maximum Load (kN)	Stiffness (kN/mm)
IRC-E	23.9	0.69
IRC-M	24.3	0.61
SEPSTUD-E	22.9	0.52
SEPSTUD-M	23.0	0.70
3INNAIL-E	52.9	0.85
3INNAIL-M	54.0	0.90
2OSB-E	56.2	0.97
2OSB-M	51.7	0.91
IRCWIN-E	22.7	0.71
IRCWIN-M	21.1	0.71
2OSBWIN-E	54.7	0.88
2OSBWIN-M	52.7	0.82
4PNLWIN-E	22.5	0.56
4PNLWIN-M	27.3	0.47

Table 4. Percentage of Maximum Load at ASCE/SEI 41-06 Drift Criteria

Shear Wall Design Average	1% Drift	2% Drift	3% Drift
IRC	73%	94%	100%
SEPSTUD	70%	95%	100%
3INNAIL	57%	88%	99%
2OSB	60%	84%	99%
IRCWIN	80%	97%	99%
2OSBWIN	60%	87%	98%
4PNLWIN	64%	87%	97%

Table 5. Global Connection Failure Observed at Allowable Strength

Shear Wall Design Average	Computed NDS Allowable Strength (kN)	Observed Displacement at Allowable Strength (mm)	Displacement Stop at which Failure was Observed (mm)	% Global Connection Failure
IRC	8.5	5.2	8	2%
SEPSTUD	8.5	8.6	8	2%
3INNAIL	16.0	9.7	12	1%
2OSB	17.1	8.1	8	1%
IRCWIN	4.7	1.4	4	0%
2OSBWIN	9.3	2.6	4	0%
4PNLWIN	4.7	2.5	4	0%

CONCLUSIONS

Conclusions based on the results of this study include:

1) ASCE/SEI 41-06 drift criteria generally agreed with observed behavior of all shear walls. Additional observations were that 1% drift occurred between 57-80% of total wall capacity, 2% drift occurred between 84-97% of wall capacity and 3% drift occurred between 97-100% of wall capacity.
2) Besides the 2OSB and 2OSBWIN designs, substantial damage to the GWB was observed in wall designs at the ASCE 7-05 drift limit of 2% drift with a minimum of 51% global connection failure.
3) Less GWB damage was observed in the 3INNAIL, 2OSB and 2OSBWIN designs compared to the IRC or IRCWIN designs at all drifts. Increasing the stiffness and strength of a shear wall resulted in less GWB damage for a given loading or displacement.
4) Adding OSB to both sides of a shear wall (2OSB and 2OSBWIN designs) resulted in superior GWB performance up to failure. This is because the similar stiffness on both sides of the wood frame resulted in equal load sharing and less damage to the GWB.
5) Increasing the strength of the GWB connection by using a larger edge distance (SEPSTUD design) improved GWB performance up to 1% drift, but affected the performance negatively at 2% and 3% drifts.

6) Applying panels around window openings (4PNLWIN design) increased GWB performance up to 1% drift, but affected the performance negatively at 2% and 3% drifts. This is because the stiffness of the GWB, as it is applied in this design, was lower and similar to that of the OSB, allowing for equal load sharing at low drifts. Once the GWB panels begin to rack, stiffness increased along with GWB damage.
7) Little damage was observed in the GWB for walls loaded to the allowable strength. This implied that walls damaged in the Northridge Earthquake were loaded above allowable strengths. The shear walls were more likely loaded beyond 1% drift.
8) The classical linear elastic sheathing rotation and wood frame deformation model was qualitatively consistent with measured relative displacements of shear walls.
9) The visual failure limit exhibited in small GWB samples, observed to be 3 mm in this study, was consistent with behavior observed in shear wall specimens. Shear walls with larger relative displacement above this visual failure limit exhibited more visual GWB damage.
10) The 3INNAIL, 2OSB and 2OSBWIN designs exhibited more efficient use of shear wall materials at 1% and 2% drifts. The 3INNAIL design exhibited the most efficient use of shear wall materials at 1% drift and the 2OSB and 2OSBWIN designs exhibited the most at 2% drift. Because most buildings are

built to be displaced to 2% drift in an earthquake, sheathing shear walls with OSB on both sides is the most efficient use of materials.

Recommendations based on results of this study include:

1) Further instrumentation of the displacement of the wood frame and relative displacements of all GWB and OSB panels up to failure is necessary to fully determine the movement of all parts of the shear wall during its failure progression.
2) Further testing of GWB panels applied horizontally, using floating edge construction, tape, spackle and paint built by professional tradesmen is needed to fully understand visual failure and economic loss of shear walls.
3) Further testing of shear walls under cyclic loading is necessary to determine visual failures and economic loss from earthquakes.
4) Testing an adaptation of the 3INNAIL design with a window opening would better help understand the behavior of this shear wall design.
5) If a homeowner wants a shear wall to exhibit only minor damage to the GWB after it has been displaced to 2% drift from an earthquake, they should sheath all shear walls with OSB on both sides of the wood frame. This demonstrates the most efficient use of shear wall materials in this application.

6) The 3INNAIL design provides a more efficient use of shear wall materials than the IRC design and should be implemented in residential construction to reduce damage from earthquakes.
7) The SEPSTUD and 4PNLWIN designs should not be implemented in residential construction due to their poor performance from earthquake loading.

REFERENCES

American Forest and Paper Association (AFPA). (2005). "National design specification® for wood construction." Washington, D.C.

American Society of Civil Engineers (ASCE) (2005). "Minimum Design Loads for Buildings and Other Structures." Reston, VA

American Society of Civil Engineers (ASCE) (2006). "Seismic Rehabilitation of Existing Buildings." Reston, VA

American Society of Testing and Materials (ASTM). (2006). "Standard Method of Static Load Test for Shear Resistance of Framed Walls for Buildings." *ASTM E 564-06,* West Conshohocken, PA.

American Society of Testing and Materials (ASTM). (2006). "Standard Specification for Gypsum Board." *ASTM C1396-06,* West Conshohocken, PA.

American Society of Testing and Materials (ASTM). (2007). "Standard Test Methods for the Physical Testing of Gypsum Panel Products." *ASTM C473-07*, West Conshohocken, PA.

Cobeen, K., Russell, J., and Dolan, D.J. (2004). "Recommendations for Earthquake Resistance in the Design and Construction of Woodframe Buildings." *CUREE Publication No. W-30b,* Richmond, CA.

Deng, Y.H. and Furno, T. (2001). "Properties of gypsum particleboard reinforced with polypropylene fibers." *Journal of Wood Science,* 47 (6), 445-450.

Filiatrault, A. (2002). "Woodframe project testing and analysis: Literature review." *CUREE Publication No. W-03,* Richmond, CA.

Folz, B., and Filiatrault, A. (2001). "Cyclic Analysis of Wood Shear Walls." *Journal of Structural Engineering*, 127(4), 433-441.

International Code Council (ICC) (2009). "2009 International Building Code." Country Club Hills, IL

International Code Council (ICC) (2009). "2009 International Residential Code for One- and Two-Family Dwellings." Country Club Hills, IL

Karacabeyli, E. and Ceccotti, A. (1996). "Test results on Lateral Resistance of Nailed Shear Walls." *Proc. 1996 International Wood Engineering Conference*, New Orleans, LA.

Lagorio, H.J. (1990). “Earthquake, An Architects Guide to Nonstructural Seismic Hazards.” John Wiley and Sons, Inc. New York, NY.

Metriguard (2008). “Model 340 E-Computer Operation and Maintenance Manual.” Pullman, WA.

McMullin, K and Merrick, D. (2002). “Seismic Performance of Gypsum Walls: Experimental Test Program.” *CUREE Publication No. W-15.* Richmond, CA.

Oakeschott, Gordon B. (1975). *San Fernando, California Earthquake of 9 February 1971*, Bulletin 196, California Division of Mines and Geology, Sacramento, CA.

Schierle, G.G. (2003). “Northridge Earthquake Field Investigations: Statistical Analysis of Woodframe Damage.” *CUREE Publication No. W-09*, Richmond, CA.

Seible, F., Filiatrault, A., and Uang, C.-M. (ed). (1999). “Proceedings of the Invitational Workshop on Seismic Testing, Analysis, and Design of Woodframe Testing”, *CUREE Publication No. W-01*, Richmond, CA.

Sinha, A. (2007). “Strain Distribution in OSB and GWB in Wood Frame Shear Walls.” MS thesis, Oregon State University, Corvallis, OR.

Toothman, A.J. (2003). “Monotonic and Cyclic performance of light- frame shear walls with various sheathing materials.” MS Thesis, Virginia Polytechnic Institute and State University, Blacksburg, VA.

Uang, C.M., and Gatto, K. (2003). “Effects of Finish Materials and Dynamic Loading on the Cyclic Response of Woodframe Shearwalls.” *Journal of Structural Engineering*, 129(10), 1394-1402.

Uang, C.M., and Gatto, K. (2003). “Cyclic Response of Woodframe Shearwalls.” *CUREE Publication No. W-13*, Richmond, CA.

USDA Forest Service. (1999). “Wood Handbook : Wood as an Engineering Material.” US Department of Agriculture, Forest Products Laboratory, Madison, WI. <http://www.fpl.fs.fed.us/documnts/fplgtr/fplgtr113/fplgtr113.pdf>

USDA Forest Service. (2004). “Mechanical Properties of Wood-Based Composites and Panel Products.” US Department of Agriculture, Forest Products Laboratory, Madison, WI. <http://www.fpl.fs.fed.us/rwu4706/mechproperties.html>

Wolfe, R.W. (1983). “Contribution of Gypsum Wallboard to the Racking Resistance of Light Frame Walls.” *FPL – 439*, U. S. Department of Agriculture, Forest Product laboratory, Madison, WI.

Appendix A: Wood Frame Materials

The modulus of elasticity (MOE) and specific gravity (SG) of each wood frame member, excluding the window headers, were determined using the Metriguard ® Model 340 E-Computer portable test system (Metriguard, 2008). To use this system for determining the MOE and SG of a piece of lumber, the lumber is positioned on two tripods. One tripod had a knife edge to hold the lumber straight while the other tripod contained a load cell which contacted the lumber. Once a vibration was induced in the middle of the lumber by the operator tapping the lumber, the resulting varying force was read by a load cell and transmitted to the interface unit. The varying force of the lumber was read by an interface unit which transmitted this information to a labtop with the E-computer software installed on it. The natural frequency of the lumber could be calculated by the E-Computer software using the varying force measurements of the lumber. Using the natural frequency, weight and dimensions of the sample, the MOE and SG of the lumber could be computed.

The specific gravity of wood is usually calculated using the oven dried weight of the sample (USDA, 1999) to account for wood and moisture interaction. It was not feasible to consider these moisture effects in this study. As a result, the specific gravity determined from the Metriguard system used the weight of the wood including the water it held inside, which resulted in a higher specific gravity than if the oven dried weight was used.

Figures A1-A4 show the makeup of each wood frame and assigns a letter to each piece of lumber. Tables A1-A14 give the values of SG and MOE for all shear walls tested in this study. The average SG was determined to be 0.54 and the average MOE was determined to be 10.8 GPa with COV's of 51% and 18%, respectively.

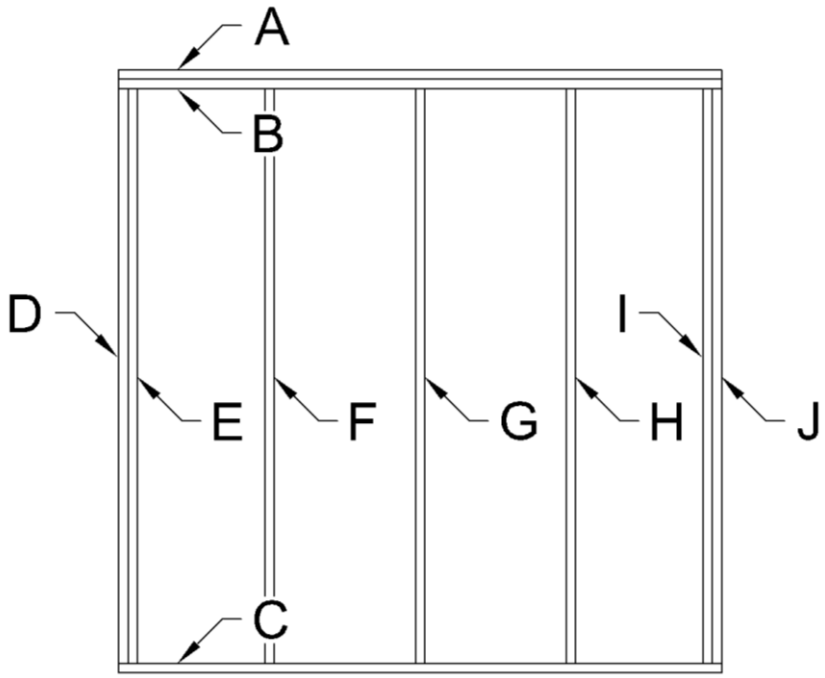

Figure A1. IRC and 2OSB Designs Wood Frame Systems

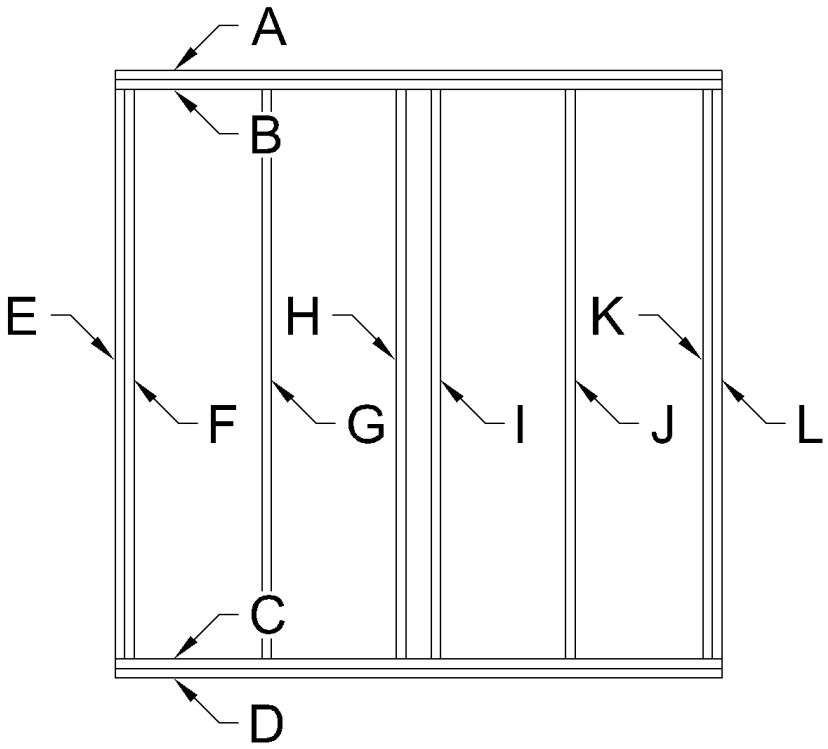

Figure A2. SEPSTUD and 3INNAIL Designs Wood Frame Systems

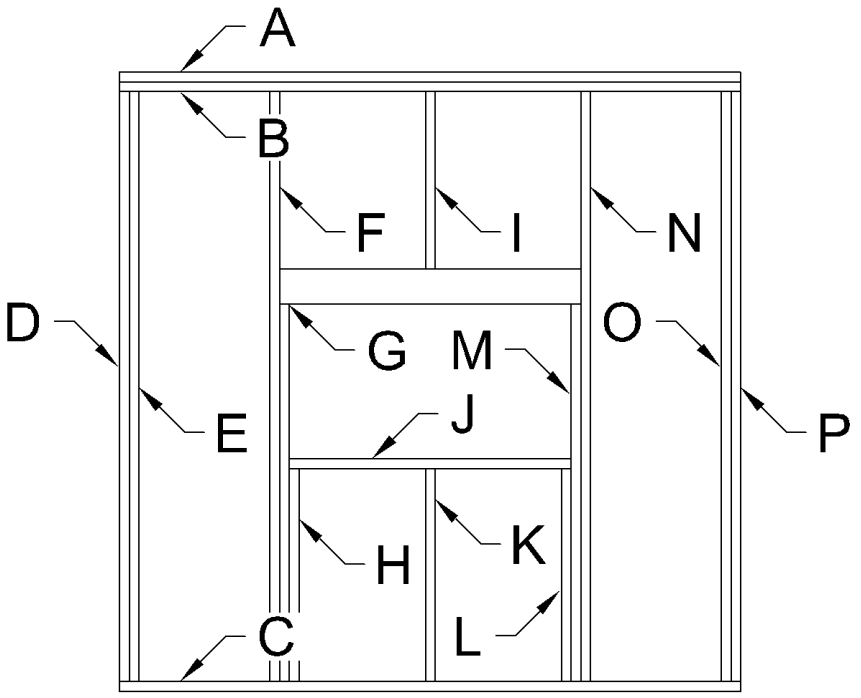

Figure A3. IRCWIN and 2OSBWIN Designs Wood Frame Systems

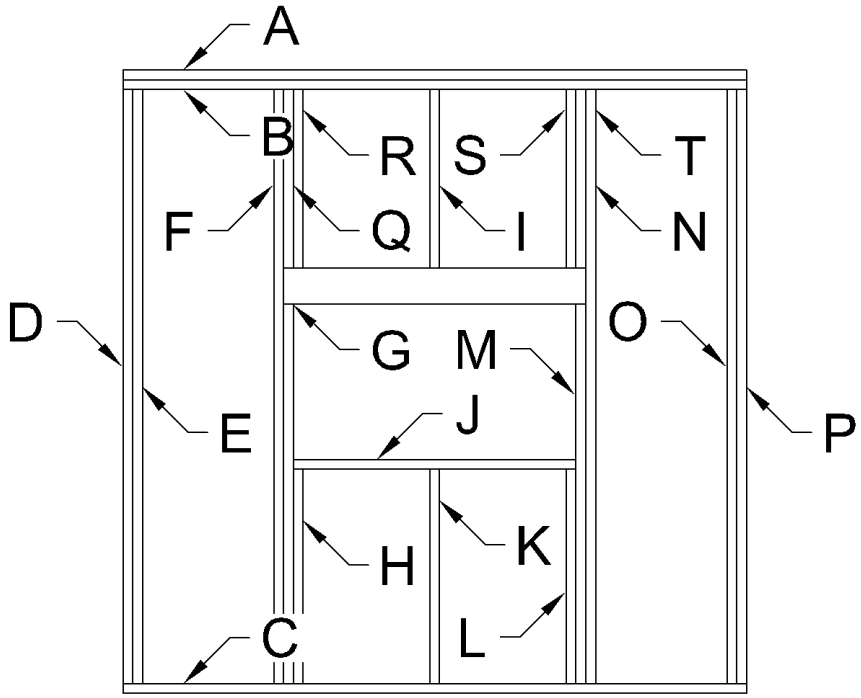

Figure A4. 4PNLWIN Design Wood Frame System

Table A1. IRC-E Wood Frame Properties

Member Location	MOE (GPa)	SG	Member Location	MOE (GPa)	SG
A	15.5	0.61	F	10.4	0.50
B	9.7	0.49	G	11.9	0.53
C	12.3	0.52	H	10.5	0.51
D	9.3	0.44	I	11.0	0.52
E	10.1	0.46	J	10.7	0.52

Table A2. IRC-M Wood Frame Properties

Member Location	MOE (GPa)	SG	Member Location	MOE (GPa)	SG
A	9.0	0.52	F	9.9	0.49
B	12.3	0.57	G	8.5	0.46
C	8.1	0.47	H	12.2	0.51
D	9.2	0.46	I	11.2	0.59
E	10.4	0.55	J	7.9	0.46

Table A3. 2OSB-E Wood Frame Properties

Member Location	MOE (GPa)	SG	Member Location	MOE (GPa)	SG
A	11.0	0.53	F	9.2	0.53
B	11.3	0.56	G	8.3	0.51
C	11.3	0.54	H	10.3	0.52
D	10.8	0.50	I	13.9	0.57
E	9.9	0.52	J	12.8	0.57

Table A4. 2OSB-M Wood Frame Properties

Member Location	MOE (GPa)	SG	Member Location	MOE (GPa)	SG
A	12.5	0.55	F	8.3	0.48
B	13.2	0.52	G	13.2	0.56
C	12.3	0.52	H	10.1	0.55
D	8.5	0.47	I	9.4	0.49
E	12.8	0.65	J	12.1	0.53

Table A5. SEPSTUD-E Wood Frame Properties

Member Location	MOE (GPa)	SG	Member Location	MOE (GPa)	SG
A	11.7	0.51	G	9.3	0.45
B	10.3	0.54	H	9.1	0.45
C	13.9	0.60	I	10.9	0.50
D	9.9	0.53	J	8.9	0.42
E	7.4	0.44	K	11.0	0.49
F	10.1	0.57	L	10.8	0.46

Table A6. SEPSTUD-M Wood Frame Properties

Member Location	MOE (GPa)	SG	Member Location	MOE (GPa)	SG
A	9.4	0.48	G	9.0	0.48
B	9.9	0.49	H	7.4	0.49
C	11.4	0.53	I	12.8	0.52
D	10.3	0.48	J	8.8	0.53
E	10.3	0.50	K	11.3	0.57
F	9.4	0.51	L	16.2	0.64

Table A7. 3INNAIL-E Wood Frame Properties

Member Location	MOE (GPa)	SG	Member Location	MOE (GPa)	SG
A	9.4	0.54	G	8.5	0.53
B	10.5	0.53	H	8.8	0.51
C	8.5	0.50	I	10.3	0.50
D	13.2	0.62	J	9.6	0.46
E	9.1	0.51	K	9.1	0.48
F	10.5	0.50	L	8.8	0.47

Table A8. 3INNAIL-M Wood Frame Properties

Member Location	MOE (GPa)	SG	Member Location	MOE (GPa)	SG
A	11.0	0.50	G	9.2	0.47
B	8.3	0.49	H	11.9	0.56
C	10.5	0.51	I	11.2	0.56
D	11.2	0.51	J	10.1	0.48
E	9.2	0.49	K	11.2	0.53
F	8.3	0.51	L	11.2	0.51

Table A9. IRCWIN-E Wood Frame Properties

Member Location	MOE (GPa)	SG	Member Location	MOE (GPa)	SG
A	11.3	0.55	I	13.9	0.57
B	10.5	0.48	J	10.7	0.52
C	16.8	0.67	K	13.9	0.57
D	9.1	0.46	L	13.7	0.53
E	10.8	0.48	M	8.3	0.48
F	11.0	0.50	N	8.1	0.47
G	10.1	0.55	O	12.4	0.57
H	8.3	0.48	P	7.9	0.46

Table A10. IRCWIN-M Wood Frame Properties

Member Location	MOE (GPa)	SG	Member Location	MOE (GPa)	SG
A	13.1	0.58	I	9.2	0.54
B	9.2	0.54	J	10.0	0.54
C	10.8	0.52	K	10.1	0.48
D	14.3	0.61	L	10.3	0.53
E	13.3	0.57	M	10.3	0.53
F	10.7	0.57	N	10.7	5.52
G	10.1	0.48	O	10.0	0.48
H	11.8	0.55	P	12.0	0.49

Table A11. 2OSBWIN-E Wood Frame Properties

Member Location	MOE (GPa)	SG	Member Location	MOE (GPa)	SG
A	12.0	0.54	I	9.4	0.48
B	9.9	0.51	J	10.0	0.54
C	13.9	0.61	K	9.4	0.53
D	11.5	0.56	L	9.9	0.49
E	9.0	0.50	M	10.2	0.51
F	12.2	0.56	N	10.6	0.50
G	9.9	0.49	O	9.0	0.52
H	10.2	0.51	P	13.0	0.60

Table A12. 2OSBWIN-M Wood Frame Properties

Member Location	MOE (GPa)	SG	Member Location	MOE (GPa)	SG
A	12.2	0.59	I	8.8	0.51
B	14.5	0.58	J	9.1	0.45
C	12.4	0.54	K	8.8	0.50
D	10.1	0.56	L	10.2	0.53
E	9.2	0.50	M	10.6	0.50
F	12.9	0.60	N	8.8	0.50
G	10.3	0.50	O	8.5	0.50
H	10.2	0.53	P	10.1	0.568

Table A13. 4PNLWIN-E Wood Frame Properties

Member Location	MOE (GPa)	SG	Member Location	MOE (GPa)	SG
A	13.7	0.60	K	9.4	0.49
B	9.0	0.61	L	10.3	0.54
C	10.5	0.57	M	8.8	0.50
D	7.0	0.50	N	10.8	0.55
E	10.1	0.57	O	11.4	0.57
F	8.8	0.51	P	10.5	0.47
G	8.8	0.51	Q	9.6	0.46
H	8.8	0.51	R	9.6	0.46
I	12.1	0.55	S	10.3	0.50
J	9.4	0.49	T	10.3	0.50

Table A14. 4PNLWIN-M Wood Frame Properties

Member Location	MOE (GPa)	SG	Member Location	MOE (GPa)	SG
A	14.3	0.62	K	9.4	0.48
B	10.6	0.51	L	12.3	0.59
C	12.1	0.54	M	12.3	0.59
D	10.6	0.58	N	9.9	0.49
E	11.6	0.57	O	12.5	0.57
F	10.3	0.59	P	9.7	0.52
G	10.3	0.54	Q	9.1	0.44
H	9.2	0.54	R	10.7	0.49
I	9.4	0.48	S	9.1	0.44
J	11.8	0.55	T	10.7	0.49

Appendix B: GWB Materials

Moisture Content of GWB Panels Applied to Shear Walls

The moisture contents of all GWB panels tested in the shear wall systems were determined in this study. All shear walls were tested in a laboratory at varying relative humidity, so the variation in moisture content was recorded to determine if this environmental change affected the results of this test. Measuring these moisture contents was accomplished by cutting a sample of the GWB panel from the shear wall after testing and weighing the sample. The sample was then placed in a drying oven at 103° C until the sample reached a constant weight. The sample was then weighed again and the moisture content was calculated using the formula:

$$Moisture\ Content = \frac{Inital\ Weight\ (g) - Oven\ Dry\ Weight\ (g)}{Oven\ Dry\ Weight\ (g)} \times 100\%$$

The moisture content of all GWB panels is shown in Table B1. The location of the GWB panel is designated by it being nearest to the hydraulic actuator or furthest from the actuator, which is shown in Figure B1. The 4PNLWIN designs required an additional panel to be cut for the middle section of the wall. This panel was designated the middle panel.

ASTM C473 GWB Flexural Strength Test

The flexural strength of the GWB shipment used in this study was calculated in accordance with Method B of the ASTM C473 Standard Test Methods for the Physical Testing of Gypsum Panel Products (ASTM, 2007). The goals of this test were to determine the variability in the GWB shipment received and to validate that the flexural strength was above ASTM C1396 requirements (ASTM, 2006). The ASTM C473 test method required that four 305 mm x 406 mm x 12.7 mm samples be tested from three GWB panels requiring a total of 12 tests. Figure B2 shows the test setup for the ASTM C473 (ASTM, 2007) GWB flexural strength test. The four samples from each panel were cut 102 mm from the edge and such that two had the 305 mm dimension perpendicular to the tapered edge of the GWB panel, and two had the 305 mm dimension parallel to the tapered edge of the GWB panel. The locations and orientations of these samples are shown in Figure B3. Of the two samples with the same orientation, one was tested with the interior finish surface up and the other with the interior finish surface down. The test procedure required that each side of the 305 mm dimension was placed on a round edge of a 3.2 mm radius support of the same

length. These supports were centered 356 mm apart from the midline of the sample such that 50.8 mm of the sample overhung outside the supports. A 305 mm long rounded support of 3.2 mm radius attached to the arm of the INSTRON 5582 applied load to the midline of the sample at a rate of 25 mm/min until failure. The breaking load recorded as the flexural strength and compared to the ASTM minimum standards.

The load displacement curves recorded from the test are shown in Figure B4. The flexural strength, or maximum load, for GWB samples in which the 305 mm dimension was perpendicular to the tapered edge of the GWB panel are shown in Table B2 and those in which the 305 mm dimension was parallel to the tapered edge of the GWB are shown in Table B3. The average flexural strength for the perpendicular and parallel GWB samples was 584 and 273 N, respectively. The average flexural strength for perpendicular and parallel samples was 23% and 71% above the ASTM C1396 (ASTM, 2006) required flexural strengths of 476 and 160 N, respectively. The COV for perpendicular and parallel GWB samples were 4% and 15% respectively. The reason for the higher variability of the parallel samples was due to the sample 3 face up test, which had a much lower flexural strength than any of the other parallel samples. If this outlier was removed, the average flexural strength of the parallel samples would be 290 N, which was 81% higher than the ASTM standard and would result in a COV of 3%. All GWB samples were conditioned in the ASTM conditioning room at 85°F at 50% relative humidity (ASTM, 2007) until constant weight. This resulted in a moisture content for all GWB flexural strength samples being 23% as shown in Table B4.

GWB Connection Tests

Fifteen GWB connection samples were tested in tension using the INSTRON 5582 universal testing machine. Each connection sample consisted of a 152 mm x 152 mm x 12.7 mm square of GWB which was attached to the side of a 584 mm length of 38 mm x 89 mm (51 mm x 102 mm or 2 x 4 nominal size) No. 1 and Better grade kiln dried Douglas-fir (*Pseudotsuga menziesii*) with one screw at one of three edge distances. These edge distances were the distance between the screw and the edge of the GWB panel. The three edge distances considered were 9.5, 19.1 and 57.2 mm which correspond to the edge distances found in all shear wall specimen design's considered in this study. GWB samples were all taken from the same GWB panel but from different locations around the perimeter. Some were taken from the tapered edge of the GWB along the long side of the panel, and some were taken from the non-tapered edge along the short side of the panel. Figure B5 shows the test setup for the

GWB connection pull tests. The load displacement curves recorded from the connection tests are shown in Figures B6, B7 and B8. The maximum load, displacement at maximum load and displacement at visual failure for the GWB tests are shown in Table B4. Connection tests were performed for edge distances of 9.5 mm, 19.1 mm and 57.2 mm and on edges which were tapered and not tapered.

The sample tests which were tapered are designated with a ‘Y’ and the others with an ‘N’. Connection tests performed on tapered edges were pulled in the same direction as the perpendicular GWB flexural test samples. Those tests not performed on tapered edges were tested in the same direction as the parallel GWB flexural test samples. Because the GWB flexural strength tests in the perpendicular direction were found to exhibit a much higher strength than for the parallel direction, it would seem that a similar trend would be present for the GWB connection tests. However, this was not the case. The only differences in strength were due to the tapered edge being much easier to attach screws to for the 9.5 mm edge distance, due to the confinement provided by the paper.

In test numbers 3, 5 and 10 no visual failure could be ascertained, so they were designated N/A for the displacement at visual failure. Test number 3 displayed initial damage so no displacement at max load could be determined. In test number 12, the sample continued to gain load until the test was stopped, so no displacement at maximum load could be determined.

As expected, as relative displacement between the GWB sample and the wood stud increased, so did damage to the GWB. Additionally, the strength and displacement at maximum load of the GWB screw connections were observed to depend on edge distance. As shown in Figure B9, the average maximum load changes little between 19.1 and 57.2 mm edge distance, but dropped by 29% between 19.1 mm and 9.5 mm. This indicated that the 9.5 mm edge distance was the weakest connection. As shown in Figure B10, the displacement at maximum load decreases by 20% between 57.2 and 19.1 mm and by 66% between 57.2 and 9.5 mm. Instead of the abrupt change in strength observed between 19.1 and 9.5 mm, the reduction in displacement at maximum load of the connection suggests a more continuous decrease with edge distance. The 57.2 mm edge distance GWB connection was used in the SEPSTUD design because it was found to be the strongest and exhibit the most displacement at maximum load.

While increased relative displacement did increase damage to the GWB, noticeable failures occurred abruptly, not slowly as displacement increased as predicted. This allowed for a visual failure limit to be observed. The visual failure limit was the relative displacement at which one of the GWB failure criteria could be visually identified in the GWB sample. The displacement of this visual failure limit was recorded and shown in Figure B11. Visual failure limits occurred at an average of 3.0 mm between 2.0 and 3.8 mm with a COV of 17%. This suggests consistent relative displacements at visual failure limits. GWB Samples 3, 5 and 10 were not included in this analysis because no visual failure could be ascertained. This may be due to initial damage, screw fracture or other failure modes which did not cause visual damage.

Photographs of selected connection tests are shown in Figure B12. While the test was running, a visual inspection was performed where the failure modes were identified and recorded on the sample as shown in the photographs. Lines drawn around the bubbles caused by local crushing of the GWB are indicated by the displacement at which they occurred.

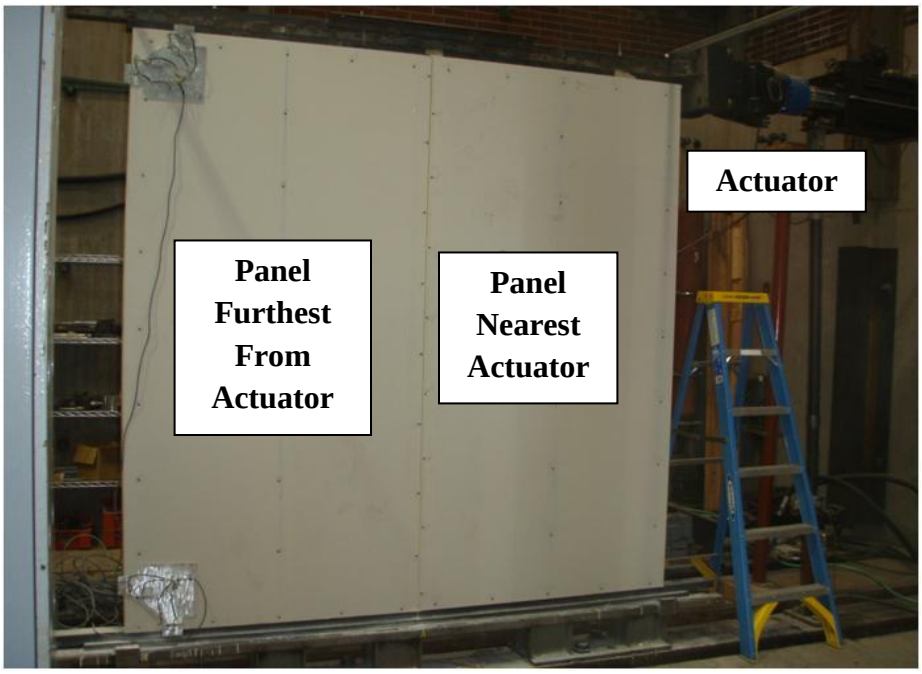

Figure B1. GWB Panel Locations

Figure B2. GWB Flexural Test Setup

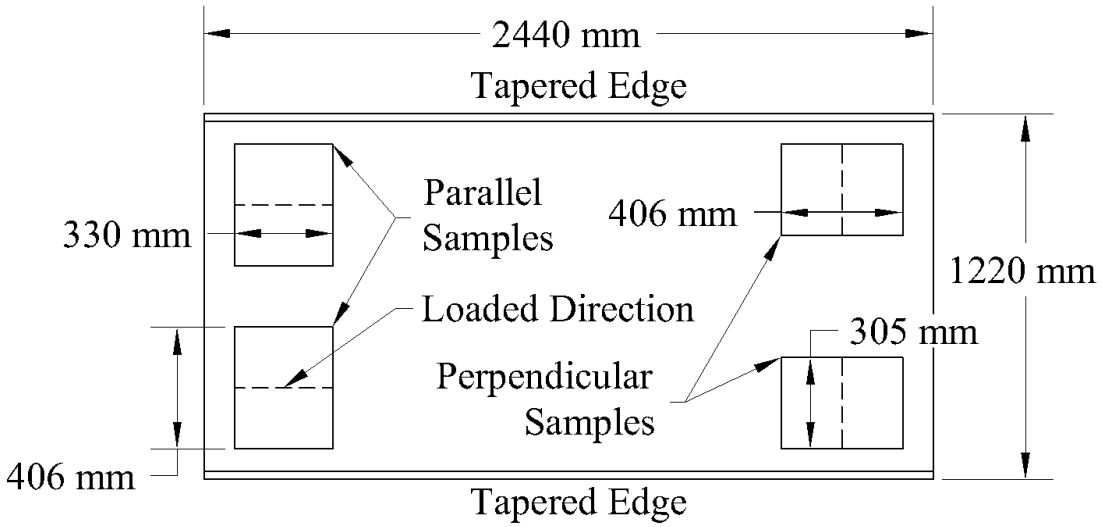

Figure B3. GWB Flexural Sample Locations

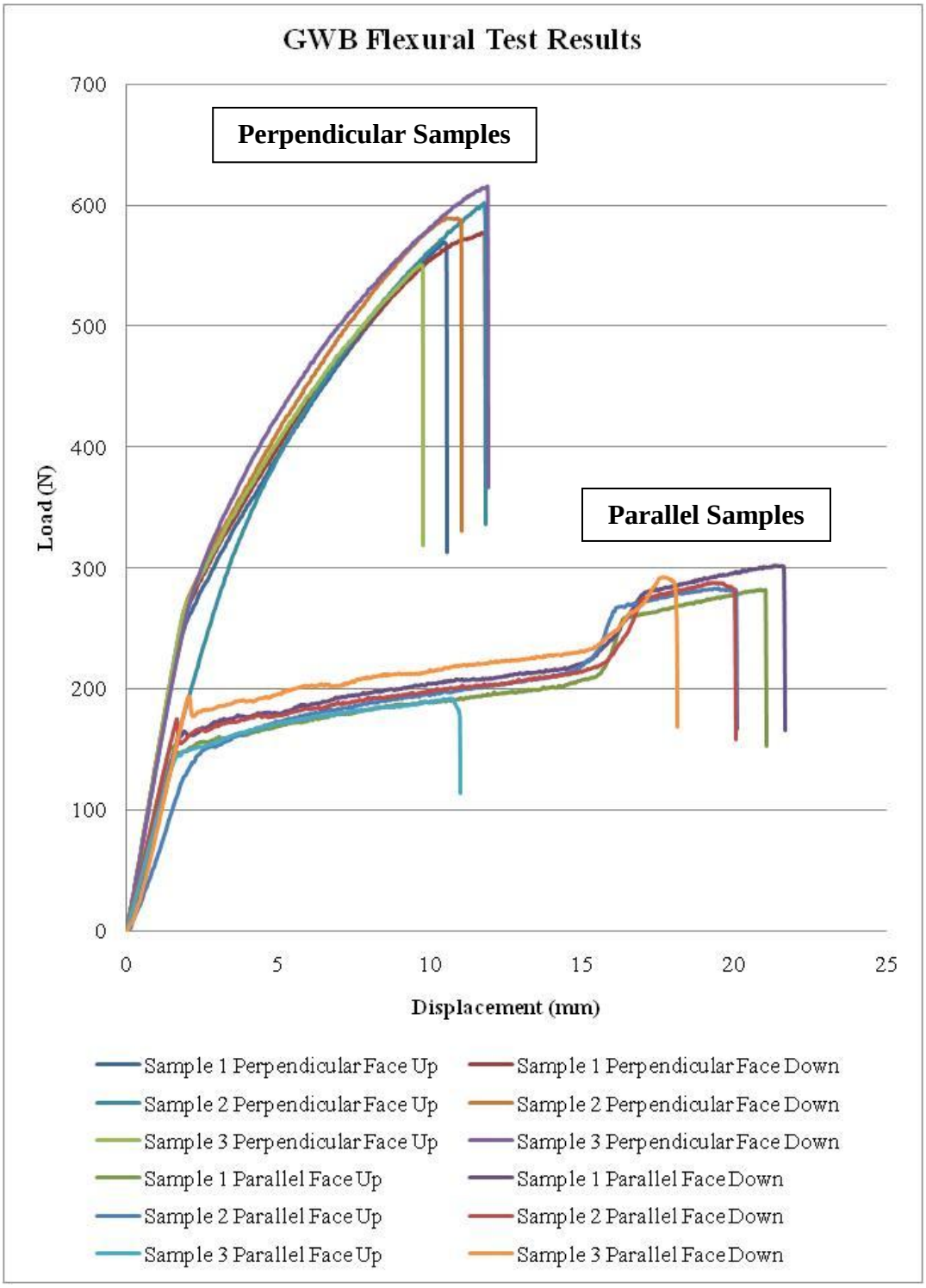

Figure B4. GWB Flexural Tests Load Displacement Curves

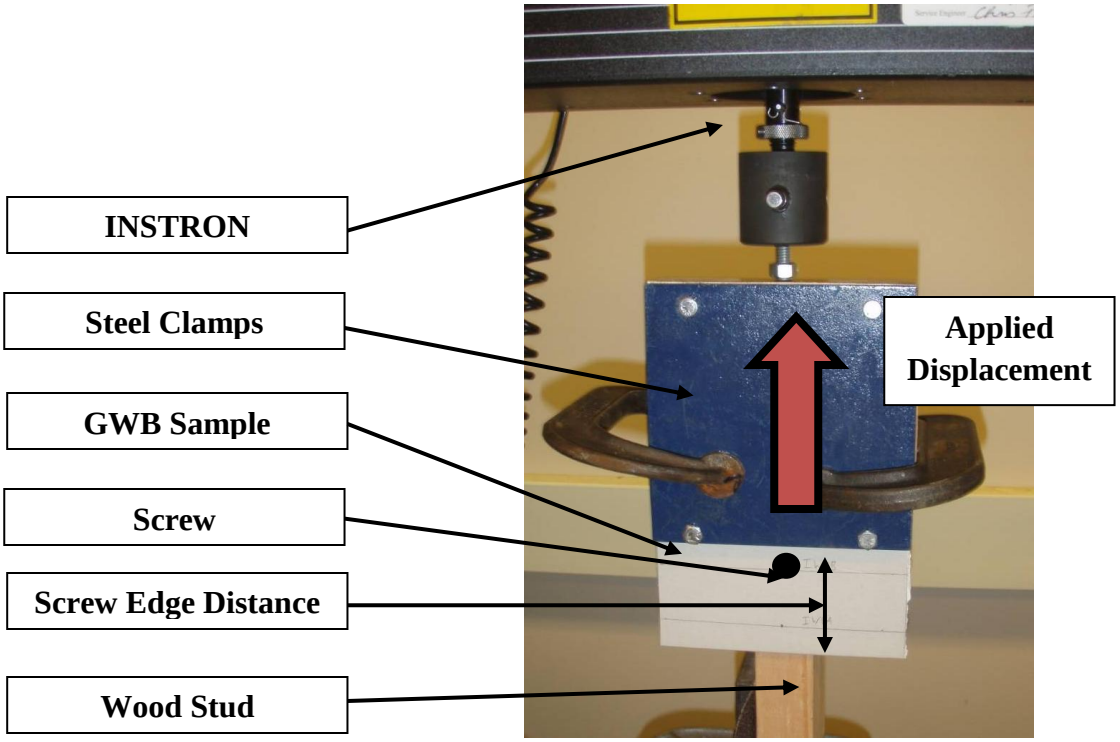

Figure B5. GWB Connection Test Setup

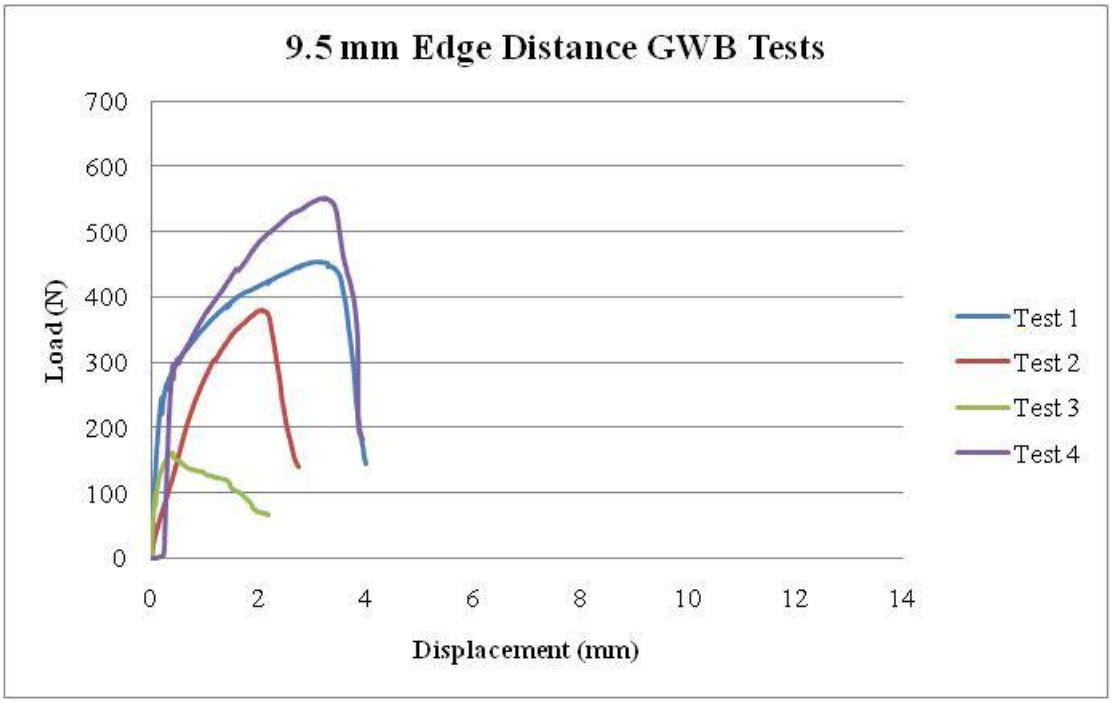

Figure B6. Load Displacement Curve for 9.5 mm Edge Distance GWB Tests

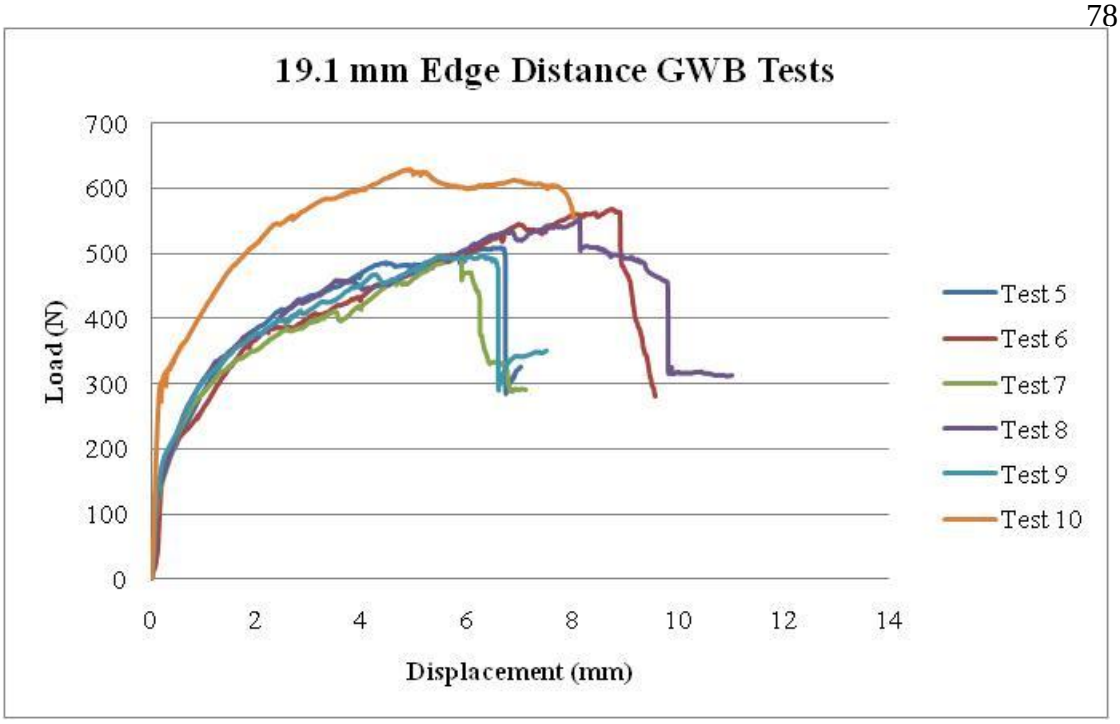

Figure B7. Load Displacement Curve for 19.1 mm Edge Distance GWB Tests

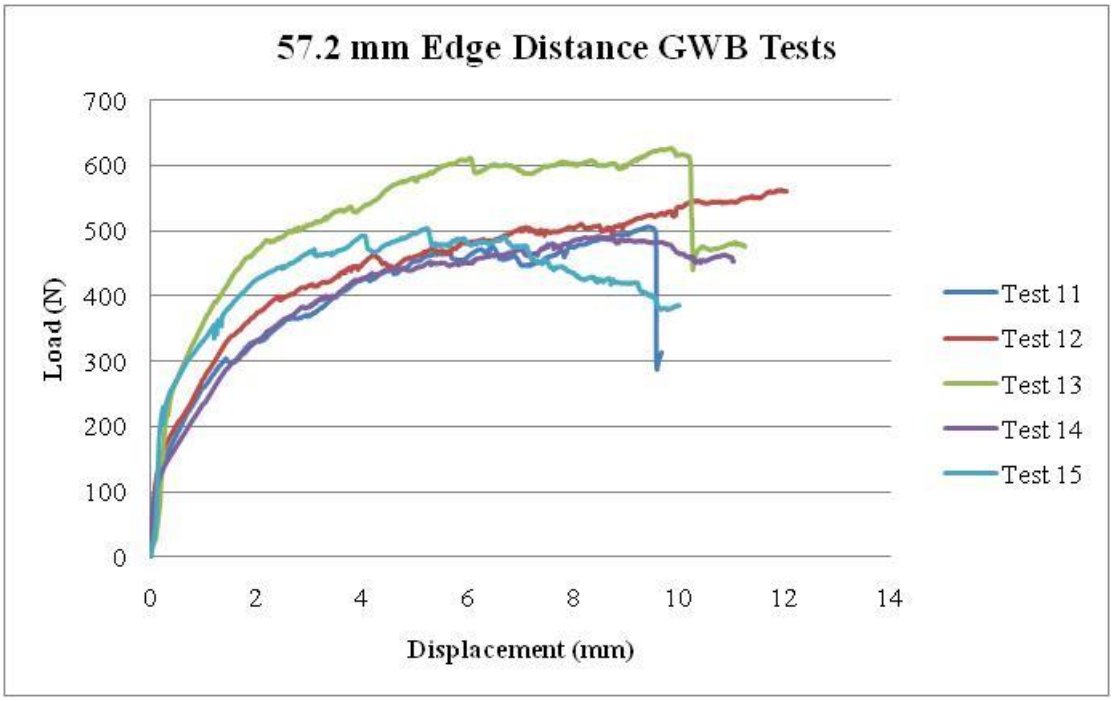

Figure B8. Load Displacement Curve for 57.2 mm Edge Distance GWB Tests

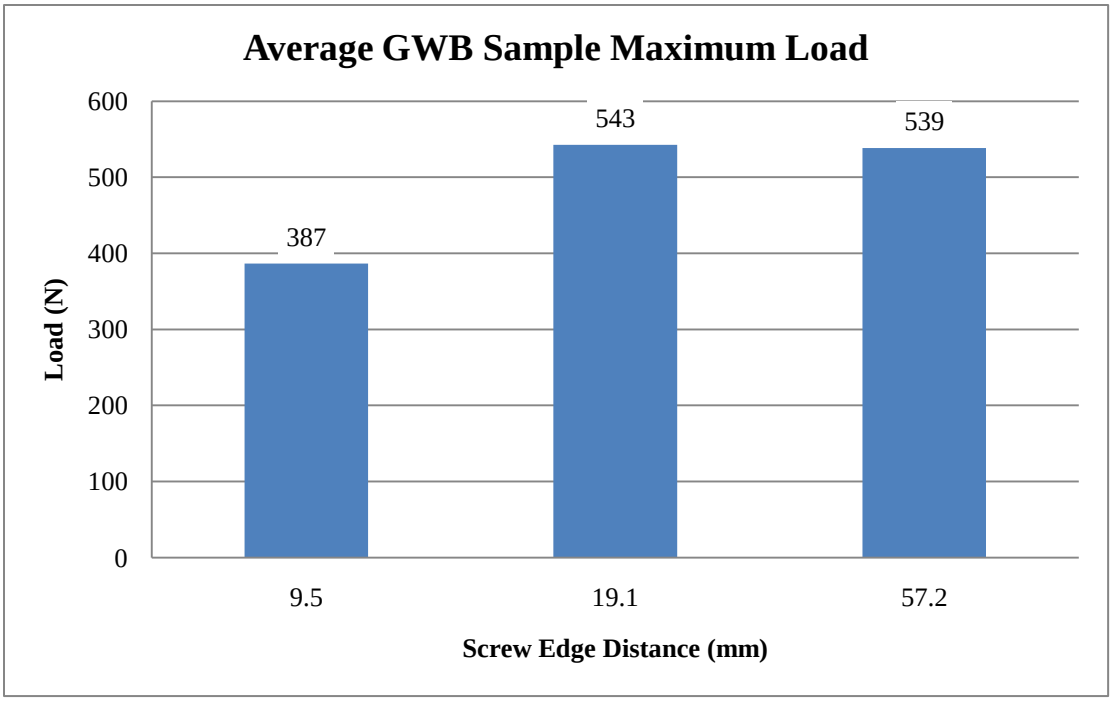

Figure B9. Average GWB Sample Maximum Load

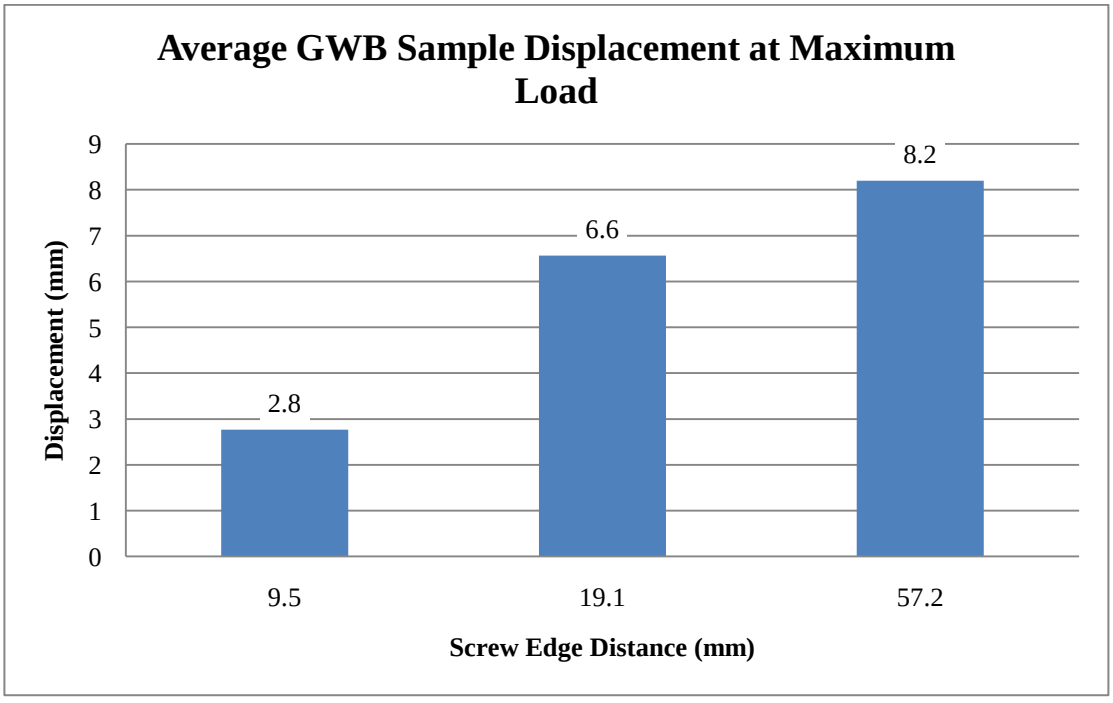

Figure B10. Average GWB Sample Displacement at Maximum Load

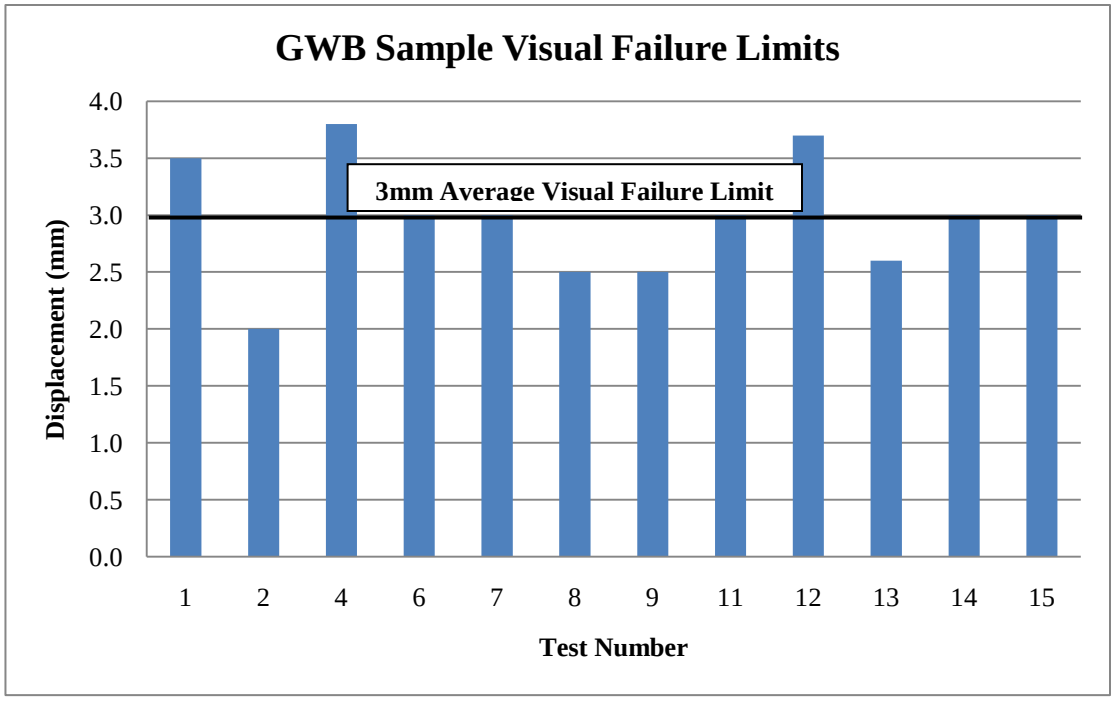

Figure B11. GWB Sample Displacement at Visual Failure

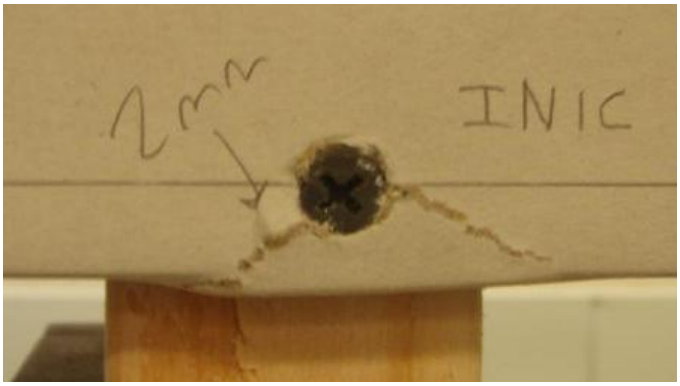

a) Sample 2 - 9.5 mm Edge Distance

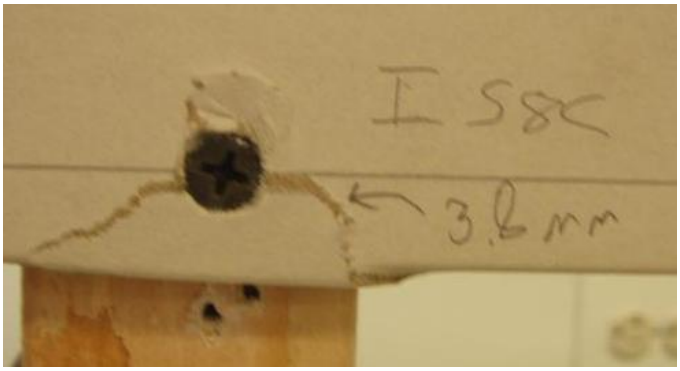

b) Sample 4 - 9.5 mm Edge Distance

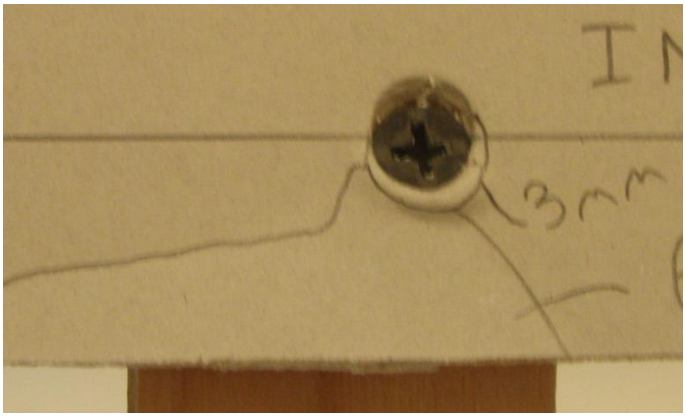

c) Sample 7- 19.1 mm Edge Distance

Figure B12. GWB Connection Test Photographs

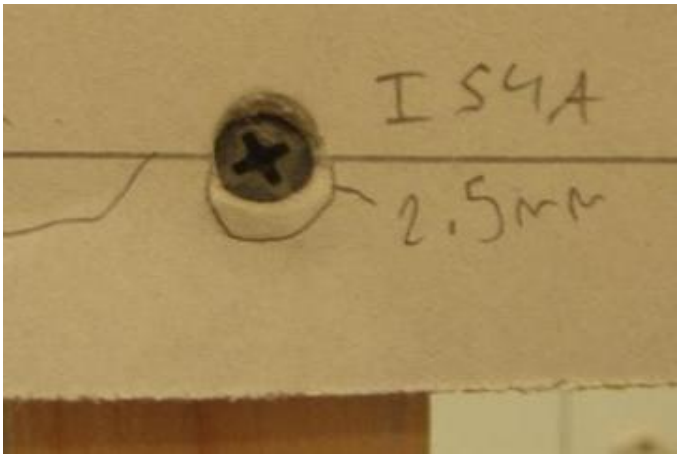

d) Sample 8 - 19.1 mm Edge Distance

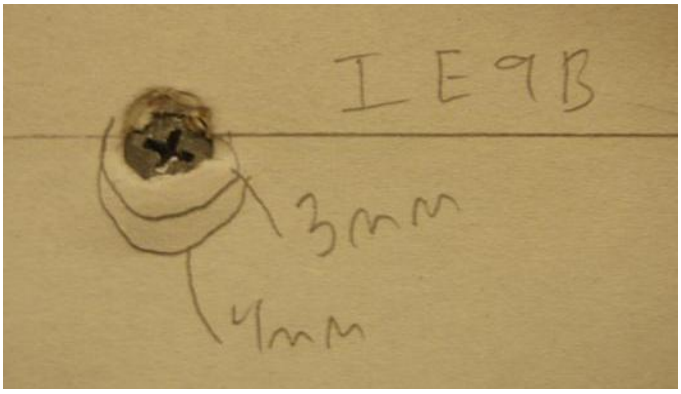

e) Sample 11 – 57.2 mm Edge Distance

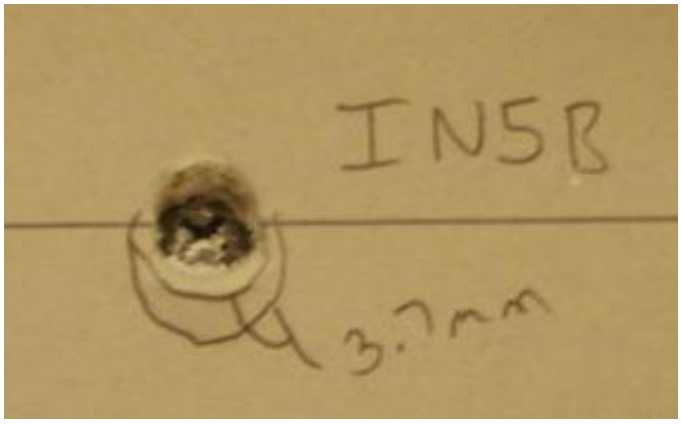

f) Sample 12 - 57.2 mm Edge Distance

Figure B12. Connection Test Photographs (Continued)

Table B1: Moisture Contents of GWB Panels Applied to Shear Walls

Shear Wall Test	Panel Location Relative to Actuator	Initial Weight (g)	Oven Dry Weight (g)	Moisture Content
IRC-E	Near	605	495	22%
	Far	776	633	23%
IRC-M	Near	617	497	24%
	Far	679	547	24%
SEPSTUD-E	Near	616	504	22%
	Far	675	552	22%
SEPSTUD-M	Near	714	586	22%
	Far	585	479	22%
3INNAIL-E	Near	445	365	22%
	Far	904	743	22%
3INNAIL-M	Near	637	520	22%
	Far	464	379	22%
2OSB-E	Near	764	624	22%
	Far	857	701	22%
2OSB-M	Near	631	519	22%
	Far	582	482	21%
IRCWIN-E	Near	607	495	23%
	Far	626	511	22%
IRCWIN-M	Near	860	701	23%
	Far	892	727	23%
2OSBWIN-E	Near	743	605	23%
	Far	826	672	23%
2OSBWIN-M	Near	709	577	23%
	Far	863	704	23%
4PNLWIN-E	Near	668	550	22%
	Far	789	650	21%
	Middle	917	755	21%
4PNLWIN-M	Near	909	744	22%
	Far	930	767	21%
	Middle	881	725	22%

Table B2. Flexural Strength of Perpendicular GWB Samples

Orientation	Sample 1	Sample 2	Sample 3
Face Up	569	602	551
Face Down	577	589	616

Table B3. Flexural Strength of Parallel GWB Samples

Orientation	Sample 1	Sample 2	Sample 3
Face Up	283	284	192
Face Down	302	288	293

Table B4. Moisture Contents of GWB Samples

	Initial Weight (g)	Oven Dry Weight (g)	Moisture Content
Sample 1	238	194	23%
Sample 2	239	194	23%
Sample 3	205	167	23%

Table B5. Test Results from Connection Tests

Test Number	Edge Distance (mm)	Tapered Edge	Max Load (N)	Displacement at Max Load (mm)	Displacement at Visual Failure (mm)
1	9.5	Y	453	3.1	3.5
2	9.5	Y	380	2	2
3	9.5	N	163	Initial Damage	N/A
4	9.5	Y	551	3.2	3.8
5	19.1	Y	510	6.6	N/A
6	19.1	N	569	8.6	3
7	19.1	N	500	5.8	3
8	19.1	N	554	8.1	2.5
9	19.1	N	496	5.5	2.5
10	19.1	Y	629	4.8	N/A
11	57.2	Y	506	9.3	3
12	57.2	N	564	N/A	3.7
13	57.2	N	628	9.6	2.6
14	57.2	N	492	8.8	3
15	57.2	Y	504	5.1	3

Appendix C: Visual Comparison Analysis

All shear wall tests were stopped at displacements of 4.0, 8.0, 12.0, 16.0, 20.0, 24.4, 48.8, 73.2 mm and at failure for a visual failure map to be recorded. At each displacement stop, the failure mode and failure location of each connection failure was recorded. Tables C1-C14 summarize the results from this visual failure comparison analysis. Each table displays data from one wall test and is divided into Table A describing failure mode and Table B describing failure location for each connection failure.

Table A for each wall test describes the failure modes recorded for each connection failure at each displacement stop. The percent global connection failure is computed by dividing the number of fasteners failed at each displacement stop by the total number of fasteners. IRC, 3INNAIL and 2OSB designs all had 64 total fasteners. SEPSTUD had 62 total fasteners. IRCWIN and 2OSBWIN had 70 fasteners and 4PNLWIN had 72 fasteners. Initial failures were removed from this analysis. The percent global connection failure observed before any displacement of the wood frame was subtracted from the subsequent percent global connection failures. This was done because some initial failures occurred due to construction error, and were not a product of wall performance.

The small and large bubble failure modes recorded in testing were combined into a singular bubble failure mode as presented in this study. This was due to the small amount of large bubble failure modes present, and the difficulty of distinguishing the two failure modes. A large bubble was generally considered to be at least 25.4 mm in diameter, with a small bubble being less in diameter. Additionally, the tear in paper failure mode and the GWB crack failure mode were combined to a GWB tear/crack failure mode presented in this study. This was done to reduce data, as both failure modes resulted from similar GWB behavior. At first the GWB paper would tear around the fastener, and then it would crack as displacement increased.

Table B for each wall test describes the failure location of each connection failure on the shear wall at each displacement stop. Figure C1 identifies where each of these failure locations presented in this study were on the wood frame. While the exact location of every failed fastener was recorded, this data analysis allows for a more condensed presentation of data. Connections failed on both intermediate studs and were recorded together as one quantity due to the small number of connection failures on the intermediate studs.

Previous testing of GWB partition walls (McMullin and Merrick, 2002) identified that damage to the GWB began at 0.25% drift. The data from the IRC wall design are consistent with this result as percent global connection failures began near 4.0 to 8.0 mm and increased substantially at 12 mm of global displacement.

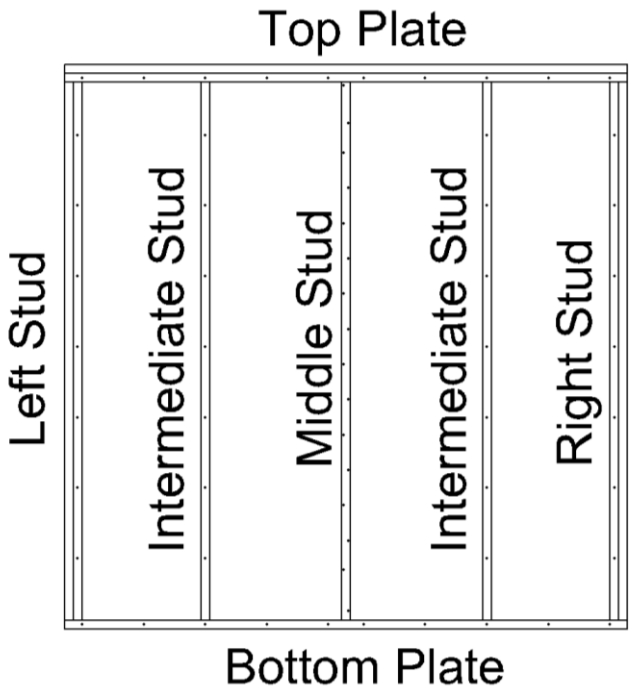

Figure C1. Visual Failure Comparison Locations

Table C1. Visual Failure Comparison Results from IRC-E

A. Failure Mode

Displacement (mm)	Small Bubble	Large Bubble	Tear in Paper	GWB Crack	Pull Through	Total	% Global Connection Failure
0	2	0	0	0	0	2	0%
4	2	1	0	0	0	3	2%
8	2	1	0	0	0	3	2%
12	4	1	1	1	1	8	9%
16	5	1	1	1	5	13	17%
20	14	1	1	1	7	24	34%
24.4	18	1	1	1	13	34	50%
48.8	3	0	1	0	44	48	72%
73.2	2	0	2	0	50	54	81%
99.6	2	0	2	0	50	54	81%

B. Failure Location

Displacement (mm)	Left Stud	Middle Stud	Right Stud	Bottom Plate	Top Plate	Intermediate Studs
0	0	2	0	0	0	0
4	0	3	0	0	0	0
8	0	3	0	0	0	0
12	0	6	0	2	0	0
16	2	7	0	4	0	0
20	5	8	5	5	1	0
24.4	6	10	7	6	5	0
48.8	7	14	7	10	10	0
73.2	7	16	7	10	10	4
99.63	7	16	7	10	10	4

Table C2. Visual Failure Comparison Results from IRC-M

A. Failure Mode

Displacement (mm)	Small Bubble	Large Bubble	Tear in Paper	GWB Crack	Pull Through	Total	% Global Connection Failure
0	0	0	2	0	0	2	0%
4	0	0	2	0	1	3	2%
8	0	0	2	0	2	4	3%
12	2	0	2	0	3	7	8%
16	2	0	2	0	3	7	8%
20	1	0	2	0	6	9	11%
24.4	7	0	2	0	12	21	30%
48.8	12	1	0	2	20	35	52%
73.2	2	1	2	3	36	46	69%
93.6	2	1	2	3	40	50	75%

B. Failure Location

Displacement (mm)	Left Stud	Middle Stud	Right Stud	Bottom Plate	Top Plate	Intermediate Studs
0	0	2	0	0	0	0
4	0	2	0	1	0	0
8	0	2	0	1	1	0
12	0	4	0	2	1	0
16	0	4	0	2	1	0
20	0	5	0	3	1	0
24.4	3	7	5	5	1	0
48.8	6	9	7	8	5	0
73.2	7	14	7	9	9	0
93.57	7	16	7	10	10	0

Table C3. Visual Failure Comparison Results from SEPSTUD-E

A. Failure Mode

Displacement (mm)	Small Bubble	Large Bubble	Tear in Paper	GWB Crack	Pull Through	Total	% Global Connection Failure
0	0	0	0	0	0	0	0%
4	0	0	0	0	0	0	0%
8	0	0	0	0	1	1	2%
12	0	0	0	0	2	2	3%
16	1	0	0	0	4	5	8%
20	1	0	0	0	6	7	11%
24.4	1	0	0	0	15	16	26%
48.8	10	0	0	0	34	44	71%
73.2	10	0	0	0	37	47	76%
92.47	2	1	2	5	40	50	81%

B. Failure Location

Displacement (mm)	Left Stud	Middle Stud	Right Stud	Bottom Plate	Top Plate	Intermediate Studs
0	0	0	0	0	0	0
4	0	0	0	0	0	0
8	0	0	0	1	0	0
12	0	1	0	1	0	0
16	0	1	1	2	1	0
20	0	1	2	3	1	0
24.4	2	1	4	4	4	1
48.8	7	11	7	10	8	1
73.2	7	13	7	10	9	1
92.47	7	14	7	10	9	3

Table C4. Visual Failure Comparison Results from SEPSTUD-M

A. Failure Mode

Displacement (mm)	Small Bubble	Large Bubble	Tear in Paper	GWB Crack	Pull Through	Total	% Global Connection Failure
0	0	0	0	0	0	0	0%
4	0	0	0	0	1	1	2%
8	0	0	0	0	1	1	2%
12	0	0	0	0	1	1	2%
16	0	0	0	0	6	6	10%
20	3	1	0	0	9	13	21%
24.4	6	0	0	0	16	22	35%
48.8	16	1	0	0	24	41	66%
73.2	5	0	0	0	39	44	71%
86.71	5	0	0	0	41	46	74%

B. Failure Location

Displacement (mm)	Left Stud	Middle Stud	Right Stud	Bottom Plate	Top Plate	Intermediate Studs
0	0	0	0	0	0	0
4	0	0	0	0	0	1
8	0	0	0	0	0	1
12	0	0	0	0	0	1
16	0	1	0	3	0	2
20	3	1	0	4	3	2
24.4	7	2	0	8	3	2
48.8	7	11	5	11	7	2
73.2	7	12	5	11	9	2
86.71	7	13	6	11	9	2

Table C5. Visual Failure Comparison Results from 3INNAIL-E

A. Failure Mode

Displacement (mm)	Small Bubble	Large Bubble	Tear in Paper	GWB Crack	Pull Through	Total	% Global Connection Failure
0	0	0	0	0	0	0	0%
4	0	0	0	0	0	0	0%
8	0	0	0	0	0	0	0%
12	0	0	0	0	0	0	0%
16	0	0	0	0	0	0	0%
20	1	0	0	0	0	1	2%
24.4	3	0	0	0	1	4	6%
48.8	20	1	0	0	17	38	59%
73.2	9	0	1	0	32	42	66%
95.34	0	0	0	0	52	52	81%

B. Failure Location

Displacement (mm)	Left Stud	Middle Stud	Right Stud	Bottom Plate	Top Plate	Intermediate Studs
0	0	0	0	0	0	0
4	0	0	0	0	0	0
8	0	0	0	0	0	0
12	0	0	0	0	0	0
16	0	0	0	0	0	0
20	0	1	0	0	0	0
24.4	0	1	0	2	1	0
48.8	7	13	4	7	7	0
73.2	7	15	4	7	9	0
95.34	7	16	7	10	10	2

Table C6. Visual Failure Comparison Results from 3INNAIL-M

A. Failure Mode

Displacement (mm)	Small Bubble	Large Bubble	Tear in Paper	GWB Crack	Pull Through	Total	% Global Connection Failure
0	1	0	0	0	0	1	0%
4	1	0	0	0	0	1	0%
8	1	0	0	0	1	2	2%
12	1	0	0	0	1	2	2%
16	1	0	0	0	1	2	2%
20	1	0	0	0	1	2	2%
24.4	1	0	0	0	6	7	9%
48.8	6	0	0	0	22	28	42%
73.2	4	1	0	0	37	42	64%
97.93	0	0	0	0	48	48	73%

B. Failure Location

Displacement (mm)	Left Stud	Middle Stud	Right Stud	Bottom Plate	Top Plate	Intermediate Studs
0	0	1	0	0	0	0
4	0	1	0	0	0	0
8	0	1	1	0	0	0
12	0	1	1	0	0	0
16	0	1	1	0	0	0
20	0	1	1	0	0	0
24.4	1	2	1	2	1	0
48.8	7	7	2	7	5	0
73.2	7	13	4	10	8	0
97.93	7	16	5	10	10	0

Table C7. Visual Failure Comparison Results from 2OSB-E

A. Failure Mode

Displacement (mm)	Small Bubble	Large Bubble	Tear in Paper	GWB Crack	Pull Through	Total	% Global Connection Failure
0	0	0	5	0	0	5	0%
4	0	0	5	0	0	5	0%
8	1	0	5	0	0	6	2%
12	1	0	5	0	0	6	2%
16	1	0	5	0	0	6	2%
20	0	0	5	0	1	6	2%
24.4	0	0	5	0	1	6	2%
48.8	1	0	5	0	3	9	6%
73.2	1	0	0	5	25	31	41%
84.22	0	0	0	0	38	38	52%

B. Failure Location

Displacement (mm)	Left Stud	Middle Stud	Right Stud	Bottom Plate	Top Plate	Intermediate Studs
0	0	5	0	0	0	0
4	0	5	0	0	0	0
8	0	6	0	0	0	0
12	0	6	0	0	0	0
16	0	6	0	0	0	0
20	0	6	0	0	0	0
24.4	0	6	0	0	0	0
48.8	1	6	1	1	0	0
73.2	6	13	2	7	3	0
84.22	7	13	3	8	7	0

Table C8. Visual Failure Comparison Results from 2OSB-M

A. Failure Mode

Displacement (mm)	Small Bubble	Large Bubble	Tear in Paper	GWB Crack	Pull Through	Total	% Global Connection Failure
0	0	0	2	0	0	2	0%
4	0	0	2	0	0	2	0%
8	0	0	2	0	0	2	0%
12	0	0	2	0	0	2	0%
16	0	0	0	2	1	3	2%
20	0	0	0	2	2	4	3%
24.4	0	0	0	2	3	5	5%
48.8	2	0	0	2	8	12	16%
73.2	2	0	0	2	12	16	22%
105.13	1	0	0	2	22	25	36%

B. Failure Location

Displacement (mm)	Left Stud	Middle Stud	Right Stud	Bottom Plate	Top Plate	Intermediate Studs
0	0	2	0	0	0	0
4	0	2	0	0	0	0
8	0	2	0	0	0	0
12	0	2	0	0	0	0
16	0	2	0	1	0	0
20	0	2	0	1	0	1
24.4	0	2	0	2	0	1
48.8	2	6	1	2	0	1
73.2	2	7	2	3	1	1
105.13	4	8	2	4	6	1

Table C9. Visual Failure Comparison Results from IRCWIN-E

A. Failure Mode

Displacement (mm)	Small Bubble	Large Bubble	Tear in Paper	GWB Crack	Pull Through	Total	% Global Connection Failure
0	0	0	0	0	0	0	0%
4	0	0	0	0	0	0	0%
8	0	0	0	0	1	1	1%
12	0	0	0	0	3	3	4%
16	3	0	2	1	4	10	14%
20	8	0	2	0	7	17	24%
24.4	14	0	1	0	13	28	40%
48.8	2	0	1	0	46	49	70%
73.2	1	0	0	0	57	58	83%
101.99	3	0	0	0	56	59	84%

B. Failure Location

Displacement (mm)	Left Stud	Middle Stud	Right Stud	Bottom Plate	Top Plate	Intermediate Studs
0	0	0	0	0	0	0
4	0	0	0	0	0	0
8	0	1	0	0	0	0
12	0	3	0	0	0	0
16	0	5	3	2	0	0
20	4	5	4	3	1	0
24.4	5	6	7	4	5	1
48.8	7	14	7	10	10	0
73.2	7	21	7	10	10	3
101.99	7	22	7	10	10	3

Table C10. Visual Failure Comparison Results from IRCWIN-M

A. Failure Mode

Displacement (mm)	Small Bubble	Large Bubble	Tear in Paper	GWB Crack	Pull Through	Total	% Global Connection Failure
0	0	0	5	0	0	5	0%
4	0	0	5	0	0	5	0%
8	0	0	6	0	0	6	1%
12	0	0	6	0	0	6	1%
16	2	0	6	0	2	10	7%
20	5	0	4	4	2	15	14%
24.4	14	0	6	4	6	30	36%
48.8	4	0	1	6	36	47	60%
73.2	0	0	0	11	40	51	66%
113.67	0	0	0	0	56	56	73%

B. Failure Location

Displacement (mm)	Left Stud	Middle Stud	Right Stud	Bottom Plate	Top Plate	Intermediate Studs
0	0	5	0	0	0	0
4	0	5	0	0	0	0
8	0	6	0	0	0	0
12	0	6	0	0	0	0
16	1	6	1	2	0	0
20	1	8	2	3	1	0
24.4	4	9	7	7	3	0
48.8	7	14	7	10	9	0
73.2	7	17	7	10	10	0
113.67	7	22	7	10	10	0

Table C11. Visual Failure Comparison Results from 2OSBWIN-M

A. Failure Mode

Displacement (mm)	Small Bubble	Large Bubble	Tear in Paper	GWB Crack	Pull Through	Total	% Global Connection Failure
0	1	0	3	0	0	4	0%
4	1	0	3	0	0	4	0%
8	1	0	3	0	0	4	0%
12	1	0	3	0	0	4	0%
16	1	0	3	0	0	4	0%
20	1	0	3	0	0	4	0%
24.4	1	0	4	0	0	5	1%
48.8	1	0	4	0	4	9	7%
73.2	1	0	3	0	18	22	26%
113.33	0	0	0	0	49	49	64%

B. Failure Location

Displacement (mm)	Left Stud	Middle Stud	Right Stud	Bottom Plate	Top Plate	Intermediate Studs
0	0	4	0	0	0	0
4	0	4	0	0	0	0
8	0	4	0	0	0	0
12	0	4	0	0	0	0
16	0	4	0	0	0	0
20	0	4	0	0	0	0
24.4	0	5	0	0	0	0
48.8	0	5	0	3	1	0
73.2	0	9	3	6	4	0
113.33	6	18	6	9	10	0

Table C12. Visual Failure Comparison Results from 2OSBWIN-E

A. Failure Mode

Displacement (mm)	Small Bubble	Large Bubble	Tear in Paper	GWB Crack	Pull Through	Total	% Global Connection Failure
0	0	0	3	0	0	3	0%
4	0	0	3	0	0	3	0%
8	0	0	3	0	0	3	0%
12	0	0	3	0	0	3	0%
16	0	0	3	0	0	3	0%
20	0	0	3	0	1	4	1%
24.4	0	0	3	0	1	4	1%
48.8	0	0	3	0	5	8	7%
73.2	0	0	2	0	8	10	10%
122.00	0	0	1	0	30	31	40%

B. Failure Location

Displacement (mm)	Left Stud	Middle Stud	Right Stud	Bottom Plate	Top Plate	Intermediate Studs
0	0	2	0	1	0	0
4	0	2	0	1	0	0
8	0	2	0	1	0	0
12	0	2	0	1	0	0
16	0	2	0	1	0	0
20	1	2	0	1	0	0
24.4	1	2	0	1	0	0
48.8	1	4	0	2	1	0
73.2	2	4	1	2	1	0
122.00	6	9	6	4	6	0

Table C13. Visual Failure Comparison Results from 4PNLWIN-E

A. Failure Mode

Displacement (mm)	Small Bubble	Large Bubble	Tear in Paper	GWB Crack	Pull Through	Total	% Global Connection Failure
0	0	0	0	0	2	2	0%
4	0	0	0	0	2	2	0%
8	0	0	0	0	3	3	1%
12	0	0	0	1	3	4	3%
16	0	0	0	1	4	5	4%
20	0	0	0	1	5	6	6%
24.4	0	0	0	1	7	8	8%
48.8	8	0	0	1	35	44	58%
73.2	5	0	0	1	54	60	81%
112.59	0	0	0	0	70	70	94%

B. Failure Location

Displacement (mm)	Left Stud	Middle Stud	Right Stud	Bottom Plate	Top Plate	Intermediate Studs
0	0	0	0	0	2	0
4	0	0	0	0	2	0
8	0	1	0	0	2	0
12	0	1	0	1	2	0
16	0	1	0	1	3	0
20	0	2	0	1	3	0
24.4	0	2	1	1	3	1
48.8	6	8	6	9	8	7
73.2	7	10	7	11	8	17
112.59	7	14	7	11	11	20

Table C14. Visual Failure Comparison Results from 4PNLWIN-M

A. Failure Mode

Displacement (mm)	Small Bubble	Large Bubble	Tear in Paper	GWB Crack	Pull Through	Total	% Global Connection Failure
0	0	0	0	1	0	1	0%
4	0	0	0	1	0	1	0%
8	1	0	0	1	0	2	1%
12	1	0	0	1	0	2	1%
16	1	0	0	1	0	2	1%
20	4	0	0	1	0	5	6%
24.4	10	0	2	2	5	19	25%
48.8	23	0	1	5	27	56	76%
73.2	0	0	0	0	66	66	90%
112.59	0	0	0	0	67	67	92%

B. Failure Location

Displacement (mm)	Left Stud	Middle Stud	Right Stud	Bottom Plate	Top Plate	Intermediate Studs
0	0	1	0	0	0	0
4	0	1	0	0	0	0
8	0	1	0	0	0	1
12	0	1	0	0	0	1
16	0	1	0	0	0	1
20	0	1	3	0	0	1
24.4	0	4	6	4	1	4
48.8	5	10	7	11	8	15
73.2	7	11	7	11	11	20
112.59	7	11	7	11	11	20

Appendix D: Displacement Sensor Configuration and Calibration

A picture of the instrumentation panel is shown in Figure D1 and a schematic is shown in Figure D2. Each of these panels contained the displacement sensors which measured the relative displacements discussed in Appendix E. Because only two of the panels could be manufactured, each was attached to one side of the shear wall according to the test setup. For each shear wall design, one shear wall sample had the panels attached to the end stud and one had the panels attached to the middle stud. The locations of these panel attachments are shown in Figure D3.

All displacement sensors were calibrated before use in the relative displacement measurements. The spring return linear position sensors used as displacement sensors in this study employ a variable resistor which alters the output voltage according to the position of the sensor. A five volt power source was imputed into the sensor and the output voltage was measured. The change in voltage corresponded to a change in position, or a displacement.

To calibrate these sensors, a mechanical position gauge was used to displace the sensor such that the output voltage changed between zero and five volts. The output voltage was measured at 20 known displacements and linear regression was used to fit a trendline to the data. The coefficient in the equation of this trendline could be used determine a displacement from a change in voltage. Figure D4 displays this calibration in graphical form. The sensor output for the given imposed displacements is shown by the sensor output series. As expected, this is very linear. The linear trendline shows the agreement between the sensor output and a linear regression analysis. This analysis was performed for all sensors, and the maximum error for each sensor is shown in Table D1. Sensor 1 broke during installment of the panels on test IRCWIN-M and was replaced with Sensor 1* for IRCWIN-M, 2OSBWIN-E, 2OSBWIN-M, 4PNLWIN-E and 4PNLWIN-M. Sensor 4 broke during installment of the panels on test 4PNLWIN-M and was replaced with Sensor 4*.

The maximum error of all sensors was measured as 0.134 mm. This is 1.06% of the entire range of the sensors which is 12.7 mm. This error was deemed acceptable for this study.

Figure D1. Instrumentation Panel

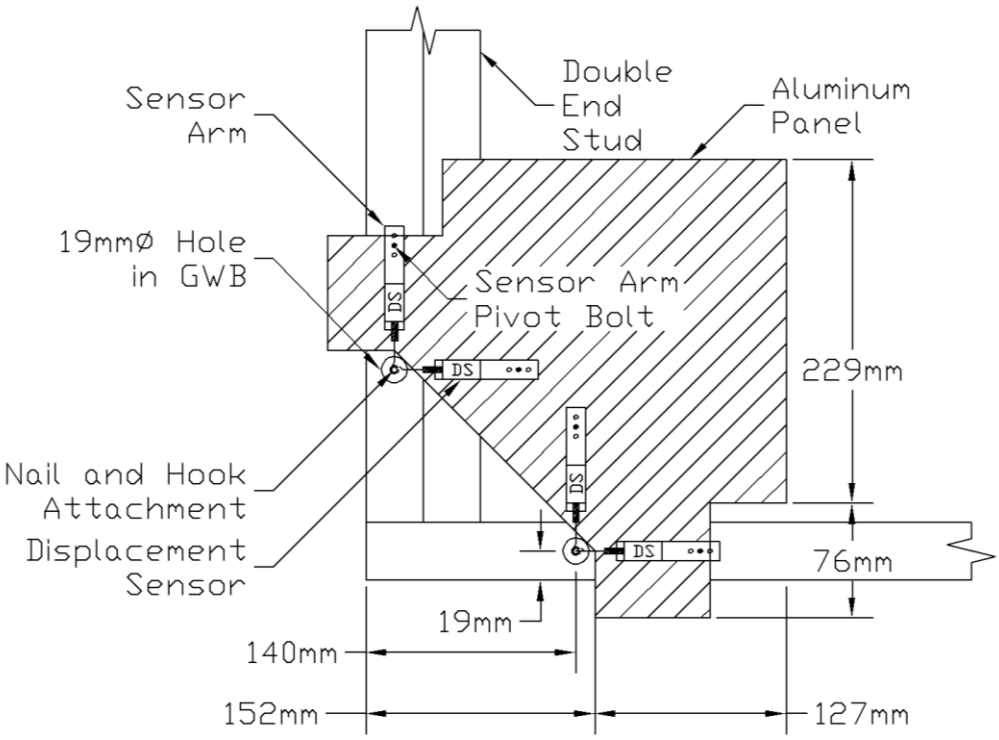

Figure D2. Displacement Sensor Schematic

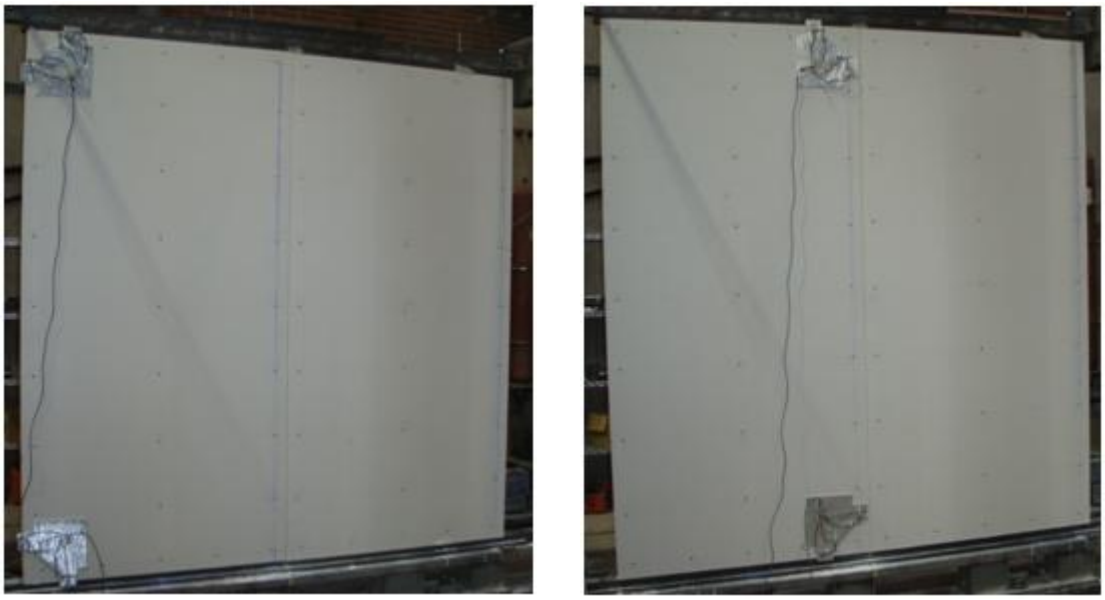

End Stud Setup **Middle Stud Setup**

Figure D3. Instrumentation Setups

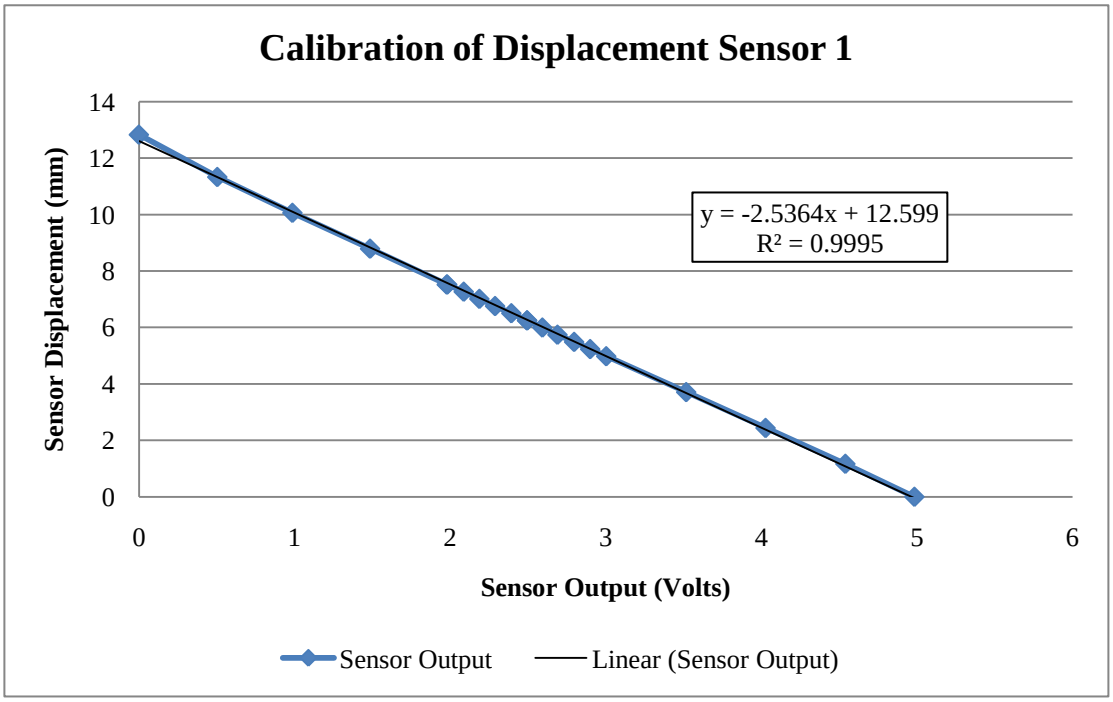

Figure D4. Displacement Sensor 1 Calibration Summary

Table D1. Maximum Displacement Sensor Error Summary

Sensor	Maximum Error (mm)
1	0.070
2	0.031
3	0.037
4	0.038
5	0.041
6	0.041
7	0.036
8	0.076
1*	0.058
4*	0.134
Maximum	0.134

* Indicates a new sensor replaced the previous sensor at the same location

Appendix E: Shear Wall Test Raw Data

The raw data for all shear wall tests are presented in this appendix. Figure E1 shows the displacement sensors locations and the names of the paired perpendicular displacement sensors. The extension and contraction data from these sensors are presented as data from each panel in Figures E2-15. The upper measurement is from the panel which was attached to the top plate and studs and includes sensor names which begin with 5, 6, 7 and 8. The lower measurement is from the panel which was attached to the bottom plate and studs which includes sensors which begin with 1, 2, 3 and 4. The locations of the graphs on the page correspond to the physical locations of the panels when tested i.e. the upper measurement for a "–M" wall test would be in the upper right corner of the page.

The sign notation for the displacement data is contraction of the sensor is positive, while extension is negative. The local displacement on the y-axis shows how much the sensor contracted or extended in relation to the global displacement of the entire wall by the hydraulic actuator, which is shown on the x-axis. The movement of the sensor in relation to a global coordinate system is described in Appendix G and uses this extension and contraction data along with the location and orientation of each sensor to calculate a displacement vector.

The load displacement curves for each wall test are also shown in Figures E2-15. Each displacement stop can be seen by each wall unloading some degree during the visual inspection, and reloading as displacement was again applied. Walls were loaded until a clear maximum load was reached or the limits of the hydraulic actuator were reached.

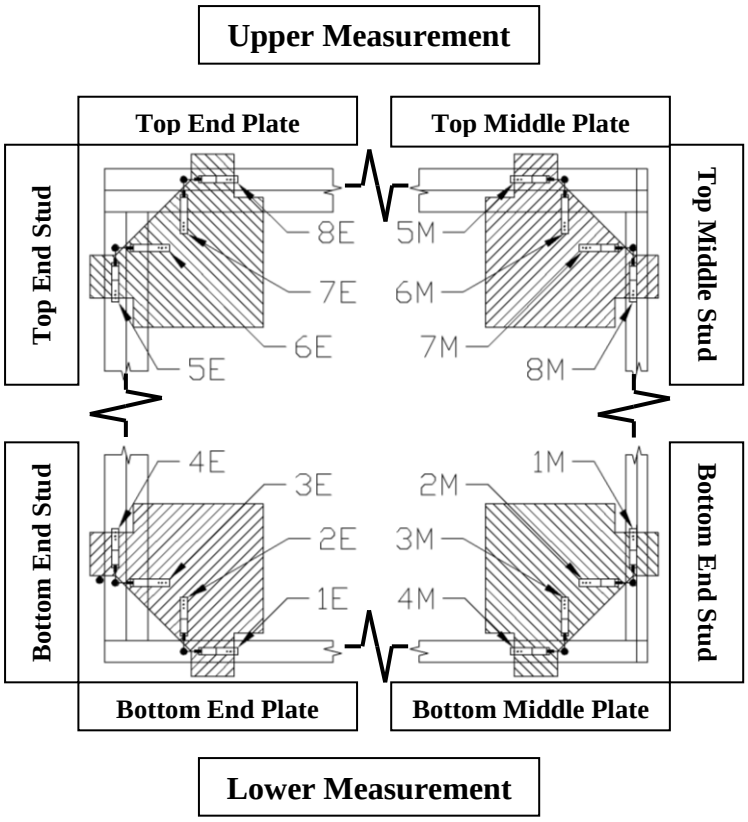

Figure E1. Displacement Sensor Locations

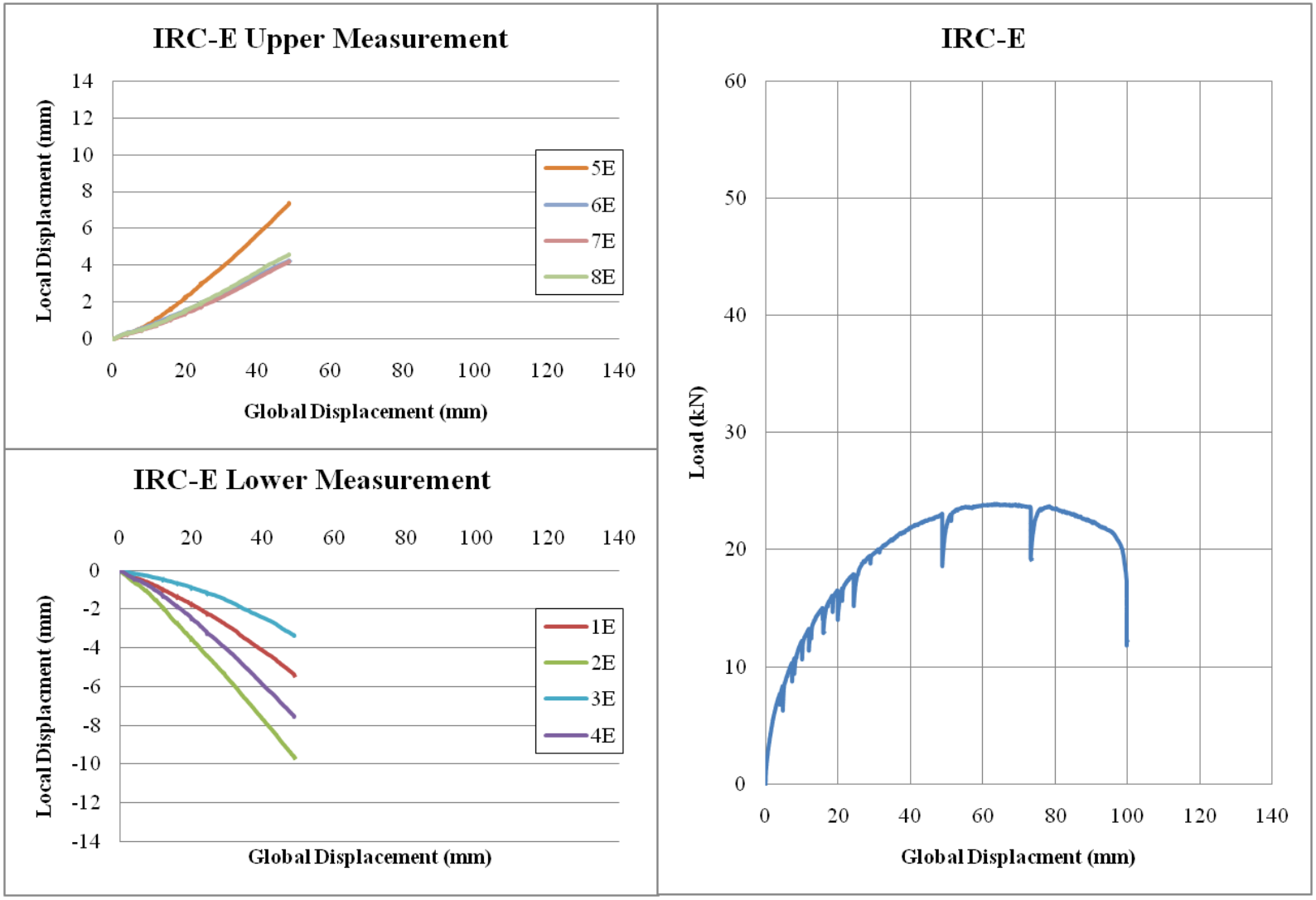

Figure E2. IRC-E Displacement Sensor and Load Displacement Curve Raw Data

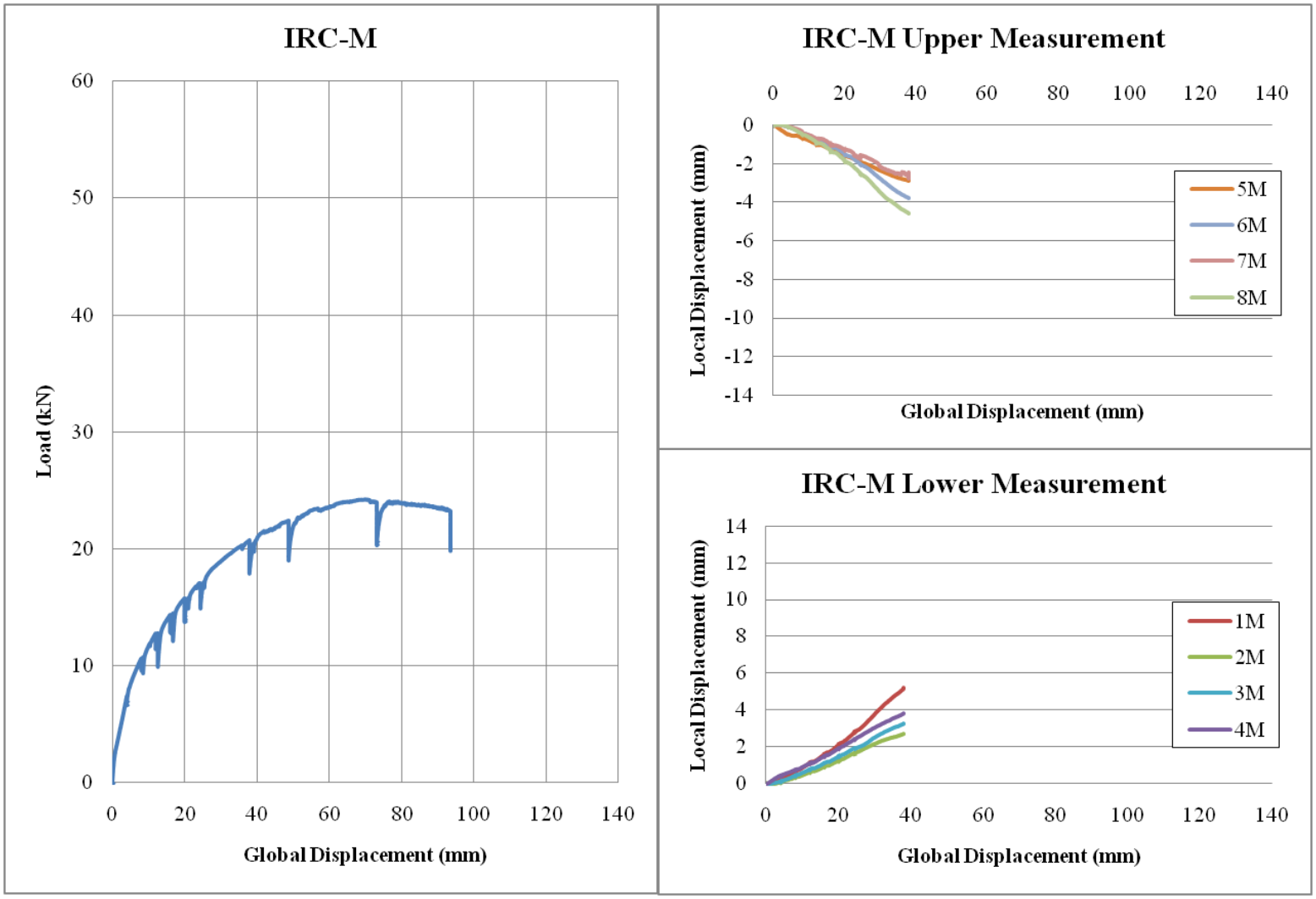

Figure E3. IRC-M Displacement Sensor and Load Displacement Curve Raw Data

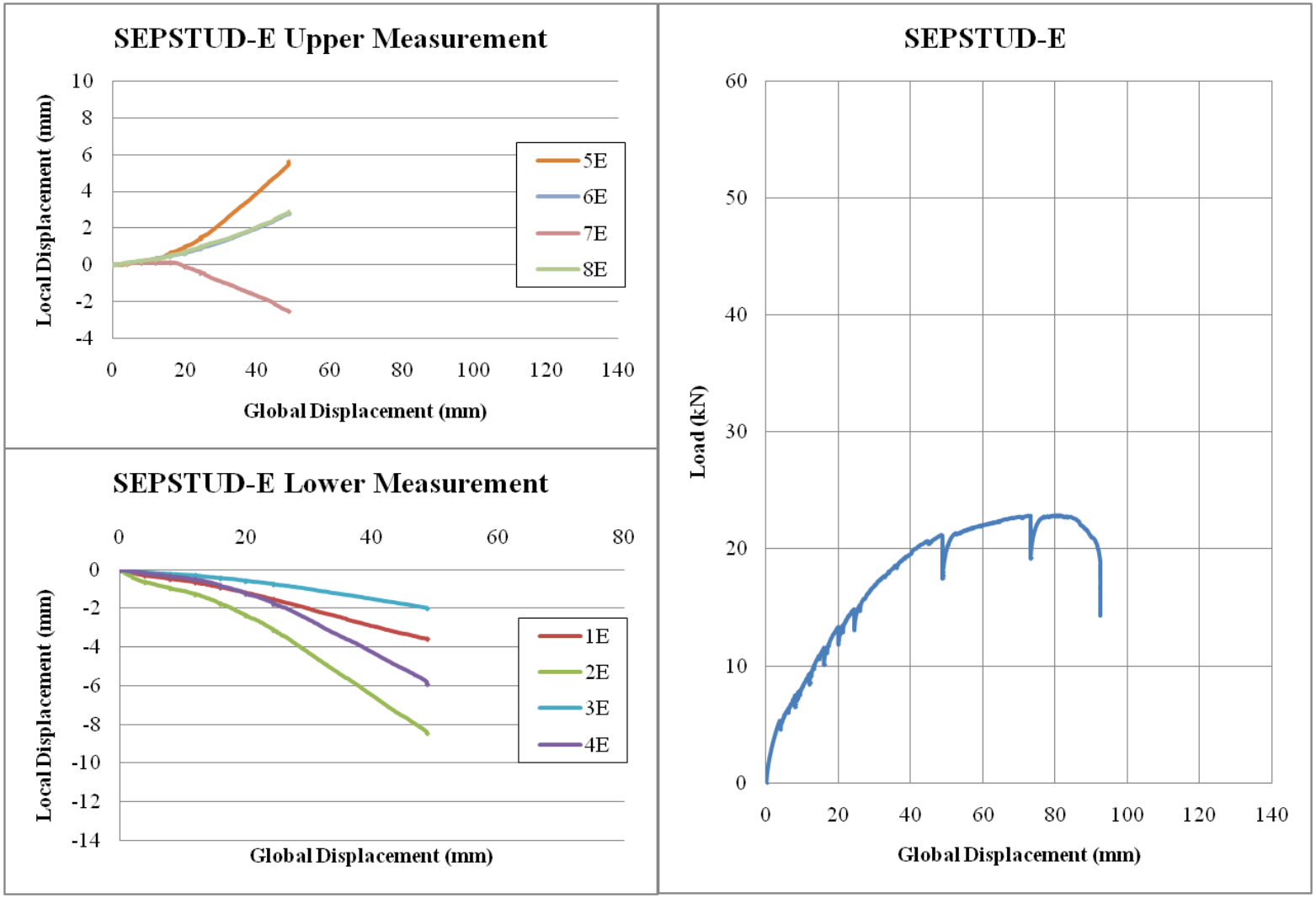

Figure E4. SEPSTUD-E Displacement Sensor and Load Displacement Curve Raw Data

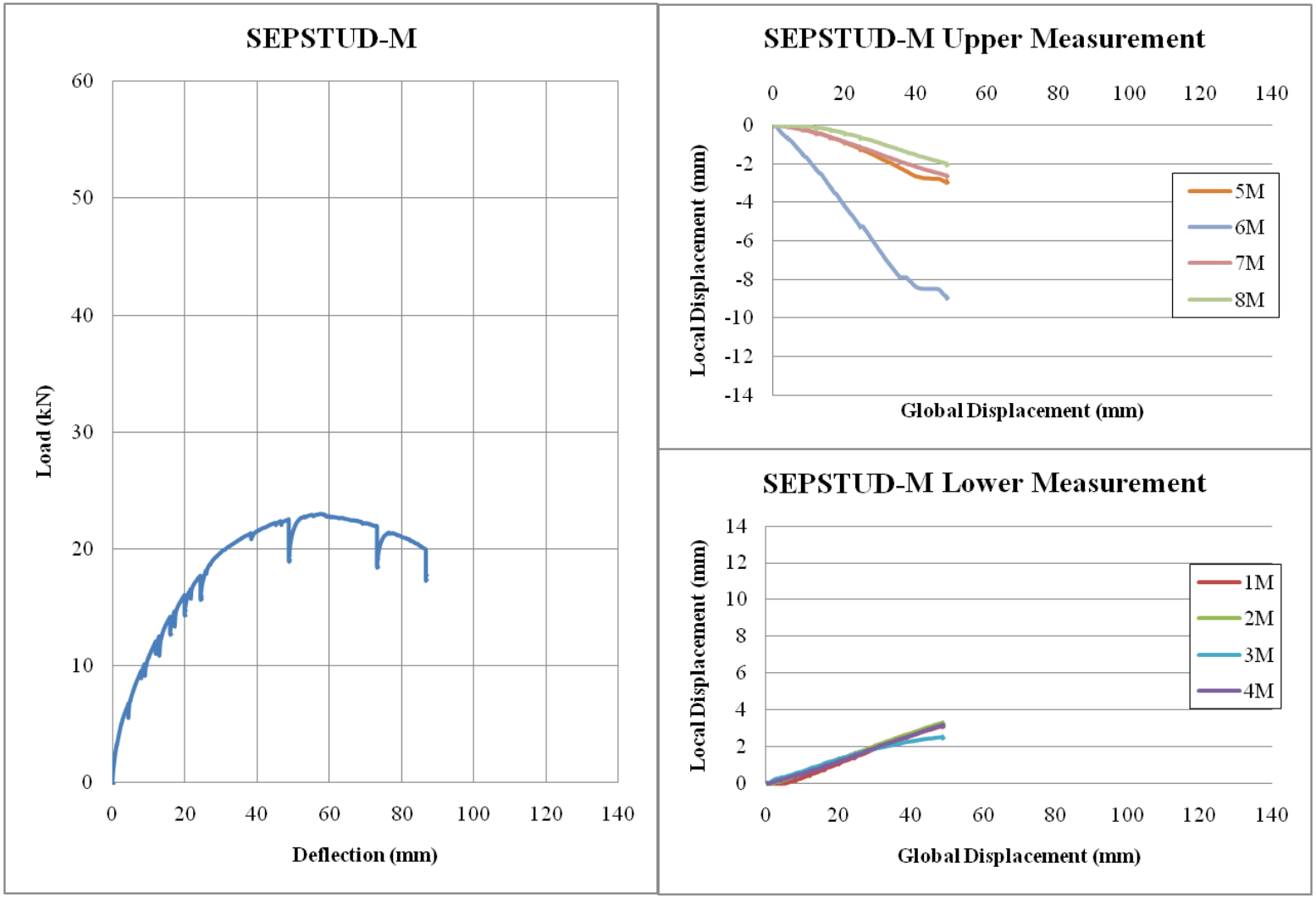

Figure E5. SEPSTUD-M Displacement Sensor and Load Displacement Curve Raw Data

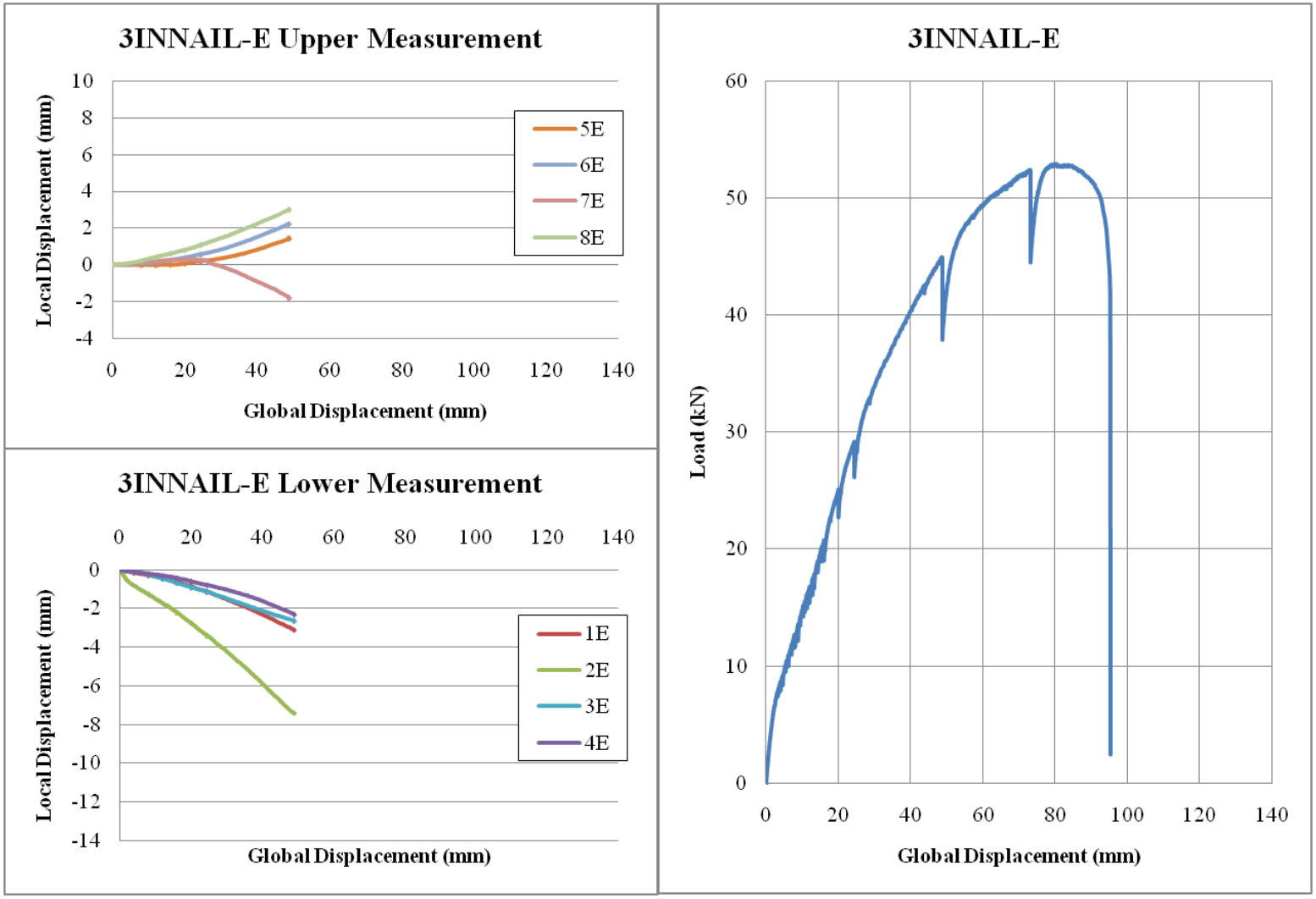

Figure E6. 3INNAIL-E Displacement Sensor and Load Displacement Curve Raw Data

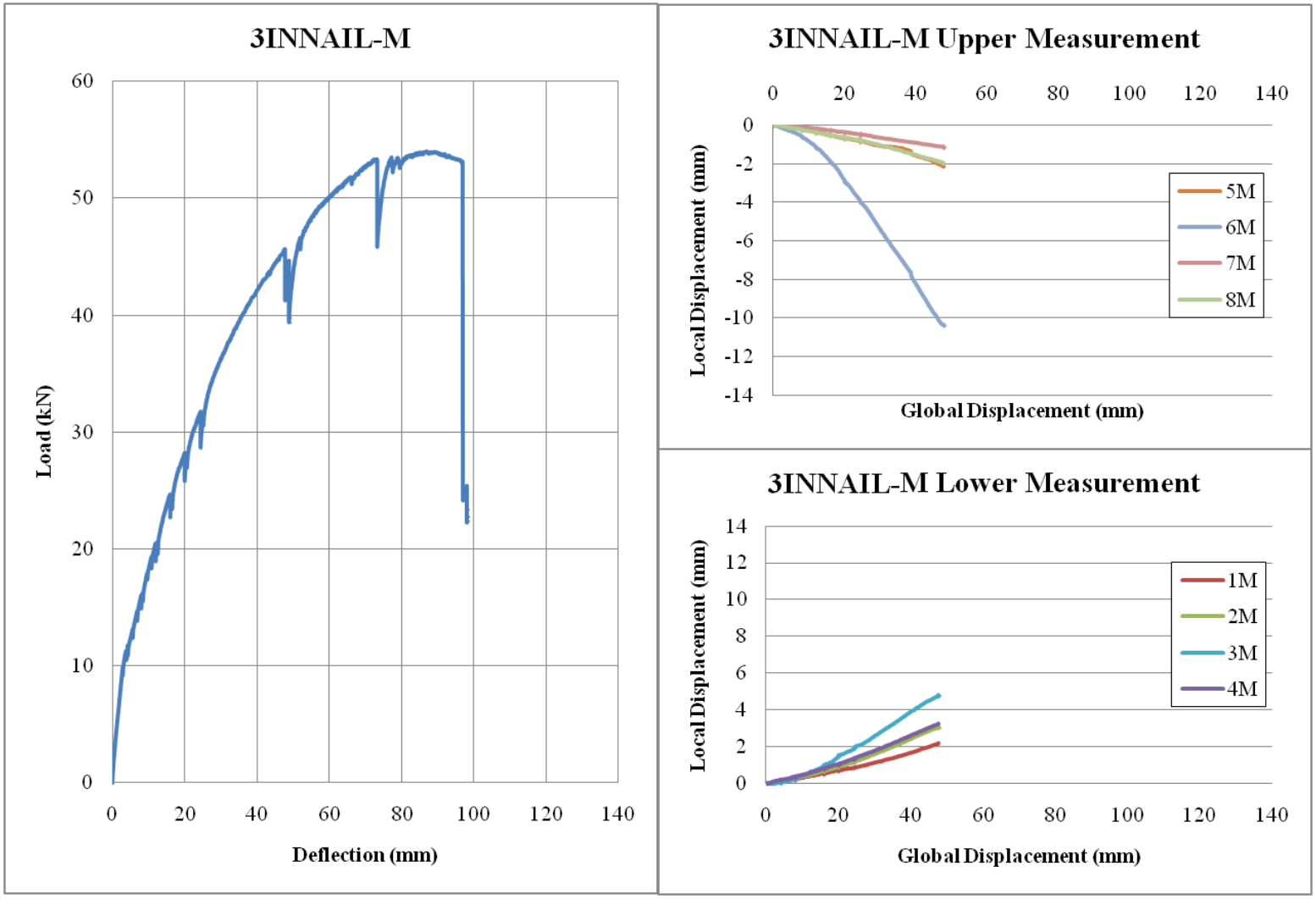

Figure E7. 3INNAIL-M Displacement Sensor and Load Displacement Curve Raw Data

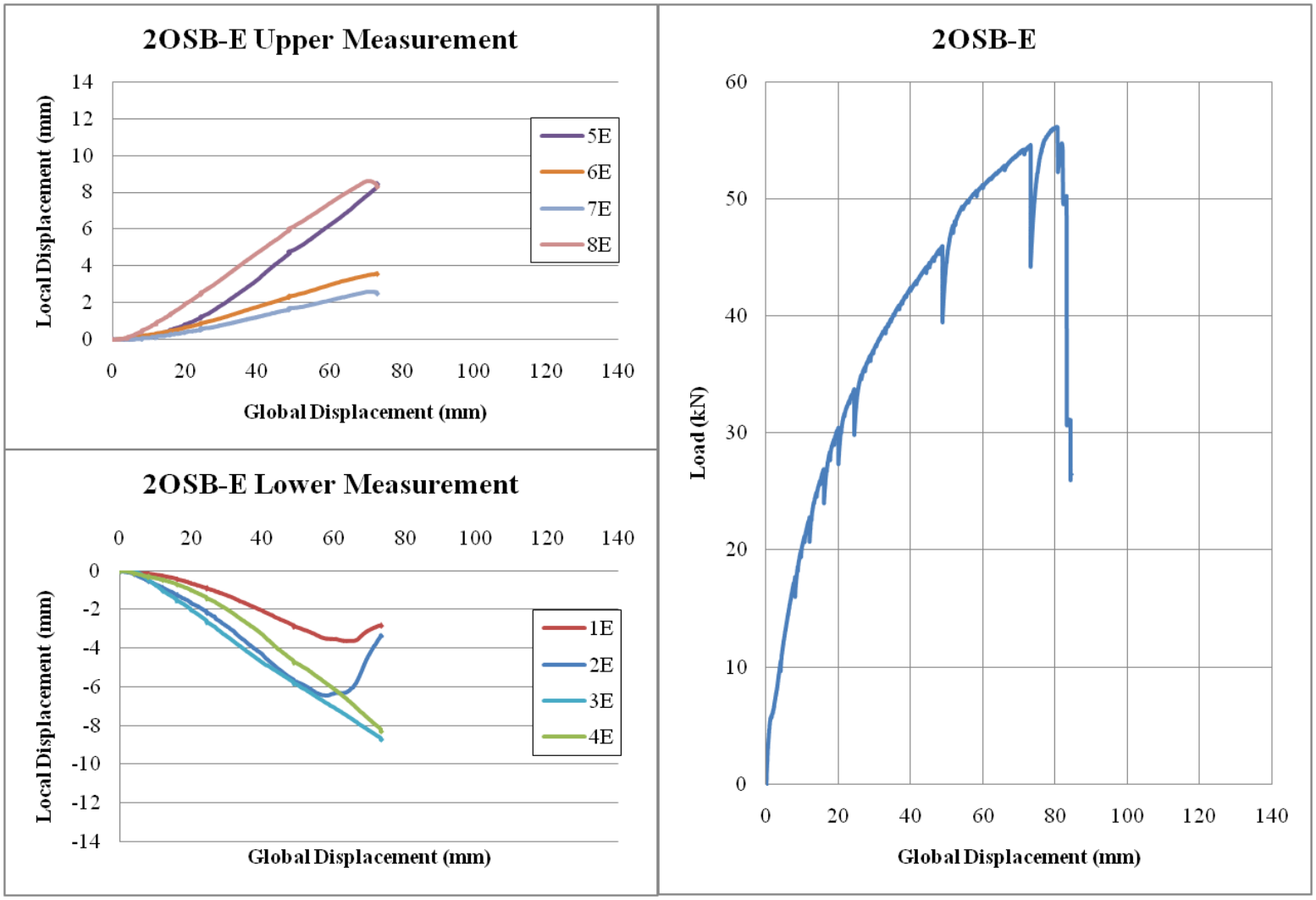

Figure E8. 2OSB-E Displacement Sensor and Load Displacement Curve Raw Data

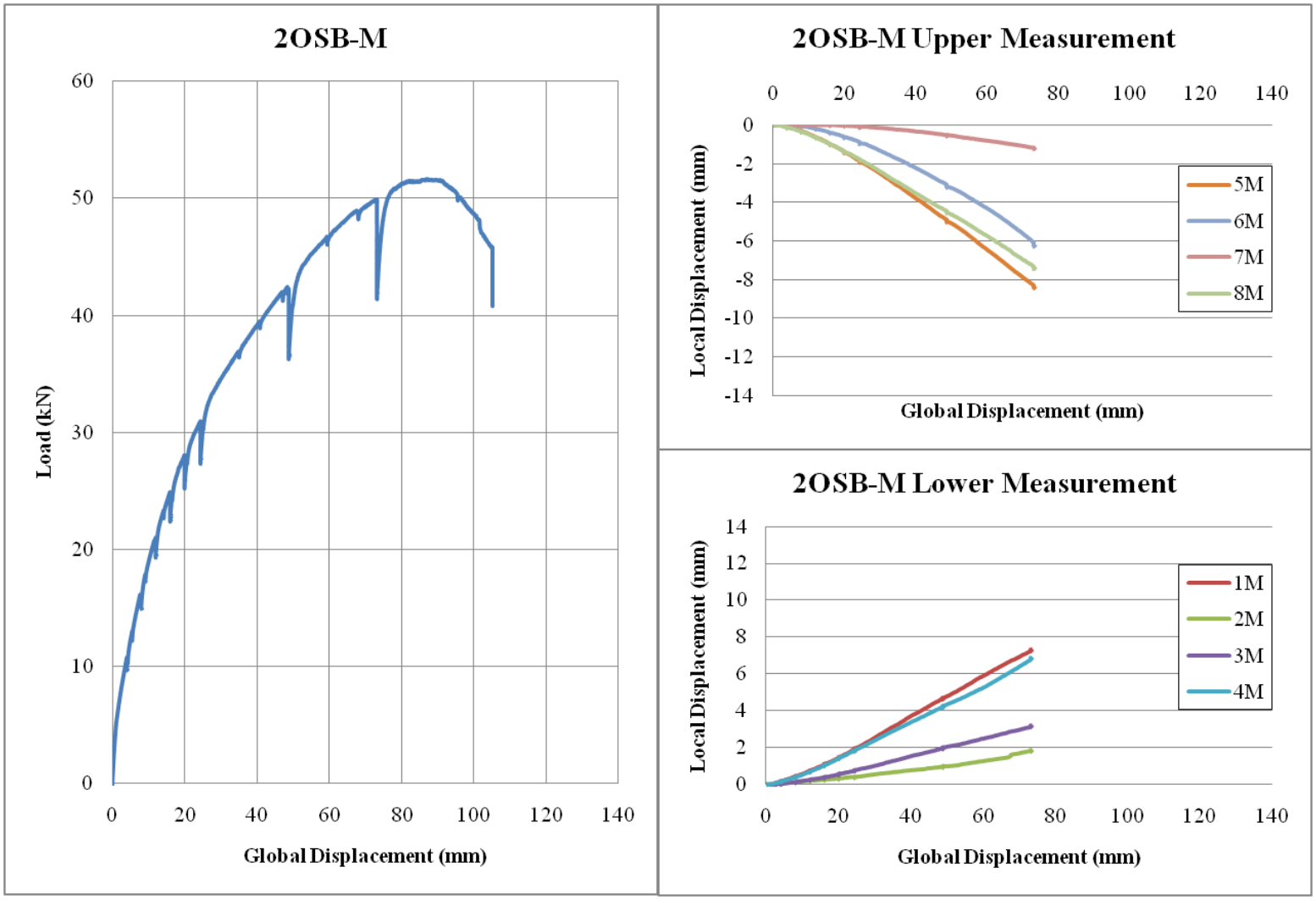

Figure E9. 2OSB-M Displacement Sensor and Load Displacement Curve Raw Data

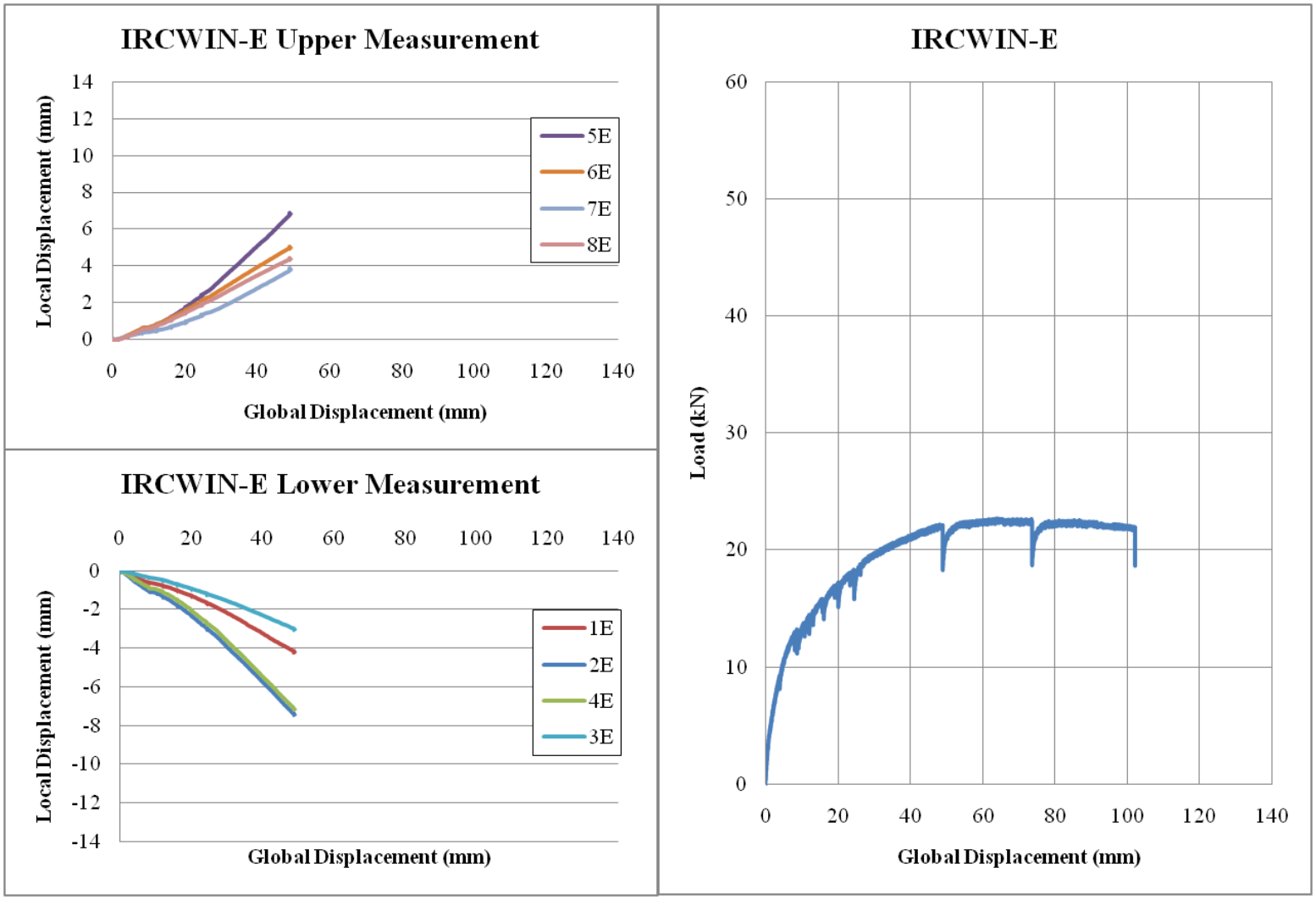

Figure E10. IRCWIN-E Displacement Sensor and Load Displacement Curve Raw Data

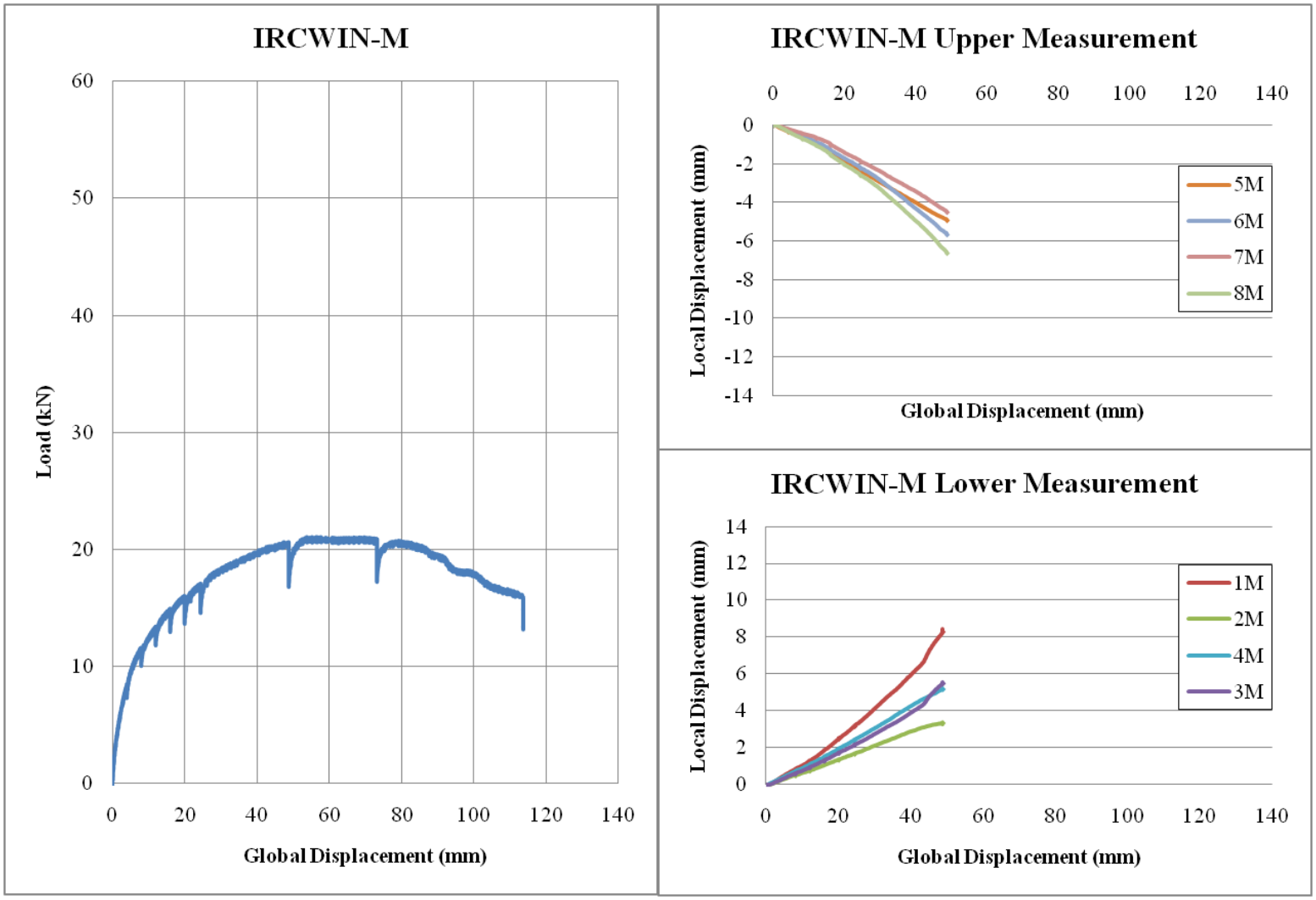

Figure E11. IRCWIN-M Displacement Sensor and Load Displacement Curve Raw Data

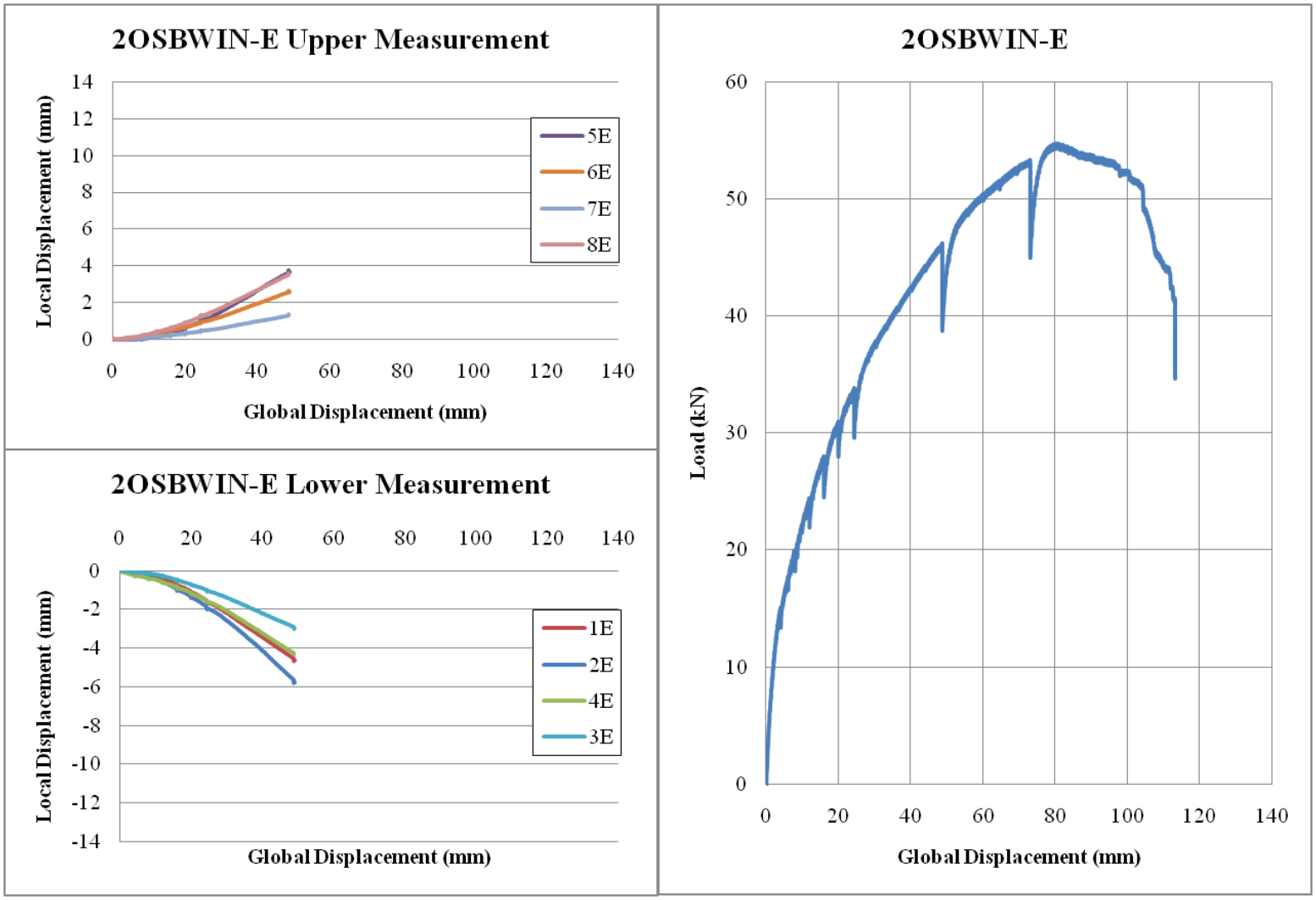

Figure E12. 2OSBWIN-E Displacement Sensor and Load Displacement Curve Raw Data

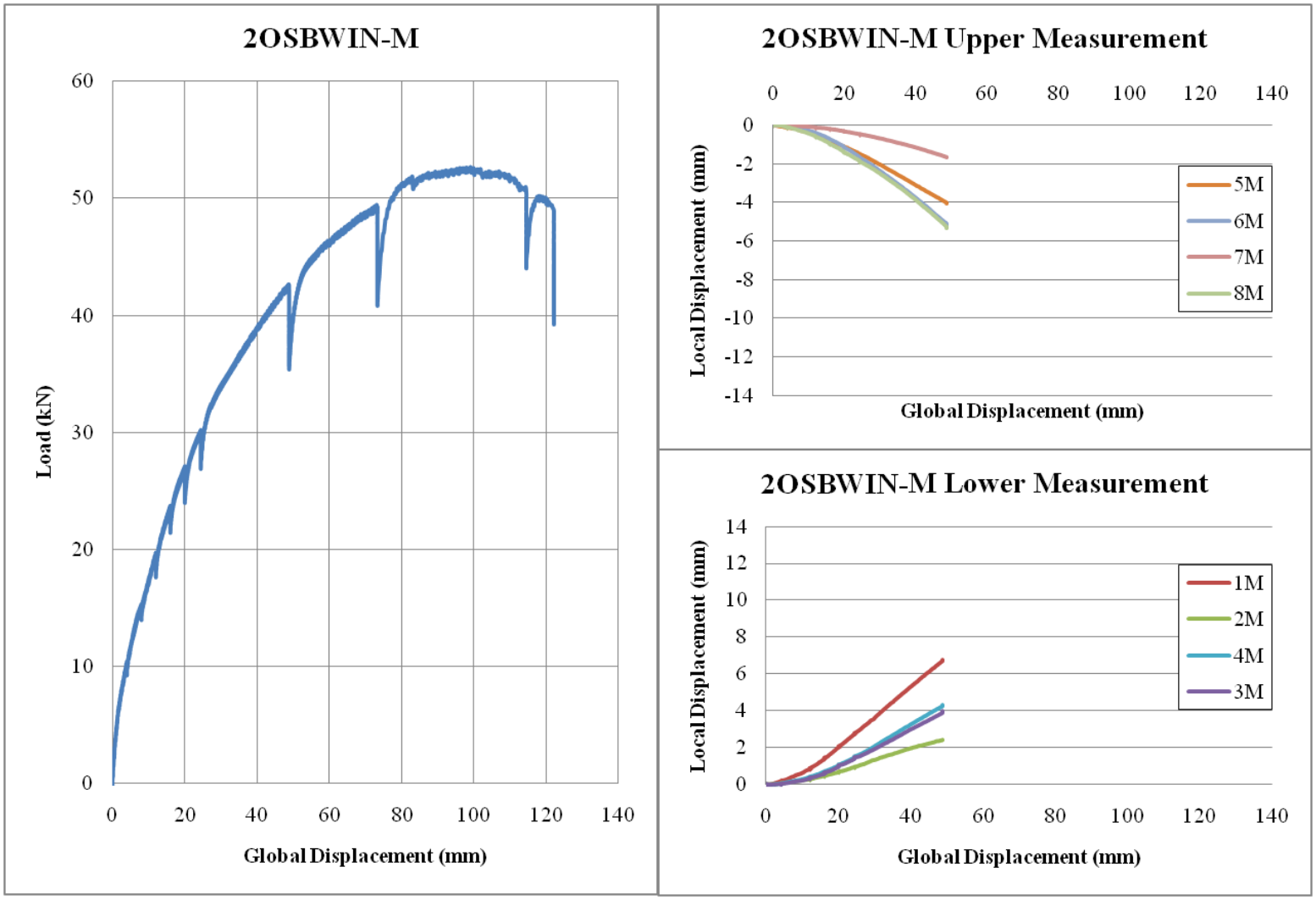

Figure E13. 2OSBWIN-M Displacement Sensor and Load Displacement Curve Raw Data

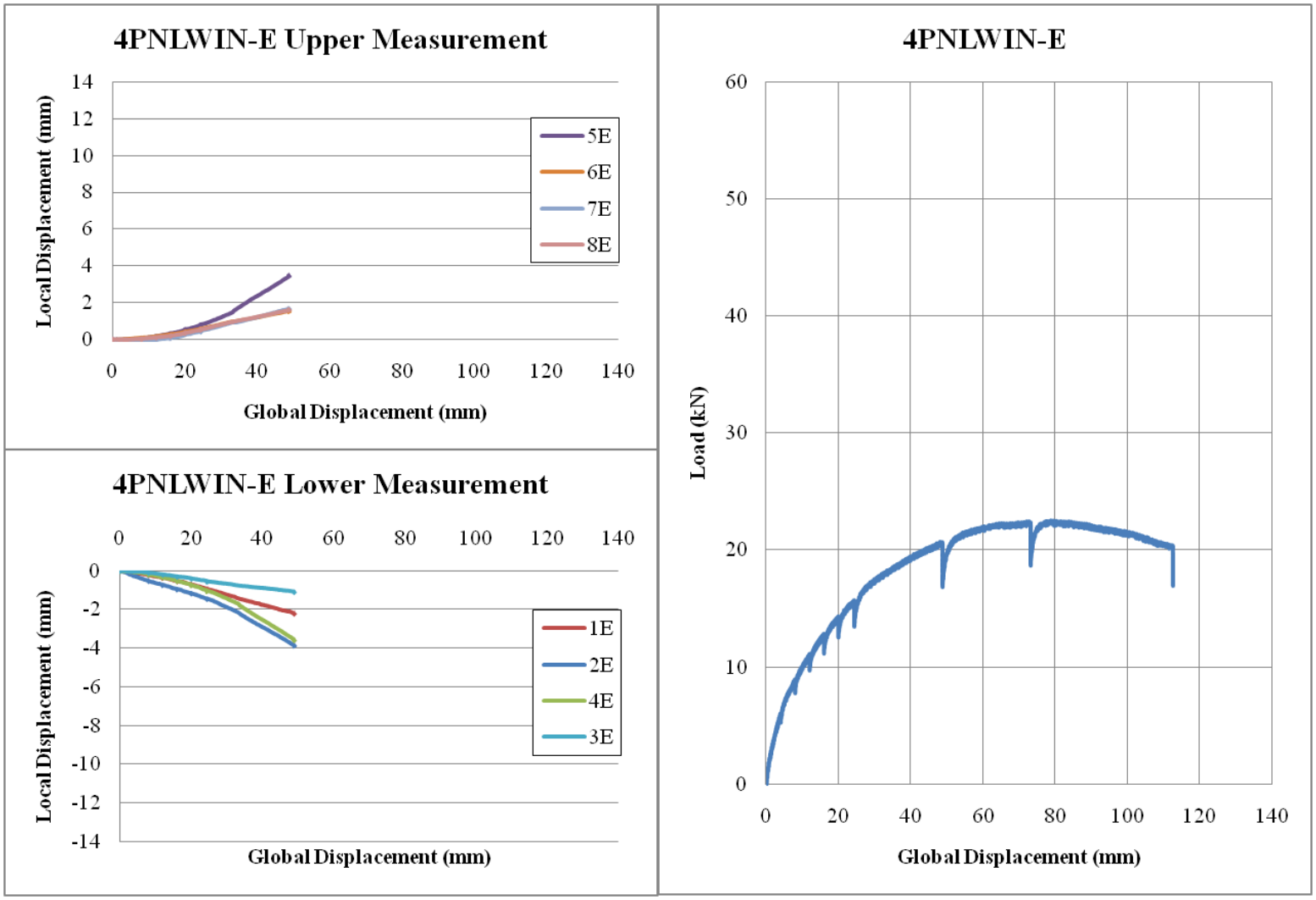

Figure E14. 4PNLWIN-E Displacement Sensor and Load Displacement Curve Raw Data

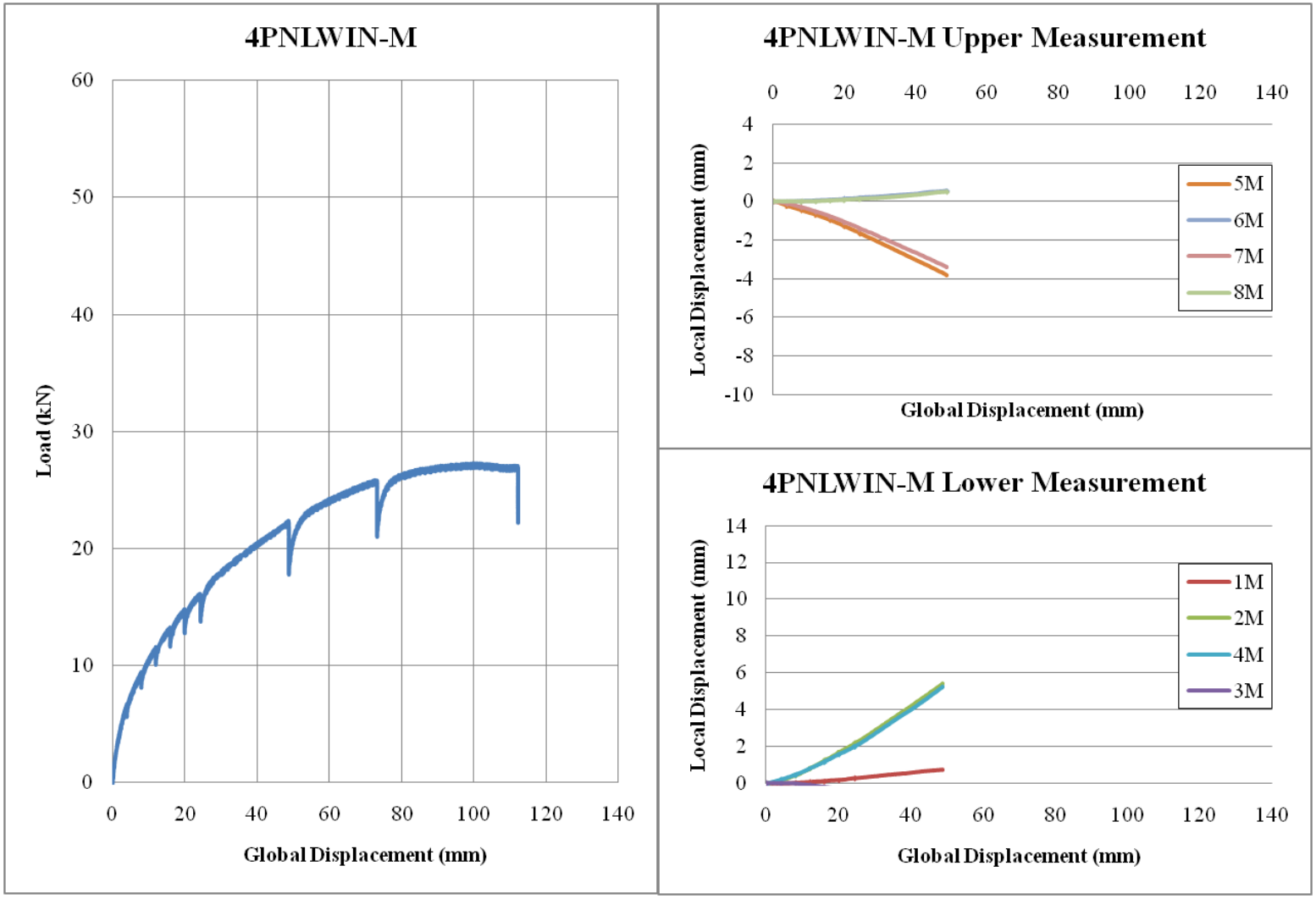

Figure E15. 4PNLWIN-M Displacement Sensor and Load Displacement Curve Raw Data

Appendix F: Shear Wall Backbone Curves

The load displacement backbone curves of all shear wall tests are shown in this appendix. The data points taken during the visual inspections were removed in these plots. As shown in Appendix E, each raw data load displacement curve contained an unloading and reloading section of the graph at each displacement stop. This section of the graph was removed in these backbone curves to represent behavior of the wall if these displacement stops were not included in the test.

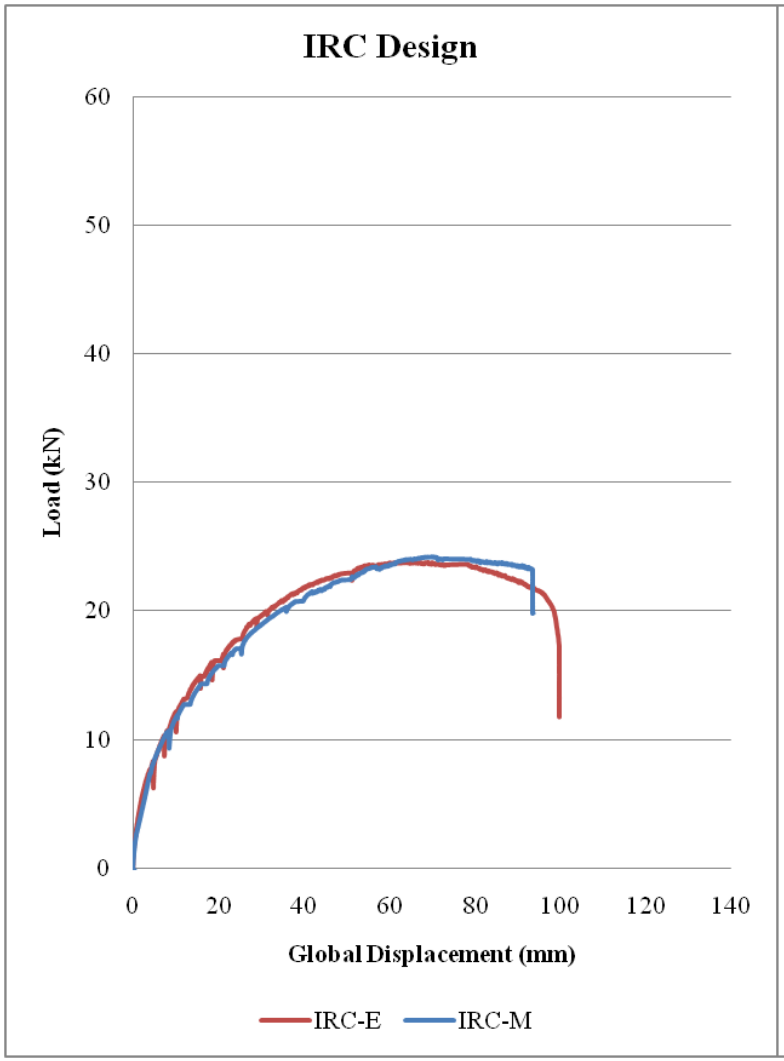

Figure F1. IRC Design Backbone Curves

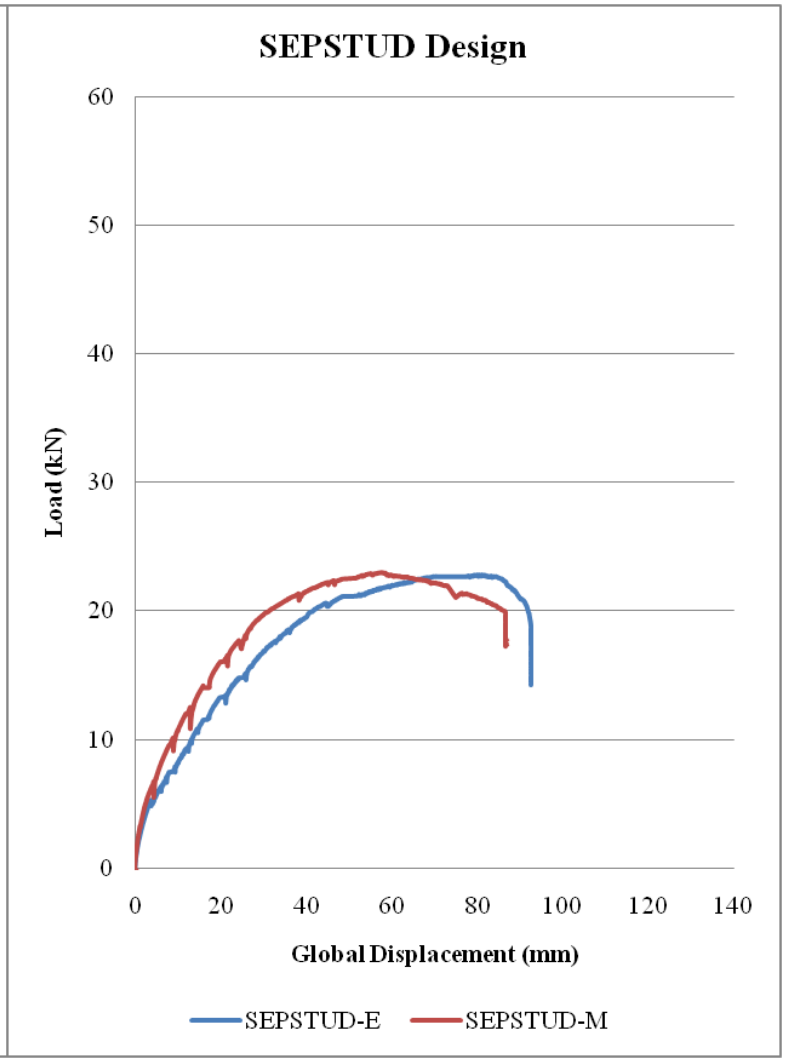

Figure F2. SEPSTUD Design Backbone Curves

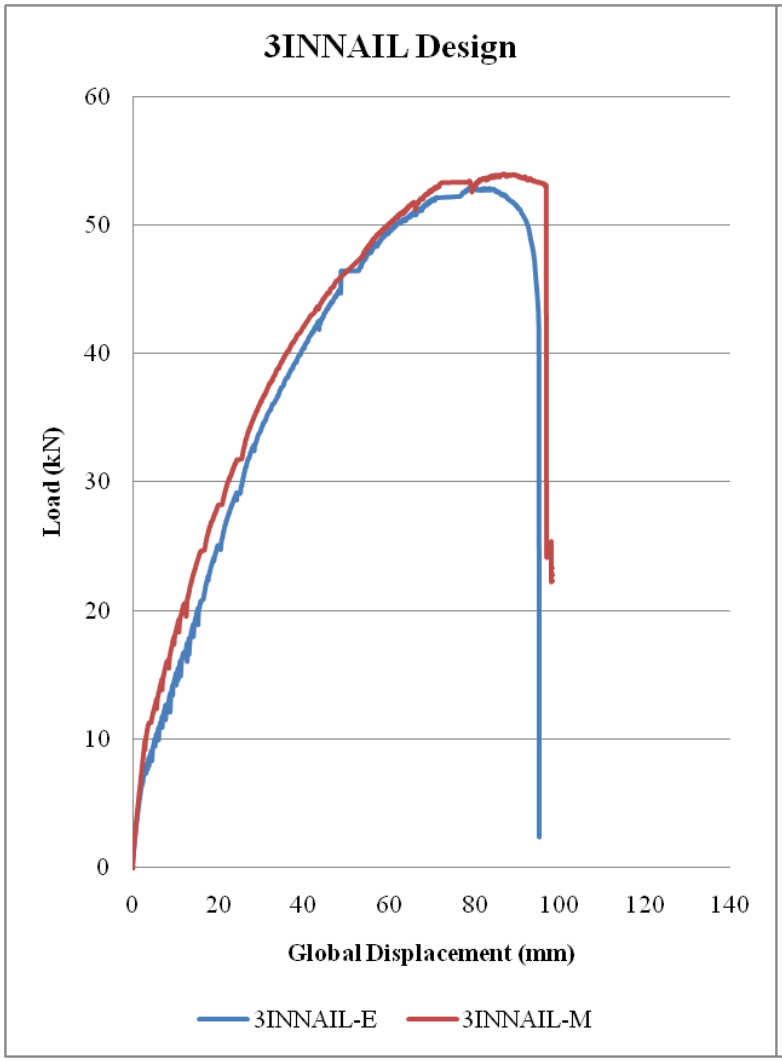

Figure F3. 3INNAIL Design Backbone Curves

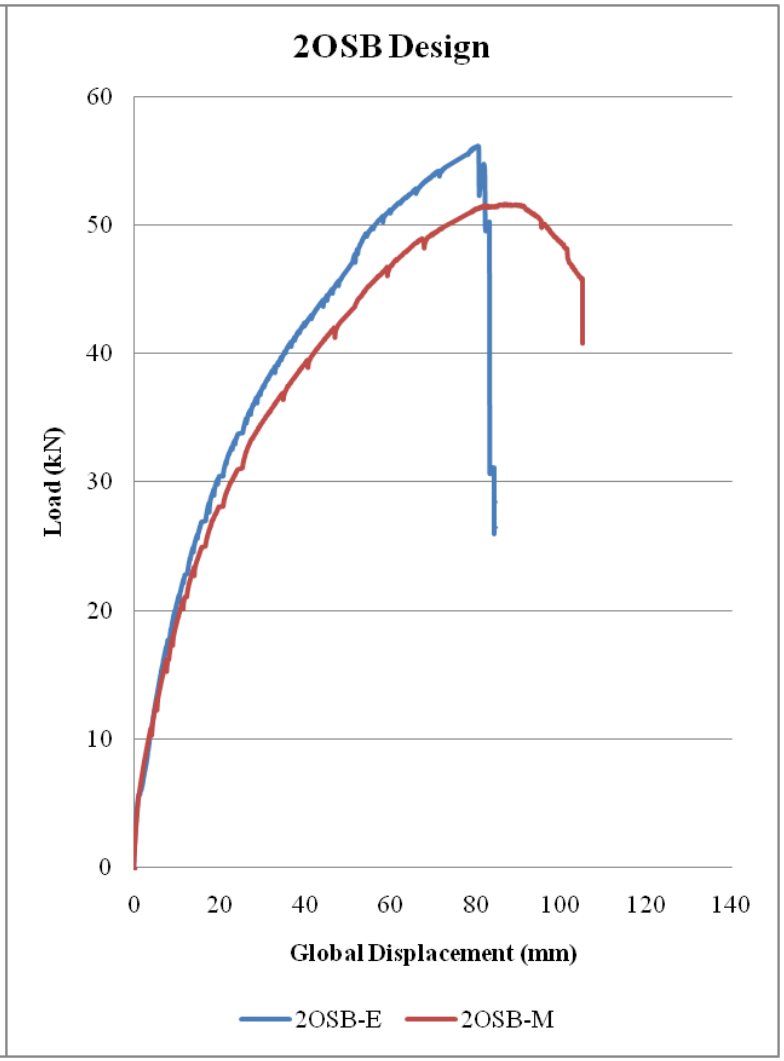

Figure F4: 2OSB Design Backbone Curves

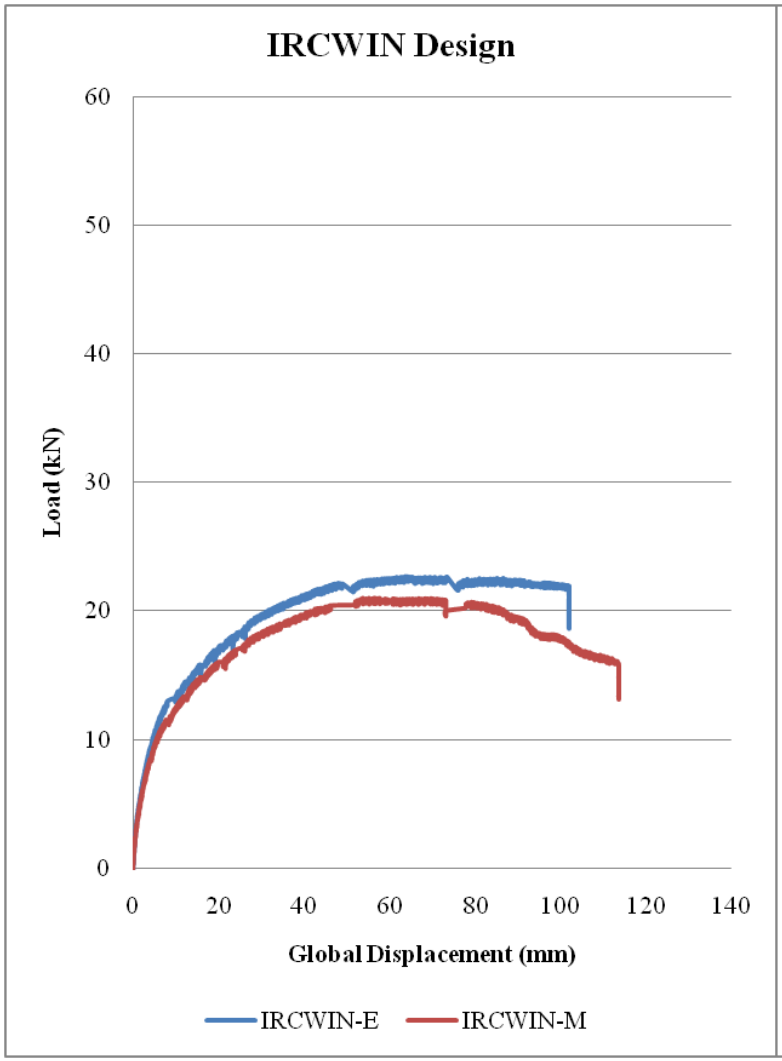

Figure F5. IRCWIN Design Backbone Curves

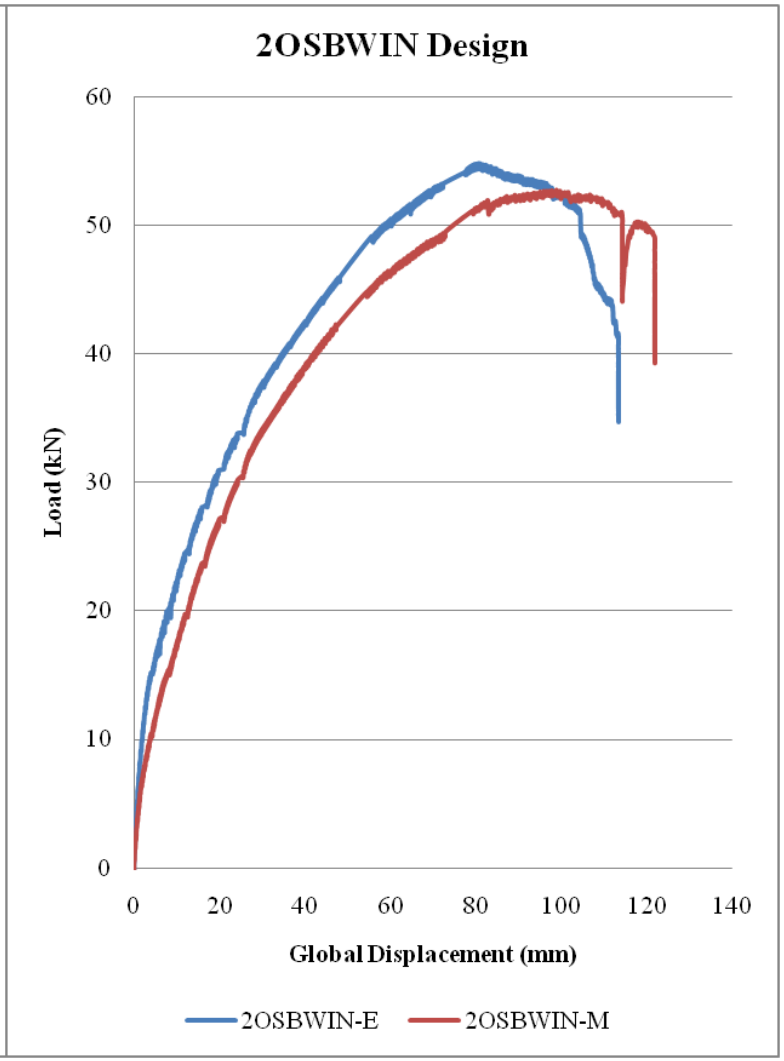

Figure F6: 2OSBWIN Design Backbone Curves

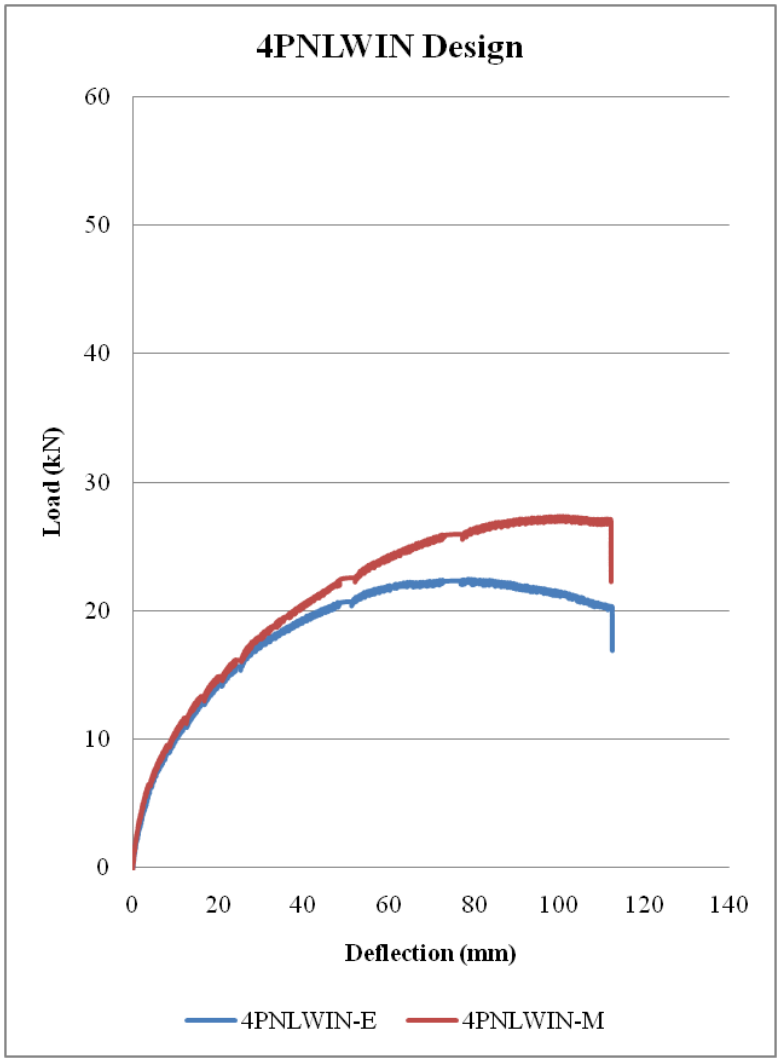

Figure F7. 4PNLWIN Design Backbone Curves

Appendix G: Sensor Vectors and Angles

The displacement sensor data from all wall tests is presented in this appendix. Using the sensor location, orientation and extension or contraction data the relative motion of the sensors and the GWB to the wood studs could be calculated. These relative displacements were calculated using a fixed coordinate system with the origin at the base of the uplift stud as shown in Figures G1 and G2. The positive x axis points in the direction of the applied displacement while the positive y axis points upward.

Figure G1 shows names and the directions of all displacement sensors and vectors in reference to this coordinate system for all wall designs except 4PNLWIN. The magnitudes of the vectors are not presented in this figure and the vector directions only show the quadrant which the angle lies in. For all of these wall tests, sensor 7E moved in the positive x direction initially. However, for SEPSTUD and 3INNAIL, sensor 7E changed direction to the negative x direction at 19.2 mm and 28.5 mm respectively, which is indicated by the asterisk '*' by 7E. This in turn caused the vector angle to become larger than 180°. All other vectors and displacement directions are consistent within all designs except 4PNLWIN.

Figure G2 shows the names and directions of all displacement sensors and vectors for wall design 4PNLWIN. The sensors and vector directions are the same for 4PNLWIN as other designs on the end stud, but different on the middle stud. This is because the sensors were placed in the middle of the GWB panel instead of the edges, resulting in different sensor and vector directions.

Figures G3-G30 display the magnitudes of all displacement sensors and vectors along with the direction of the resultant vector for all wall designs. These displacement graphs for each pair of sensors show the local displacement of the sensors along with the magnitude of their resulting vector in relation to the global displacement of the entire wall by the actuator. These resulting vector magnitudes were determined by taking the sum of the squares of each sensor local displacement. The vector angle graphs show the angle of the vector taken counterclockwise from the positive x direction in relation to the global displacement of the entire wall by the actuator. This vector angle was not recorded for global displacements below 4 mm. This was because the very small local displacements below 4 mm of global displacement gave extremely variable angles which were not representative of actual behavior.

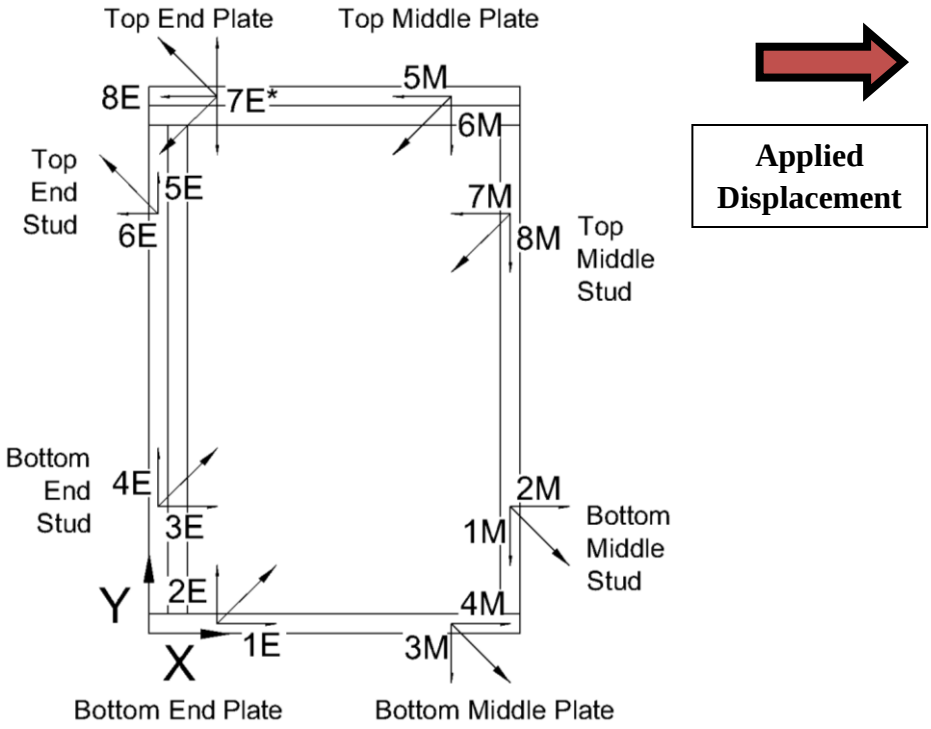

Figure G1. Sensor and Vector Directions for Shear Walls besides 4PNLWIN

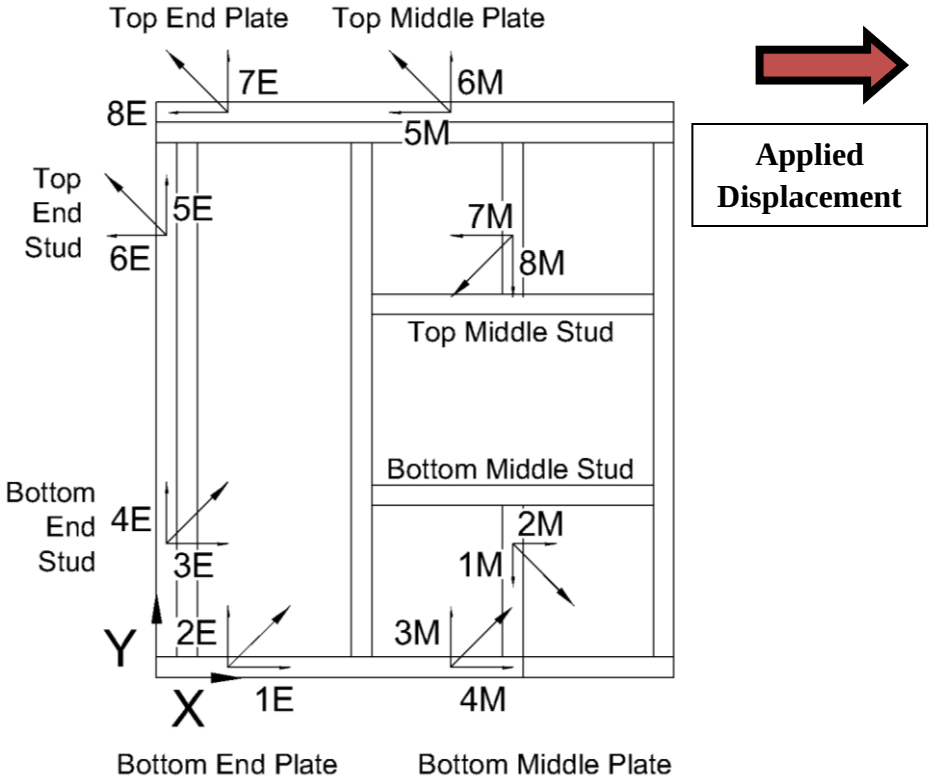

Figure G2. Sensor and Vector Directions for 4PNLWIN

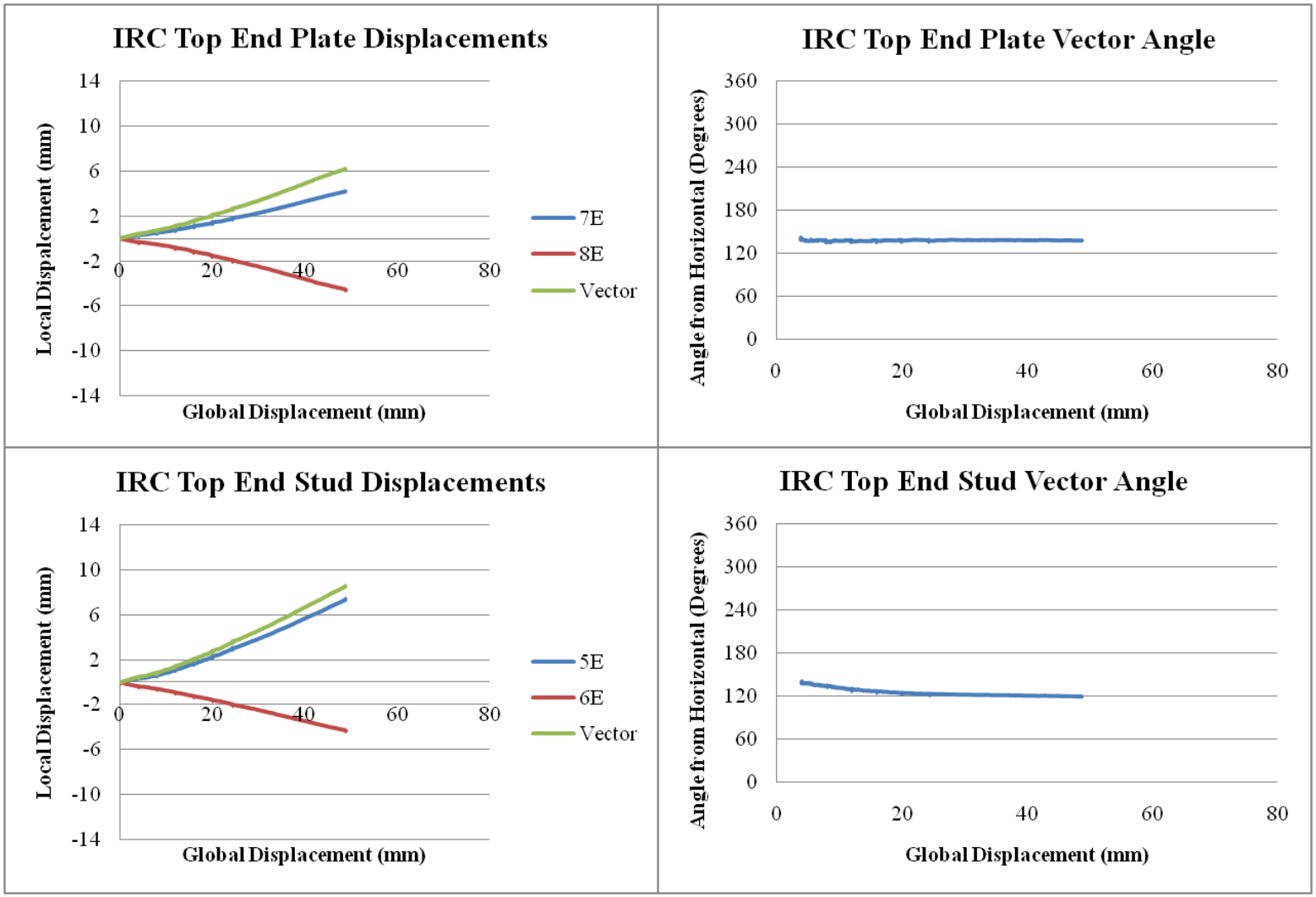

Figure G3. IRC Top End Sensor Displacements and Vector Angles

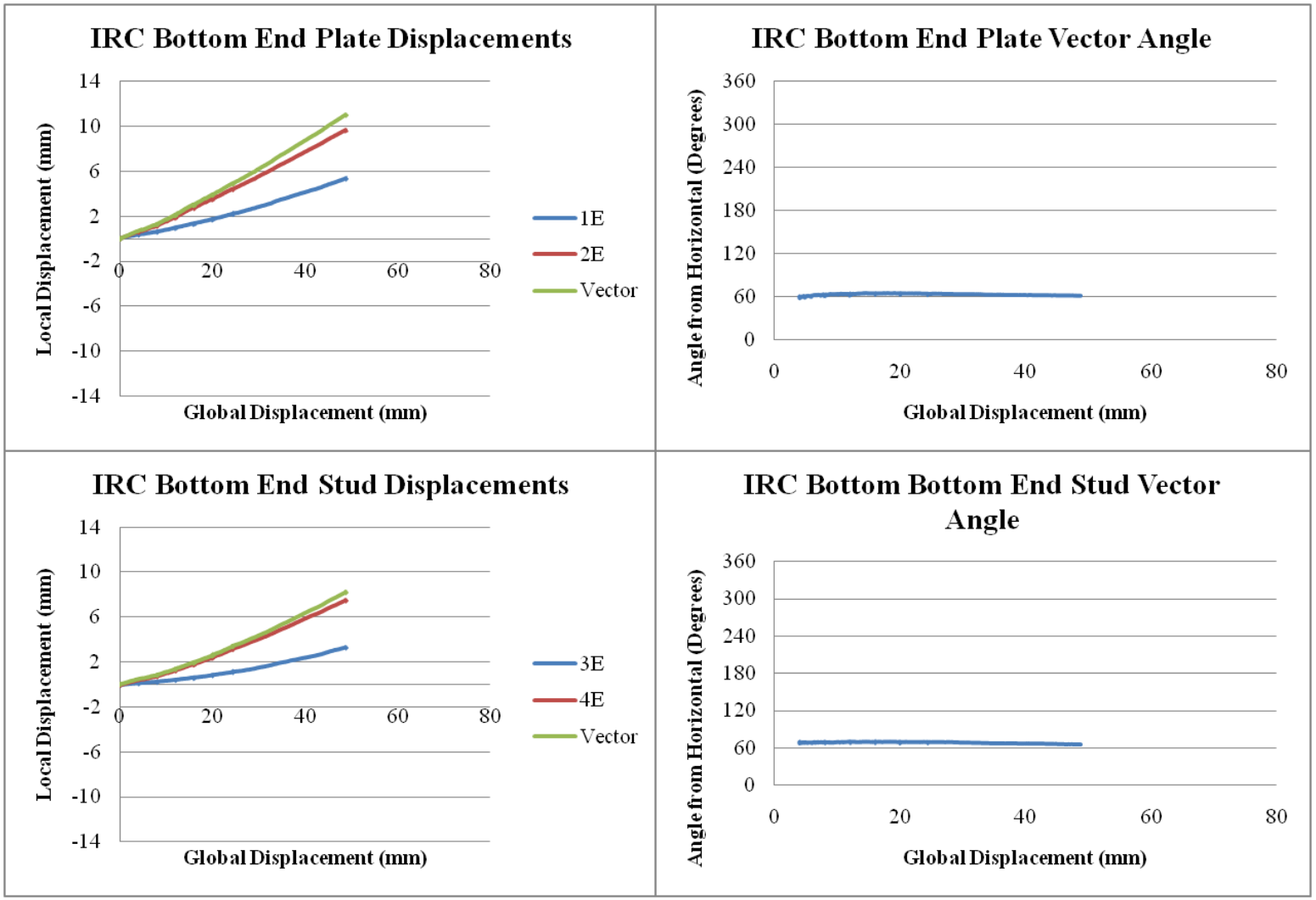

Figure G4. IRC Bottom End Sensor Displacements and Vector Angles

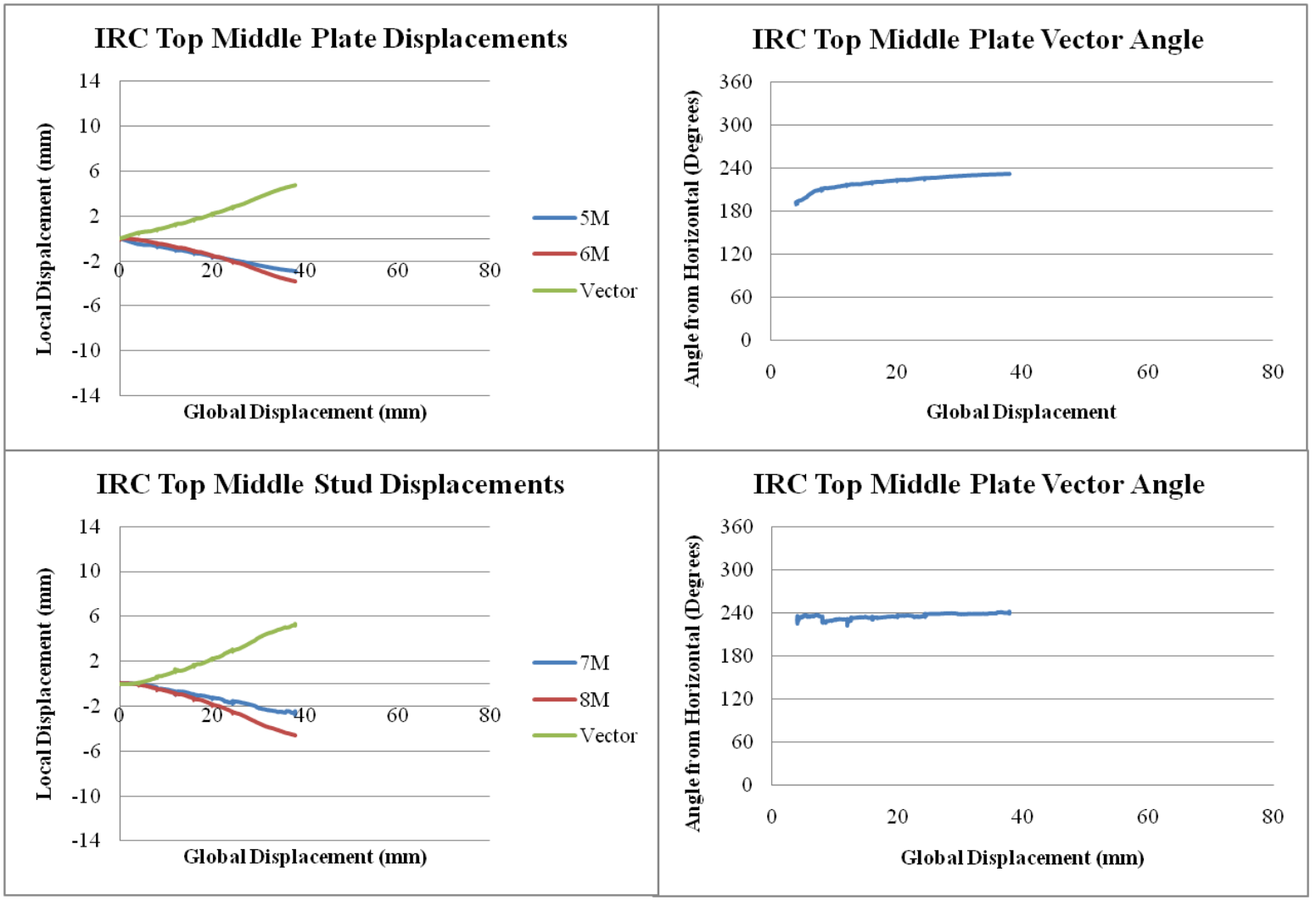

Figure G5. IRC Top Middle Sensor Displacements and Vector Angles

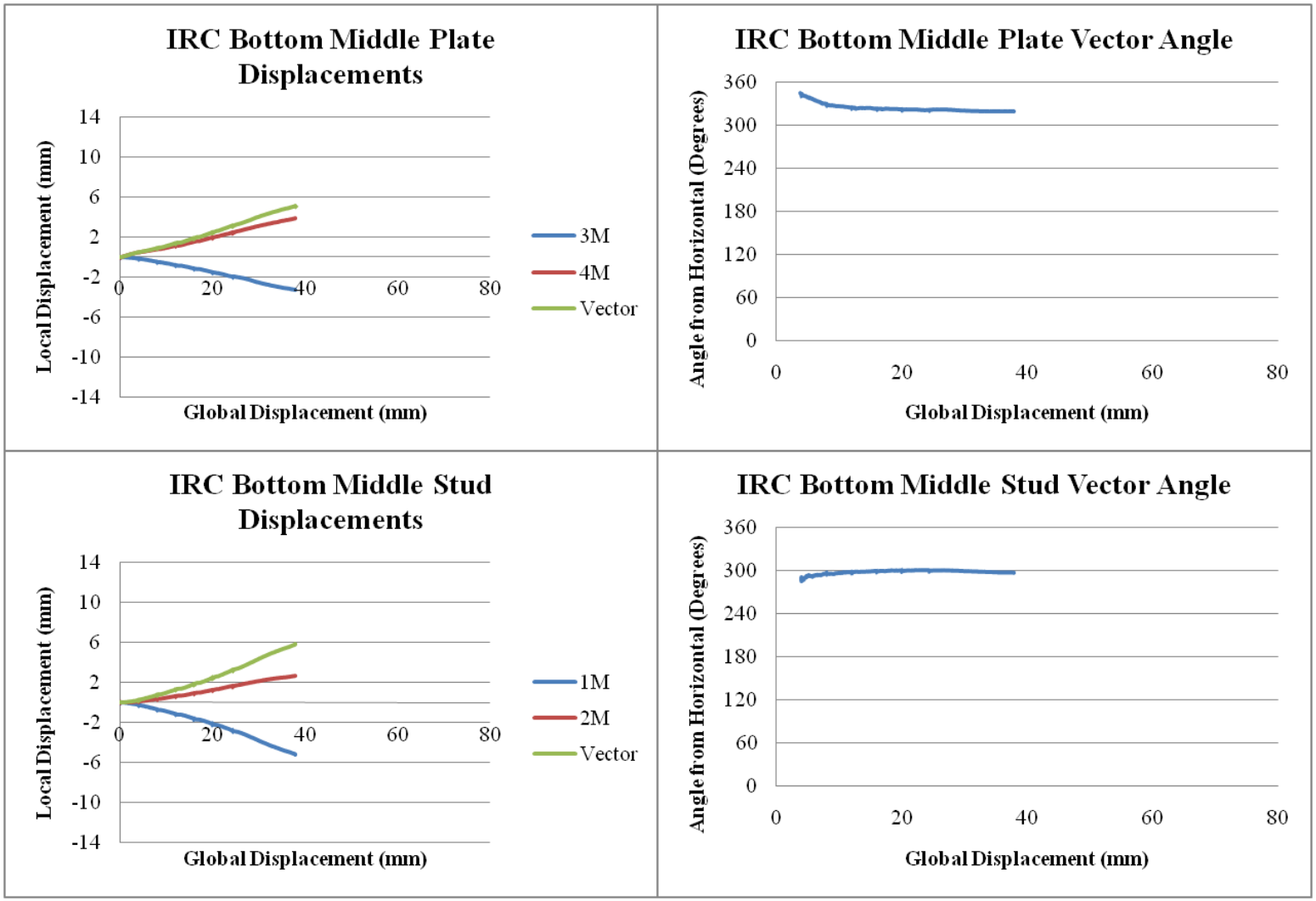

Figure G6. IRC Bottom Middle Sensor Displacements and Vector Angles

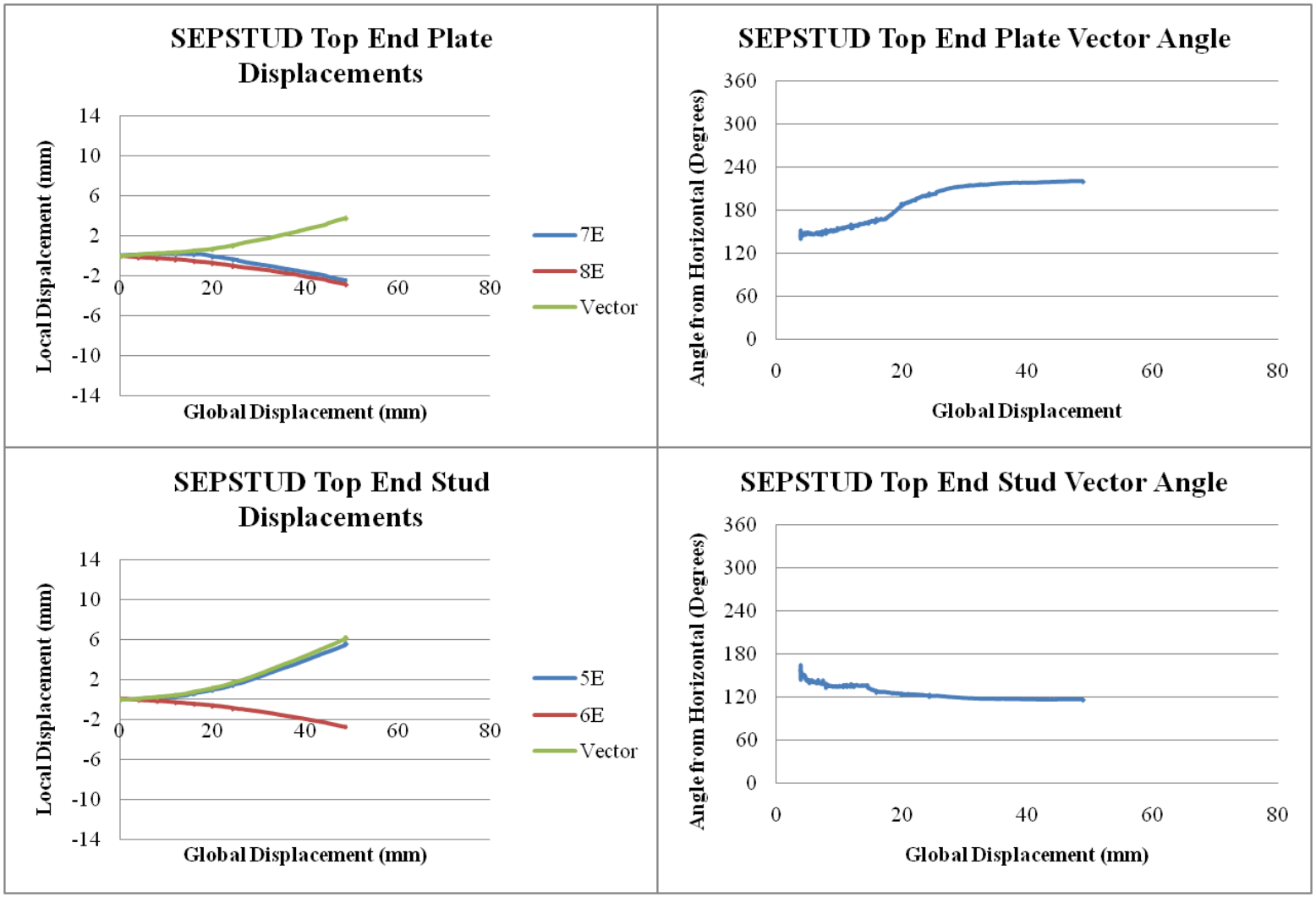

Figure G7. SEPSTUD Top End Sensor Displacements and Vector Angles

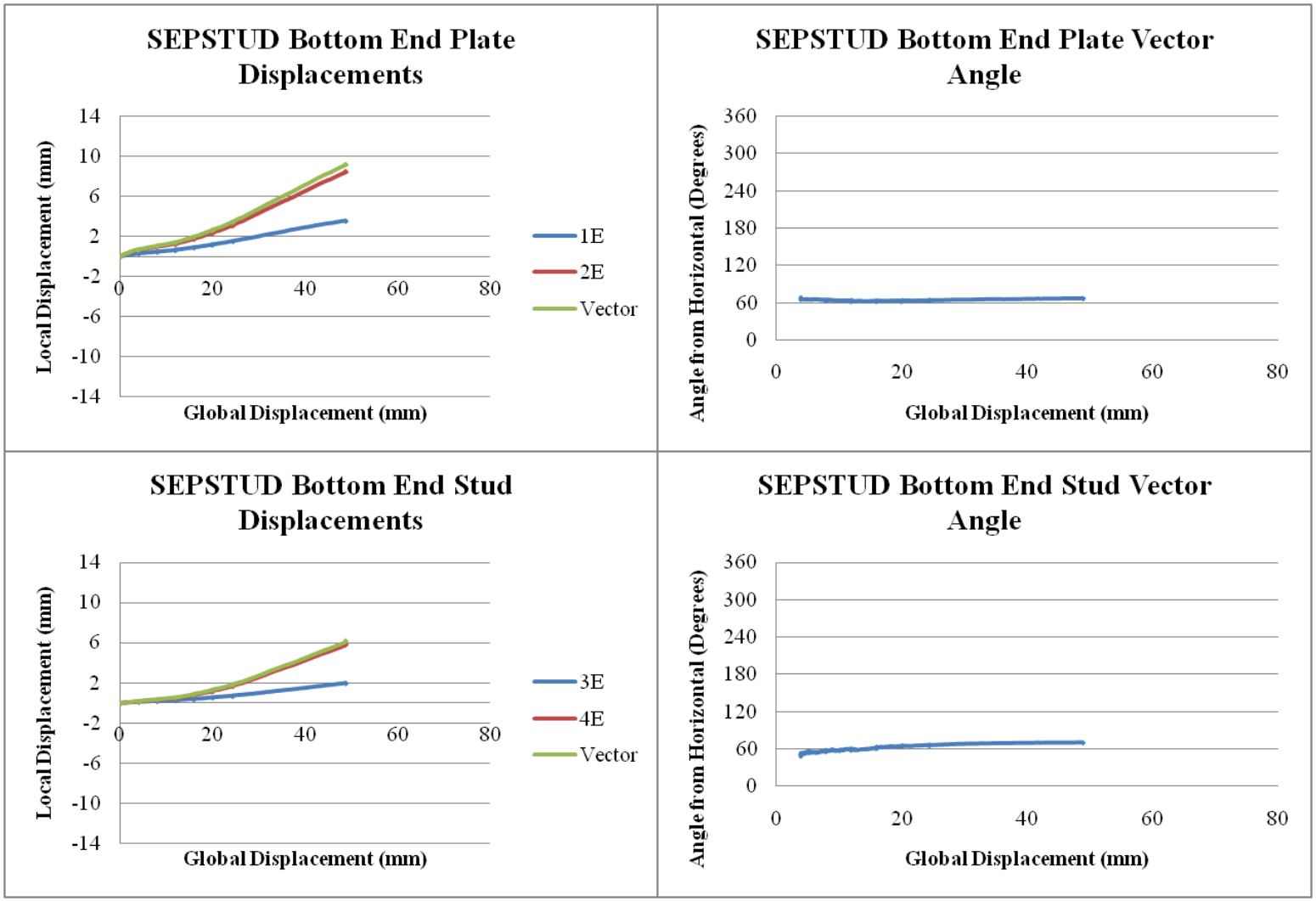

Figure G8. SEPSTUD Bottom End Sensor Displacements and Vector Angles

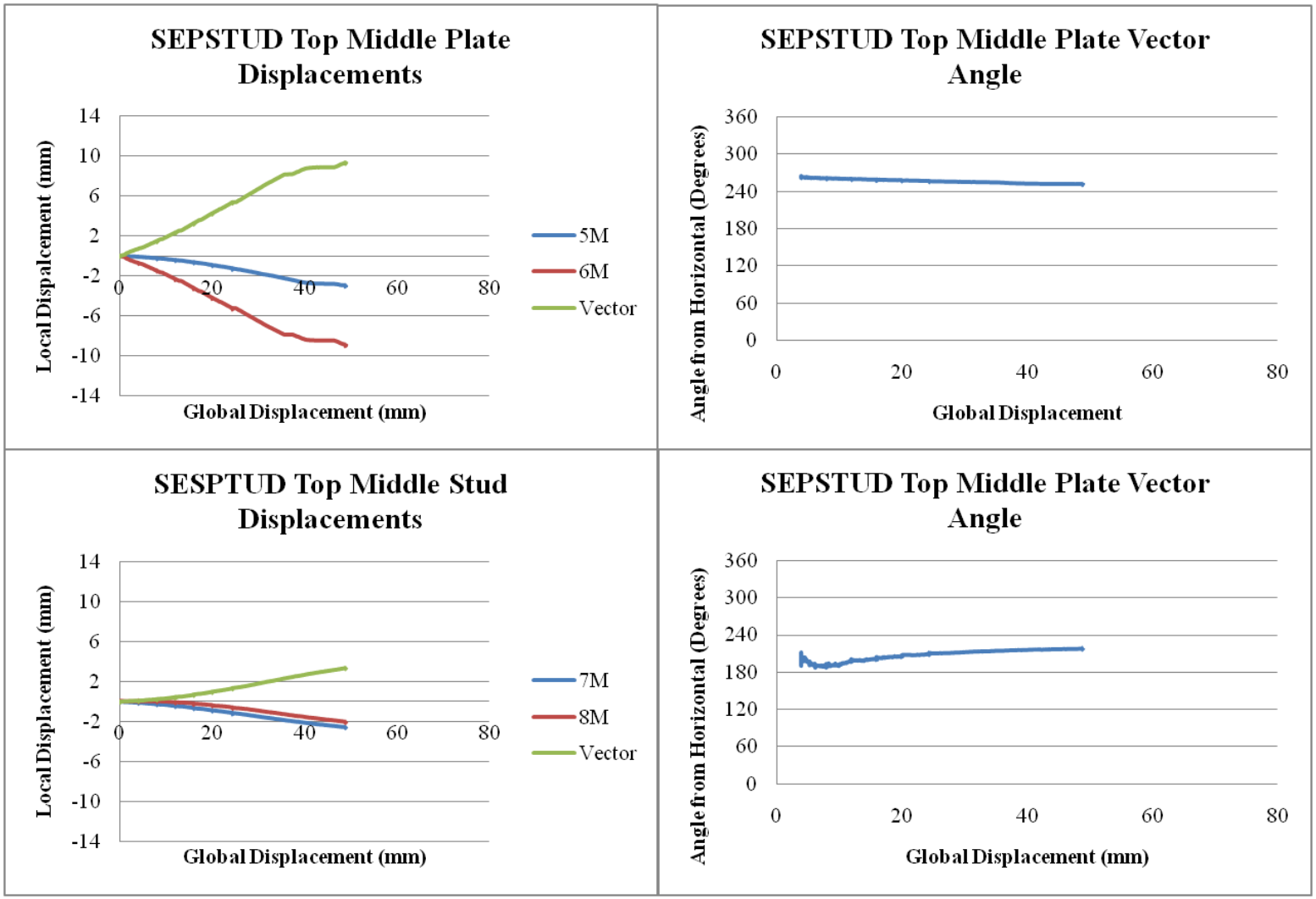

Figure G9. SEPSTUD Top Middle Sensor Displacements and Vector Angles

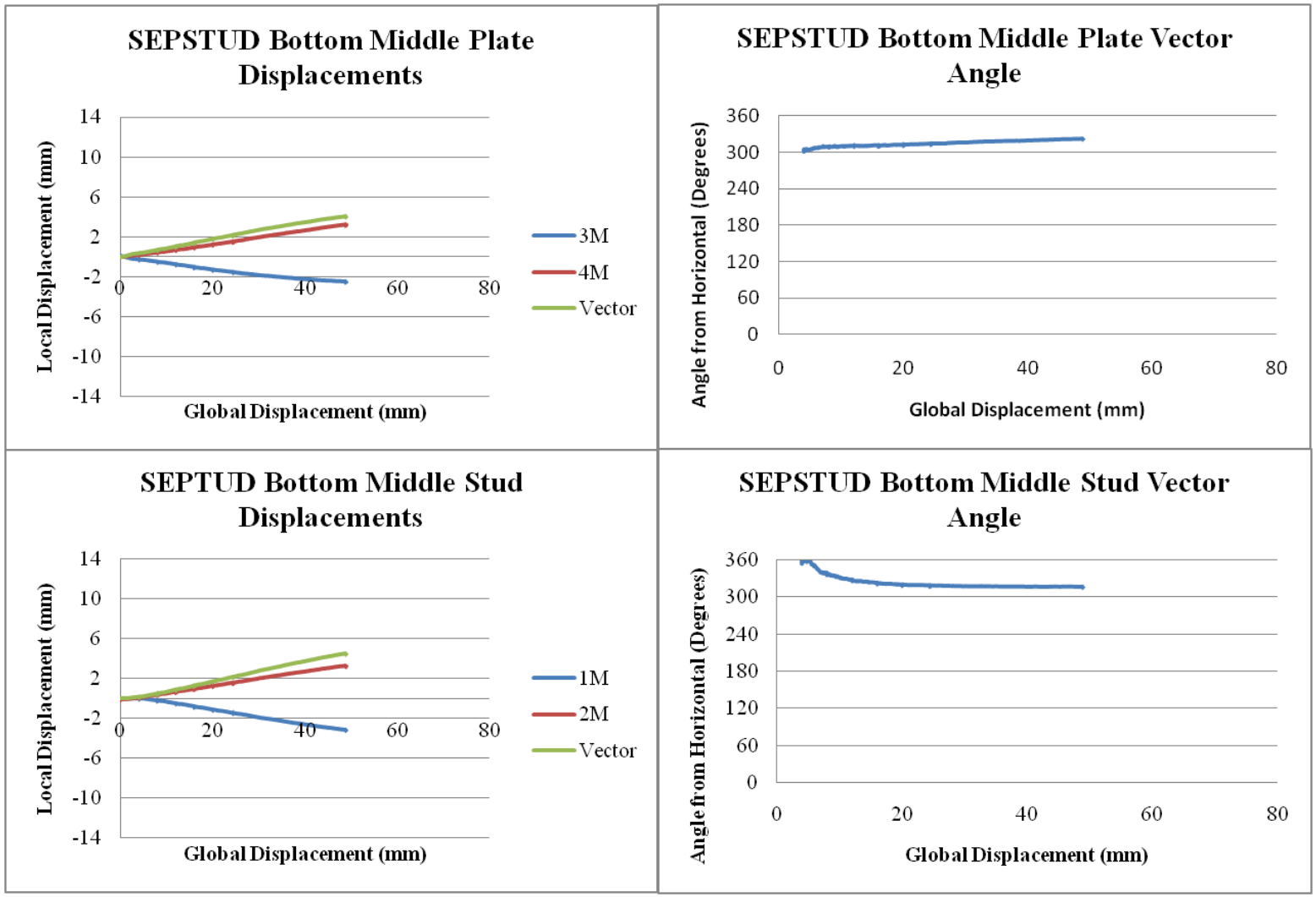

Figure G10. SEPSTUD Bottom Middle Sensor Displacements and Vector Angles

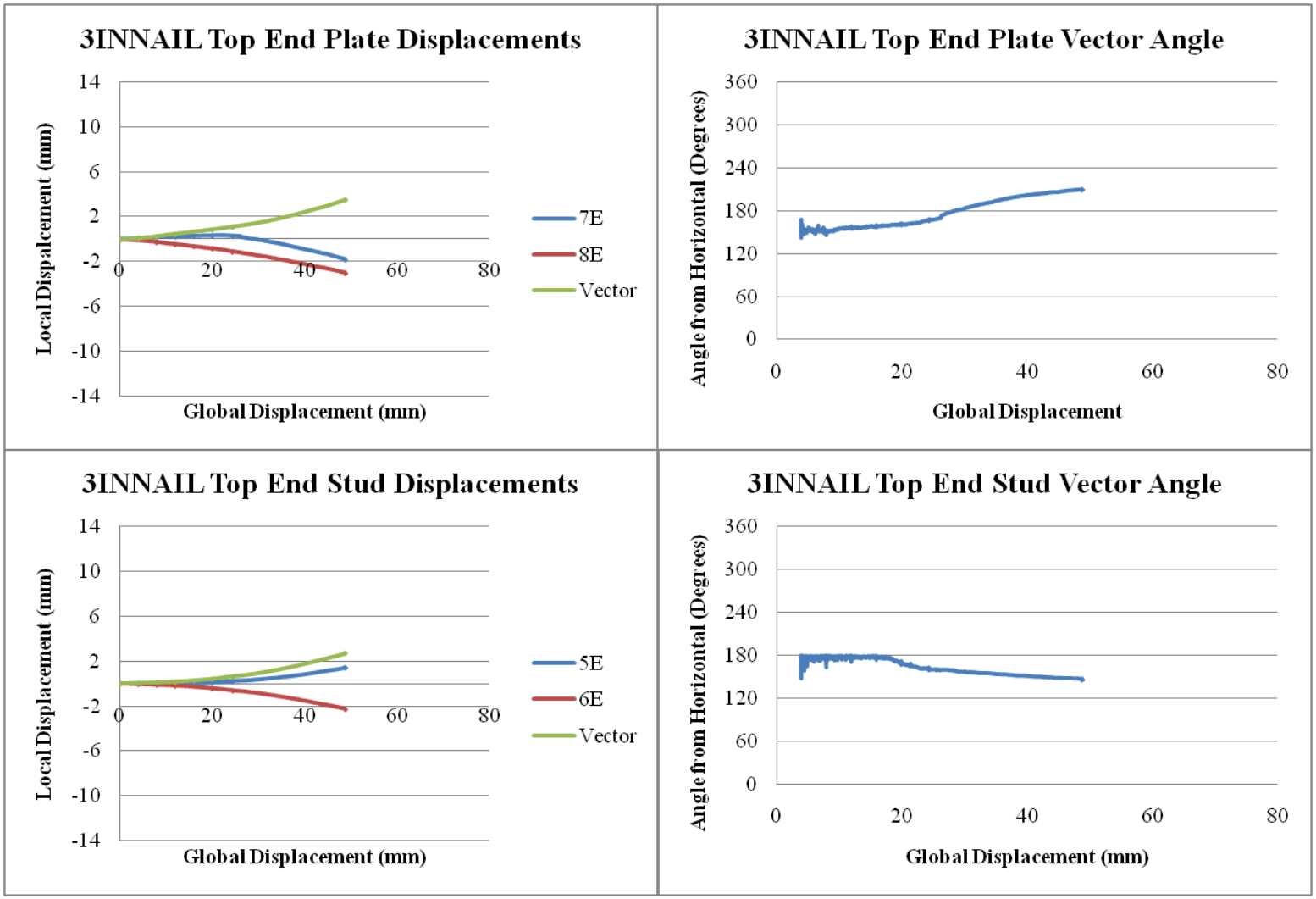

Figure G11. 3INNAIL Top End Sensor Displacements and Vector Angles

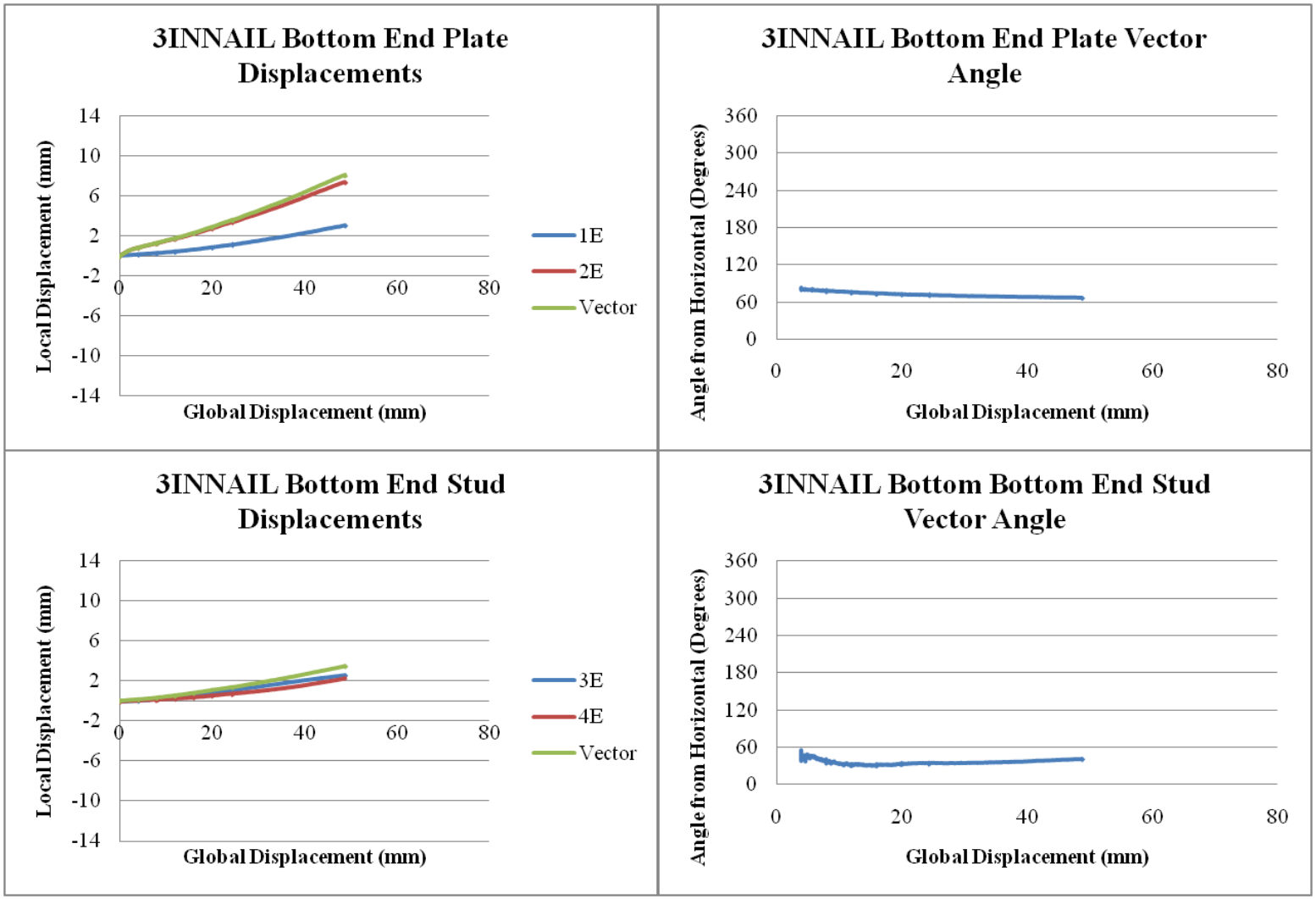

Figure G12. 3INNAIL Bottom End Sensor Displacements and Vector Angles

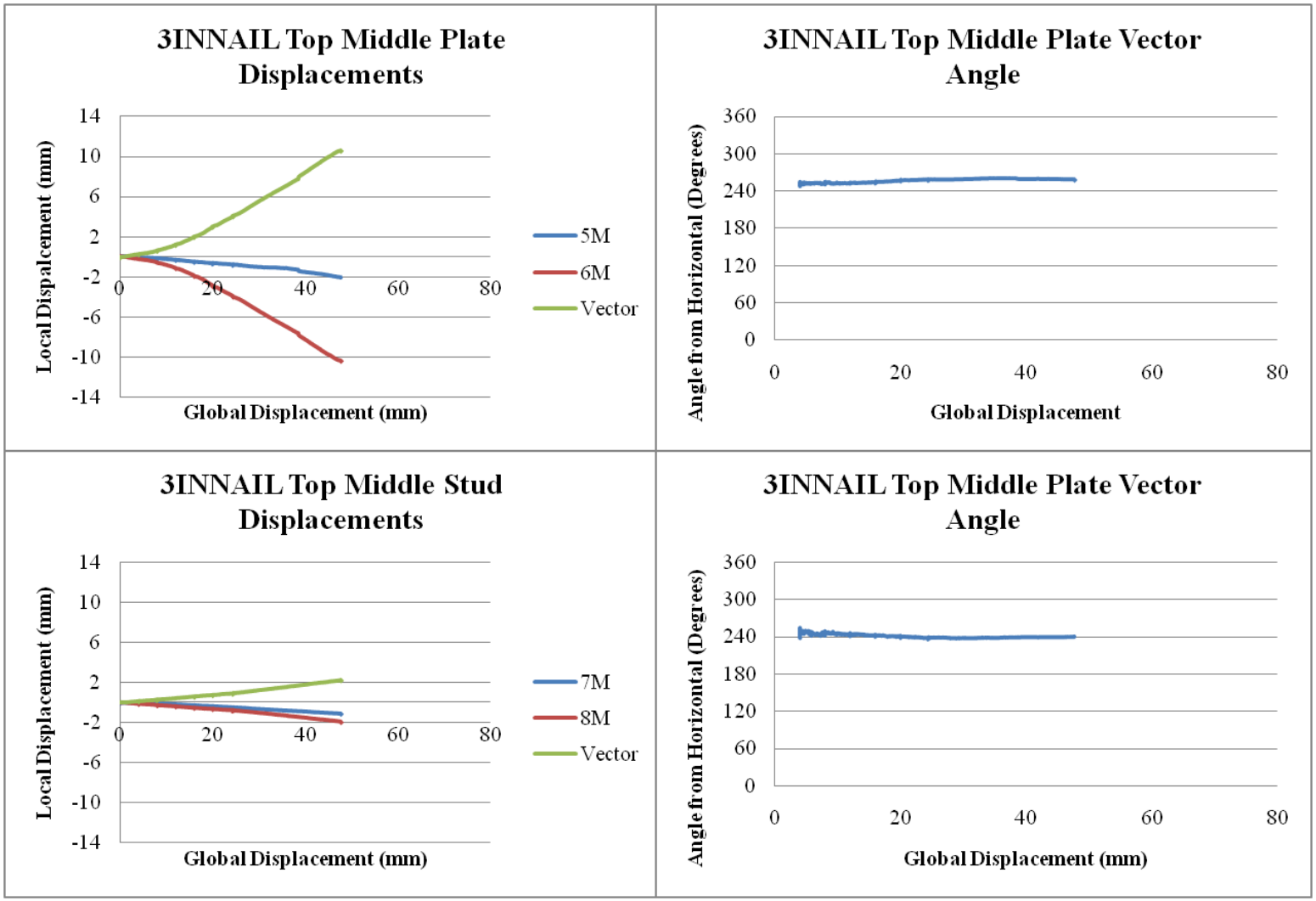

Figure G13. 3INNAIL Top Middle Sensor Displacements and Vector Angles

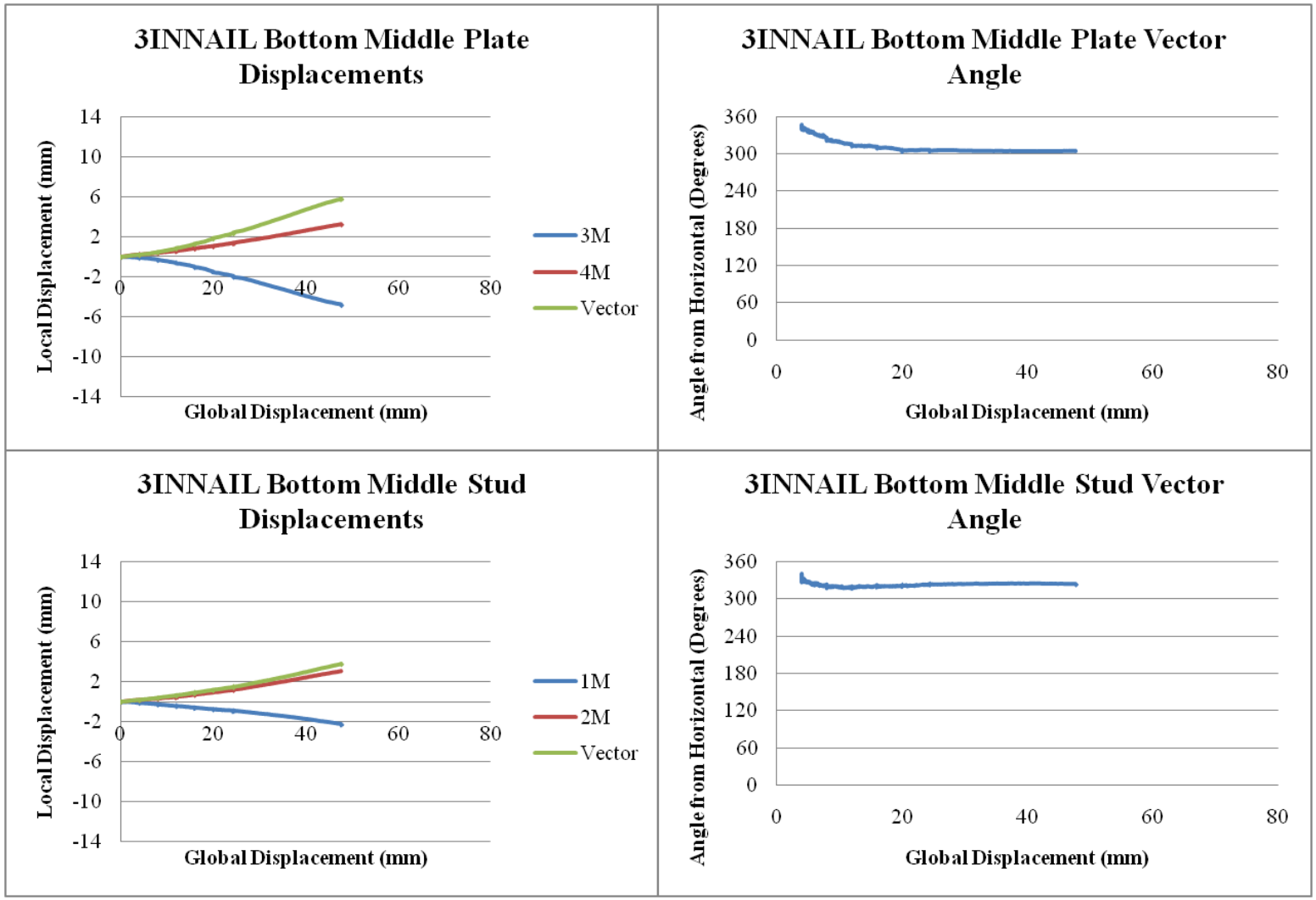

Figure G14. 3INNAIL Bottom Middle Sensor Displacements and Vector Angles

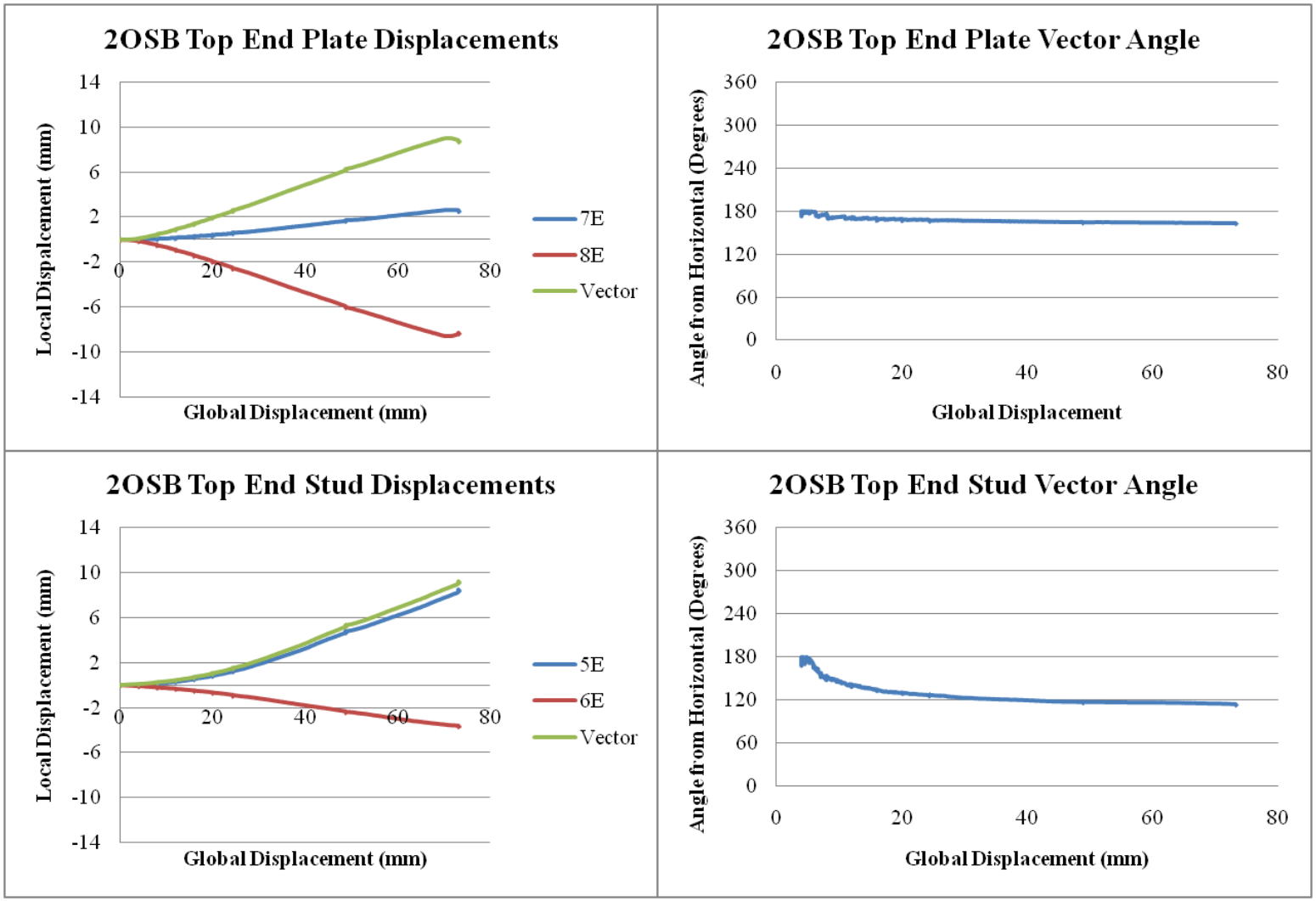

Figure G15. 2OSB Top End Sensor Displacements and Vector Angles

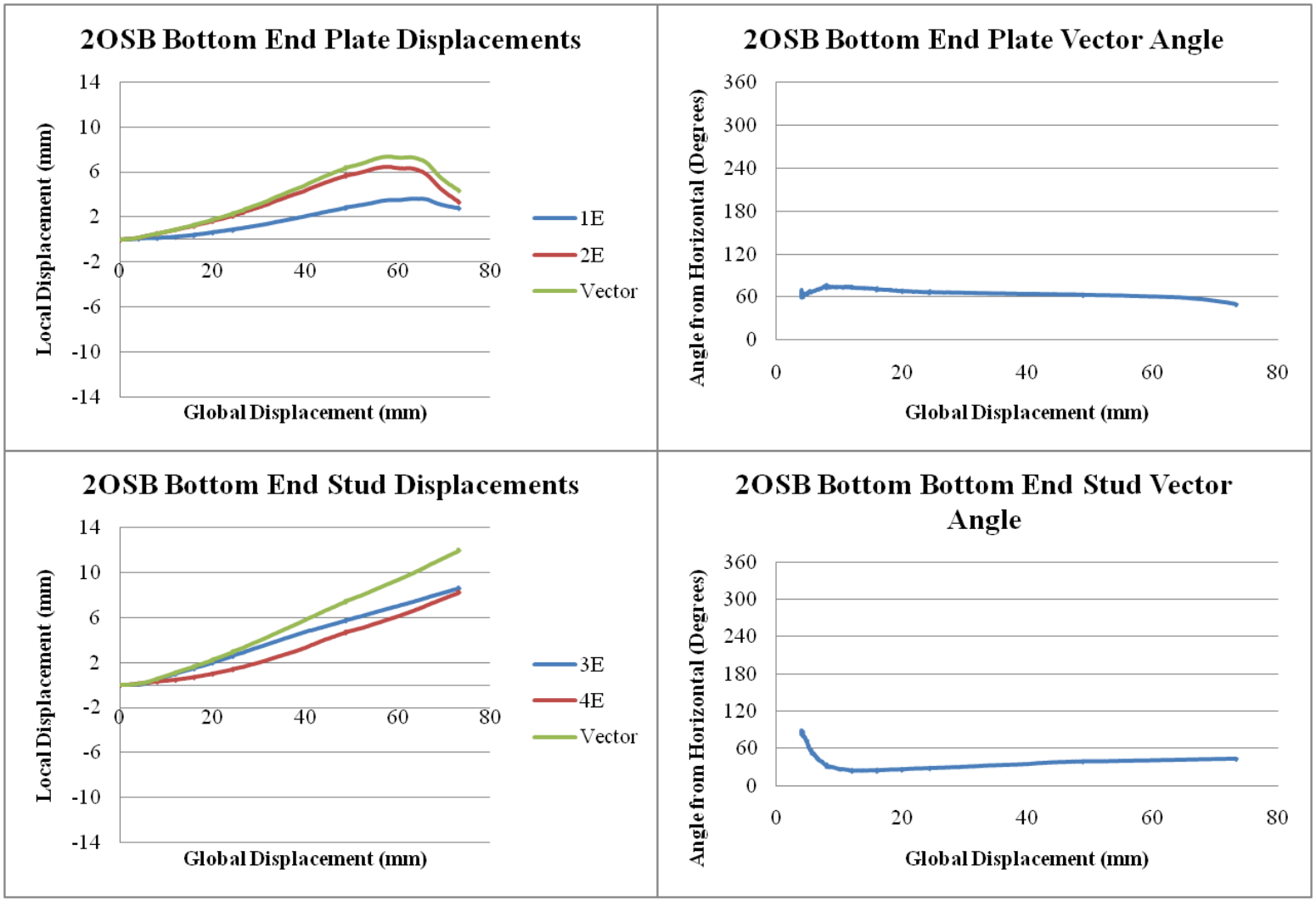

Figure G16. 2OSB Bottom End Sensor Displacements and Vector Angles

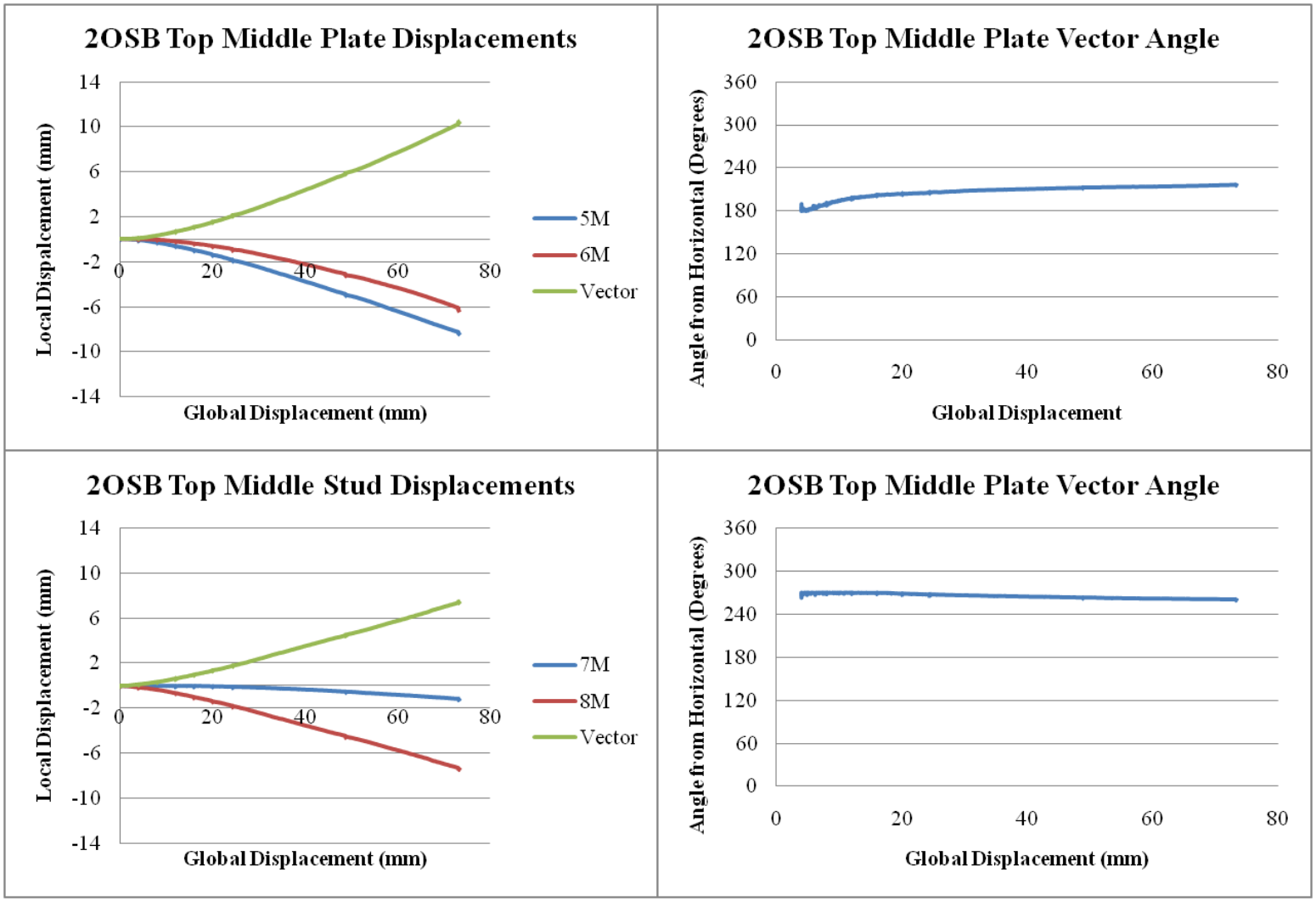

Figure G17. 2OSB Top Middle Sensor Displacements and Vector Angles

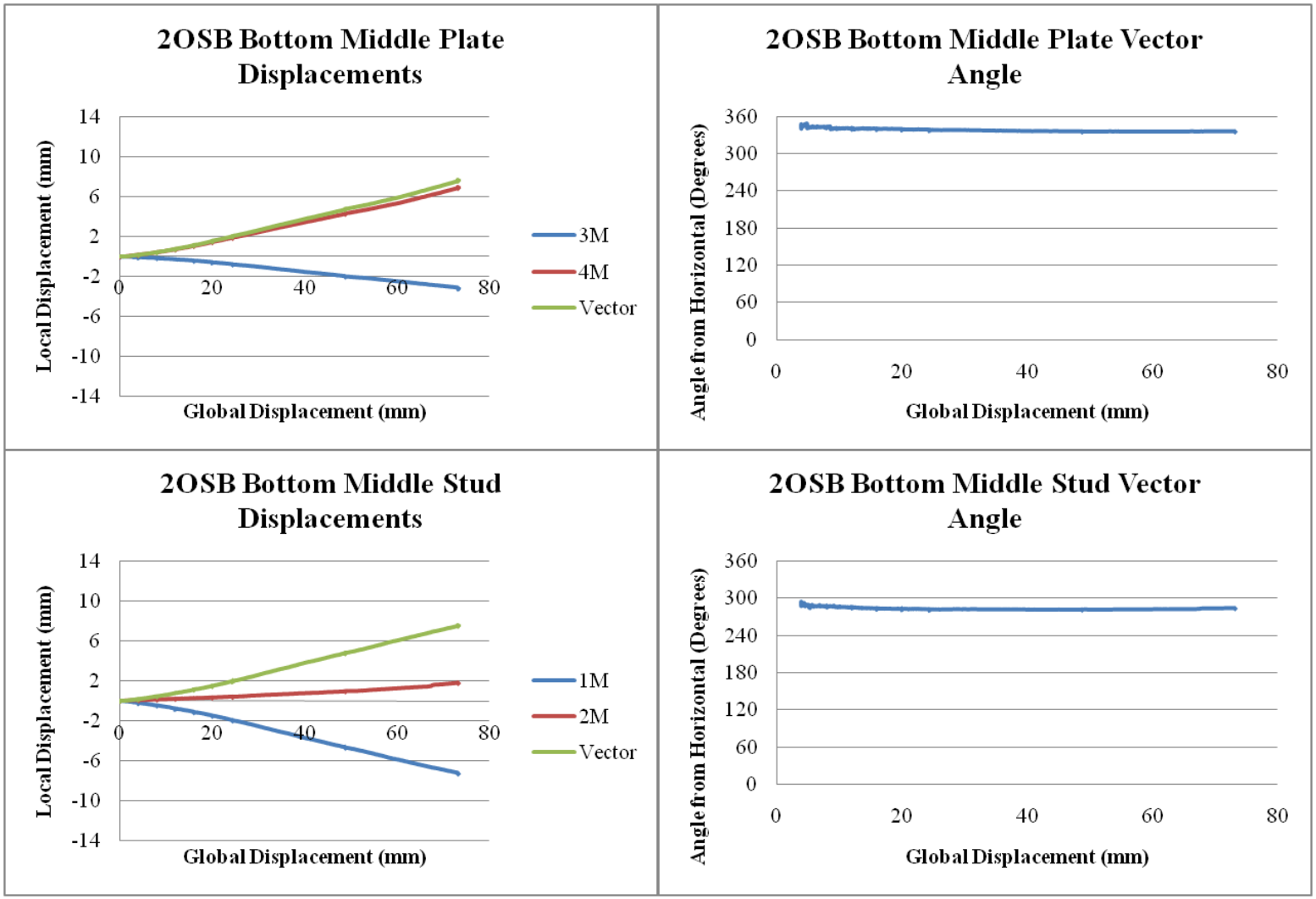

Figure G18. 2OSB Bottom Middle Sensor Displacements and Vector Angles

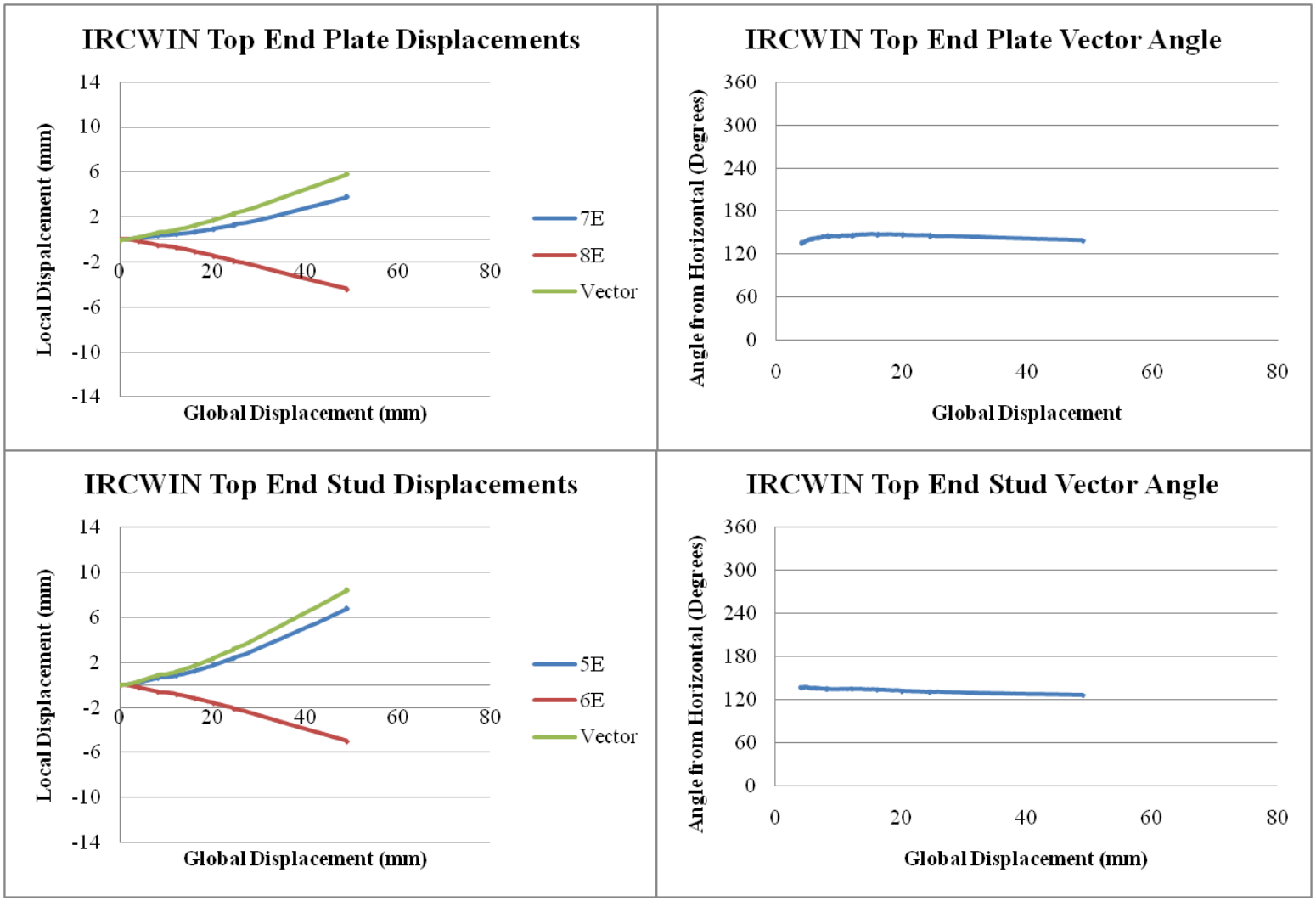

Figure G19. IRCWIN Top End Sensor Displacements and Vector Angles

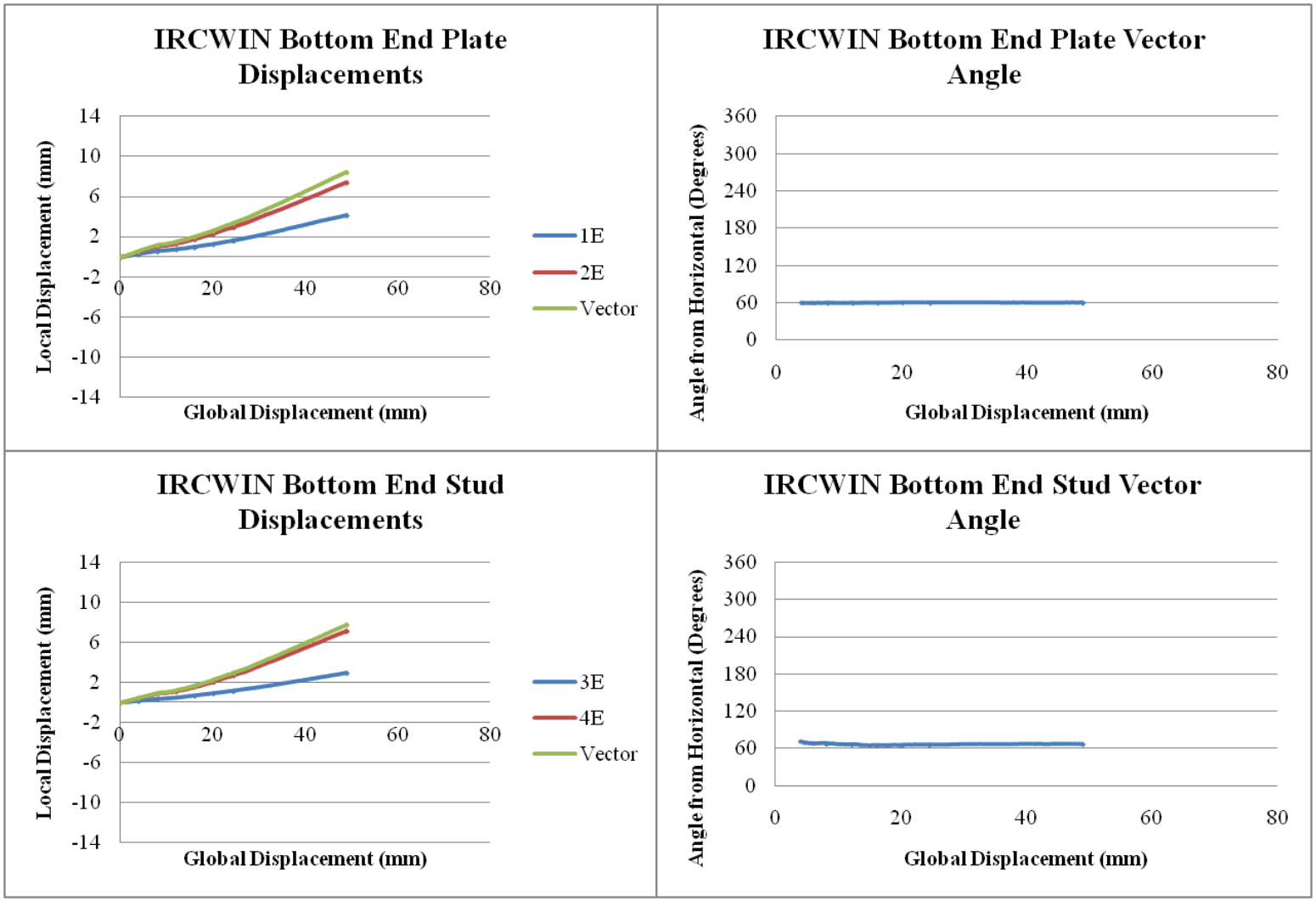

Figure G20. IRCWIN Bottom End Sensor Displacements and Vector Angles

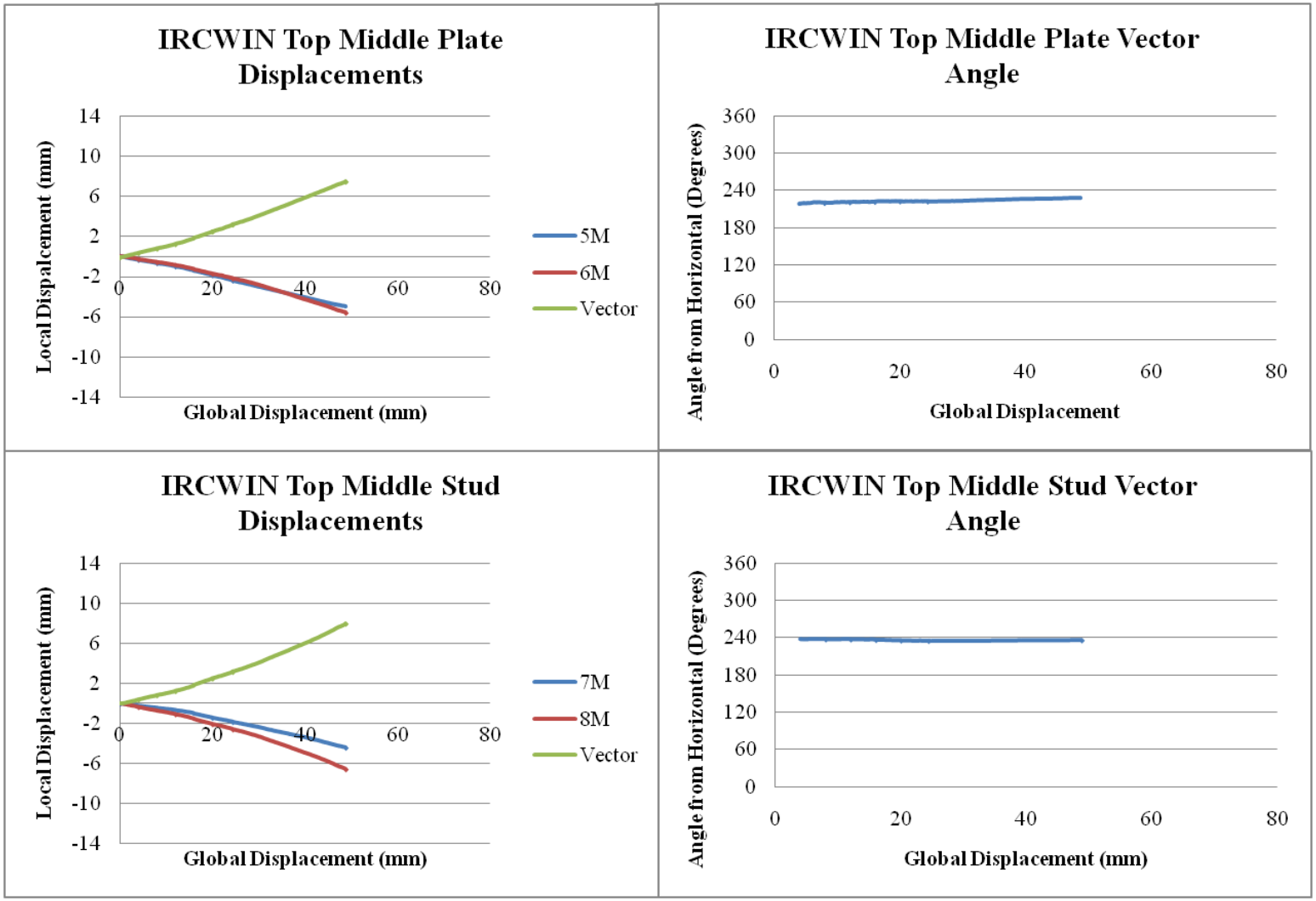

Figure G21. IRCWIN Top Middle Sensor Displacements and Vector Angles

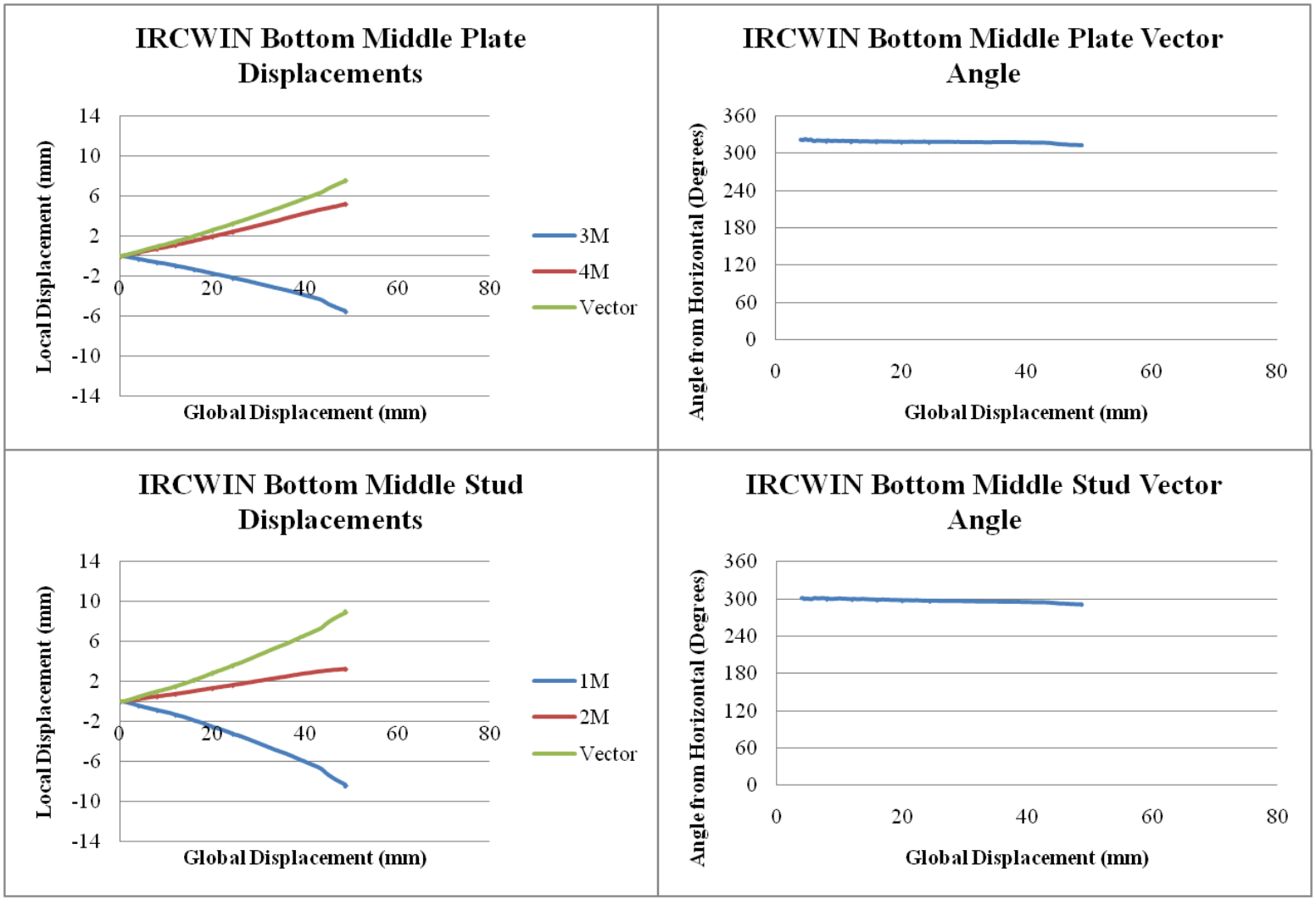

Figure G22. IRCWIN Bottom Middle Sensor Displacements and Vector Angles

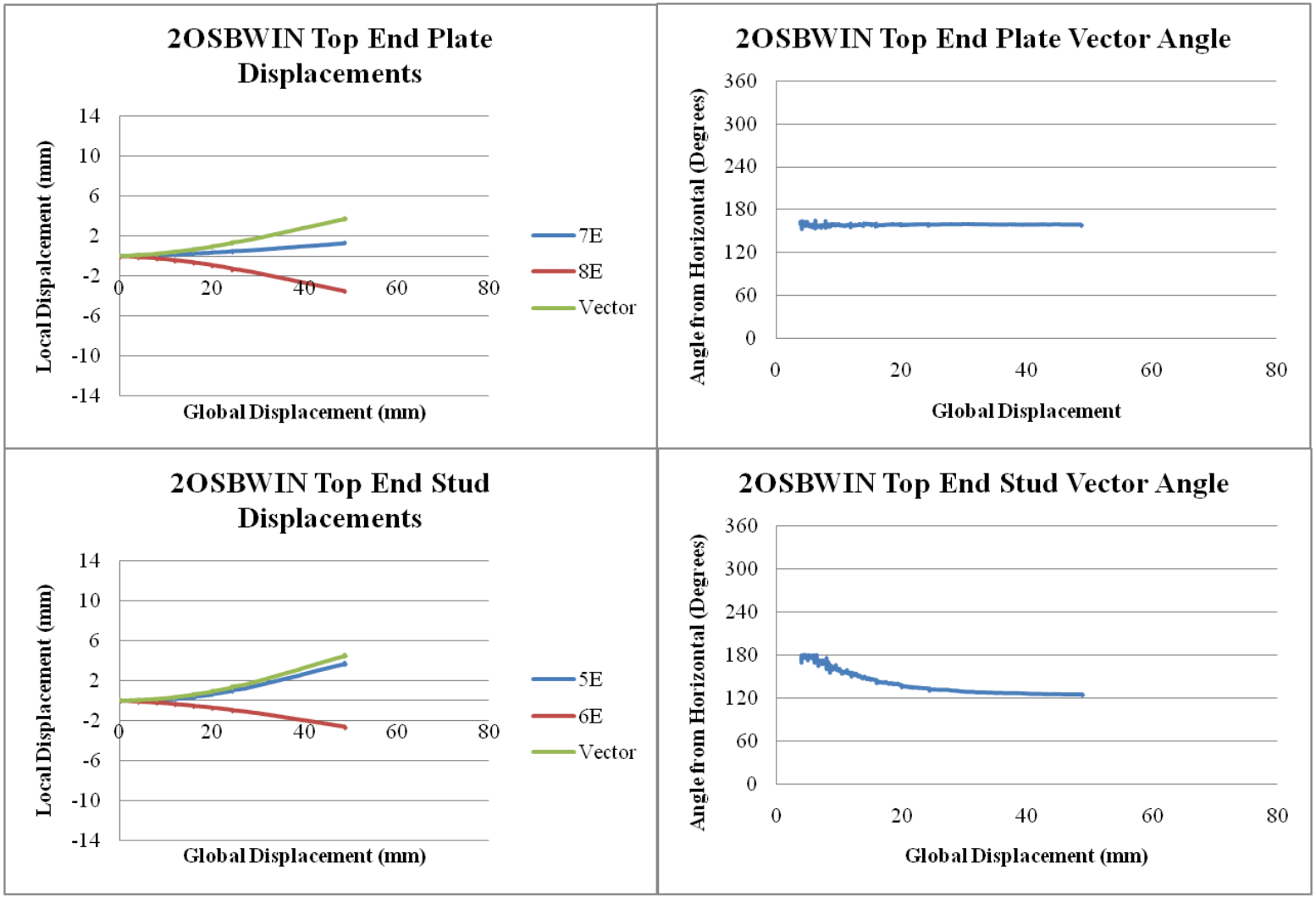

Figure G23. 2OSBWIN Top End Sensor Displacements and Vector Angles

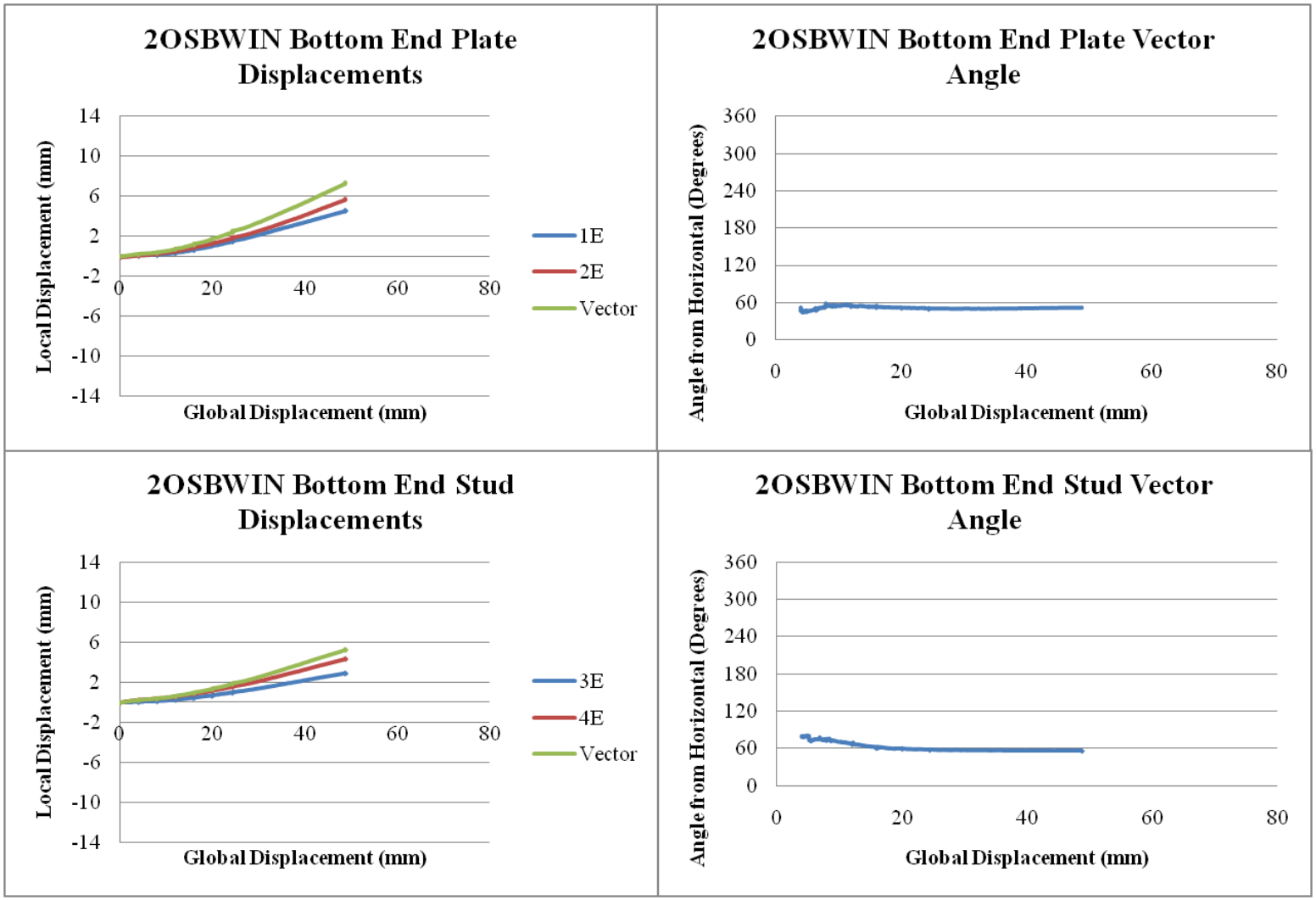

Figure G24. 2OSBWIN Bottom End Sensor Displacements and Vector Angles

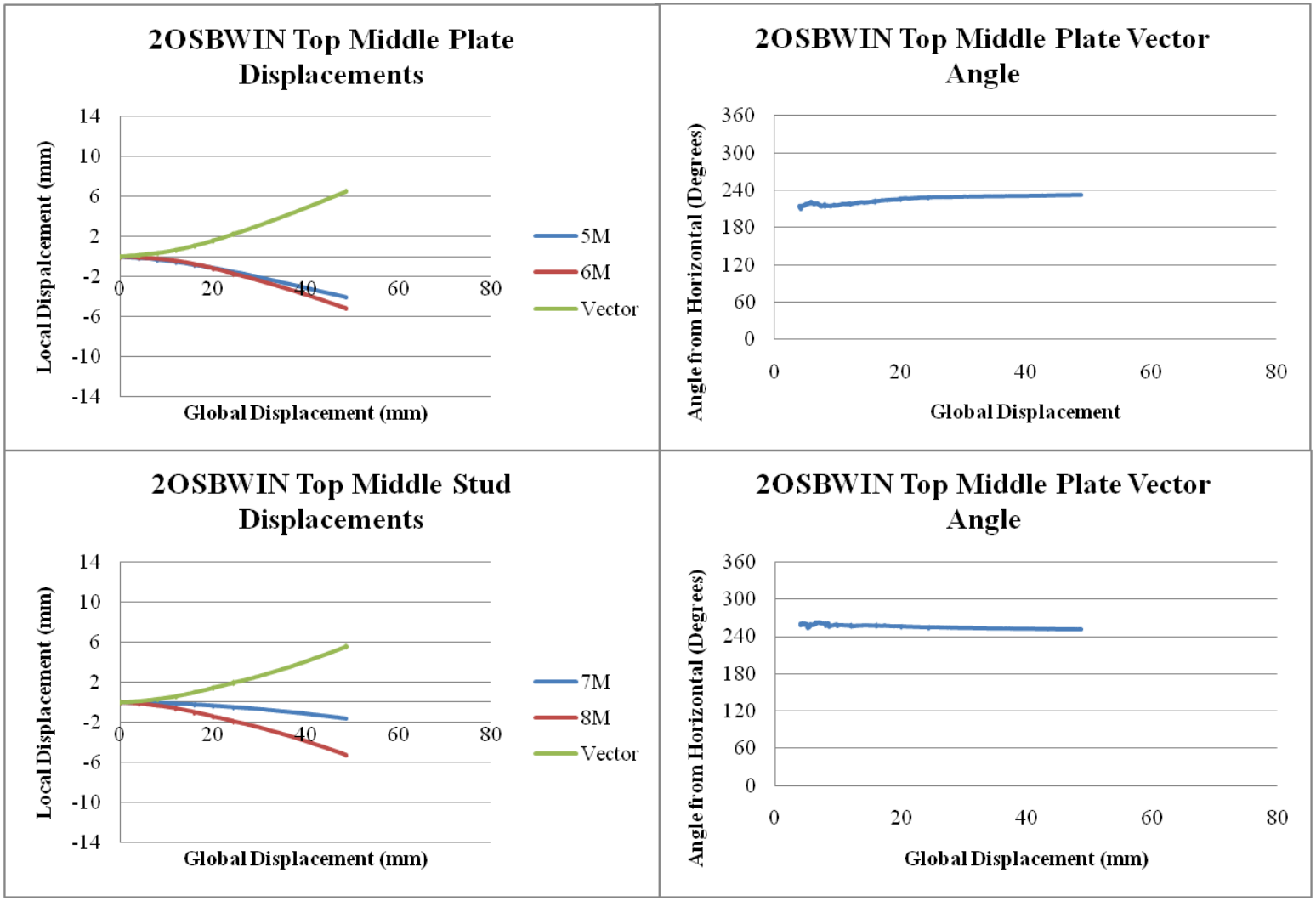

Figure G25. 2OSBWIN Top Middle Sensor Displacements and Vector Angles

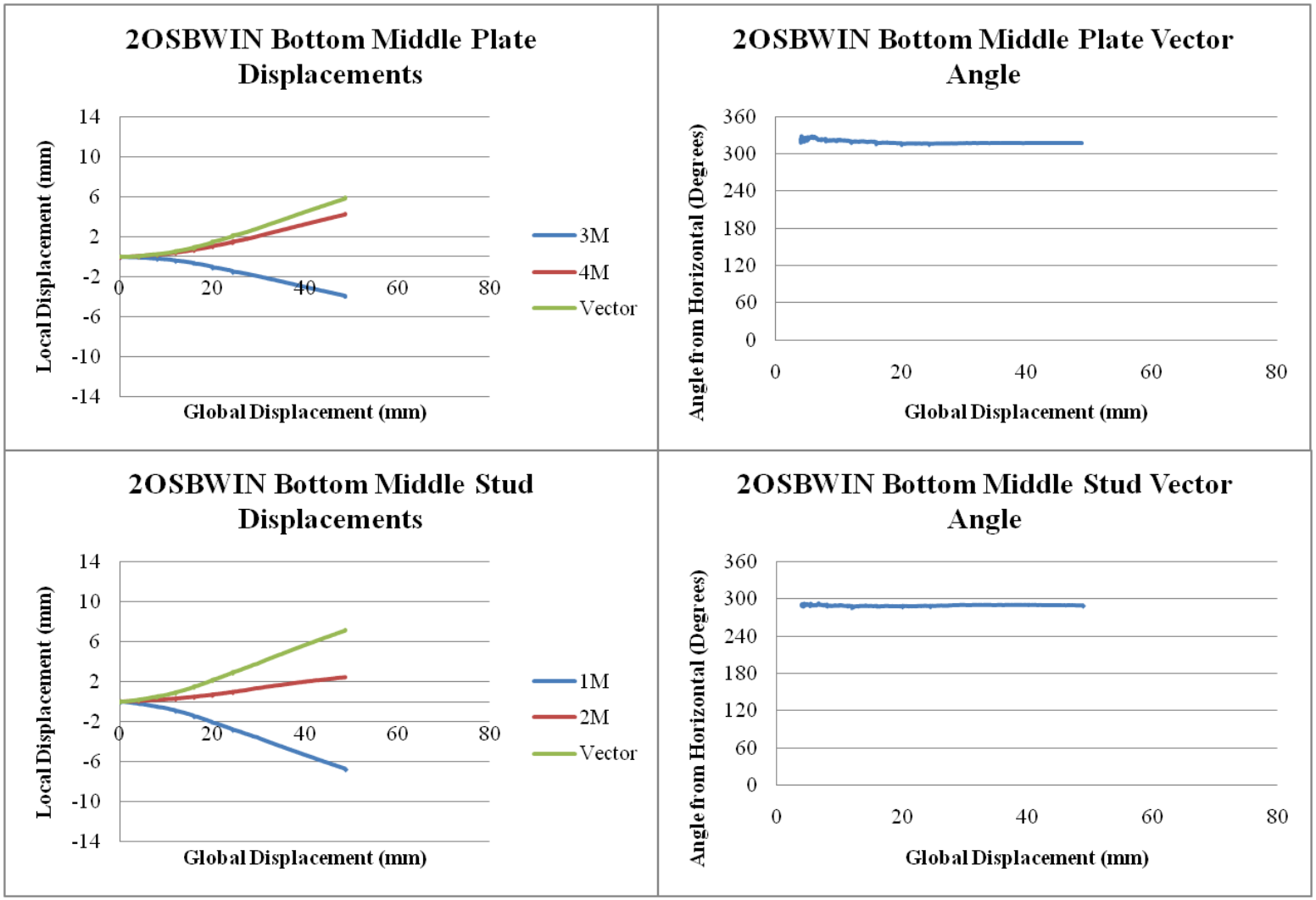

Figure G26. 2OSBWIN Bottom Middle Sensor Displacements and Vector Angles

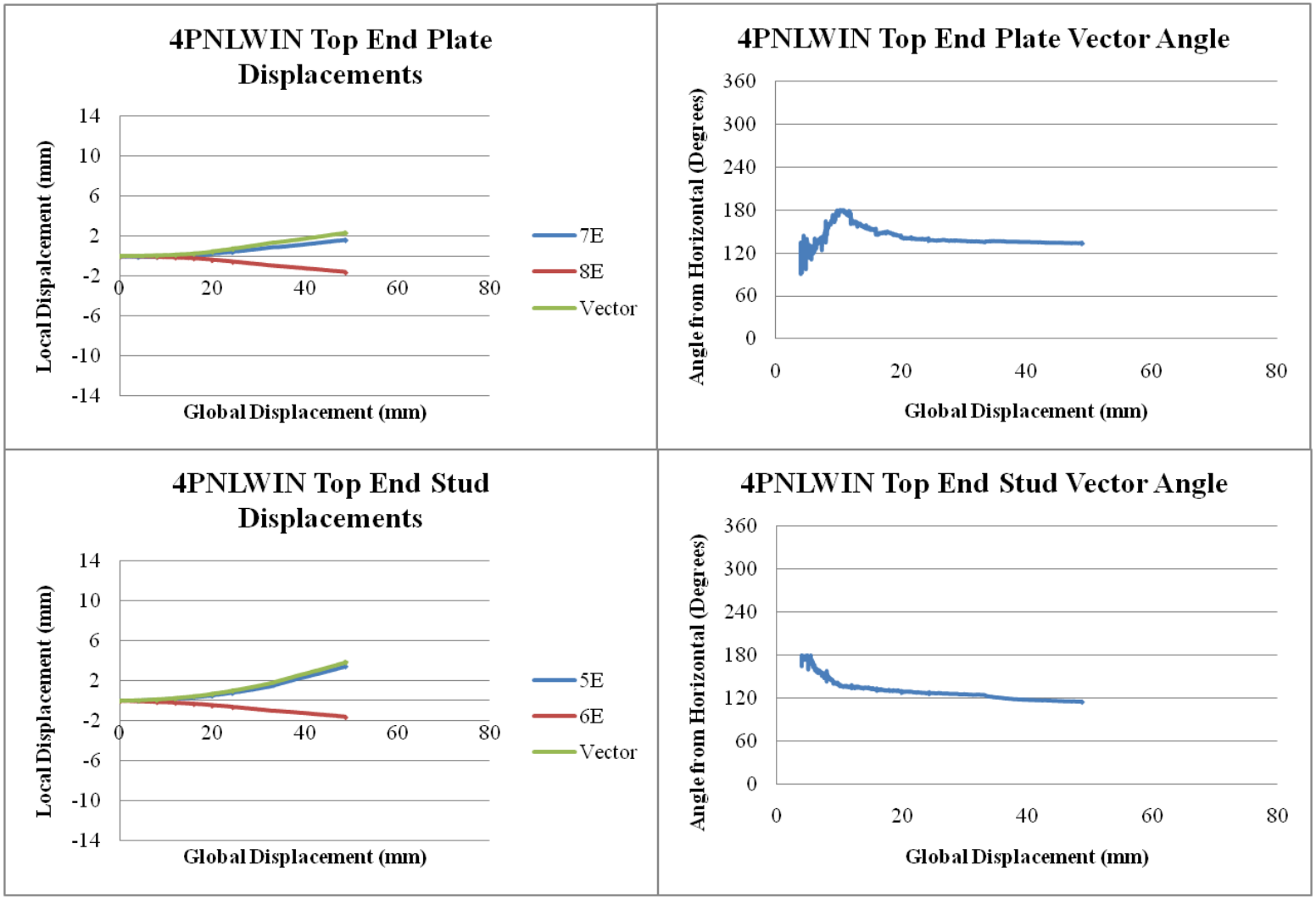

Figure G27. 4PNLWIN Top End Sensor Displacements and Vector Angles

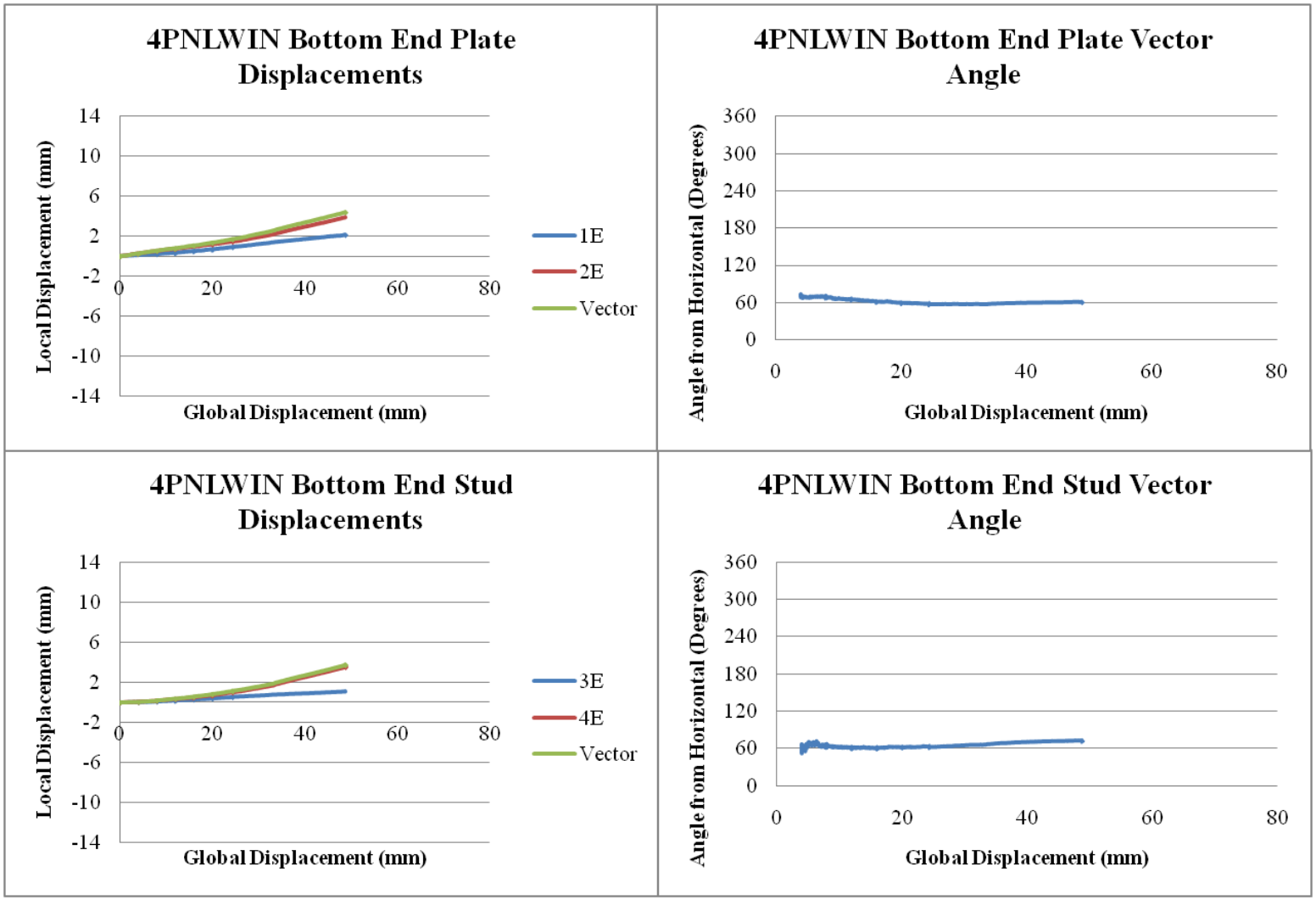

Figure G28. 4PNLWIN Bottom End Sensor Displacements and Vector Angles

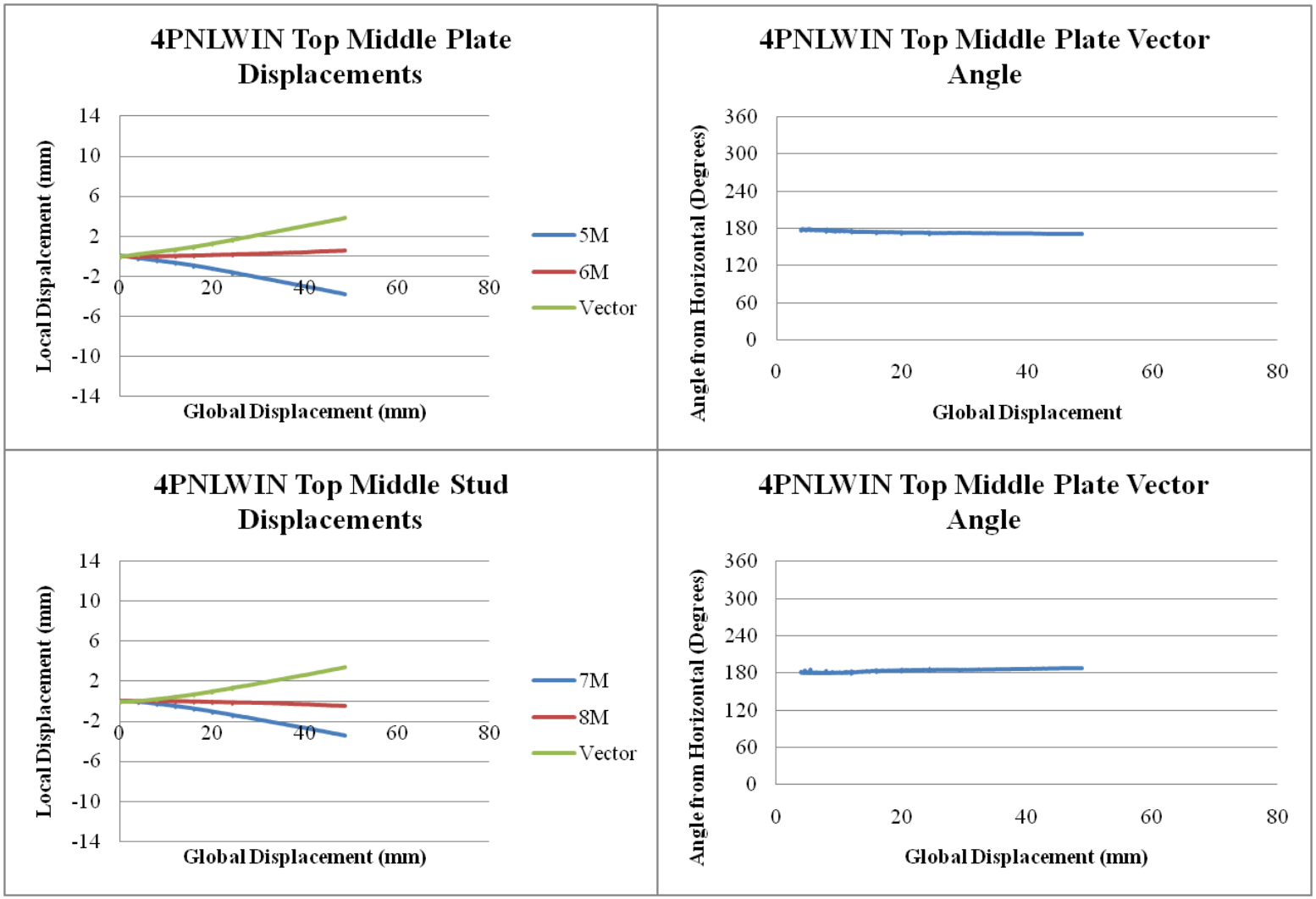

Figure G29. 4PNLWIN Top Middle Sensor Displacements and Vector Angles

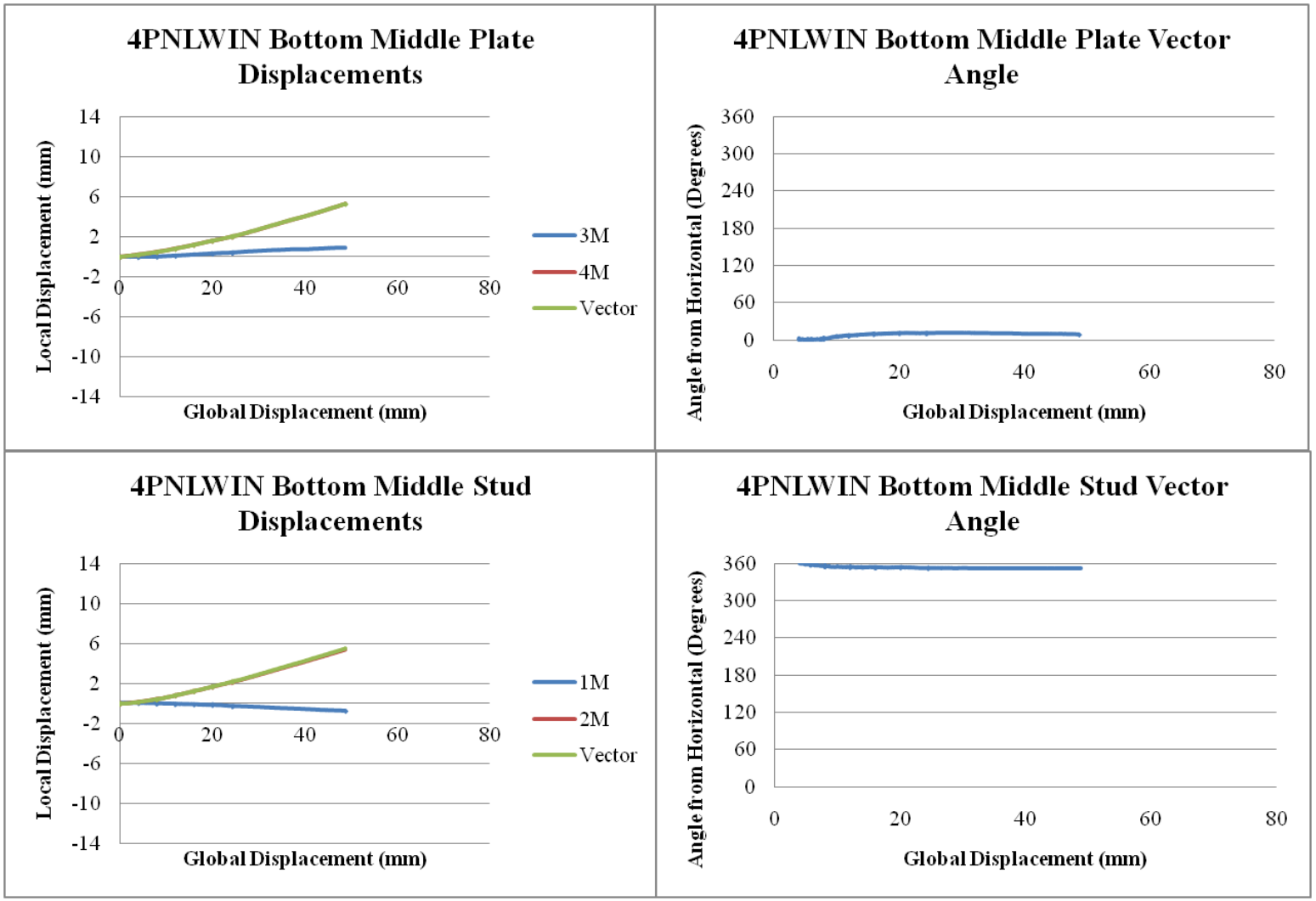

Figure G30. 4PNLWIN Bottom Middle Sensor Displacements and Vector Angles

Appendix H: Further Discussion of Relative Displacement Vectors

The directions of the relative displacement vectors calculated from the displacement sensors are consistent with those predicted by the classical GWB rotation model shown in Figure H1 and with those observed qualitatively in Figure H2. The recorded displacement vectors for all wall designs at 1% drift are shown in Figure H3 for shear walls without openings and in Figure H4 for shear walls with openings. These vectors are shown at their true angles and scaled 100 times their length. This similarity between the predicted and actual model is especially noticeable for the IRC, 2OSB, IRCWIN and 2OSBWIN designs. These designs had wood frames and sheathing attachments most like those used in the classical model. However, the altered wood frames and sheathing attachment of the SEPSTUD, 3INNAIL and 4PNLWIN designs caused different displacement vector directions and magnitudes than the classical model.

All bottom plate and bottom stud vectors were qualitatively consistent with what was expected from the classical model, except for the 4PNLWIN design middle stud vectors. This similarity is because all bottom plates were rigidly attached to the metal foundation, and did not deform as the rest of the wood frame did. This similarity suggests that the GWB absolute rotation was similar for all walls, while the wood frame absolute deflection was not. This observation is consistent with the fact that all GWB panels had similar properties as discussed in the preliminary results, but the wood frames designs contained much more variability. Despite the variability in wood frame designs, the qualitative similarity of all wall designs to the classical model was generally preserved.

Shear Walls without Openings

For shear walls without openings, relative displacement vectors for IRC and 2OSB, shown in Figure H3a and H3d, were both qualitatively comparable to the classical GWB rotation model and wood frame deformation model shown in Figure H1. For shear walls without openings, some differences between the classical model predictions and the observed results were the directions and magnitudes of the vectors on the top end stud and plate, top middle stud and plate in the 3INNAIL and SEPSTUD designs shown in Figure H3b and H3c. These designs incorporated a double middle stud which was separated by 114 mm in the SEPSTUD design and attached with two 10d nails 610 mm on center in the 3INNAIL design. This double middle stud nearest the applied displacement uplifted as shown in Figure H5 in the SEPSTUD and 3INNAIL designs. As can be seen, the right middle stud in the picture

is completely attached to the top plate, while the left stud is not attached and out of view. This uplift middle stud caused uplift of the top plate. This uplift resulted in a separation of the top plate at failure which is documented in Figure H5a for the SEPSTUD design and Figure H5b for the 3INNAIL design.

The load path which caused this uplift of the top plate is shown in Figure H6 to be caused by the tensile force in the middle stud nearest the applied displacement (uplift middle stud). Failed connections are circled in Figure H6. If only considering the forces in the wood frame, studs on the side of the applied displacement should be in compression and those on the uplift side should be in tension, with the neutral axis being in the middle of the wall. This force would change linearly between the maximum compression force near the applied displacement, and the maximum tension force on the uplift side of the wall. This would imply a small tension force in the compression middle stud and a small compression force in the uplift stud middle stud. However, the larger shear forces from the compression stud were transferred to the uplift middle stud through the OSB sheathing fasteners. This sheathing shear transfer caused a tension force in the uplift middle stud greater than the small compression force contribution from the wood frame. Uplift of the tension middle stud compromised the connection to the bottom plate and caused uplift of the top plate. The end nailing of studs to the bottom plate was a weak connection, and was always the first to fail.

The uplift stud was rigidly attached to the foundation by a tie down and did not uplift despite having a large tension force. The connection of the top plate to the tension stud was a much weaker connection than the tie down and resulted in a compromised connection at the top plate, which is evident in Figure H5. The tension forces from the uplift stud were transferred to the compression middle stud through the OSB sheathing fasteners as shown in Figure H6. While a small tension force was added from load transfer of the wood frame, the larger compression forces from load transfer of the sheathing caused the member to be in compression. Due to the uplift of the top plate, the connection of the compression middle stud and top plate was compromised.

The deflected shape of a shear wall with a double middle stud was different from that of a shear wall with one middle stud. Shear walls with one middle stud did not exhibit uplift of the middle stud because both OSB sheathing panels were attached to one stud. This stud has equal tension and compression forces from each sheathing panel and zero force contribution from the wood frame, as it is at the neutral axis. Thus, it does not uplift.

The different deflected shape for the double middle stud design wood frame resulted in a different wood frame deformation and GWB rotation behavior as shown in Figure H3. The largest change is the direction of the vectors on the top plate. The top middle plate vector is pointing nearly straight down. This is because the counterclockwise rotation of the GWB panel and the uplift of the top plate caused the top middle GWB corner to move down, while the wood frame moves up. The magnitude of this vector is much higher in the SEPSTUD and 3INNAIL designs as shown in Figure H3b and H3c due to the uplift of the top plate relative to the compression middle stud. The GWB stays mostly attached to the compression middle stud as shown in Figure H5, which results in the small magnitude of the top middle stud vector. The strong force transfer in the 3INNAIL design, due to the strong OSB sheathing attachment of nails at 76.2 mm on center, resulted in an opposite vector in direction to that of the top middle plate at the bottom end plate. This is also true of the top middle stud and bottom end stud. This behavior is not as obvious in the SEPSTUD design due to its weaker OSB sheathing connection of 152 mm on center. However, the top middle plate vector magnitude in SEPSTUD is much higher for the 3INNAIL due to the lack of attachment between the middle studs. This resulted in much more uplift of the uplift middle stud and top plate than in for the 3INNAIL design. The 3INNAIL design had a nailed connection between the two middle studs which resisted this uplift motion.

The top end plate and top end stud vectors for both the 3INNAIL and SEPSTUD designs are small at 1% drift. This is because the counterclockwise rotation of the GWB panel and the uplift of the top plate are in the same direction, leading to a large absolute displacement in each element, but little relative displacement. In fact, the direction of the SEPSTUD top end plate vector at 1% drift was pointing in a different direction than for all other designs. The top plate moved above the GWB, as shown at failure in Figure H5. This behavior begins at 19.2 mm of global displacement for the SEPSTUD design at which the top end plate vector was pointing 180°. The 3INNAIL design also exhibited this type of behavior at 28.5 mm of global displacement.

Shear Walls with Openings

For shear walls with openings, calculated relative displacement vectors for IRCWIN and 2OSBWIN, shown in Figure H4a and H4b, both qualitatively compare to the classical wood frame deflection and GWB rotation model. However, the 4PNLWIN design had a much different GWB attachment than other designs. The four panels attached above, below and to the sides of the window opening rotated

independently of each other until they begin racking against each other which was observed after 1% drift. This four panel flexible GWB attachment moved (absolutely) much more than the more rigid two panel attachment. Because the flexible wood framed moved (absolutely) similar to the GWB panels, the difference between the two absolute movements was small. This small relative displacement is shown in Figure H4. The end stud and plate vectors were consistent with other designs, but those on the middle stud and plate were much different. While the sensors in 4PNLWIN were attached to the same location in the wood frame as all other walls, the sensors were attached to the middle of the GWB panel in 4PNLWIN and the corner of the panel in all other designs. This different location explains the difference in vector direction. Assuming a linear change in relative displacement vector angle between the corners of a panel, the classical model predicts the horizontal angle shown on the top and bottom plates as observed in 4PNLWIN. The horizontal angle is approximately half of the minimum angle change between the corners of the panel predicted by the classical model.

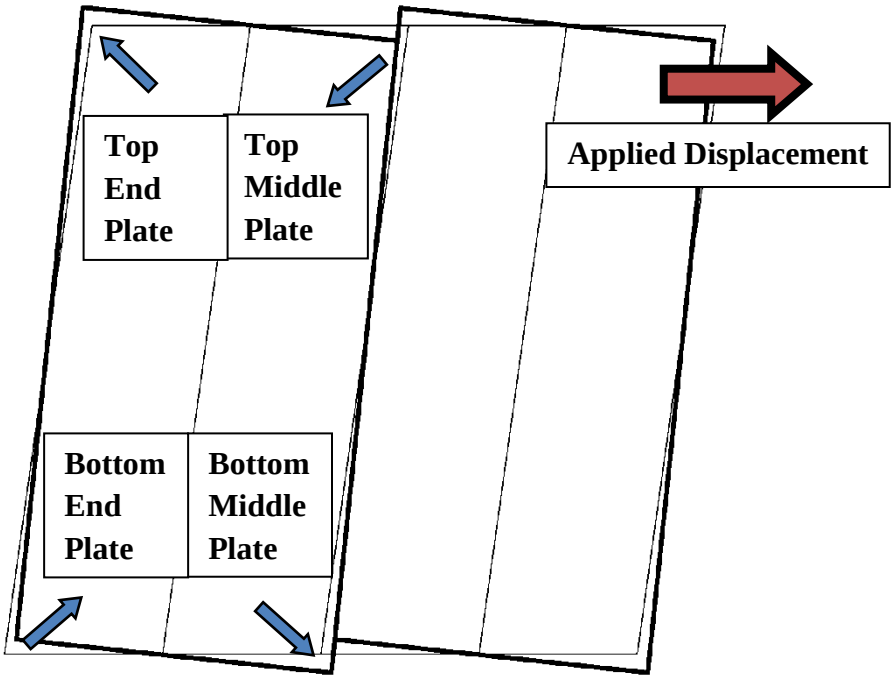

Figure H1. Classical Wood Frame Deformation and GWB Rotation Model

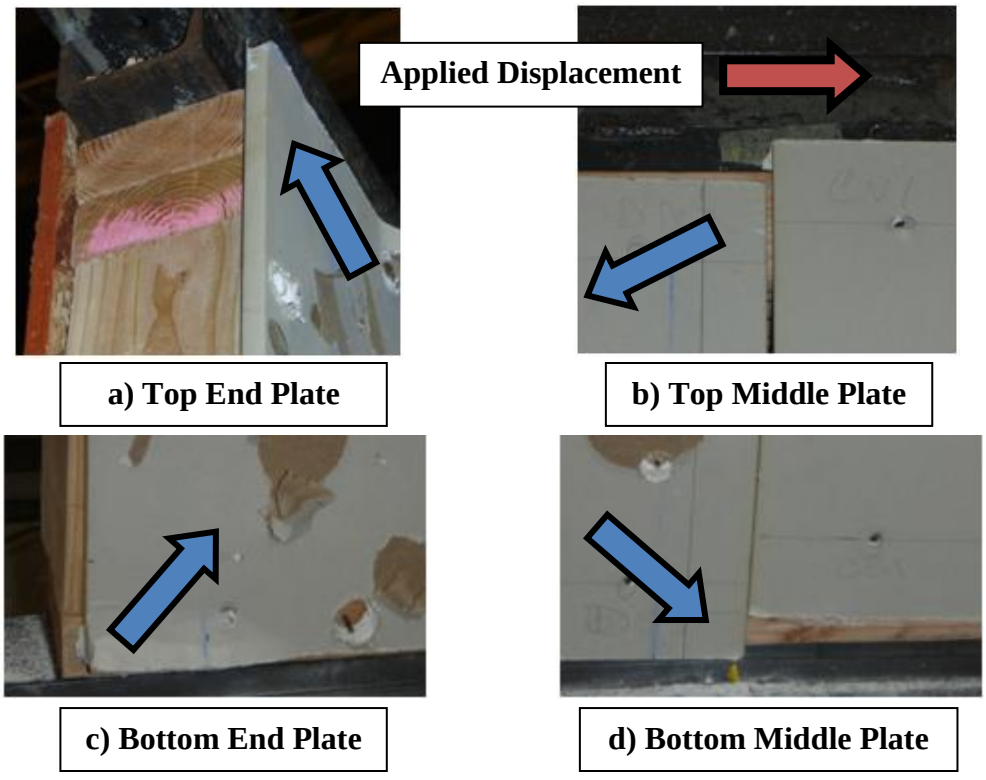

Figure H2. Relative Displacement Photos of Shear Walls at Failure

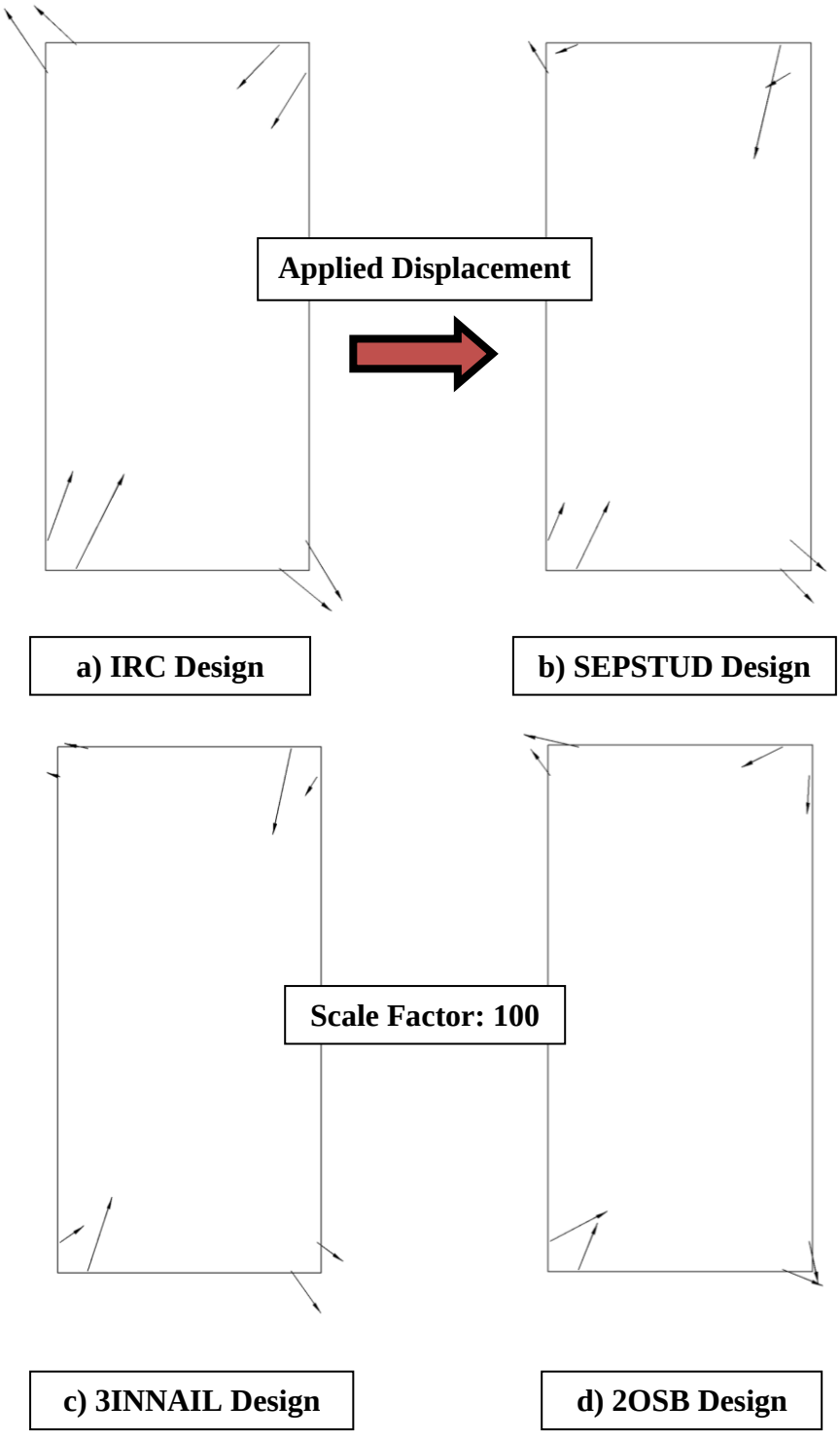

Figure H3. GWB Relative Displacement Vectors at 1% Drift for Shear Walls without Openings

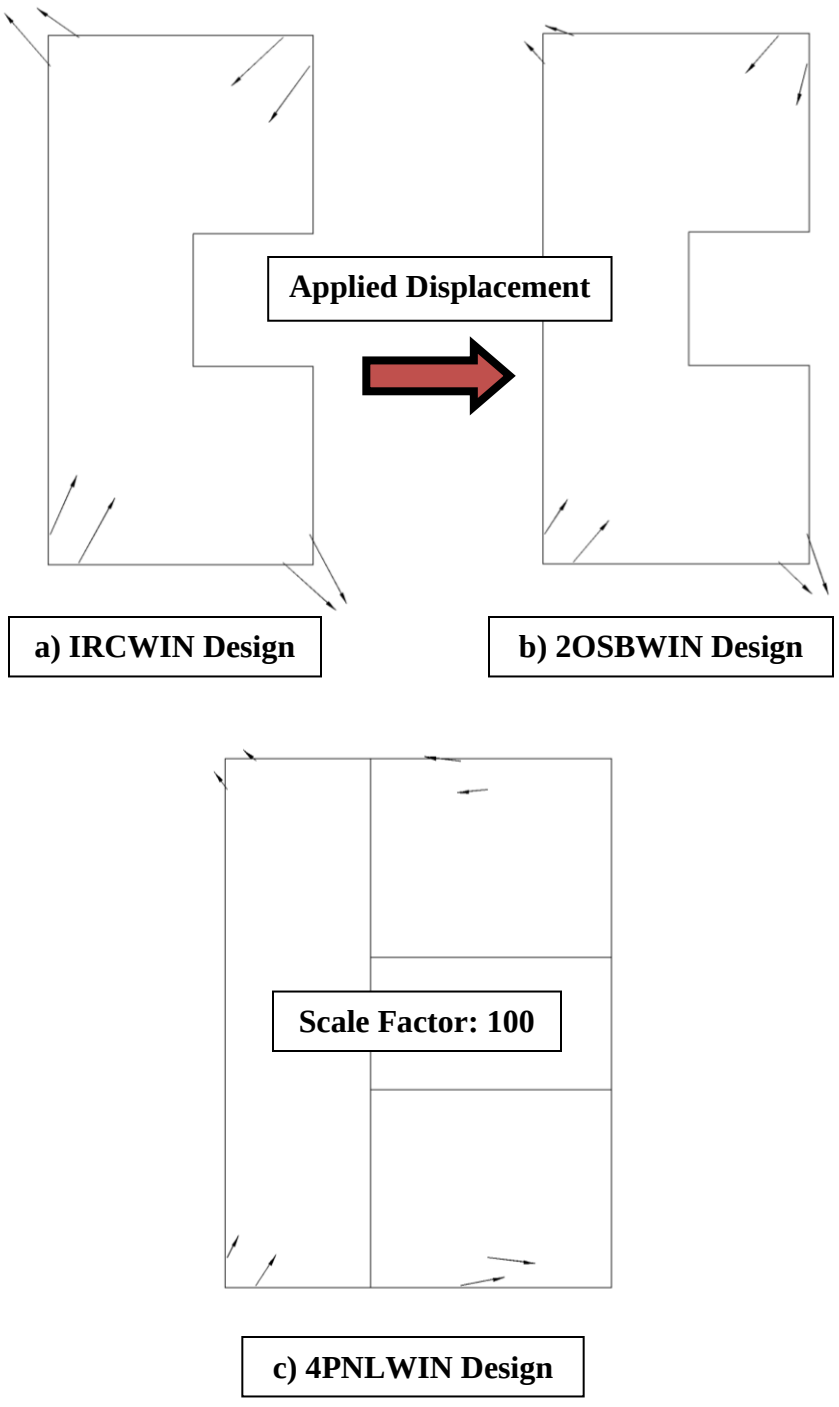

Figure H4. GWB Relative Displacement Vectors at 1% Drift for Shear Walls with Openings

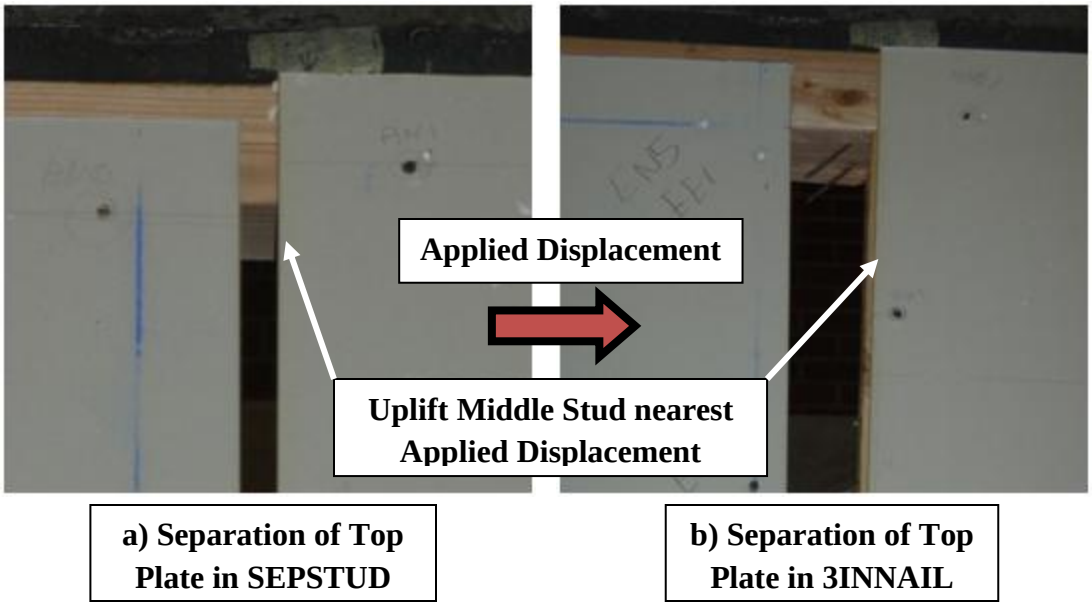

Figure H5. Uplift of the Middle Stud at Failure in Double Middle Stud Designs

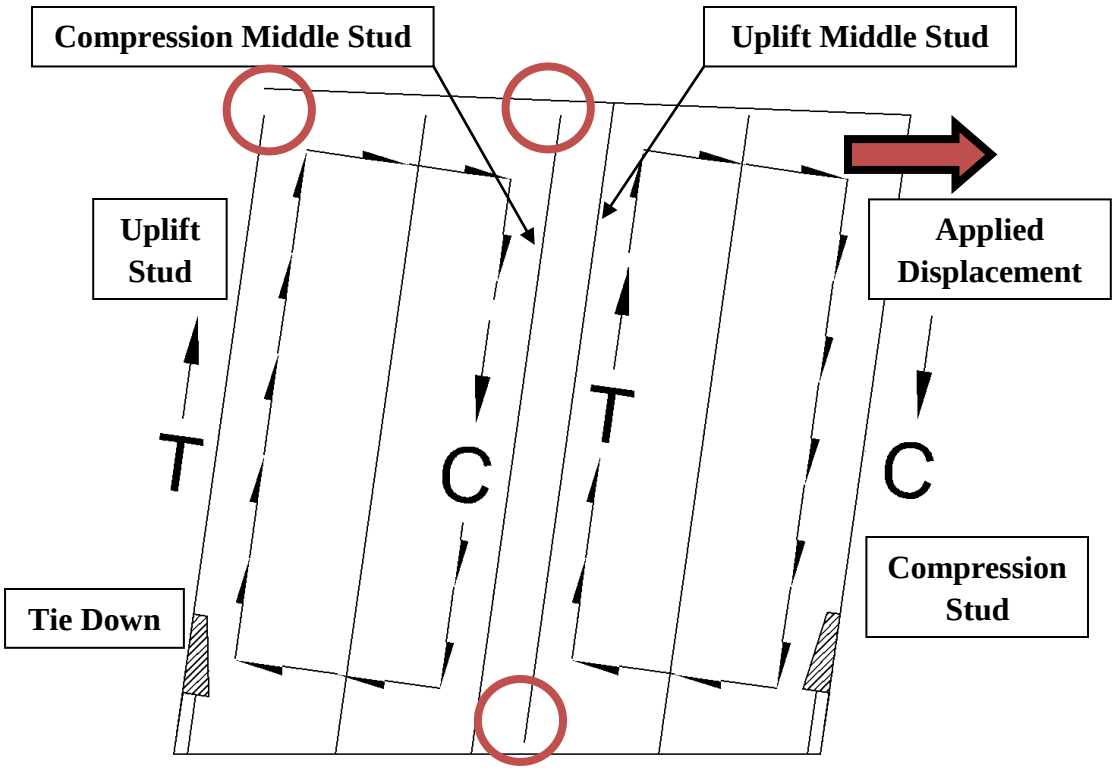

Figure H6. Load Path Schematic of Double Middle Stud Shear Walls

Appendix I: Discussion of Shear Wall Performance at Low Displacements

A visual comparison between shear walls without openings is shown at low displacements in Figure I1. As can be seen from Figure I1, even small shear wall displacements can cause substantial fastener failure. At low global displacement levels of 12, 16 and 20 mm, the IRC and SEPSTUD designs both exhibited noticeable connection failures. At 20 mm global displacement the IRC and SEPSTUD designs had 23% and 16% respective global connection failures. The 3INNAIL and 2OSB designs had almost no global connection failures for this displacement range. However, all innovative shear wall designs outperformed the control design (IRC) at all of these low displacements.

A visual comparison between shear walls with openings is shown at low displacements in Figure I2. At the low displacements of 12, 16 and 20 mm, the IRCWIN design exhibited a noticeable connection failure of 19% at 20 mm. The other designs, 2OSBWIN and 4PNLWIN, exhibited lower connection failures of 1% and 6% at 20 mm, respectively. Like shear walls without openings, both innovative designs performed better at all displacements than the control, the IRCWIN design.

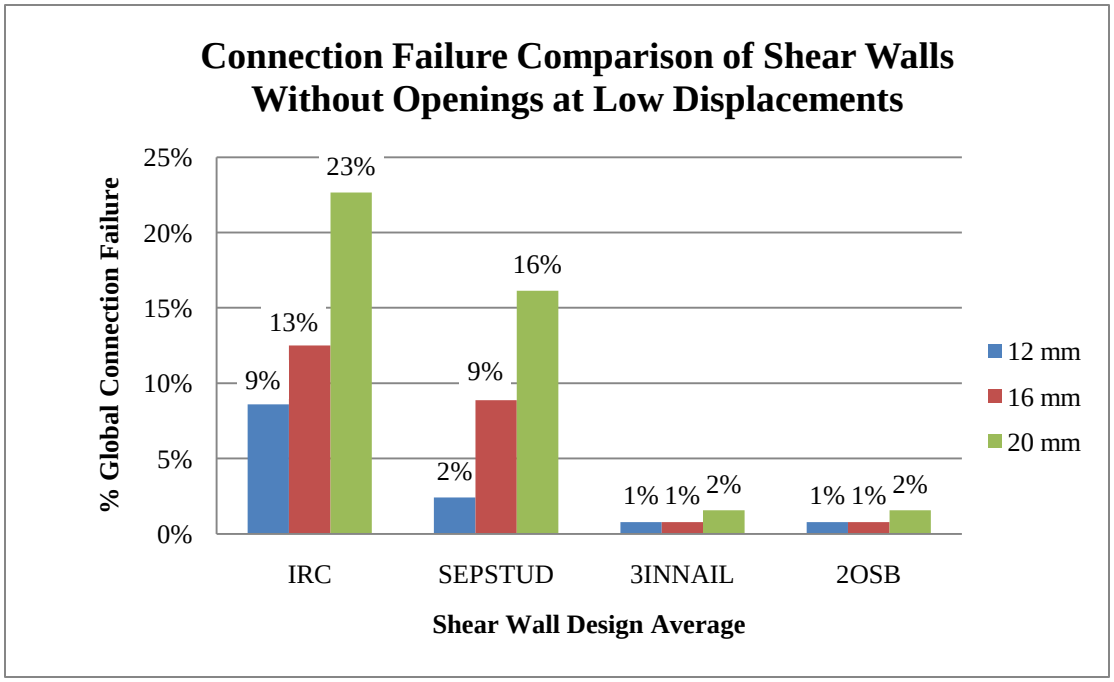

Figure I1: Connection Failure Comparison of Shear Walls without Openings at Low Displacements

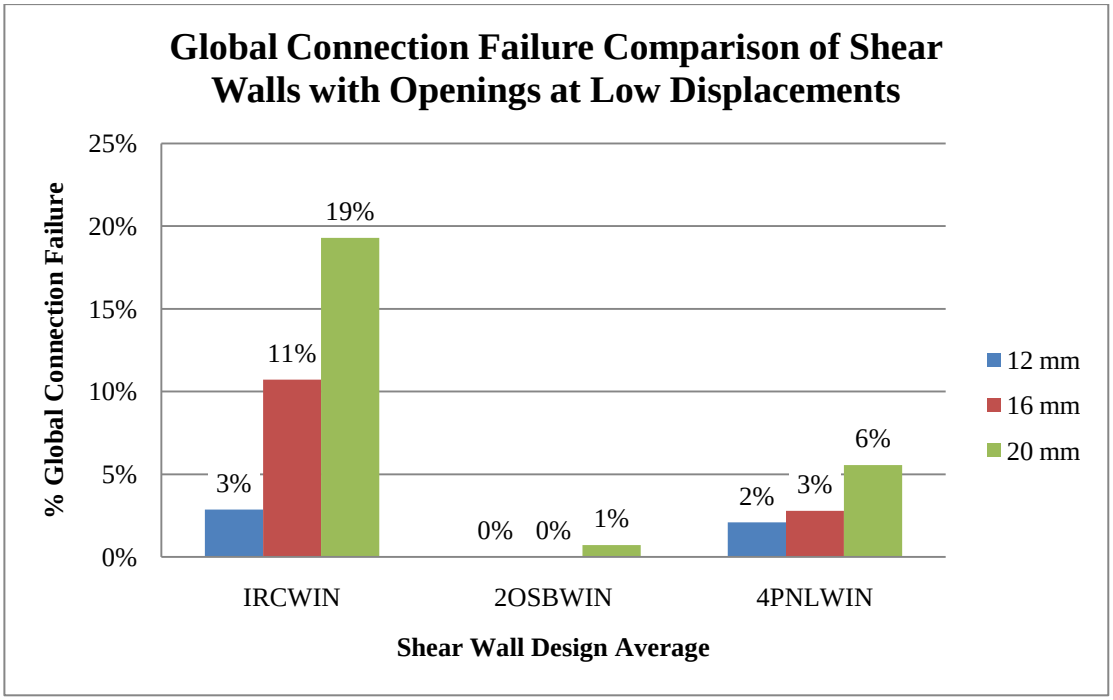

Figure I2: Connection Failure Comparison of Shear Walls with Openings at Low Displacements

Appendix J: Shear Wall Value Comparison Figures

Figures J1-J4 show the material cost of each shear wall design on left vertical axis and the percent global connection failure on the right vertical axis. Shear walls without openings are examined in Figures J1 and J2 for 1% and 2% drift, respectively. Shear walls with openings are examined in Figures J3 and J4 for 1% and 2% drift, respectively. OSB panels were purchased for $5.29 a sheet, GWB was purchased for $6.29 a sheet, 2438 mm length 38 mm x 89 mm wood studs were purchased for $1.90 a board, precut 2324 mm length 38 mm x 89 mm wood studs were purchased for $2.23 a board and the 38 mm x 140 mm header pieces were purchased for $3.39 a board.

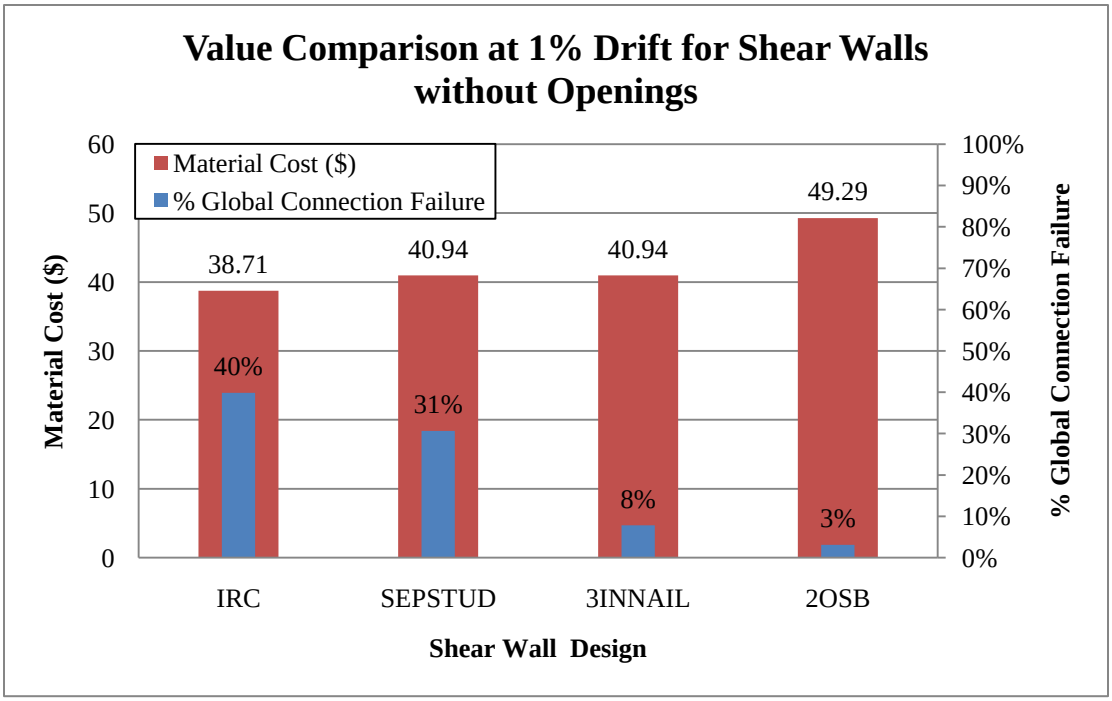

Figure J1. Value Comparison at 1% Drift for Shear Walls without Openings

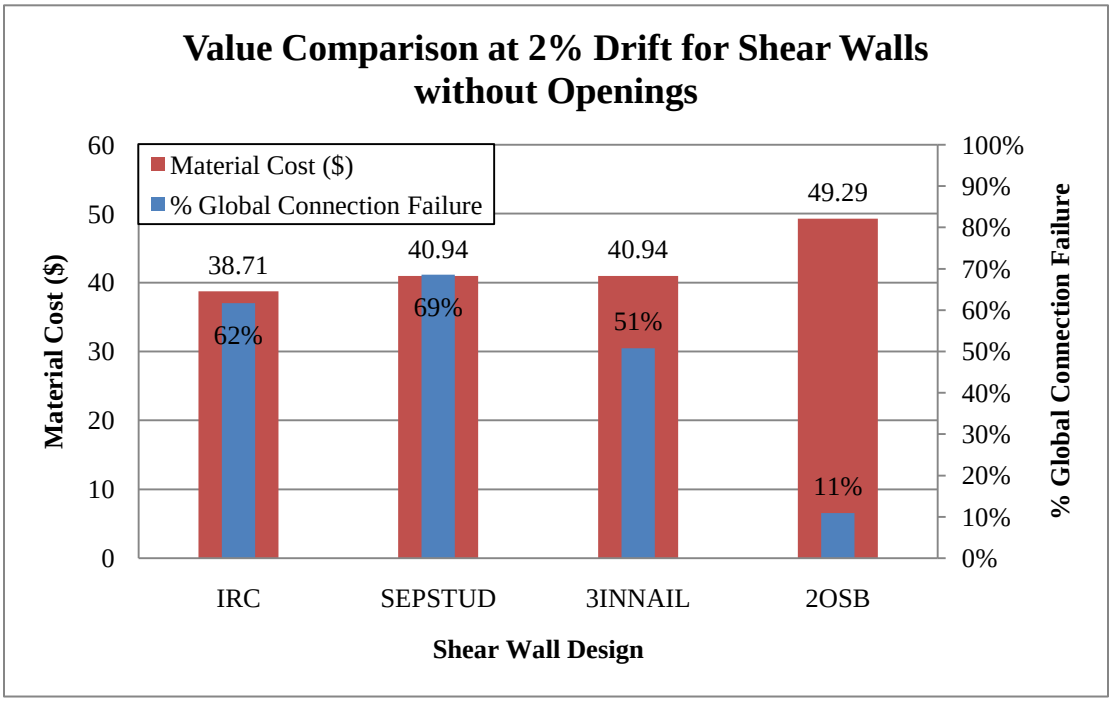

Figure J2. Value Comparison at 2% Drift for Shear Walls without Openings

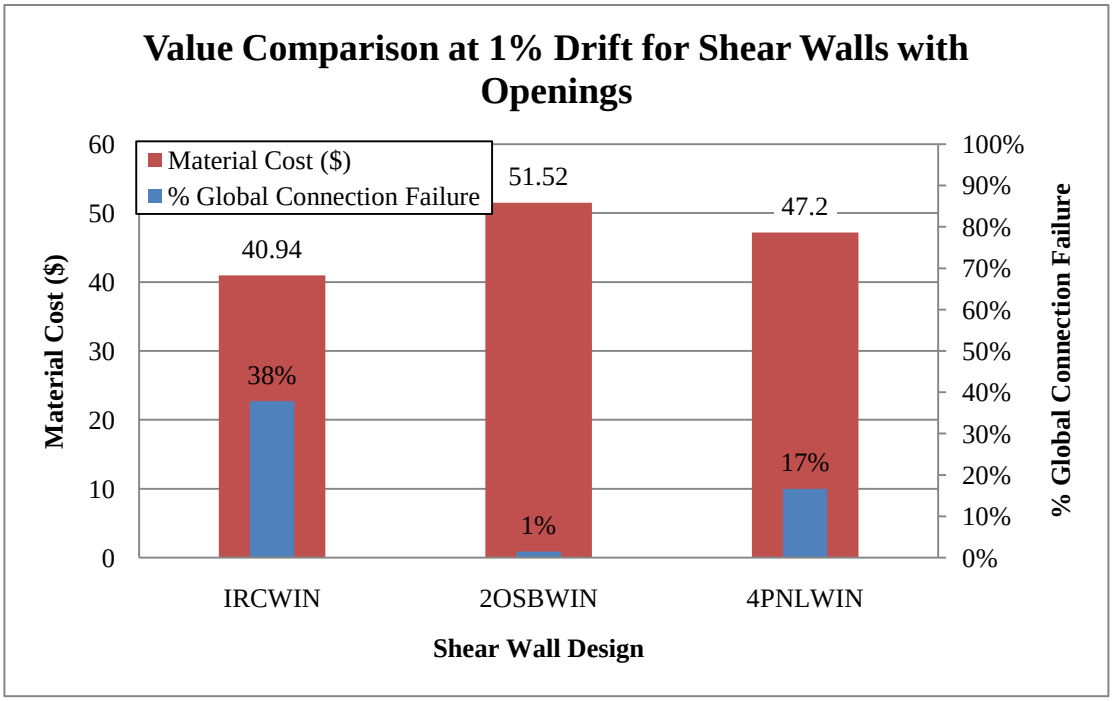

Figure J3. Value Comparison at 1% Drift for Shear Walls with Openings

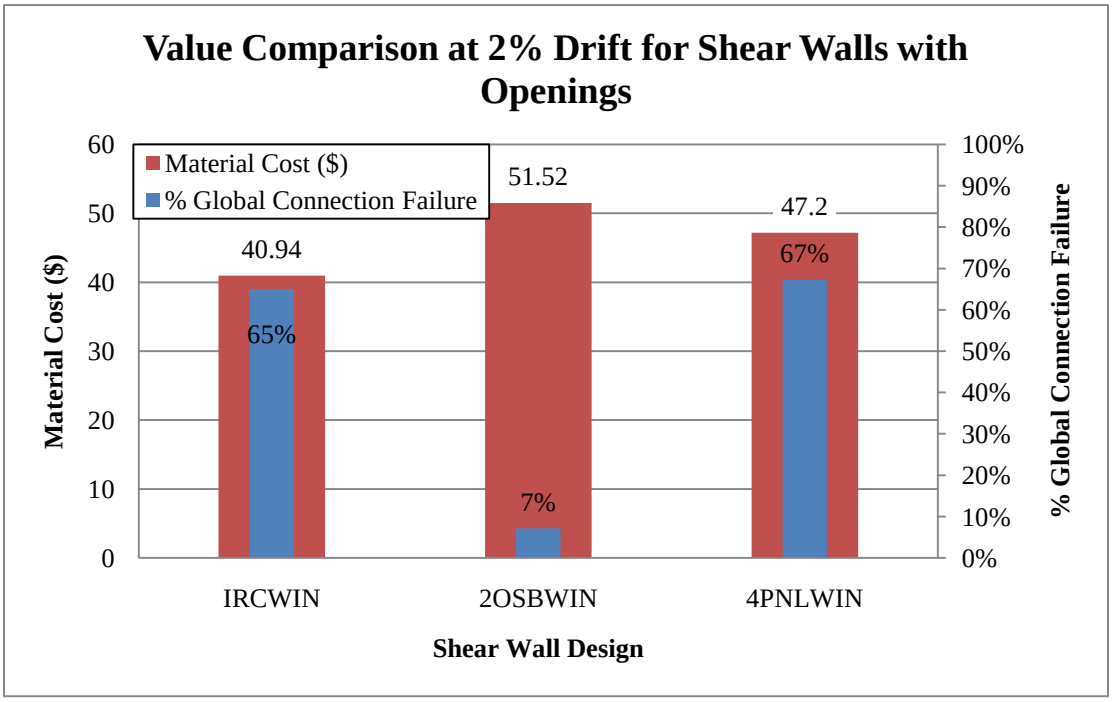

Figure J4. Value Comparison at 2% Drift for Shear Walls with Openings

Appendix K: Discussion of Variability in Results

Variation in Mechanical Property Results

Variability of strength and stiffness measurements in walls of the same design was high in this study for the more unconventional walls designs with variations in the GWB connection. The greatest variability seen in strength was 18% for the 4PNLWIN design and 25% for the stiffness of the SEPSTUD design walls. These two types of walls were very sensitive to changes in construction. The 4PNLWIN design had twice as many GWB joints as other designs, all of which were cut by hand through the middle of each panel. The GWB panels began to rack against each other at different global displacements during the test due to small differences in construction. This caused a variation in strength and stiffness. In the two SEPSTUD design walls, one wall failed by the middle studs buckling out of plane and the other by uplift of the top plate. This difference in failure modes described the instability of this design and the variation in strength and stiffness. Another possibility for this variation is the amount of displacement stops. Each wall was stopped ten times while failure maps of the GWB were made. Walls unloaded differently from these displacement stops, especially in the inelastic range, which could cause variation in strength and stiffness. In the other three designs, the greatest variability in strength and stiffness between walls of the same design were 8% and 12%, respectively. These designs represent what is more commonly used in industry, and variability which is more commonly seen in the literature (ASTM, 2006).

Variation in Visual Failure Comparison Method

While visual failure criteria were quantified and administered as objectively as possible, variation in results of the visual failure method did occur. Table K1 displays the difference of the percent global connection failure recorded at 1%, 2% and 3% drifts between the identical shear wall specimens of each design. Variations of 17% to 20% were recorded for all designs except SEPSTUD for at least one drift level. There seems to be no connection between the variation in mechanical properties of the shear wall and variation in visual failure criteria. This high level of variation is consistent with the first time employment of a visually graded system. For this reason, the relative displacement movements were measured to add credibility to the findings of this study. Using the data from the visual grading system and the relative displacement measurements, conclusions can be drawn about the performance of these shear walls.

Table K1: Difference in Percent Global Connection Failure

Shear Wall Design	1% Drift	2% Drift	3% Drift
IRC	20%	20%	13%
SEPSTUD	10%	5%	5%
3INNAIL	3%	17%	2%
2OSB	3%	9%	19%
IRCWIN	4%	10%	17%
2OSBWIN	1%	7%	18%
4PNLWIN	17%	18%	10%

Appendix L: Shear Wall Allowable Strengths

Calculations for the allowable strength of all shear wall designs are shown in this appendix. All unit shear capacities (v_s) were taken from the Special Design Provisions for Wind and Seismic with Commentary 2005 Edition Table 4.3A and Section 4.3.3 (AFPA, 2005)

IRC and SEPSTUD Shear Wall Designs

Seismic Allowable Strength
Sheathing Material: 7/16" OSB
Fastener Type and Size: 8d Nails
Panel Edge Fastener Spacing (in): 6 in o.c.
Length (L): 8 ft
Reduction Factor (RF): 2.0

$$V = \frac{v_s}{RF} \times L = \frac{480\,plf}{2.0} \times 8\,ft = 1920lb = 8.54kN$$

3INNAIL Shear Wall Design

Seismic Allowable strength
Sheathing Material: 7/16" OSB
Fastener Type and Size: 8d Nails
Panel Edge Fastener Spacing: 3 in o.c.
Length (L): 8 ft
Reduction Factor (RF): 2.0

$$V = \frac{v_s}{RF} \times L = \frac{900\,plf}{2.0} \times 8\,ft = 3600lb = 16.0kN$$

2OSB Shear Wall Design

Seismic Allowable Strength
Sheathing Material: 7/16" OSB on both sides

The unit shear capacity can be doubled for shear walls sheathed with the same construction and materials on both sides per Special Design Provisions for Wind and Seismic with Commentary 2005 Edition Section 4.3.3.2

Fastener Type and Size: 8d Nails
Panel Edge Fastener Spacing: 6 in o.c.
Length (L): 8 ft
Reduction Factor (RF): 2.0

$$V = \frac{v_s}{RF} \times L = \frac{480\,plf \times 2}{2.0} \times 8\,ft = 3840lb = 17.1kN$$

IRCWIN and 4PNLWIN Shear Wall Designs

Seismic Allowable Strength
Sheathing Material: 7/16" OSB
Fastener Type and Size: 8d Nails
Panel Edge Fastener Spacing (in): 6 in o.c.
Length (L): $L = 96in - 43.5in = 4.375\,ft$
Reduction Factor (RF): 2.0
Opening Height: 2 ft
Maximum Opening for 8 ft High Wall: 2'-8" (h/3)
Percent Full-Height Sheathing $\frac{4.375\,ft}{8\,ft} = 0.55 = 55\%$
Use $C_0 = 1.0$

Table 4.3.3.4 in Special Design Provisions for Wind and Seismic with Commentary 2005 Edition

$$V = \frac{v_s}{RF} \times L \times C_0 = \frac{480\,plf}{2.0} \times 4.375\,ft \times 1.0 = 1050lb = 4.67kN$$

2OSBWIN Shear Wall Designs

Seismic Allowable Strength
Sheathing Material: 7/16" OSB on both sides

The unit shear capacity can be doubled for shear walls sheathed with the same construction and materials on both sides per Special Design Provisions for Wind and Seismic with Commentary 2005 Edition Section 4.3.3.2

Fastener Type and Size: 8d Nails
Panel Edge Fastener Spacing (in): 6 in o.c.
Length (L): $L = 96in - 43.5in = 4.375\,ft$
Reduction Factor (RF): 2.0
Opening Height: 2 ft
Maximum Opening for 8 ft High Wall: 2'-8" (h/3)
Percent Full-Height Sheathing $\frac{4.375\,ft}{8\,ft} = 0.55 = 55\%$
Use $C_0 = 1.0$

Table 4.3.3.4 in Special Design Provisions for Wind and Seismic with Commentary 2005 Edition

$$V = \frac{v_s}{RF} \times L \times C_0 = \frac{480\,plf \times 2}{2.0} \times 4.375\,ft \times 1.0 = 2100lb = 9.34kN$$